LITHIUM DIAMIDOBINAPHTHYL CATALYSTS FOR ASYMMETRIC

HYDROAMINATION

By

LISA HURD

A Dissertation submitted to the

Graduate School-New Brunswick

Rutgers, The State University of New Jersey

in partial fulfillment of the requirements

for the degree of

Doctor of Philosophy

Graduate Program in Chemistry and Chemical Biology

written under the direction of

Prof. Kai C. Hultzsch

and approved by

_____

_____

_____

_____

New Brunswick, New Jersey

October 2013

ABSTRACT OF THE DISSERTATION

LITHIUM DIAMIDOBINAPHTHYL CATALYSTS FOR ASYMMETRIC

HYDROAMINATION

by LISA HURD

Dissertation Director: Prof. Kai C. Hultzsch

Lithium catalyzed intramolecular hydroamination of unactivated alkenes has been known for over 20 years, although growth in this field has been limited. Deduction of structure activity relationships for these systems is a challenge because of their complex solution behavior. A series of axially chiral C_2-symmetric diamidobinaphtyl dilithium salts given by the formula $[\{C_{10}H_6N(CH_2CH_2X)\}_2Li_2]_n$ where $n = 2, 6$ for X = NMe_2, $n = 2$ for X = OMe, and $n = 1$ for X = NEt_2 or $N(CH_2)_5$ were synthesized. Solid state characterization of these dilithium salts free of outside donor solvents allowed ligands to direct aggregation based on their steric hindrance and flexibility. All complexes showed π interactions between lithium and the naphthyl rings playing a significant role in the stabilization of the metal center. The complexes based on the sterically least demanding N-dimethyl-substituted ligand $[\{C_{10}H_6N(CH_2CH_2NMe_2)\}_2Li_2]_n$ crystallize as a dimer in enantiopure form and as a hexameric cycle in racemic form.
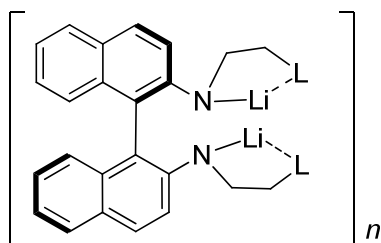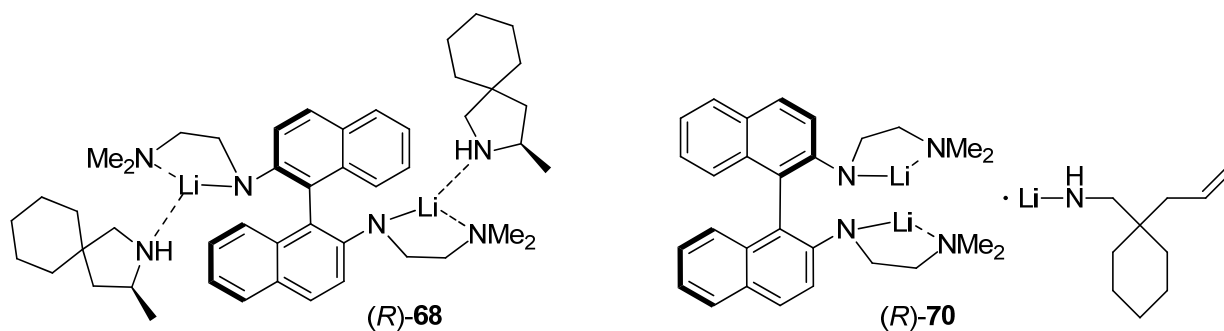
L = NMe_2; $n=2$ (R)-**64**
   NMe_2; $n=6$ (rac)-**64**
   NEt_2; $n=1$ (R)-**65**
   -$N(CH_2)_5$-; $n=1$ (R)-**66**
   OMe; $n=2$ (R)-**67**
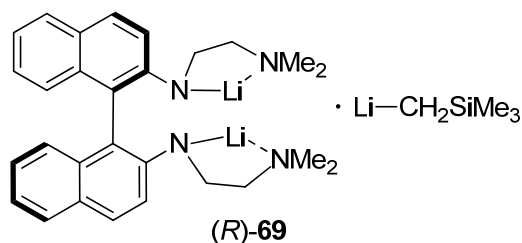
When used in combination with excess LiCH$_2$SiMe$_3$ various *gem*-dialkyl substituted aminopentenes were cyclized in up to 67% *ee* at 22°C. Cyclization of aminopentene at 40°C was also performed producing 2-methylpyrrolidine in up to 64% *ee*. The precatalysts were studied using DOSY, ^{7}Li and variable temperature NMR spectroscopy. DOSY NMR spectroscopy suggests that solutions of (*rac*)-**64** and (*R*)-**64** exist as a mixture of monomers and dimers at 25°C, while (*R*)-**65** and (*R*)-**66** are monomeric. Addition of one equivalent LiCH$_2$SiMe$_3$ to (*R*)-**64** resulted in a sharpening of ^{1}H NMR spectra and produced a single peak in the ^{7}Li NMR spectra, suggesting the formation of a new mixed aggregate, (*R*)-**69**.

Kinetic studies for the cyclization of *C*-(1-allyl-cyclohexyl)-methylamine demonstrated a first order rate dependence on substrate and catalyst concentrations. A first order rate dependence on LiCH$_2$SiMe$_3$ was also observed, with enantioselectivity decreasing linearly as the concentration of LiCH$_2$SiMe$_3$ was increased. (*R*)-**70** is a general representation of components found in the rate limiting transition state for the hydroamination/cyclization of *C*-(1-allyl-cyclohexyl)-methylamine. Solid state characterization of (*R*)-**64** with two equivalents of 3-methyl-2-aza-spiro[4.5]decane bound to it revealed the formation of a monomeric species, (*R*)-**68**.

(*R*)-**68**   (*R*)-**70**

TABLE OF CONTENTS

CHAPTER ONE: INTRODUCTION

CHAPTER   TWO: INTRAMOLECULAR   HYDROAMINATION   WITH

DIAMIDOBINAPHTHYL BASED LITHIUM AMIDES

LIST OF TABLES

LIST OF SCHEMES

LIST OF FIGURES

LIST OF ABBREVIATIONS AND SYMBOLS

α	Alpha
Å	Angstrom
Agg.	Aggregation
Ar	Aryl
β	Beta
Bn	Benzyl, amine protecting group
Boc	*tert*-Butyloxycarbonyl, amine protecting group
br	Broad
n-Bu	*n*-Butyl
n-BuLi	*n*-Butyllithium
cat.	Catalyst
Cbz.	Benzyloxycarbonyl, amine protecting group
COD	Cyclooctadiene
COE	Cyclooctene
config.	Configuration
conv.	Conversion
Cp	η^5-Cyclopentadienyl
Cp*	η^5-Pentamethylcyclopentadienyl
Cy	Cyclohexane
δ	Delta, chemical shift
d	Doublet
D	diffusion coefficient
DABN	2,2'-Diamino-1,1'-binaphthyl
Dbppste	DOSY Bipolar Pulse Pair Stimulated Echo
Dbppste_cc	DOSY Bipolar Pulse Pair Stimulated Echo with Convection Compensation
DCE	Dichloroethane
DFT	Density functional theory
DMF	*N,N*-Dimethylformamide
DMSO	Dimethylsulfoxide
DOSY	Diffusion Ordered Spectroscopy
η	Eta; hapticity OR viscosity
ee	Enantiomeric excess
eq.	Equivalent
equiv.	Equivalent
Et	Ethyl
Et_2O	Diethylether
f	Frictional coefficient
FW	Formula Weight
γ	Gamma
gem	geminal
g	gram
HMPA	Hexamethylphosphoramide
HMDS	Hexamethyldisilazide, $-N(SiMe_3)_2$

hr	Hours
IR	Infrared
KIE	Kinetic isotope effect
κ	*Kappa*, denticity
k_b	Boltzman constant, 1.3806×10^{-23} kg·m^2·s^{-2}·K^{-1}
L	Lone pair donor ligand
LAH	Lithium aluminum hydride
LDA	Lithium diisopropyl amide
Ln	Rare earth metal (Sc, Y, La – Lu)
m	Multiplet
m	meta
M	Metal
Me	Methyl
NMR	Nuclear magnetic resonance
NOBIN	2-amino-2'-hydroxy-1,1'-binaphthyl
*N*t	Turnover Number
o	ortho
ORTEP	Oak Ridge Thermal Ellipsoid Plot
p	para
Ph	Phenyl
π	Pi, 3.14
PMDTA	*N,N,N',N',N''*-Pentamethyl-diethylene-triamine
POV-ray	Persistence of Vision Raytracer
i-Pr	*iso*-Propyl
n-Pr	*n*-Propyl
q	Quartet
quint	Quintet
r	radius
R	Organic substituent
R*	Chiral organic substituent
R_H	Hydrodynamic radius
σ	Sigma
s	Singlet
sept	Septet
sext	Sextet
SQU	Squalene
Sub.	Substrate
t	Triplet
T	Temperature
*t*Bu	*tert*-butyl, tertiary butyl
TDE	Tetradecene
TEA	Triethylamine
TFA	Trifluoroacetic acid
OTf	Trifluoromethanesulfonate
THF	Tetrahydrofuran
THP	Tetrahydropyran

TMEDA N,N,N',N'-Tetramethylethylendiamine
TMS   Tetramethylsilane
TON   Turnover Number
Ts   Tosyl, toluenesulfonyl
VT   Variable Temperature

1

Introduction

1.1 Lithium Amides: Applications and Solution Behavior

Although lithium reagents are frequently used in both academic and industrial synthesis,[1] their structures in solution often remain ambiguous. Susceptible to solvent effects, salt effects and changes in temperature, concentration or stoichiometry the reproducibility of a given process can be compromised if all of these variables are not controlled. Publications in this field typically focus on empirical results and worldwide, only a few groups have identified solution structures and reaction intermediates with confidence.[2]

The study of lithium complexes in the solid state has advanced significantly since the 1980's[3] due to wider availability of x-ray crystallography, its use at low temperatures and advances in crystal mounting techniques.[4] Understanding these complexes in the solid state has allowed the field to advance, although the elucidation of solution structures remains the final frontier. Accounts of inconsistent structures in the solid state and in solution have been documented necessitating independent studies for the assignment of solution structures.[5] Low temperature NMR studies of isotopically labeled compounds, the method of continuous variation (Job plots) and DFT studies have allowed chemists to probe the solution behaviour of these compounds.[6] Kinetic studies have also assisted in the identification of transition states.[7] Recently, DOSY-NMR[8] has been utilized in conjunction with these classical techniques to study lithium amides/alkyls[9] and bimetallic lithium containing superbases.[10]

1.2 Amines: Applications and Synthesis

Many amine containing molecules demonstrate biological activity of a medicinally applicable nature. Phenethylpiperazines[11] and β-arylethylamines[12] are examples of molecular skeletons used to treat a variety of medical conditions (Figure 1-1). These compounds are also target molecules for the *anti*-Markovnikov hydroamination of styrene derivatives (Section 1.3.1).
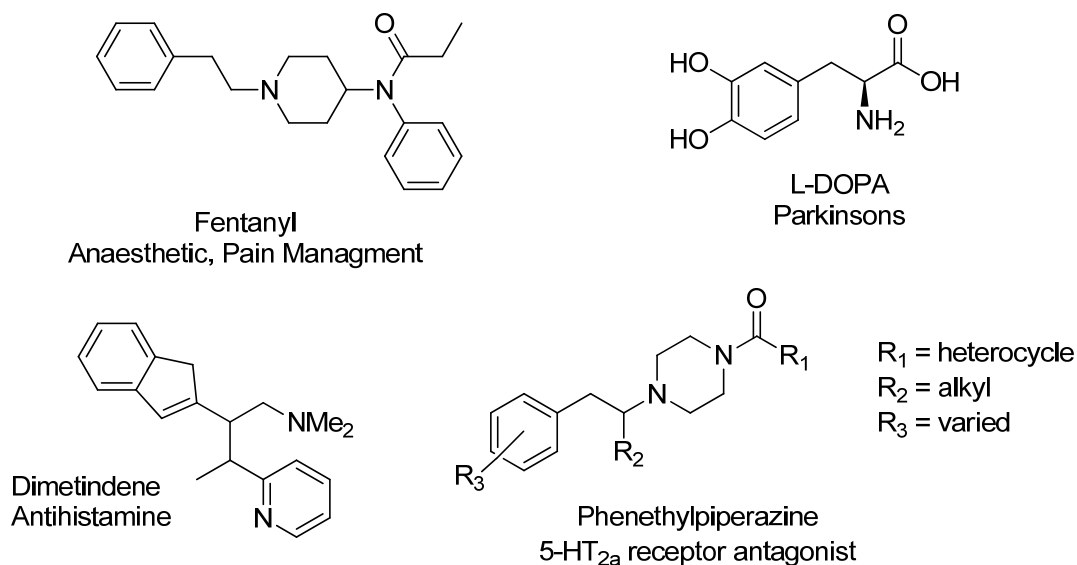
Figure 1-1. Structures and pharmaceutical applications of selected β-arylethylamines and a general phenethylpiperazine skeleton.

Development of methodology for the efficient synthesis of amine containing compounds is useful to the pharmaceutical and specialty chemical industries. Challenges typically encountered during the synthesis of amines include low selectivity and difficulty during purification. These processes often generate significant amounts of waste and become an environmental burden. Historical approaches to amine synthesis include alkylation of amines (Eq. 1-1), reduction of nitrogen containing functionalities (Eq. 1-2) and amine synthesis via addition reactions (Eq. 1-3). Other approaches included the use of organometallic reagents (boranes, Grignard reagents), hydrolysis (cleavage of a nitrogen-carbonyl bond) or molecular rearrangements (Hoffmann, Curtis, etc.).[13]

$$\text{R'}-\text{X} \quad + \quad \text{H}_2\text{N}-\text{R} \quad \longrightarrow \quad \text{R'}-\overset{\text{H}}{\underset{}{\text{N}}}-\text{R} \quad + \quad \text{R'}_2-\text{N}-\text{R} \qquad (1\text{-}1)$$

R, R' = alkyl

$$+ \quad \text{H}_2\text{N}-\text{R} \quad \underset{-\text{H}_2\text{O}}{\rightleftharpoons} \quad \text{=N}-\text{R} \quad \xrightarrow{\text{reduction}} \quad \overset{\text{H}}{\underset{}{\text{N}}}-\text{R} \qquad (1\text{-}2)$$

R = alkyl, aryl

$$+ \quad \text{HNEt}_2 \quad \xrightarrow{\textit{n}\text{-BuLi}} \quad \text{NEt}_2 \qquad (1\text{-}3)$$
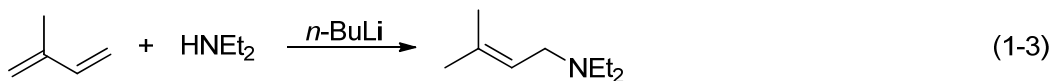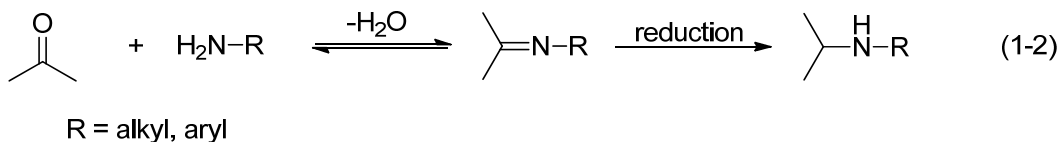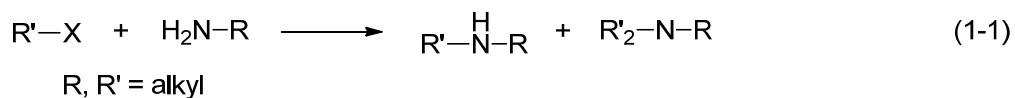
Homogeneous catalysis is increasingly important to the field of organic synthesis,[14] because it allows access to target molecules with high selectivity and a minimal amount of waste. Methods applicable to the synthesis of amines include the hydroaminomethylation (Eq. 1-4),[15] Buchwald – Hartwig amination (Eq. 1-5),[16] hydroamination, and reductive alkylation of imines and enamines.[17]

$$R \diagup\!\!\diagdown \xrightarrow[CO, H_2]{catalyst,} R \diagup\!\!\diagdown\!\!\diagup\!\!\diagdown\overset{O}{\underset{H}{\diagdown}} \xrightarrow[HNR_2/H_2]{catalyst,} R \diagup\!\!\diagdown\!\!\diagup\!\!\diagdown NR_2 \qquad (1\text{-}4)$$

R = alkyl, aryl

$$Ar-X \ + \ HNR_2 \xrightarrow[-HX]{catalyst,} Ar-NR_2 \qquad (1\text{-}5)$$
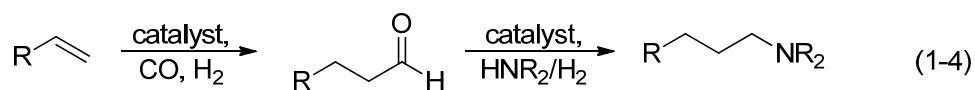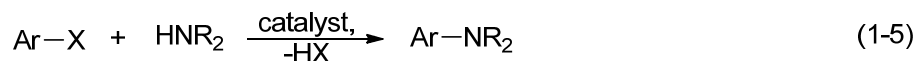
X = Cl, Br, I, OTs

1.3 Catalytic Hydroamination of Unactivated Olefins

1.3.1 General Overview

Hydroamination[18] describes the addition of an amine to an aliphatic or aromatic alkene, alkyne,[19] allene or diene (Scheme 1-1). The past two decades have seen the development of several asymmetric catalysts[20] to effect this transformation. The most active and selective catalysts for the intramolecular variant of this transformation are mediated by rare earth metals.[21] Intermolecular transformations are showing increasing potential, particularly the anti-Markovnikov addition of amines to styrene derivatives. Moderate to high reactivity has been observed in systems based on alkali, alkaline earth and rare earth metals. The development of catalysts for intermolecular hydroamination reactions has proven challenging due to an imbalance between alkene and amine binding in most catalyst systems.
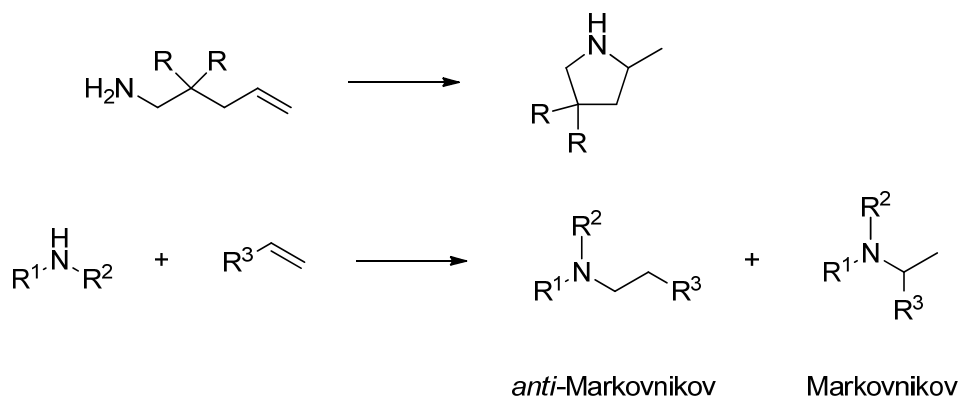
Scheme 1-1. Intramolecular Hydroamination (top), Intermolecular Hydroamination leading to *anti*-Markovnikov and Markovnikov regioselectivity (bottom).

Investigation of this transformation has uncovered several catalyst systems which prefer C-H activation instead of N-H activation. After activation these catalysts can undergo intramolecular cyclization or intermolecular addition to alkenes. Commonly referred to as hydroaminoalkylation[22] (Scheme 1-2), these reactions have been performed in an intra- and intermolecular fashion mediated by Group 1, 4 and 5 metals. The asymmetric variant of this transformation is also of interest.[23]
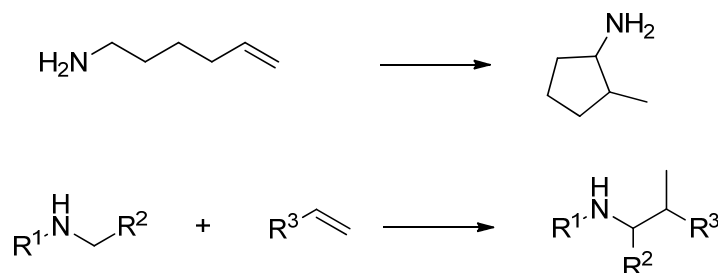
Scheme 1-2. Intramolecular Hydroaminoalkylation (top) and Intermolecular Markovnikov Hydroaminoalkylation (bottom).

Polar Organometallic Reagents – Mechanistic Considerations

Similarities in the reactivity of Group 1 – 3 complexes exist due to their polar nature and the presence of one stable oxidation state. Because they cannot undergo oxidative addition and reductive elimination, their range of mechanistic options is somewhat limited. Amine activation is the accepted mode of delivery for these metals into their catalytic cycles. Subsequent olefin insertion and protonolysis occurs in either a stepwise or concerted fashion. The tendency of

Group 1 and 2 based complexes undergo facile ligand redistribution[24] adds additional difficulty to the understanding and elucidation of their behavior in solution.

M = Li, Na, K, Mg, Ca, Sr, Sc, Y, lanthanide
X = alkyl, aryl, amido
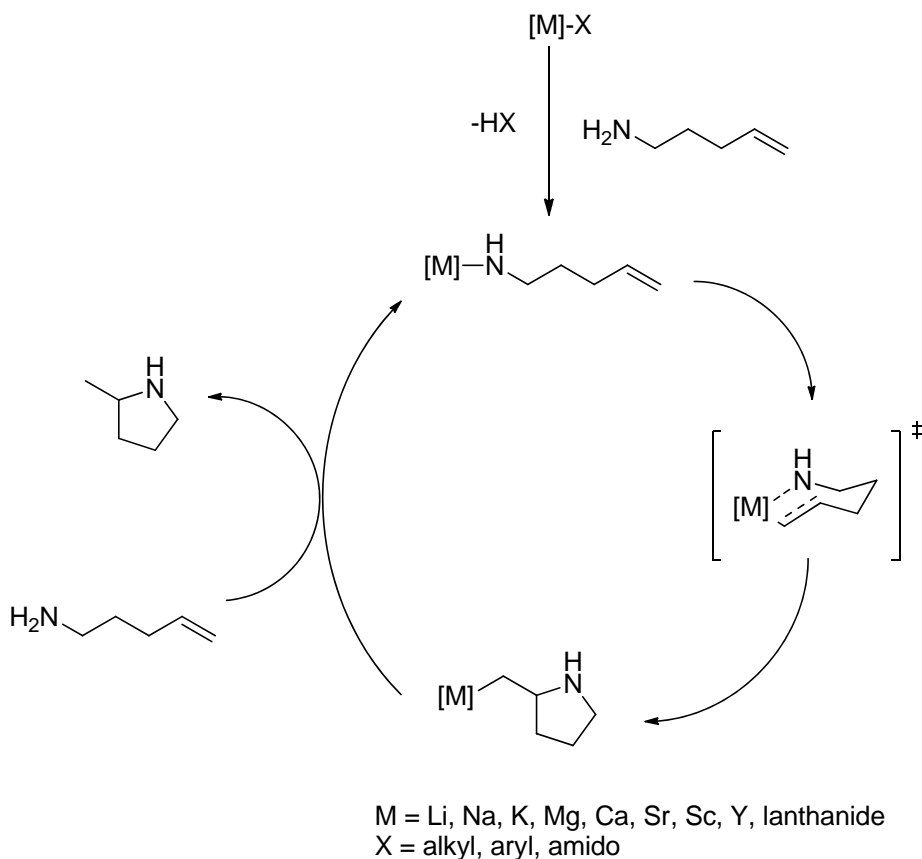
Scheme 1-3. Generalized Mechanism for Intramolecular Hydroamination of Aminoalkenes with catalysts based on metals from Group 1 – 3.

The mechanism of rare earth metal-catalyzed hydroamination is well understood and many catalysts are believed to proceed by σ bond metathesis (Scheme 1-3).[25] A zero order rate dependence on substrate concentration suggesting rate limiting olefin insertion[26] is often observed. The concurrent observation of kinetic isotope effects (KIE's) complicates the interpretation of these studies and a similar trend is developing for alkaline earth based systems. Rationalizations of these KIE's include the presence of a concerted non-insertive mechanism[27] and proton assistance from a proximal amine.[26a] For the intramolecular cyclization of aminoalkenes, DFT studies have supported a σ-insertive mechanism with rate limiting protonolysis for alkaline earth metals[28] and rate limiting olefin insertion for rare earth metals.[29]

1.3.2 Rare Earth Metal-Catalyzed Hydroamination

Rare Earth Metal-Catalyzed Hydroamination: Intramolecular Examples

Hydroamination catalysts based on rare earth metals are currently the most active and selective for intramolecular cyclizations.[21] Lanthanides have one stable oxidation state (+3), and thus cannot undergo oxidative addition or reductive elimination. Electrophilic in nature, these complexes typically react by σ bond metathesis (Scheme 1-4).[25] Initial catalysts were based on cyclopentadienyl ligands in the form of either half sandwich complexes or metallocenes. The steric environment around the metal center has a significant impact on catalytic activity. The use of more open ligand scaffolds and metals with larger Ln^{3+} ionic radii[30] led to more active catalysts. Exposure of the metal center has allowed product inhibition to occur in several lanthanide catalysts.
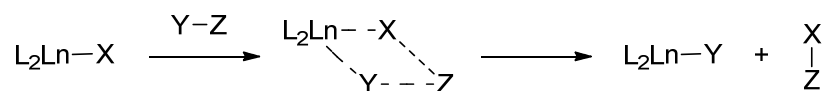
Scheme 1-4. General representation of a rare earth metal mediated σ bond metathesis.

These seminal catalysts[31] underwent rapid olefin insertion into Ln-C and Ln-H bonds during the polymerization of ethylene. Its capacity to perform the analogous process with M-N bonds was realized shortly thereafter.[32] Substitution of the labile hydride with an alkyl ligand allowed the formation of a more active monomeric precatalyst **1**.[33] The synthesis of ansa-complexes **2**[26a] allowed enhanced reactivity by exposing the metal center. Further improvement in rate was observed with half-sandwich "constrained geometry" catalysts **3**.[34]
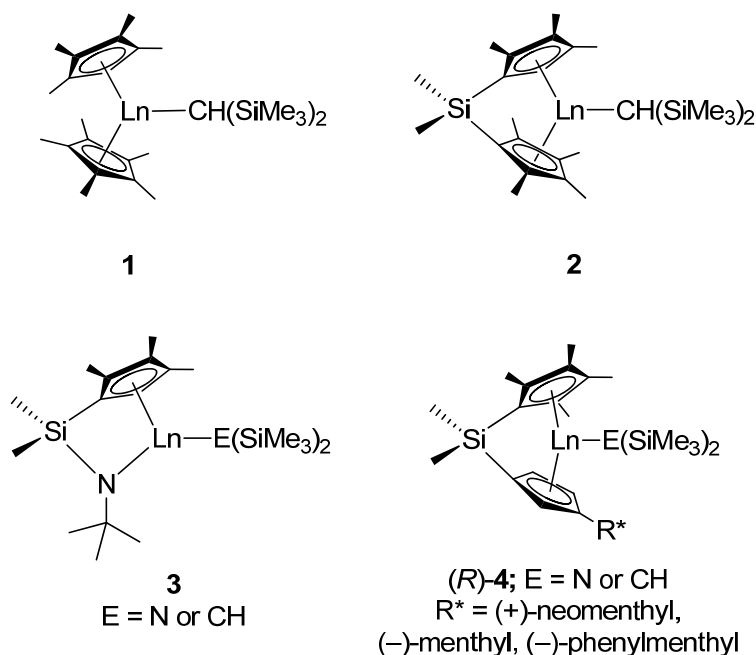
Figure 1-2. Cyclopentadienyl-based hydroamination catalysts.

The first asymmetric catalysts[20] in this class, **4**,[35] incorporated an optically active menthyl group attached to the cyclopentadienyl ring and efficiently cyclized terminal aminoalkenes. Catalyst epimerization (Scheme 1-5) proved problematic and prevented *ee*'s from rising above 74%. One isomer is typically favored in a ratio typically >90:10 depending on the chiral substituent R*, solvent and temperature. In addition to lowering enantioselectivity, this also prevents access to both product enantiomers from the diastereomeric precatalyst. The limitations of lanthanocene catalysts in asymmetric hydroamination necessitated the creation of catalysts based on other ligand sets.
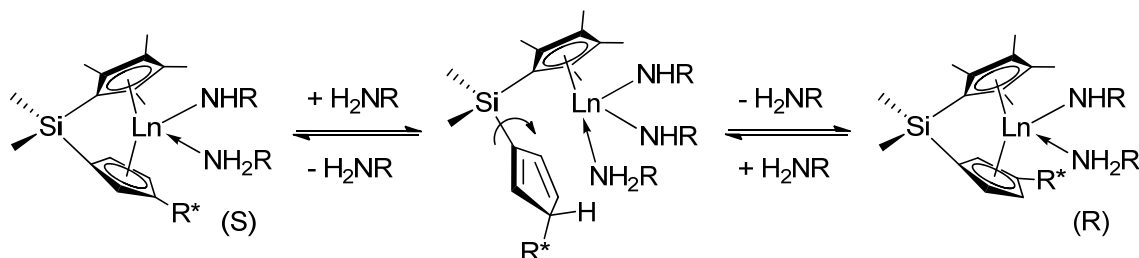
Scheme 1-5. Enantioselectivity limiting epimerization of chiral ansa-lanthanocene catalyst.

The development of post-metallocene catalysts was influenced by the realization that simple lanthanide amides[36] mediated the hydroamination of aminoalkenes, albeit slowly and

under more forcing conditions. Configurational stability of non-cyclopentadienyl complexes was improved because ligands were bound to metals through σ-oxygen and σ-nitrogen bonds rather than π and σ-carbon bonds. Chelating diamides and bis(thiophosphinic amides)[37] demonstrated ligand acceleration and good *cis/trans* diastereoselectivity for intramolecular hydroamination of aminoalkenes. Structure – activity relationships were not determined due to a lack of detailed information on the solid state and solution structures for many of these complexes. The first well defined system incorporated diamidoamine complexes **5a – c, 6a – c** and **7** and demonstrated high *trans/cis* diastereoselectivity at room temperature for the cyclization of 1-methyl-pent-4-enylamine.[36b]
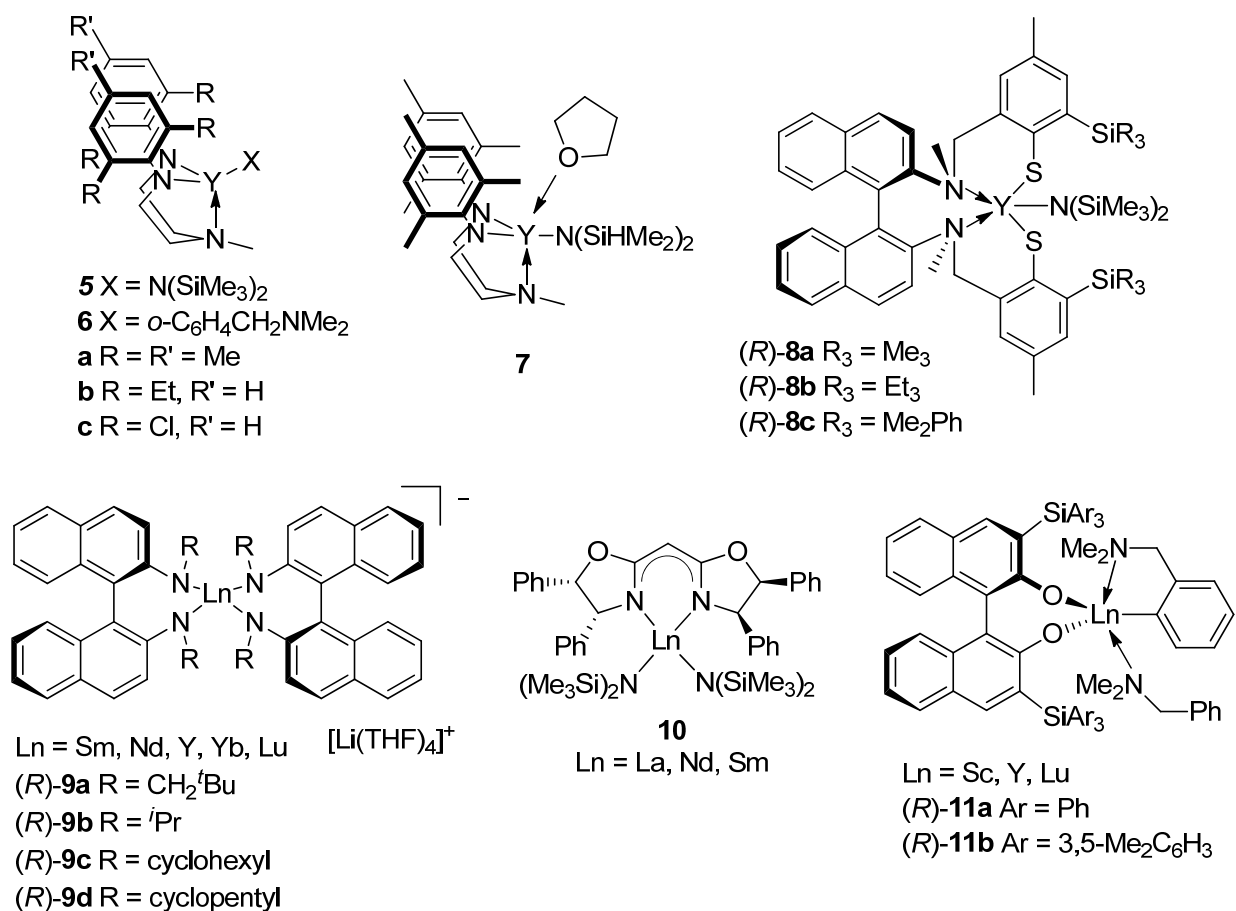
Figure 1-3. Post-metallocene hydroamination catalysts.

Many chiral post-metallocene catalysts have been reported over the last 15 years, although few have achieved the level of activity and stereoinduction reported in their

cyclopentadienyl-based predecessors. The majority of ligand scaffolds incorporated have been C_2 symmetric and include biaryl diamides, diamidobinaphthyls, aminophenolates, aminothiophenolates, biphenolates and binaphtholates.

Aminothiophenolate catalyst (*R*)-**8** has achieved high levels of enantioselectivity in spite of the higher temperatures required for activity and it was applicable across a range of substrates including internal alkenes and secondary amines.[38] Electronic saturation of the metal center by this multidentate ligand is a likely cause of its low activity, while high enantioselectivities have been attributed to its large bite angle. Electron rich ate complexes **9a** – **d** also demonstrated lower activity than lanthanocene catalysts; however, enantiomeric excess of up to 87% were reported.[39] Related neutral complexes containing LiCl and THF were also reported and achieved similar or higher enantiomeric excess and higher activity.[40] Bisoxazoline based systems including **10** have demonstrated ligand acceleration and enantiomeric excess of up to 67%.[41]

Activities comparable to lanthanocene catalysts were achieved with 3,3'-bis(tri(aryl/alkyl)silyl binaphtholate rare earth metal complexes **11a** – **d**.[26b] The bulky silyl groups prevent complex aggregation and are essential for enantioselectivity. A wide range of substrates are cyclized by this catalyst with up to 95% enantiomeric excess being reported.

Rare Earth Metal-Catalyzed Hydroamination: Intermolecular Examples

Although rare earth metal-based catalysts are the most active and selective for intramolecular hydroamination, they are not as efficient for intermolecular reactions. A large excess of olefin and a higher reaction temperature is required to achieve conversion and increase reaction rate. Olefin insertion, which is postulated to be the rate determining step, is hindered by competitive binding with substrate and product amines. Nonetheless, the intermolecular hydroamination of olefins has been documented on multiple occasions in the groups of Marks and Hultzsch (Scheme 1-6).[42] Lanthanocene and binaphtholate catalysts have mediated the addition of primary amines to styrene derivatives (*anti*-Markovnikov) and aliphatic olefins (Markovnikov) with the binaphtholate catalyst (**16**) achieving up to 61% enantiomeric excess.
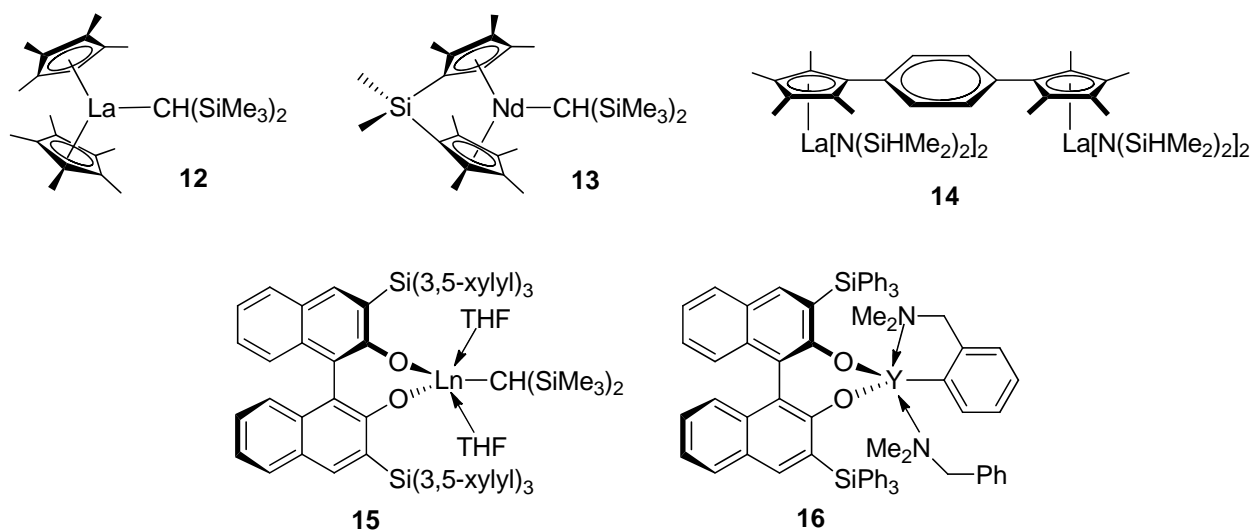
Figure 1-4. Rare earth metal-based catalysts for intermolecular hydroaminations.

Amine:Olefin	Catalyst	T (°C)	Conv(%), Nt
1:10	**12** (10%)	90°C	93%, 2.0 h⁻¹
1:1.3	**15** (2%)	60°C	74%, 0.7 h⁻¹
1:10	**14** (2%)	90°C	>95%, 0.02⁻¹
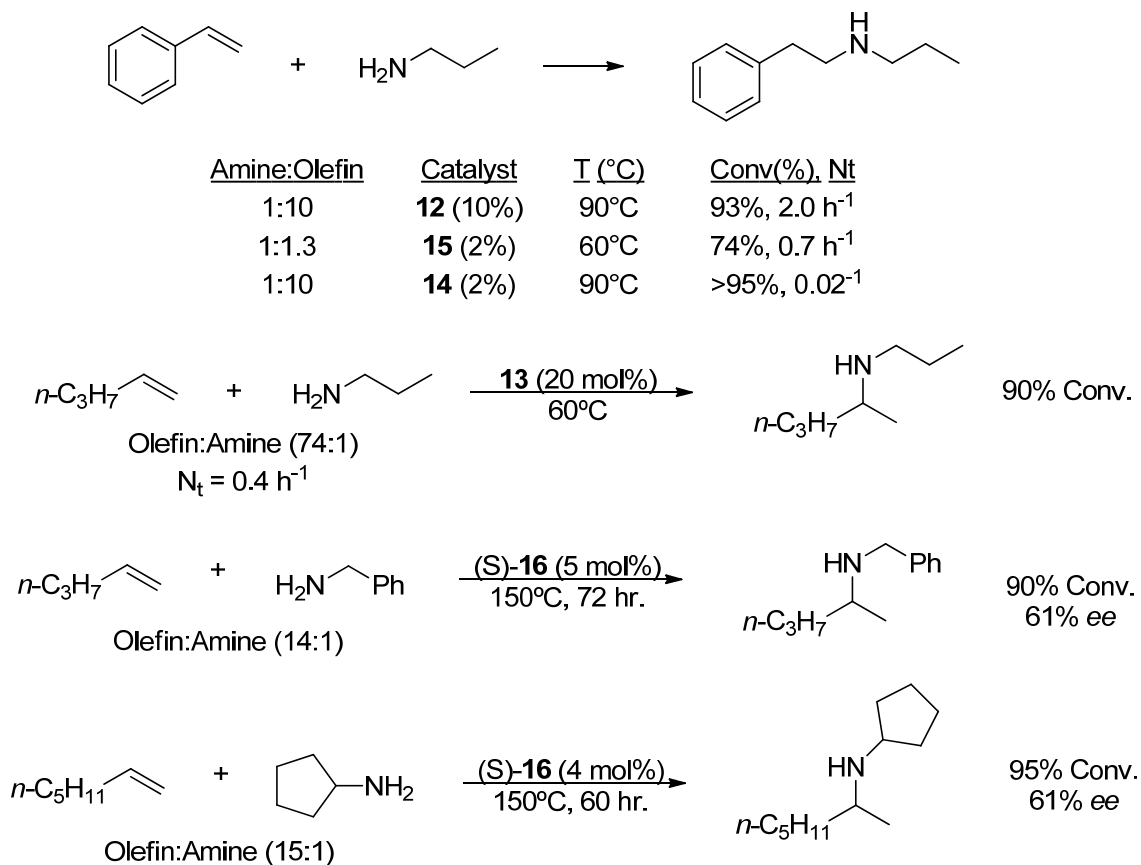
Scheme 1-6. Rare earth metal-mediated intermolecular hydroaminations.

1.3.3 Alkaline Earth Metal-Catalyzed Hydroamination

Alkaline Earth Metal-Catalyzed Hydroamination – Intramolecular Examples

      The use of alkaline earth metals for hydroamination catalysis is of particular interest due to their natural abundance, low toxicity[43] and potential to act as both nucleophiles and electrophiles.[44] The development of alkaline earth metal complexes suitable for hydroamination has been hindered by their tendency to exist in a Schlenk equilibrium (Eq. 1-6) and their low solubility in non-coordinating solvents.

$$2RMgX \rightleftharpoons MgR_2 + MgX_2 \qquad (1\text{-}6)$$
$$R = \text{alkyl}; X = Cl, Br, I$$
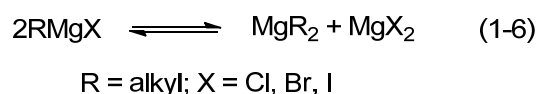
      Many well defined Group 2 complexes demonstrating hydroamination activity have been reported, and some exhibit activity comparable to rare earth metal-based systems. Group 2 complexes enter their catalytic cycle by amine activation with substrate deprotonation typically initiated by an amido[45] or alkyl[46] leaving group. Alkyl leaving groups are advantageous because of their high basicity and irreversible catalyst activation after protonation. The high basicity of Group 2 metal alkyls is problematic and competing deprotonation[47] can prevent the synthesis of the desired complexes. Lewis basic solvents, including THF, are used to solubilize precatalysts, potentially leading to ambiguous aggregates or stabilizing the ground states of catalytic species.

(R,R)-**17**[R]

18a M = Mg, R = Me
18b M = Ca, R = C(SiHMe$_2$)$_3$
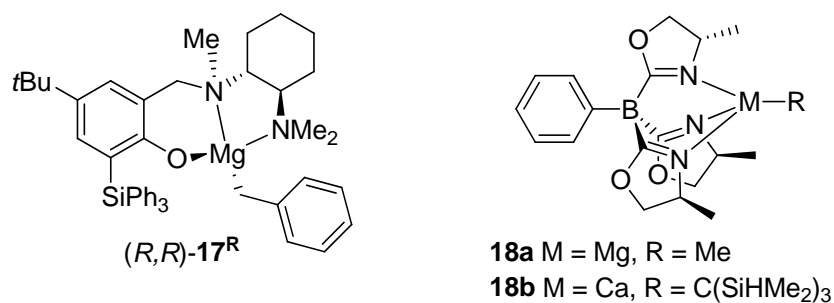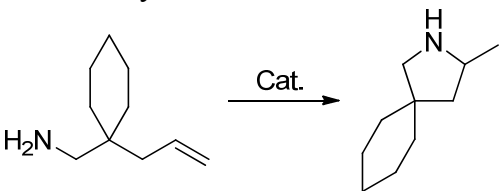
Figure 1-5. Chiral Alkaline earth metal-based catalysts for intramolecular hydroamination/cyclization.

Table 1-1. Catalytic data for the intramolecular hydroamination/cyclization mediated by selected chiral Alkaline earth metal-based catalysts.

Cat. (mol%)	Time, Temp. (°C)	Conv. (%), ee
17^R (5%)	48 hr, -20°C	>95, 90% *ee*
17^R (5%)	2 hr, 22°C	>95, 84% *ee*
18a (10%)	26 hr, 60°C	93, 36% *ee*
18b (10%)	5 min, RT	99, 18% *ee*

Bulky multidentate ligands have demonstrated their capacity to prevent Schlenk equilibria, solubilize metal centers and generate a chiral environment. Early chiral catalysts suffered from low enantioselectivities[48] caused by ligand redistribution. Recently, a phenoxyamine magnesium catalyst (*R,R*)-**17^R** has induced up to 93% enantiomeric excess on the intramolecular hydroamination/cyclization of aminoalkenes.[49] Previously reported multidentate system **18a** achieved a maximum of 36% enantiomeric excess.[50]

Alkaline Earth Metal-Catalyzed Hydroamination – Intermolecular Examples

While some studies suggest that the reactivity of alkaline earth metal-based catalysts increases with increasing metal size,[51] (Mg^{2+}(6), 0.65 Å; Ca^{2+}(6), 0.99 Å; Sr^{2+}(6) 1.13 Å; Ba^{2+}(6) 1.35 Å),[52] While some other experimental and computational studies calculations contradict this observation.[53] The evaluation of this trend is difficult with a single ligand because the metals vary in size and can form unstable complexes or mixtures of aggregates upon metalation.

19 [Ca{N(SiMe$_3$)$_2$}$_2$]$_2$
20 [Sr{N(SiMe$_3$)$_2$}$_2$]$_2$
21 [Sr{CH(SiMe$_3$)$_2$}$_2$(THF)$_2$]

Ar = 2,6-*i*Pr$_2$-C$_6$H$_3$
22 M = Ca; *n* = 1
23 M = Sr; *n* = 2
24 M = Ba; *n* = 3
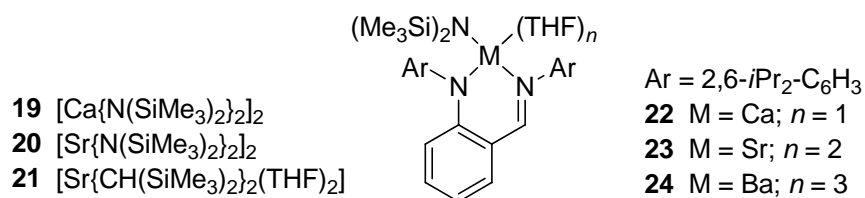
Figure 1-6. Selected alkaline earth metal-based catalysts for the intermolecular hydroamination.[51]

Table 1-2. Selected examples of intermolecular hydroamination mediated by alkaline earth metal catalysts.

R'	R"	Amine:Olefin	Catalyst	Time, T (°C)	Conv(%), N_t	Ref
-(CH$_2$)$_5$-		1:1	**20** (5%)	72 hr, RT	92%, 0.28 h^{-1}	52
-(CH$_2$)$_5$-		1:1	**21** (5%)	10 min, RT	70%, 120.0 h^{-1}	52
-(CH$_2$)$_4$-		1.2:1	(R,R)-**17** (5%)	16 hr, 60°C	87%	50
H	Bn	1:1	**22** (2%)	18.5 hr, 60°C	34%	52
H	Bn	1:1	**23** (2%)	18.5 hr, 60°C	71%	52
H	Bn	1:1	**24** (2%)	18.5 hr, 60°C	86%	52
H	Bn	1:1	**19** (5%)	48 hr, 60°C	92%	52
H	Bn	1:1	**20** (5%)	24 hr, 60°C	78%	52

Excellent activity for the intermolecular hydroamination of styrene derivatives (*anti*-Markovnikov selectivity) and 1,3-dienes has been demonstrated by alkaline earth metal-based complexes **17** and **19 – 24**.[49,51,53] Catalysts containing alkyl leaving groups show higher activity than their amido containing counterparts; however, they are more prone to side reactions including the anionic polymerization of styrene. Activity comparable to, or better than, the most active rare earth metal-based systems for *anti*-Markovnikov hydroamination of styrene has been reported. Their capacity to perform this transformation with both secondary and primary amines in the presence of equimolar amounts of olefin makes their further development a worthy pursuit. The optimization of amine/olefin ratios has not been addressed extensively, and it is plausible that adding excess olefin when polymerization is a side reaction or excess amine when overalkylation of primary amines is problematic will further increase yields of the desired product.

1.3.4 Alkali Metal-Catalyzed Hydroamination

Alkali Metal-Catalyzed Hydroamination: Intermolecular Examples

Interest in the development of alkali metal-based catalysts for hydroamination is driven by their low cost and low toxicity, and is largely hindered by their low solubility in non-coordinating solvents as well as the propensity to undergo rapid ligand redistribution. The base-

catalyzed hydroamination[54] of olefins and 1,3 dienes can be traced back to the 1940's.[55] The following decade a widely reproducible process[56] was applied to various amines and olefins including the addition of ammonia across ethylene with lithium, sodium and their hydrides. High temperatures (200 – 250°C) and pressures (200 – 1000 atm) were needed to achieve conversion which reached a maximum of 42%.

Metal amides were later pre-formed to allow more uniform reaction conditions.[57] Stoichiometric amounts of sodium amide allowed for correlations to be made between amine pK_a and reactivity. More basic amines required lower temperatures to achieve conversion and deviations from this trend were attributed to steric strain. The use of pyridine allowed for catalyst synthesis to occur under less harsh conditions, and demonstrated the potential of Lewis basic amines to affect the aggregation states of alkali metal amides.

The addition of dimethyl- or diethylamine to ethylene was assisted by TMEDA.[58] A five to ten fold drop in pressures and temperatures 50 – 100°C lower than previously required with sodium catalysts were reported. A mechanistic study of this process was later undertaken[59] and amides of cesium and rubidium were found to add ammonia across ethylene. Further investigation of this system was undertaken more recently.[60] The use of toluene as a solvent prevented degradation of TMEDA into *N,N*-dimethylaminoethene which occurs in neat reactions. Catalyst deactivation remained a problem, possibly due to β-hydride elimination from the lithium diethylamide leading to LiH, which was found to be an inactive hydroamination catalyst under the conditions used.[61] Ligand screening revealed TMEDA and PMDTA as most effective under the conditions used with sparteine also showing activity. Yields of 1 – 15% were also obtained in the intermolecular hydroamination of piperidine with 1-hexene and mixtures of regioisomers were obtained with Markovnikov selectivity being favored.
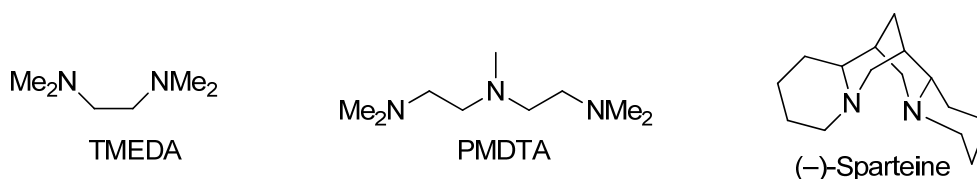
Figure 1-7. Multi-dentate amine ligands commonly used with alkali metals.

TMEDA/LiHMDS was used shortly thereafter[62] in the base catalyzed hydroamination of vinylarenes with *anti*-Markovnikov selectivity.[63] Several examples used (–)-sparteine as a

substitute for TMEDA and stereoinduction, albeit low, was reported.[64] KHMDS/TMEDA demonstrated an increase in activity which was accompanied by a decrease in regioselectivity and hydroamination products. Other accounts of base-catalyzed hydroamination of styrenes,[65] 1,3 dienes,[66] ethylene[67] and aliphatic amines[68] have been reported.

<u>Alkali Metal-Catalyzed Hydroamination: Intramolecular Examples</u>
<u>Achiral Systems</u>

The earliest examples of lithium-mediated intramolecular hydroamination/cyclization utilized *n*-butyllithium in THF (Eq. 1-7). It was noted that catalytic rather than stoichiometric amounts of base mediated this process more efficiently.[69a]

$$X = 0.1; \text{ yield} = 99\%$$
$$X = 1.2; \text{ yield} = 65\%$$
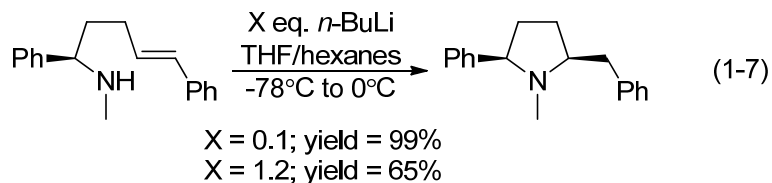
In a later study, *n*-butyllithium cyclized several Thorpe – Ingold activated primary and secondary aminoalkenes (Eq. 1-8), aminopentene (Eq. 1-9), and performed several hydroamination/bicyclizations (Eq. 1-10).[69c] Isomerization was noted as a major competing process in the cyclization of aminopentene with *n*-butyllithium in THF, although use of 1:1 THP:THF as a solvent yielded only hydroamination products (Eq. 1-9). Catalytic and stoichiometric amounts of LDA were reported to mediate the cyclization of aminopentene with similar rates.[70]

$$(1\text{-}10)$$
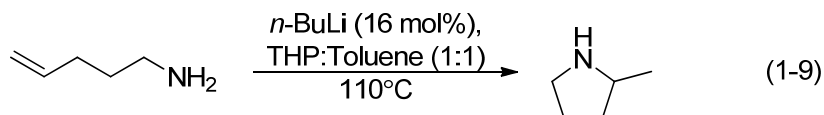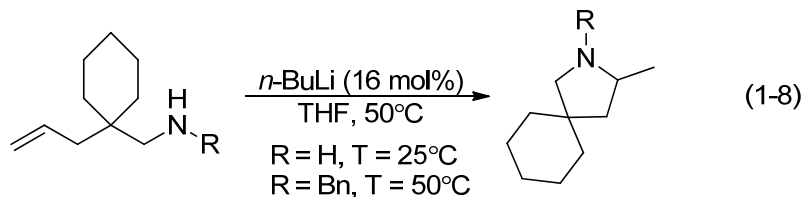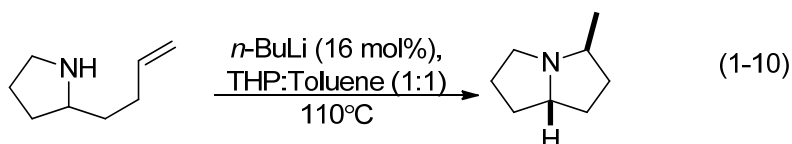
The intramolecular aminolithiation-carbolithiation of styrene derivatives was also investigated (Scheme 1-7).[71] Catalytic amounts of bulky secondary lithium amides allowed hydroamination products to form under ambient conditions. Stoichiometric amounts of base allowed tandem aminolithiation-carbolithiation products to form in high yield and diastereoselectivities.
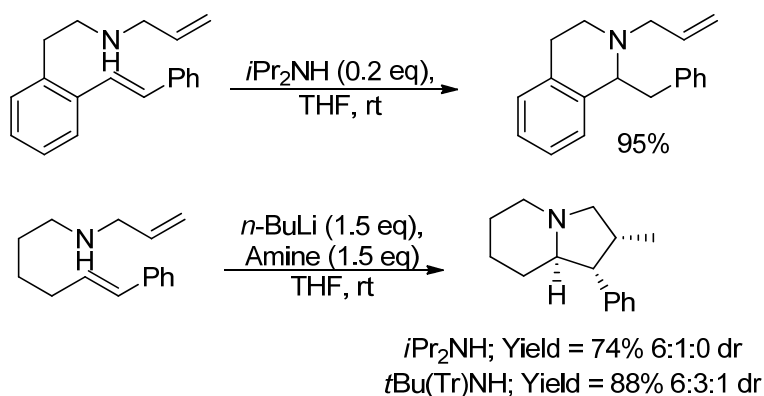
Scheme 1-7. Intramolecular hydroamination and tandem aminolithiation-carbolithiation of styrene derivatives mediated by achiral lithium reagents.[71]

Asymmetric Systems

The first asymmetric intramolecular hydroamination was mediated by a chiral dilithium salt (*S,S,S*)-**25** containing a diaminobinaphthyl (DABN) backbone (Scheme 1-8).[72] Reactions proceeded rapidly at room temperature on a series of *gem*-dialkyl-activated substrates with up to 75% enantiomeric excess at 22°C and 85% at −10°C. The catalyst was soluble in benzene and toluene, and the addition of THF caused a drop in reactivity and enantioselectivity.
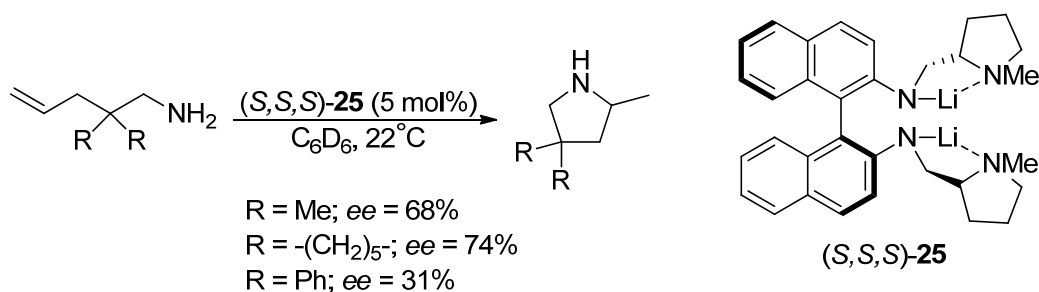
Scheme 1-8. Intramolecular hydroamination cyclization with dilithium salt (*S,S,S*)-**25**.[72]

Related ligands (*R*)-**26a** – **d** were applied similarly in combination with commercial alkyl lithium reagents in the hydroamination/cyclization of aminoalkenes and aminodienes (Scheme 1-9).[73] Enantioselectivities of up to 65% were reported with aminodienes and up to 58% for one aminoalkene substrate. The rate enhancing effect of excess base in these reactions was empirically demonstrated. The ligands, which do not contain L-donor sidearms,[74] formed homogeneous solutions in benzene when $LiCH_2SiMe_3$ was used as a base. A reversal in the trends for stereoinduction induced with (*S,S,S*)-**25** and (*R*)-**26** was observed. The lowest *ee* (31%) reported with (*S,S,S*)-**25** was on the sterically hindered *gem*-diphenyl substituted aminopentene, on which the highest *ee*'s (58%) were reported with (*R*)-**26**. Other enantioselectivities reported on terminal aminopentenes with (*R*)-**26** were below 12%, where (*S,S,S*)-**25** consistently produced higher *ee*'s (64-75%) on the same substrates.
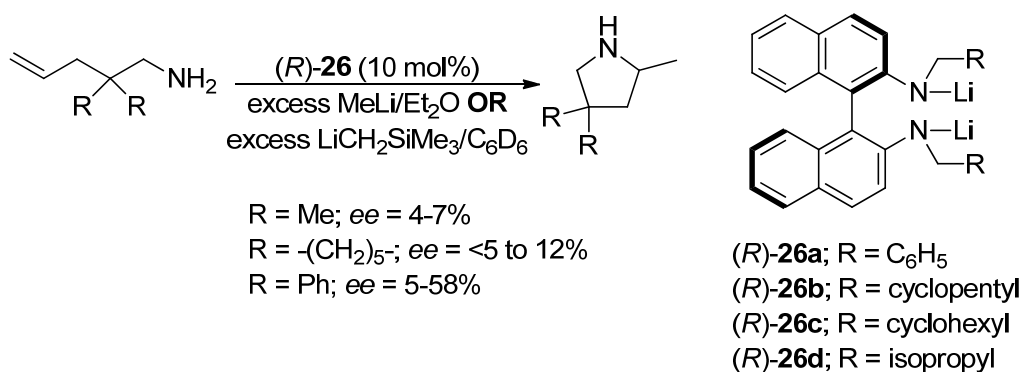
Scheme 1-9. Intramolecular hydroamination cyclization with ligands (*R*)-**26a–d** and excess lithium alkyl.[73]

R = Ph, R' = Me; 95% yield, >95% de
R = 3,5-(MeO)$_2$Ph, R' = Me; 46% yield, >95% de
R = CH$_2$OBn, R' = Me; 82% yield, >95% de
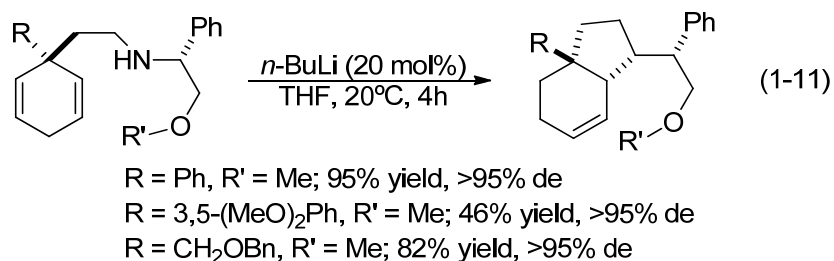
The hydroamination cyclization of a chiral substrate with *n*-butyllithium (Eq. 1-11) was performed and generated a diastereomeric excess of >95% at 20°C.[75] A series of chiral bisoxazoline ligands, including **27**, were used with *n*-butyllithium to perform intramolecular cyclizations of aminostilbenes in up to 91% *ee* at -60°C (Scheme 1-10).[76] Kinetic conditions favored *exo*-cyclization and thermodynamic conditions allowed formation of the *endo*-cyclization product. An excess of bisoxazoline ligand with respect to the lithium base was required to achieve conversion.

Time	*exo*-product	*endo*-product
15 min	94%	5%
5 hr	65%	34%
24 hr	32%	67%
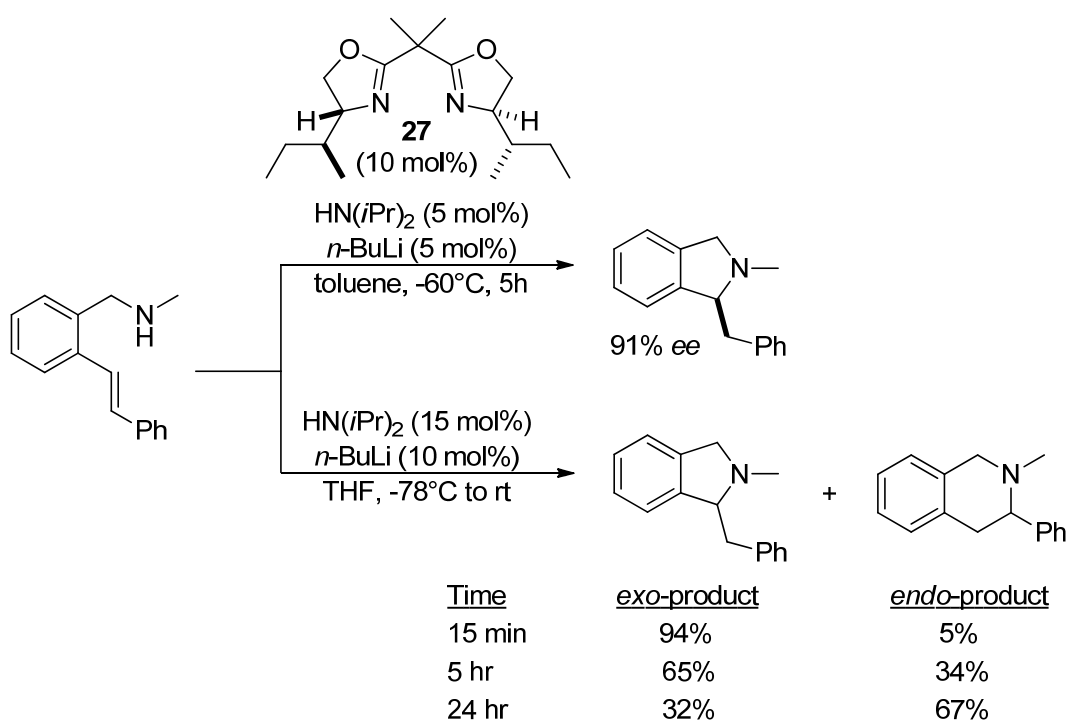
Scheme 1-10. Lithium catalyzed intramolecular hydroamination/cyclization of aminostilbenes favoring *exo*-cyclization under kinetic conditions and *endo*-cyclization under thermodynamic conditions.

1.3.5 Group 4 Metal-Catalyzed Hydroamination

A significant portion of literature on Group 4 metal-based hydroamination catalysts has focused on the addition of amines to allenes and alkynes.[18,19] Olefins are less expensive and easier to synthesize and catalyst development for these substrates is of great interest. The past ten years has seen the development of catalysts for the intramolecular hydroamination of aminoalkenes based on both cationic (for secondary amines) and neutral Group 4 complexes (for primary amines).[77] Activities in all but one system[78] are lower than rare earth metal-based systems, and high catalyst loadings and temperatures are often required for conversion. These complexes are still of interest because they are easier to prepare and catalyst precursors are commercially available.

Reaction conditions for group 4 and 5 metal-mediated hydroamination reactions are often harsh, leading to the formation of hydroaminoalkylation by-products.[79] Concurrent development of catalysts for both transformations has occurred. Hydroaminoalkylation catalysts have generated stereoinduction and mediated intermolecular reactions which favor Markovnikov selectivity.

Cationic Group 4 Metal Complexes

The development of Group 4 metal-based catalysts for intramolecular hydroamination/cyclization of aminoalkenes was inspired by complexes for olefin polymerization.[80] Lanthanocenes and isoelectronic cationic Group 4 metal complexes undergo 1,2-migratiory insertion (Scheme 1-11) allowing high activity for homogeneous Ziegler-Natta and single site polymerizations. Cationic Group 4 complexes are far less efficient for hydroamination than their rare earth metal-based counterparts; however, their activity is noteworthy. The scope of these catalysts is limited to secondary amines because exposure to primary amines leads the formation of inactive neutral metal imido complexes. The solubility of these catalysts is low in benzene and toluene, and reactions are typically performed in bromobenzene without a significant decrease in enantioselectivity.
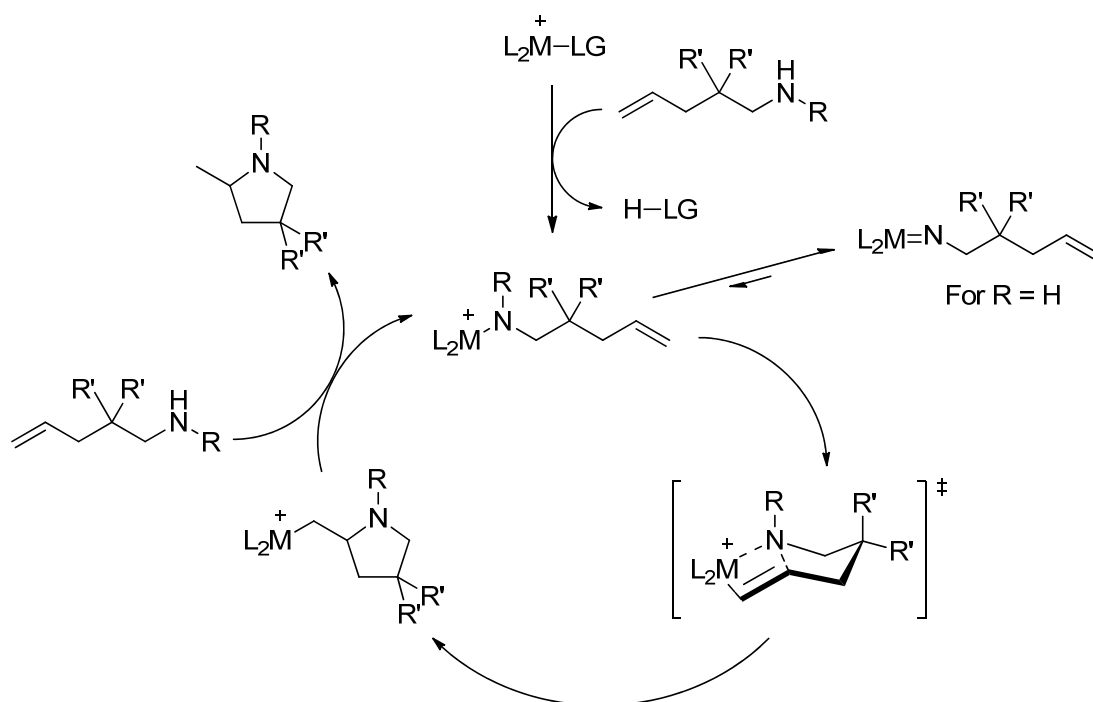
Scheme 1-11. Proposed mechanism for the intramolecular hydroamination/cyclization of aminoalkenes mediated by cationic Group 4 metal complexes.

The mechanism for cationic Group 4 mediated hydroamination is believed to occur in a manner analogous to that proposed for rare earth metals. Amine activation is followed by insertion and subsequent protonolysis. The zirconocene complex **29** is the most active catalyst in this class,[81] and functions efficiently at low catalyst loading even without *gem*-dialkyl activation of the substrate. The chiral zirconium aminophenolate complex **28** generated enantioselectivities of up to 82% for piperidine products and 64% for pyrrolidine products.[82]
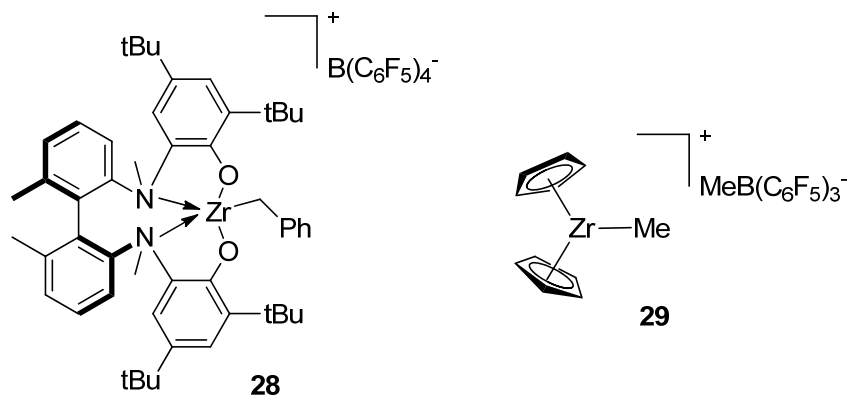
Figure 1-8. Cationic Group 4 catalysts for intramolecular hydroamination/cyclization of aminoalkenes.

Table 1-3. Intramolecular hydroamination/cyclization of aminoalkenes mediated by cationic group 4 based complexes.
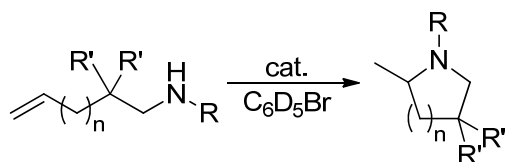
R	R'	n	Catalyst	Time, T (°C)	Conv(%), *ee*(%)
Me	H	1	**29** (2%)	1 hr, 100°C	97, —
Bn	H	1	**29** (2.5%)	6 hr, 100°C	94, —
Me	H	2	**29** (2%)	87 hr, 100°C	>98, —
Me	H	1	**28** (10%)	4 hr, 100°C	100, 64
Me	Me	2	**28** (10%)	3 hr, 100°C	100, 82

Neutral Complexes

Shortly after the disclosure of cationic Group 4 complexes for intramolecular hydroamination of aminoalkenes, it was reported that neutral $Ti(NMe_2)_4$ could mediate the transformation.[83] This system was effective at the cyclization of primary aminoalkenes and not secondary aminoalkenes. Hydroamination mediated by neutral Group 4 complexes are believed to proceed through a metal imido species which is formed by α-deprotonation of the precatalyst (Scheme 1-12). A [2+2]-cycloaddition is followed by protonation to form the product.[84] Sufficient steric bulk must be present in either the ligand or substrate to prevent the formation of inactive dimeric metal imido species. Zirconium catalysts are slightly more reactive than those based on titanium, and *gem*-dialkyl activation is required for all but a few catalytic systems.[78,85]
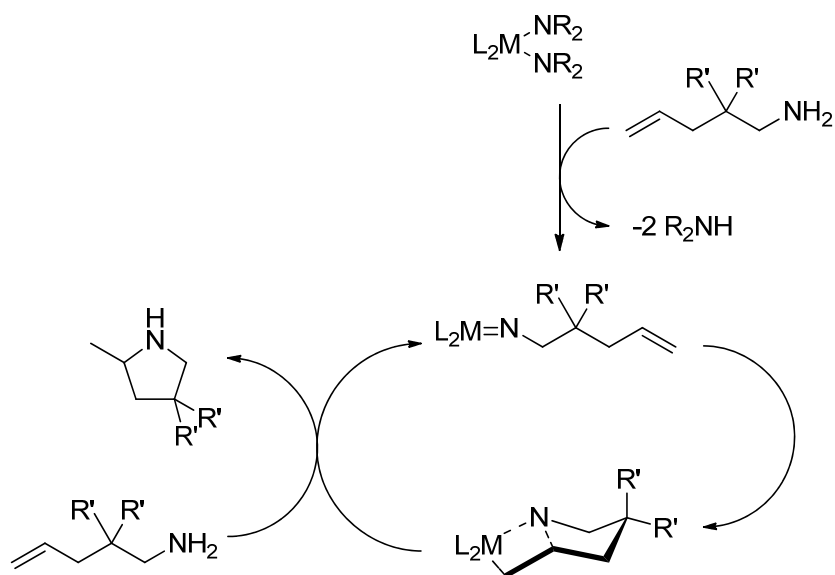
Scheme 1-12. Postulated mechanism for the intramolecular hydroamination/cyclization of aminoalkenes mediated by a neutral group 4 metal based catalyst.

The cyclization of secondary aminoalkenes with neutral Group 4 metal complexes has been reported and it is believed that a σ-insertive mechanism similar to that observed for rare earth metals is operative.[86] Thorpe Ingold activation of substrates is typically required for catalyst activity, although the cyclization of aminopentene has been reported with neutral complexes at high temperatures with low conversions.[87] The intermolecular hydroamination of anilines to norbornene[88] and styrene derivatives[89] has also been reported although the transformation is not regioselective and may be acid catalyzed.[90]

The highest levels of stereoinduction in this class of compounds were observed with a zirconium amidate **30**[91] and a borate zirconium complex **31**[78a] inducing enantioselectivities up to 93% and 98% respectively. The zwitterionic complex **31** demonstrates activity unrivaled by other compounds in this class. Activity was documented at temperatures as low as -30°C and catalyst loadings as low as 2%. Isotopic perturbation of enantioselectivity was reported to result in 2 − 7% higher enantiomeric excess for N-deutero substrates compared with their proteo counterparts. This, combined with a high primary KIE raises speculation about a concerted proteo mechanistic pathway for this system.
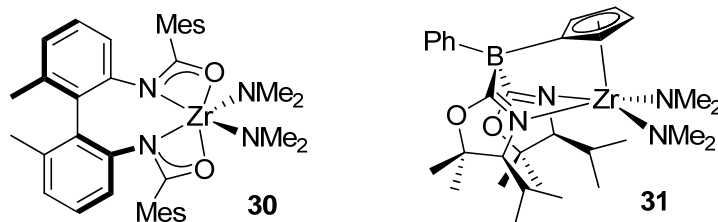
Figure 1-9. Neutral Group 4 metal-based catalysts for the intramolecular hydroamination/cyclization of aminoalkenes.

Table 1-4. Cyclization of primary aminoalkenes catalyzed by neutral Group 4 based catalysts.

R	Catalyst	Time, T (°C)	Conv(%), *ee*(%)
H	**31**	5 hr, 110°C	24, —
Me	**31**	7 hr, RT	89, 89
Me	**30**	3 hr, 110°C	>98, 93
-(CH$_2$)$_5$-	**31**	1.25 hr, RT	>95, 90
-(CH$_2$)$_5$-	**30**	3 hr, 110°C	96, 82
Ph	**31**	1.25, RT	>95, 93
Ph	**30**	1.25 hr, 110°C	>98, 74

1.3.6 Group 5 Metal-Catalyzed Hydroamination

Group 5 metal mediated intramolecular hydroamination has been reported, and catalysts show similar activity to their neighbors in Group 4 with primary aminoalkenes.[92] These complexes can form metallaziridines[79a] when exposed to certain secondary amines and subsequently undergo olefin insertion to form hydroaminoalkylation[79b] products. Research on Group 5 catalysts has focused on hydroaminoalkylation[93] instead of hydroamination.

1.3.7 Late Transition Metal-Catalyzed Hydroamination

A number of late transition metal-based catalysts[94] for hydroamination have been developed, however this field has largely focused on the hydroamination of activated substrates including alkynes, allenes and dienes. The past fifteen years have seen a number of reports on the

intermolecular hydroamination of styrene derivatives along with the hydroamination/cyclization of aminoalkenes demonstrating the potential of complexes within this class.

Late transition metal catalysts frequently operate by alkene activation instead of amine activation which distinguishes them from the more polar reagents typically employed in this transformation. The presence of multiple stable oxidations states and sensitivity to the steric bulk on substrates allows catalysts to operate under a broader range of mechanisms than observed with complexes from Groups 1–3. The three common scenarios include coordination of an alkene, alkyne or allylic complex to a catalyst which allows nucleophilic attack from an amine. Alkene insertion into late transition metal hydride complexes have been documented although it is uncommon.[95] Redox couples are known to undergo oxidative addition with amines, and the catalytic cycle for the iridium catalyzed intermolecular hydroamination of norbornene begins by amine activation.[96] For intermolecular transformations which proceed by alkene activation, Markovnikov regioselectivity typically ensues. Nucleophilic attack occurs at the most electrophilic carbon adjacent to the aromatic ring, which makes design of catalysts for *anti*-Markovnikov transformations challenging. This mechanism also contains a β-amino alkyl metal intermediate which is susceptible to β-hydride elimination leading to oxidative amination by-products (Scheme 1-14).

The propensity of late transition metal catalysts to operate by alkene activation accounts for the choice of substrates in many studies. Alkenes are more desirable starting materials for hydroamination because they are less expensive, more stable and more easily synthesized than alkynes and allenes. However, they contain less electron density which makes binding to a metal center more difficult. In spite of this obstacle, the inter- and intramolecular hydroamination of alkenes has been documented.

Late transition metal-based complexes have good functional group tolerance and low sensitivity to oxygen and moisture compared with other classes of catalysts. Acid co-catalysts are known to increase reaction rates and yields by accelerating turnover limiting protonolysis of the M-C bond. They may also suppress competitive amine binding to the metal center. Bulky, weakly coordinating counterions, frequently triflate (TfO- = F_3CSO_3-) are commonly used, and many of these reactions may be acid catalyzed.[90]

Intramolecular Hydroamination/Cyclization

The hydrate $FeCl_3 \cdot 6H_2O$ demonstrated activity at 80°C in the intramolecular hydroamination/cyclization of toluenesulfonyl protected aminopentenes containing both internal and terminal olefins (Eq. 1-12).[97]

$$(1\text{-}12)$$
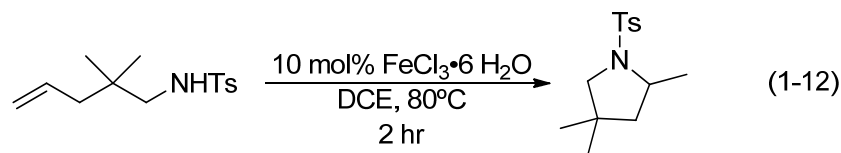
Group 9: Rh(I) and Ir(I)

Enantioselectivities up to 91% (Table 1-5) were reported for the cyclization of secondary aminoalkenes mediated by $[Rh(COD)_2]BF_4$ and several MOP derived ligands (**32**).[98] Aminopentene protected by various benzyl derivatives was cyclized at 70°C in 83 – 90% *ee*.

Table 1-5. Enantioselective rhodium catalyzed intramolecular hydroamination/cyclization.

R^1	R^2	Time	T (°C)	Conv(%)	*ee*(%)
Ph	C_6H_5	24 hr	50°C	90	83
Ph	$2\text{-}CH_3C_6H_4$	24 hr	50°C	91	88
Me	$2\text{-}CH_3C_6H_4$	20 hr	70°C	75	62
$-(CH_2)_5-$	$2\text{-}CH_3C_6H_4$	20 hr	70°C	80	63
H	C_6H_5	20 hr	70°C	48	90
H	$2\text{-}CH_3C_6H_4$	20 hr	70°C	50	86

$[Rh(COD)_2]BF_4$ in the presence of biarylphosphines (**33**)[99] and POP-pincer ligands (**34**)[100] have cyclized a variety of primary and secondary aminoalkene substrates, including N-benzyl aminopentene (Table 1-6). An unexpected $\eta^6\text{-}\kappa^1$ binding of rhodium to a biarylphosphine

ligand[99] was also disclosed (Figure 1-10). The intramolecular *endo*-cyclization of aminoalkenes to form 3-arylpiperidines was also mediated by [Rh(COD)$_2$]BF$_4$ in the presence of DPPB (**35**).[101]
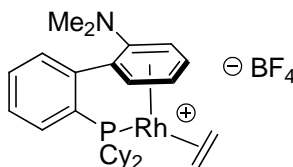
Figure 1-10. Unique crystallographically characterized η^6-κ^1 binding of rhodium to a biarylphosphine ligand.

Table 1-6. Intramolecular hydroamination/cyclization mediated by a unique rhodium complex bound η^6-κ^1 to a biarylphosphine ligand.
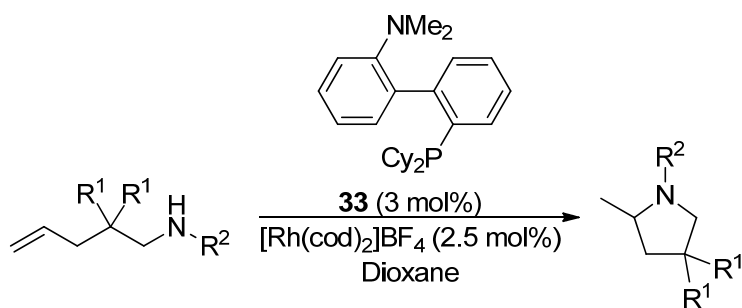
R^1	R^2	Time	T (°C)	Conv(%)
Ph	Bn	7 hr	70°C	91
Ph	H	10 hr	100°C	83^a
Me	Bn	7 hr	70°C	83
-(CH$_2$)$_5$-	Bn	7 hr	70°C	92
-(CH$_2$)$_5$-	H	10 hr	100°C	74^a

a = **33** (6 mol%), [Rh(cod)$_2$]BF$_4$ (5 mol%)

Rhodium and iridium complexes of CCC-NHC pincer ligands (**36**) were also reported to cyclize a variety of benzyl protected Thorpe-Ingold-activated aminoalkenes.[102] In another study, secondary aminoalkenes were cyclized at 110°C with [Ir(COD)Cl]$_2$ as a precatalyst and addition of HNEt$_3$Cl (2 equiv. relative to [Ir(COD)Cl]$_2$) allowed cyclization of primary aminoalkenes.[103]
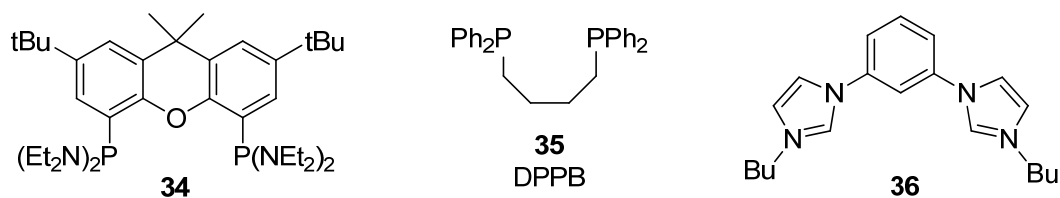
Figure 1-11. Pincer and phosphine ligands applied to hydroamination/cyclization reactions with rhodium and iridium.

A bifunctional Cp* iridium pyrazolato complex (**37**)[104] cyclized benzyl aminopentene along with other primary and secondary aminoalkenes between 50–110°C (Table 1-7). Group 9 based complexes for intramolecular hydroamination/cyclization are known to enter their catalytic cycles by olefin activation, and DFT studies support a similar mode of activation for this system. Stabilization derived from unique hydrogen bonding interactions between this catalyst and substrates likely enhance its activity.

Table 1-7. Intramolecular hydroamination/cyclization mediated by a bifunctional Cp* iridium pyrazolato complex.

R^1	R^2	**37** (mol %)	T (°C)	Conv(%)
Ph	H	2.5	50°C	89
Me	Bn	0.5	50°C	66
Ph	Bn	0.5	50°C	99
H	Bn	2.5	80°C	98
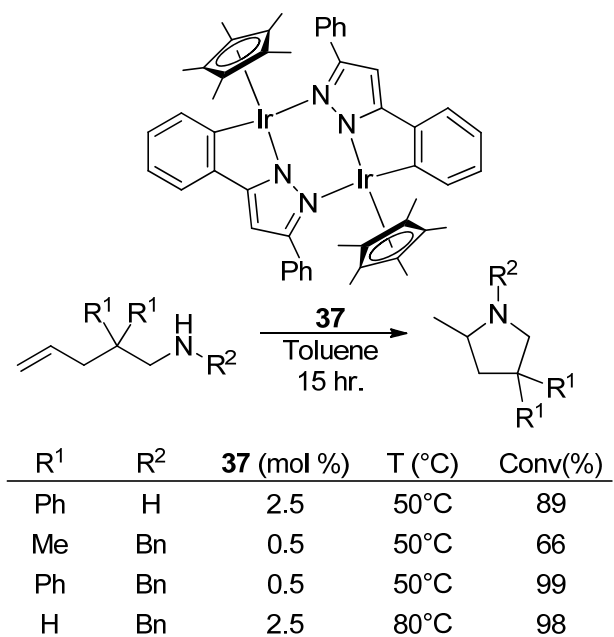
Group 10: Pd(II) and Pt(II)

The cyclization of secondary aminoalkenes mediated by Zeise's dimer, $[PtCl_2(H_2C=CH_2)]_2$ and triphenylphosphine[105] or $PtCl_2$ and biarylphosphines (**38a-c**)[106] at

elevated temperatures (60–120°C) was documented (Table 1-8). Excellent functional group compatibility was reported with ethers, esters, halogen, cyano, thienyl and nitro groups. The phosphine free catalyst, (COD)PtCl$_2$ was also found to cyclize secondary and primary aminoalkenes at 110°C (Table 1-8).[106b]

Palladium pincer complexes (**39**)PdCl$_2$/AgBF$_4$ cyclized carbamate protected aminoalkenes and piperazines at ambient temperatures.[107] Steric hindrance of the metal center by the tridentate ligand prevented β-hydride elimination. An uncommon inverse dependence on substrate concentration was observed because the Brønsted basic carbamate protecting group hindered the rate limiting protonolysis step.[108]

38a R^1 = R^2 = R^3 = *i*-Pr
38b R^1 = R^2 = R^3 = H
38c R^1 = NMe$_2$, R^2 = R^3 = H
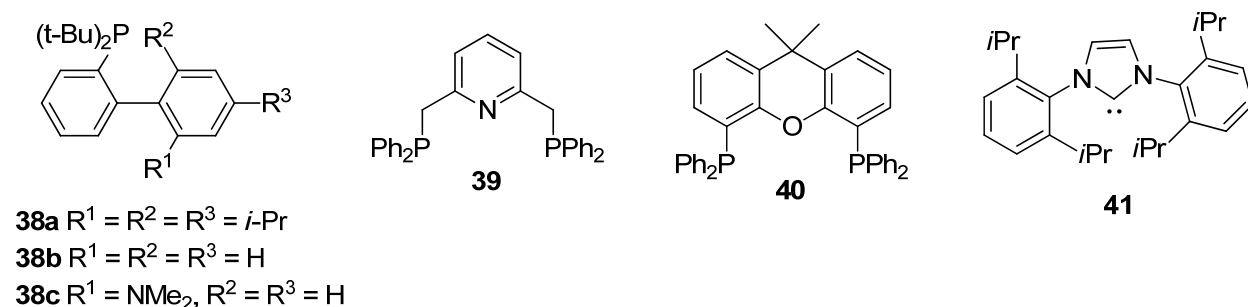
Figure 1-12. Ligands used for intramolecular hydroamination/cyclization reactions with metals from groups 10 and 11.

Table 1-8. Intramolecular hydroamination/cyclization mediated by Platinum.

R^1	R^2	Cat. (mol %)	Ligand (mol %)	T (°C)	Time (hr)	Conv(%)	Ref.
Cy	Bn	[PtCl$_2$(H$_2$C=CH$_2$)]$_2$ (2.5)	PPh$_3$ (5)	120°C	6	57^a	105
Cy	Bn	(COD)PtCl$_2$ (5)	none	110°C	5	82	106b
Cy	Bn	PtCl$_2$ (5)	none	110°C	5	79	106b
Cy	Bn	PtCl$_2$ (5)	**38a** (5)	80°C^b	6	100	106a
Cy	Bn	PtCl$_2$ (5)	**38b** (5)	80°C^b	6	98	106a
Cy	Bn	PtCl$_2$ (5)	**38c** (5)	80°C^b	6	100	106a
Me	Bn	[PtCl$_2$(H$_2$C=CH$_2$)]$_2$ (2.5)	PPh$_3$ (5)	120°C	9	65	105
Ph	Bn	[PtCl$_2$(H$_2$C=CH$_2$)]$_2$ (2.5)	PPh$_3$ (5)	120°C	16	75	105
Ph	H	(COD)PtCl$_2$ (5)	none	110°C	5	61	106b

a = Substrate slowly added to mixture; b = digylme used instead of dioxane

Group 11: Gold(I) and Copper(I)

The intramolecular hydroamination/cyclization of primary and secondary amines was catalyzed at elevated temperatures (60–140°C) by Cu(OtBu)(**40**).[109] The system demonstrated compatibility with multiple functional groups including halogens, alcohols, ethers, esters, and cyano groups.

The intramolecular cyclization of carbamates[110] and carboxamides[111] initiated by Au[P(tBu)$_2$(o-biphenyl)]OTf was reported at 60–100°C. Aminopentene protected by benzyloxycarbonyl (Cbz) was cyclized at 100°C. The use of an N-heterocyclic carbene ligand allowed Au(**41**)OTf to cyclize N-alkenyl ureas at room temperature and carboxamides at 45°C.[112] Aminopentene protected by N-alkenyl urea was cyclized at 45°C. The tetrafluoroborate salts of several intramolecular hydroamination substrates were cyclized at 80°C using AuOTf as a catalyst.[113] Tosylated amino olefins were also cyclized with Ph$_3$PAuCl/AgOTf at 85°C.[114]

Intermolecular Hydroamination

Group 8: Ru(II)

Ru(COD)(2-Me-allyl)$_2$ (**42**), DPPPent (**43**) and triflic acid is one of the most selective catalytic systems for the intermolecular *anti*-Markovnikov hydroamination of styrene derivatives.[115] Its d^6 configuration allows unique binding to the arene system of the substrate (**44**, Eq. 1-13), favoring nucleophilic attack at the terminal carbon (Scheme 1-13). Moderate to high yields were reported for the addition of morpholine and piperidines to styrene at 100°C.

Scheme 1-13. Mechanism for the Ruthenium-catalyzed *anti*-Markovnikov hydroamination of styrene.

Group 9: Rh(I) and Ir(I)

Intermolecular hydroamination mediated by Rh(I)- and Ir(I)- based systems have been known since 1971,[116] although their applications are limited. Rhodium-based systems form *anti*-Markovnikov hydroamination products upon addition to styrene; however, oxidative amination is a major side-product.[117] The metal alkyl intermediate generated tends to undergo β-hydride elimination, behaving similarly to palladium complexes (Scheme 1-14). High selectivity for the hydroamination product has been demonstrated when DPEphos (**45**) is used as a ligand,[118] although enamines are observed as a side-product.
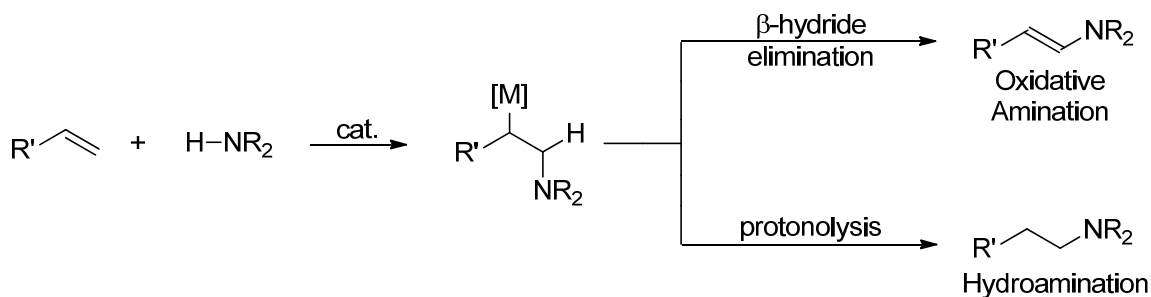
Scheme 1-14. The *anti*-Markovnikov addition of an amine to styrene forms a metal alkyl intermediate which can undergo β-hydride elimination or protonolysis leading to oxidative amination or hydroamination products.[94c]
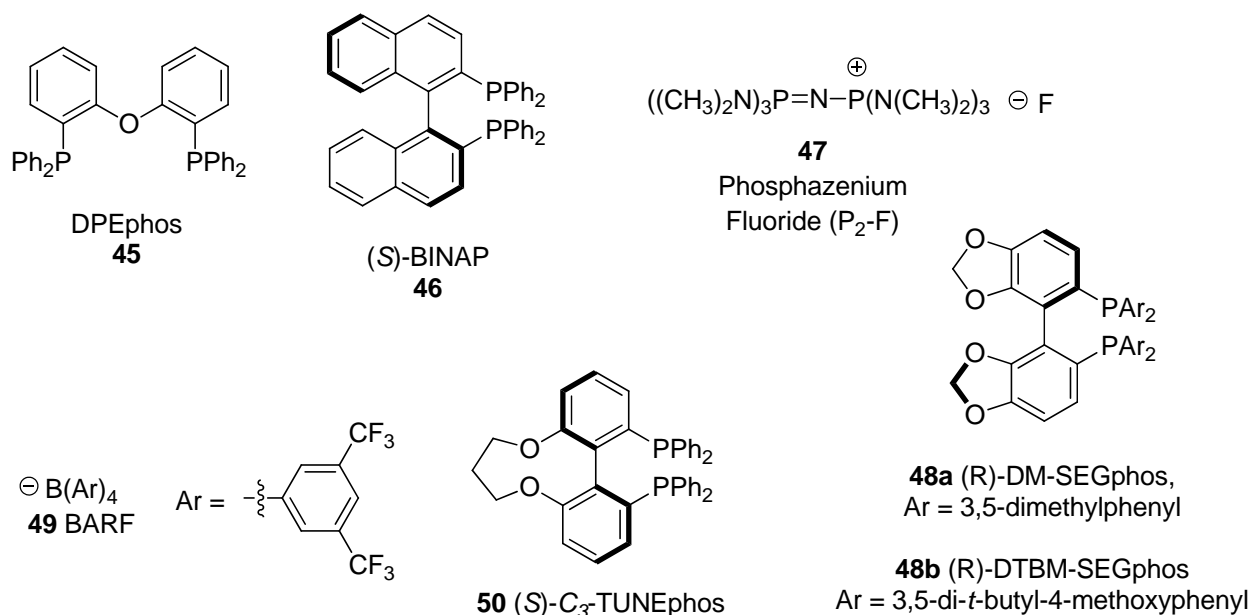
Figure 1-13. Phosphine ligands and other additives used to form Iridium catalysts for intermolecular hydroamination reactions.

The majority of intermolecular Ir(I)- mediated hydroaminations have been documented on norbornene and its derivatives. Enantioselectivities of up to 95%[96b] were reported with [IrCl((S)-**46**)]$_2$ and phosphazenium fluoride (**47**) although low TON's in addition to low substrate scope limit the utility of this catalyst (Eq. 1-14). A catalytic mixture of (R)-**48a**, [Ir(COE)$_2$Cl]$_2$ and KHMDS in yielded *ee*'s up to 99% and yields up to 94% on the intermolecular addition of aniline derivatives to norbornene (Eq. 1-15).[96d] The combination of high yield and enantioselectivity distinguish this system from others. The intermolecular addition of amides and sulfonamides to norbornene (in up to 93% *ee*) and aliphatic olefins was catalyzed by **48b** and [Ir(COE)$_2$Cl]$_2$.[119] Up to 83% *ee* was induced with [Ir(COD)$_2$]/**49** and (S)-C$_3$-TUNEPHOS (**50**) for the intermolecular Markovnikov addition of heteroaromatic amines to styrene and styrene derivatives.[120]

$$[Ir(COE)_2Cl]_2 \ (0.5 \ mol\%)$$
$$(R)\text{-}\mathbf{48b} \ (2 \ mol\%)$$
$$KHMDS \ (2 \ mol\%)$$
$$70°C, 12 \ hr.$$

2 equiv.

94% yield, 95% ee

(1-15)
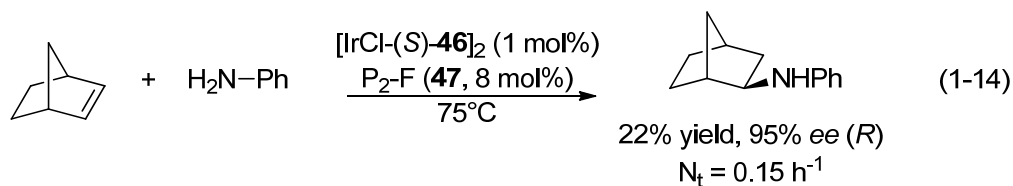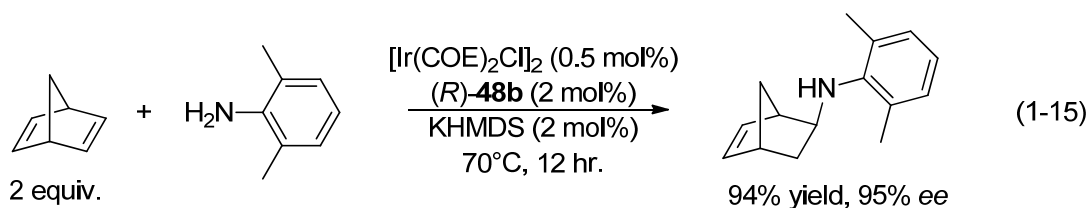
The propensity of Ir(I) catalysts to undergo oxidative addition with amine N-H bonds,[96c] distinguishes them from other systems, although this mechanism appears specific to the intermolecular addition to norbornene.[96a] In contrast, kinetic and DFT studies favor olefin activation[103b;104a,b] for the intramolecular cyclization of aminoalkenes.

Group 10: Pd(II)

The Markovnikov addition of anilines to styrenes was mediated by $Pd(PPh_3)_2(OTf)_2$ and $(\mathbf{51})Pd(TFA)_2$ in the presence of excess triflic acid.[95a] $(\mathbf{51})Pd(O_2CCF_3)_2$ and triflic acid were also effective for this transformation.[121] $[(R)\text{-}\mathbf{46}]Pd(OTf)_2$ induced *ee*'s of 81% at 25°C (Eq. 1-16) and 64% at 45°C for the addition of aniline to *p*-trifluoromethyl styrene and 2-vinyl naphthalene.[95a]

$$[(R)\text{-}\mathbf{46}]Pd(OTf)_2$$
$$(10 \ mol\%)$$
$$25°C, 72 \ hr.$$

80% yield, 81% ee (S)

(1-16)
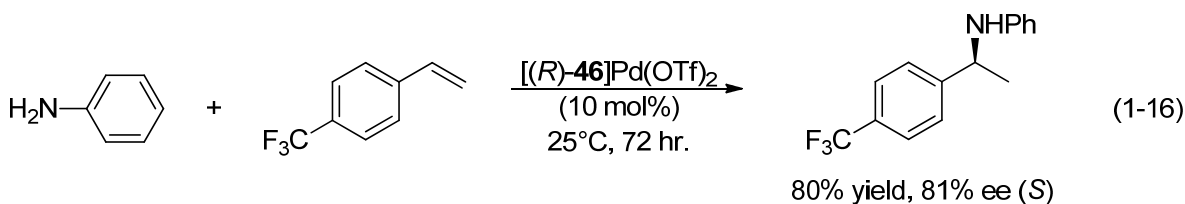
A unique crystallographically characterized η^3–benzyl intermediate[95b] allows mechanistic insight into this process and rationalization for the Markovnikov selectivity (Scheme 1-14). The benzyl group binds in an η^3-fashion to the metal center, which activates the benzylic carbon for nucleophilic attack. Inversion of configuration at this carbon upon nucleophilic attack serves as proof of concept. In depth analysis on these systems revealed higher rates of nucleophilic attack on $[Pd(\eta^3\text{-allyl})Cl]_2$ complexes relative to those containing triflate and tetrafluoroborate counterions. The η^3-benzyl derivative of this complex, $[Pd(\eta^3\text{-benzyl})OTf]_2$ also demonstrated counterion effects, with tetrafluoroborate showing higher activity than triflate. Larger P-Pd-P bite angles increased their activity with Xantphos (**40**) being the most effective ligand.[95c] Additional crystallographic and catalytic data were reported for other Pd(II) complexes chelated

by bidentate phosphine ligands. The intermolecular Markovnikov hydroamination of aniline to styrene or *p*-fluoro styrene was reported in up to 70% *ee* with [Pd((*R*)-**46**)(NCMe)(H$_2$O)](OTf)$_2$[122] and 84% *ee* with [Pd(**52**)(NCMe$_2$)$_2$](OTf)$_2$.[123]
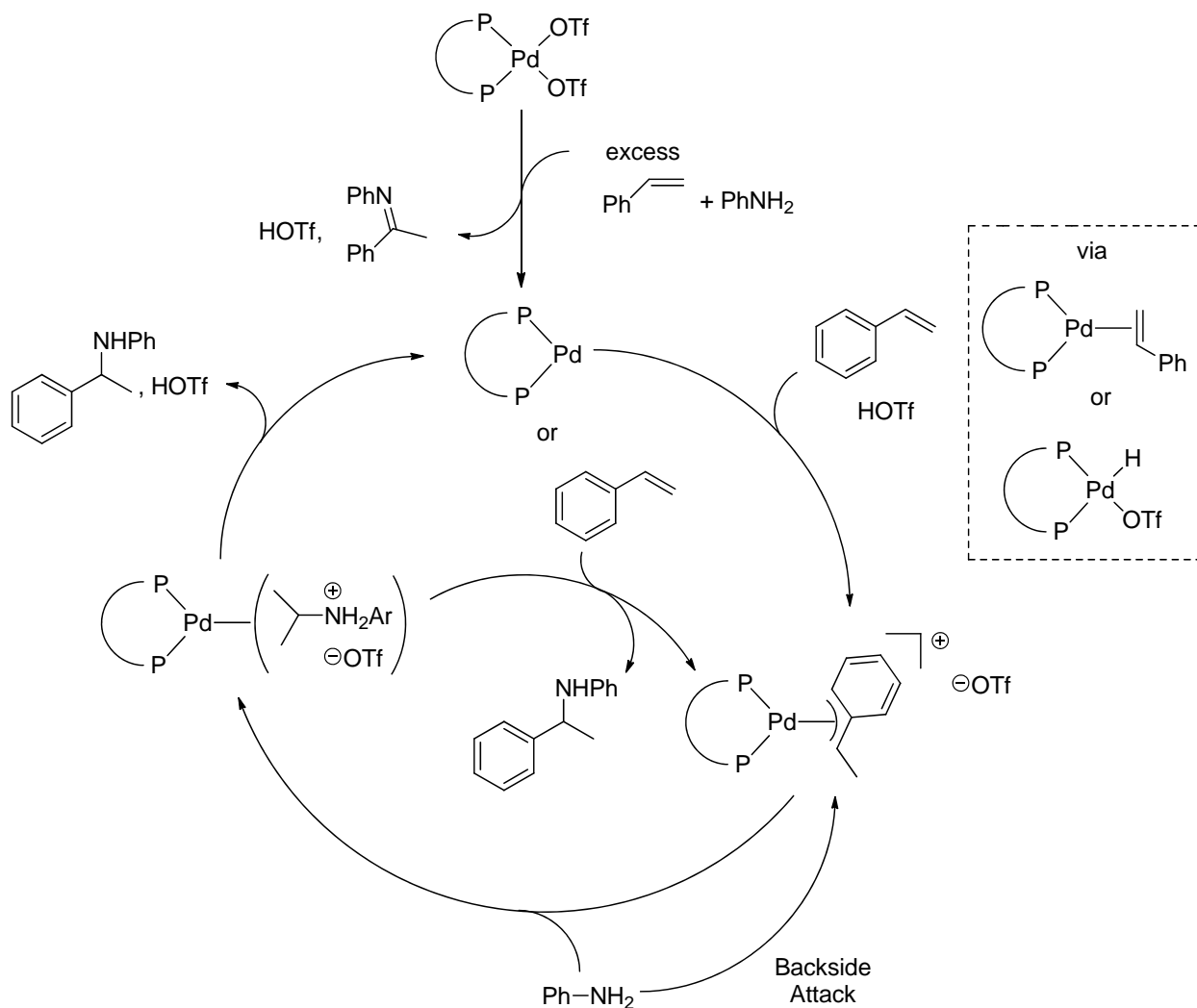
Scheme 1-15. Mechanism for the Palladium catalyzed Markovnikov hydroamination of styrene through a unique η^3-benzyl intermediate.
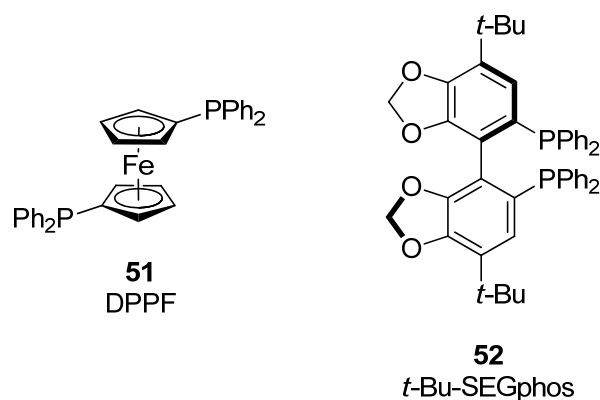
Figure 1-14. Phosphine ligands used to form Palladium catalysts for intermolecular hydroamination reactions.

Group 11: Gold(I)

Although multiple accounts of late transition metal-based hydroamination of dienes[124] and ethylene have been documented, this transformation is much more difficult with unactivated aliphatic amines. These transformations are seemingly more difficult with free amines and many systems were reported only with protected amines including sulfonamides.[125]

The Markovnikov addition of urea to unactivated alkenes and ethylene has been reported in up to 78% *ee* catalyzed by a mixture of [(*S*)-**53**](AuCl)$_2$ and AgOTf (Table 1-9).[126] Much like the rare earth metal-mediated intermolecular hydroamination of unactivated olefins, a large excess of olefin (10–60 equivalents) was used in this study.

Table 1-9. Gold catalyzed enantioselective intermolecular Markovnikov hydroamination of unactivated alkenes with Imidazolidin-2-ones.
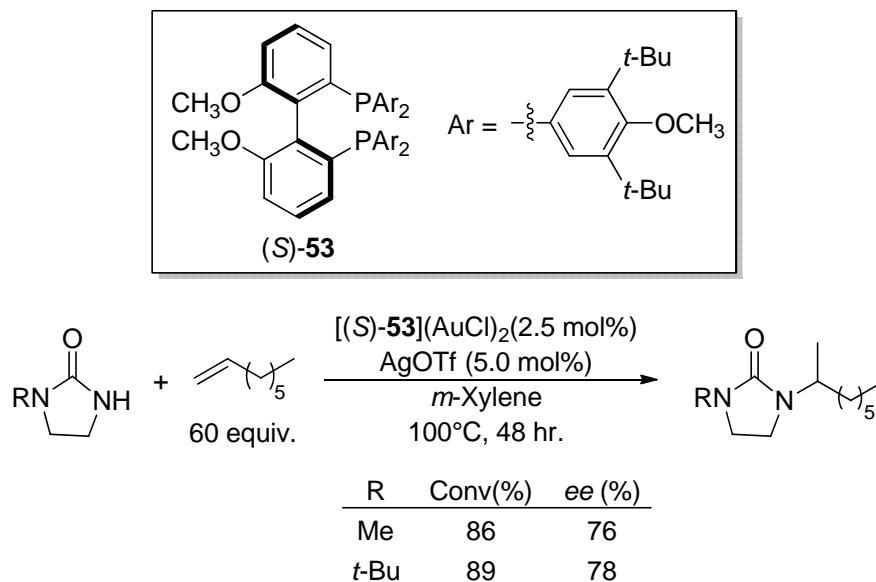
1.3.8 Objectives of this work

The hydroamination reaction has made significant progress in the last 25 years, largely due to advances in rare earth metal-based catalyst systems. The rising costs of these metals could hinder their future development, and their efficiency as intermolecular catalysts is limited A large excess of olefin is required for activity because rate limiting olefin insertion is hindered by competitive binding from substrate and product amines. Group 4 and 5 metal-based systems are limited because high temperatures are required to achieve conversion, and intermolecular reactions often occur in competition with hydroaminoalkylation.

The full potential of alkali, alkaline-earth and transition metal-based systems has not been realized, and advances in this field will likely be derived from these portions of the periodic chart. The *anti*-Markovnikov hydroamination of styrene derivatives has been efficiently mediated by these systems, and warrants further investigation. The proper characterization of precatalysts along with information from kinetic studies will allow the behavior of these complexes to be understood on a fundamental level. If structure activity relationships can be derived, it will allow rational design of future generation catalysts and they will surpass the activity and selectivity of their predecessors.

The high enantioselectivities induced with (*S,S,S*)-**25** demonstrate the potential of chiral alkali metal-based salts for intramolecular hydroamination/cyclization. Broadening the substrate scope of this system along with increasing its activity and selectivity are objectives for this project. Understanding and gaining control of the precatalyst and rate limiting transition state(s) in the catalytic cycle are long term goals of this project. Based on the limited information regarding (*S,S,S*)-**25**, modification of its structure may allow a deeper understanding of this system. Removal of internal chirality from the catalyst sidearms will allow their impact on catalyst structure, activity and selectivity to be studied. Characterization of the modified precatalysts, particularly in solution will allow their aggregation behavior to be understood and kinetic studies will show the behavior of these complexes during reactions. A more complete understanding of this system will allow the design of new catalysts.

The intermolecular *anti*-Markovnikov hydroamination of styrene derivatives has been mediated by LiHMDS and TMEDA at 120°C. Low levels of stereoinduction were observed when sparteine was used as a ligand. The reactivity of alkali metal mediated hydroamination of styrene derivatives under milder conditions will also be studied with the goal of improving enantioselectivity.

1.4 References

(1)   (a) Wu, G.; Huang, M. *Chem. Rev.* **2006**, *106*, 2596. (b) Dugger, R. W.; Ragan, J. A.; Ripin, D. H. B. *Org. Process Res. Dev.* **2005**, *9*, 253. (c) Hoppe, D.; Hense, T. *Angew. Chem., Int. Ed. Engl.* **1997**, *36*, 2282.

(2)   Reviews: (a) Reich, H. J. *Chem. Rev.* **2013**, DOI: 10.1021/cr400187u. (b) Reich, H. J. *J. Org. Chem.* **2012**, *77*, 5471. (c) Collum, D. B.; McNeil, A.J.; Ramirez, A. *Angew. Chem., Int. Ed.* **2007**, *46*, 3002. (d) von Ragué Schleyer, P. *Lithium Chemistry*; Wiley Interscience: New York, NY, **1995**. (e) Seebach, D. *Angew. Chem. Int. Ed. Engl.* **1988**, *27*, 1624.

(3)   (a) Wardell, J. L. *Comprehensive Organometallic Chemistry I*; Wilkinson, G., Ed.; Pergamon Press: Oxford, **1982**; Vol. 1. (b) Beswick, M. A.; Wright, D. S. *Comprehensive Organometallic Chemistry II*; Abel, E. W., Stone, F. G. A., Wilkinson, G., Eds.; Elsvier: Oxford, **1995**; Vol. 1.

(4)   (a) Hope, H. *Prog. Inorg. Chem.*; Wiley: New York, NY, 1994; Vol. 41, p 1. (b) Ruhlandt-Senge, K.; Henderson, K. W.; Andrews, P. C. *Comprehensive Organometallic Chemistry III*; Elsevier: **2007**; Vol. 1.

(5)   (a) Collum, D. B.; Kahne, D.; Gut, S. A.; DePue, R. T.; Mohamadi, F.; Wanat, R. A.; Clardy, J.; Van Duyne, G. *J. Am. Chem. Soc.* **1984**, *106*, 4865. (b) Xu, F.; Reamer, R. A.;

Tillyer, R.; Cummins, J. M.; Grabowski, E. J. J.; Reider, P. J.; Collum, D. B.; Huffman, J. C. *J. Am. Chem. Soc.* **2000**, *122*, 11212.

(6) Reviews: See also reference 2. (a) Lucht, B. L.; Collum, D. B. *Acc. Chem. Res.* **1999**, *32*, 1035. (b) Günther, H. *J. Braz. Chem. Soc.* **1999**, *10*, 241. (c) Collum, D. B. *Acc. Chem. Res.* **1993**, *26*, 227. (d) Collum, D. B. *Acc. Chem. Res.* **1992**, *25*, 448.

(7) Selected studies identifying transition states: (a) Riggs, J. C.; Singh, K. J.; Yun, M.; Collum, D. B. *J. Am. Chem. Soc.* **2008**, *130*, 13709. (b) Remenar, J. F.; Lucht, B. L.; Collum, D. B. *J. Am. Chem. Soc.* **1997**, *119*, 5567. (c) Lucht, B. L.; Bernstein, M. P.; Remenar, J. F.; Collum, D. B. *J. Am. Chem. Soc.* **1996**, *118*, 10707.

(8) Reviews − DOSY study of reactive intermediates: (a) Li, D.; Keresztes, I.; Hopson, R.; Williard, P. G. *Acc. Chem. Res.* **2008**, *42*, 270. DOSY for determining aggregation states: (b) Macchioni, A.; Ciancaleoni, G.; Zuccaccia, C.; Zuccaccia, D. *Chem. Soc. Rev.* **2008**, *37*, 479. DOSY Theory and applications: (c) Brand, T.; Cabrita, E. J.; Berger, S. In *Modern Magnetic Resonance*; Webb, G. A., Ed.; Springer: **2006**; Vol. 1, p 135. (d) Cohen, Y.; Avram, L.; Frish, L. *Angew. Chem. Int. Ed.* **2005**, *44*, 520.

(9) (a) Kagan, G.; Li, W.; Li, D.; Hopson, R.; Williard, P. G. *J. Am. Chem. Soc.* **2011**, *133*, 6596. (b) Armstrong, D. R.; García-Álvarez, P.; Kennedy, A. R.; Mulvey, R. E.; Robertson, S. D. *Chem. Eur. J.* **2011**, *17*, 6725. (c) Kagan, G.; Li, W.; Sun, C.; Hopson, R.; Williard, P. G. *J. Org. Chem.* **2010**, *76*, 65. (d) Lecachey, B.; Oulyadi, H.; Lameiras, P.; Harrison-Marchand, A.; Gérard, H.; Maddaluno, J. *J. Org. Chem.* **2010**, *75*, 5976. (e) Li, D.; Kagan, G.; Hopson, R.; Williard, P. G. *J. Am. Chem. Soc.* **2009**, *131*, 5627. (f) Kagan, G.; Li, W.; Hopson, R.; Williard, P. G. *Org. Lett.* **2009**, *12*, 520. (g) Lecachey, B.; Duguet, N.; Oulyadi, H.; Fressigné, C.; Harrison-Marchand, A.; Yamamoto, Y.; Tomioka, K.; Maddaluno, J. *Org. Lett.* **2009**, *11*, 1907. (h) Liu, J.; Li, D.; Sun, C.; Williard, P. G. *J. Org. Chem.* **2008**, *73*, 4045. (i) Li, D.; Sun, C.; Liu, J.; Hopson, R.; Li, W.; Williard, P. G. *J. Org. Chem.* **2008**, *73*, 2373.

(10) (a) Lithium and Magnesium: García-Álvarez, P.; Mulvey, R. E.; Parkinson, J. A. *Angew. Chem. Int. Ed.* **2011**, *50*, 9668. (b) Lithium and Zinc: Armstrong, D. R.; García-Álvarez, P.; Kennedy, A. R.; Mulvey, R. E.; Parkinson, J. A. *Angew. Chem. Int. Ed.* **2010**, *49*, 3185.

(11) Kumar, K.; Michalik, D.; Garcia Castro, I.; Tillack, A.; Zapf, A.; Arlt, M.; Heinrich, T.; Böttcher, H.; Beller, M. *Chem. Eur. J.* **2004**, *10*, 746.

(12) (a) Beller, M.; Breindl, C.; Riermeier, T. H.; Eichberger, M.; Trauthwein, H. *Angew. Chem. Int. Ed.* **1998**, *37*, 3389. (b) Beller, M.; Breindl, C. *Chemosphere* **2001**, *43*, 21. (c) Seayad, J.; Tillack, A.; Hartung, C. G.; Beller, M. *Adv. Synth. Catal.* **2002**, *344*, 795.

(13) (a) Malpass, J. R. *Comprehensive Organic Chemistry*; Barton, D., Ollis, W. D., Eds.; Pergamon: Oxford, **1979**; Vol. 2, p 3. (b) Lawrence, S. A. *Amines: Synthesis, Properties and Applications*; Cambridge University Press, **2004**.

(14) (a) Krueger, K.; Tillack, A.; Beller, M. *ChemSusChem* **2009**, *2*, 715. (b) Trost, B. M. *Angew. Chem. Int. Ed. Engl.* **1995**, *34*, 259.

(15) Veige, A. S. *Polyhedron* **2008**, *27*, 3177.

(16) (a) Monnier, F.; Taillefer, M. *Angew. Chem. Int. Ed.* **2008**, *47*, 3096. (b) Beccalli, E. M.; Broggini, G.; Martinelli, M.; Sottocornola, S. *Chem. Rev.* **2007**, *107*, 5318.

(17) Nugent, T. C.; El-Shazly, M. *Adv. Synth. Catal.* **2010**, *352*, 753.

(18) General review of hydroamination: (a) Müller, T. E.; Beller, M. *Chem. Rev.* **1998**, *98*, 675. (b) Müller, T. E.; Hultzsch, K. C.; Yus, M.; Foubelo, F.; Tada, M. *Chem. Rev.* **2008**, *108*, 3795.

(19) (a) Severin, R.; Doye, S. *Chem. Soc. Rev.* **2007**, *36*, 1407. (b) Alonso, F.; Beletskaya, I. P.; Yus, M. *Chem. Rev.* **2004**, *104*, 3079. (c) Doye, S. *Synlett* **2004**, *2004*, 1653. (d) Pohlki, F.; Doye, S. *Chem. Soc. Rev.* **2003**, *32*, 104.

(20) Reviews: (a) Chemler, S. R. *Org. Biomol. Chem.* **2009**, *7*, 3009. (b) Zi, G. *Dalton Trans.* **2009**, 9101. (c) Aillaud, I.; Collin, J.; Hannedouche, J.; Schulz, E. *Dalton Trans.* **2007**, 5105. (d) Hultzsch, K. C. *Adv. Synth. Catal.* **2005**, *347*, 367. (e) Hultzsch, K. C. *Org. Biomol. Chem.* **2005**, *3*, 1819. (f) Hultzsch, K. C.; Gribkov, D. V.; Hampel, F. *J. Organomet. Chem.* **2005**, *690*, 4441. (g) Roesky, P. W.; Müller, T. E. *Angew. Chem. Int. Ed.* **2003**, *42*, 2708.

(21) (a) Hong, S.; Marks, T. J. *Acc. Chem. Res.* **2004**, *37*, 673. (b) Molander, G. A.; Romero, J. A. C. *Chem. Rev.* **2002**, *102*, 2161.

(22) (a) Lauzon, J. M. P.; Schafer, L. L. *Dalton Trans.* **2012**, *41*, 11539. (b) Roesky, P. W. *Angew. Chem. Int. Ed.* **2009**, *48*, 4892. (c) Eisenberger, P.; Schafer, L. L. *Pure Appl. Chem.* **2010**, *82*, 1503.

(23) (a) Reznichenko, A. L.; Hultzsch, K. C. *J. Am. Chem. Soc.* **2012**, *134*, 3300. (b) Zhang, F.; Song, H.; Zi, G. *Dalton Trans.* **2011**, *40*, 1547. (c) Eisenberger, P.; Ayinla, R. O.; Lauzon, J. M. P.; Schafer, L. L. *Angew. Chem. Int. Ed.* **2009**, *48*, 8361.

(24) Seyferth, D., *Organometallics* **2009**, *28*, 1598.

(25) Reznichenko, A. L.; Hultzsch, K. C.; *Structure and Bonding, Vol. 137* (Ed.: P. W. Roesky), Springer Berlin / Heidelberg, **2010**, pp. 1-48.

(26) (a) Gagné, M. R.; Stern, C. L.; Marks, T. J. *J. Am. Chem. Soc.* **1992**, *114*, 275. (b) Gribkov, D. V.; Hultzsch, K. C.; Hampel, F. *J. Am. Chem. Soc.* **2006**, *128*, 3748.

(27) (a) Liu, B.; Roisnel, T.; Carpentier, J.-F.; Sarazin, Y. *Angew. Chem. Int. Ed.* **2012**, *51*, 4943. (b) Brinkmann, C.; Barrett, A. G. M.; Hill, M. S.; Procopiou, P. A. *J. Am. Chem. Soc.* **2012**, *134*, 2193. (c) Arrowsmith, M.; Crimmin, M. R.; Barrett, A. G. M.; Hill, M. S.; Kociok-Köhn, G.; Procopiou, P. A. *Organometallics* **2011**, *30*, 1493. (d) Dunne, J. F.; Fulton, D. B.; Ellern, A.; Sadow, A. D. *J. Am. Chem. Soc.* **2010**, *132*, 17680.

(28) Tobisch, S. *Chem. Eur. J.* **2011**, *17*, 14974.

(29) Motta, A.; Lanza, G.; Fragalà, I. L.; Marks, T. J. *Organometallics* **2004**, *23*, 4097.

(30) Ln^{3+} ionic radii for C.N. = 8 decreases from La^{3+} = 1.16 Å to Lu^{3+} = 0.98 Å due to the lanthanide contraction. (a) Shriver, D. F.; Atkins, P. W. *Inorganic Chemistry*; Third ed.; W. H. Freeman and Company: New York, N. Y., **1999**. (b) Shannon, R. *Acta Crystallogr., Sect. A* **1976**, *32*, 751.

(31) (a) Jeske, G.; Lauke, H.; Mauermann, H.; Swepston, P. N.; Schumann, H.; Marks, T. J. *J. Am. Chem. Soc.* **1985**, *107*, 8091. (b) Jeske, G.; Schock, L. E.; Swepston, P. N.; Schumann, H.; Marks, T. J. *J. Am. Chem. Soc.* **1985**, *107*, 8103.

(32) Gagné, M. R.; Marks, T. J. *J. Am. Chem. Soc.* **1989**, *111*, 4108.

(33) See also reference 26a. Gagné, M. R.; Nolan, S. P.; Marks, T. J. *Organometallics* **1990**, *9*, 1716.

(34) Tian, S.; Arredondo, V. M.; Stern, C. L.; Marks, T. J. *Organometallics* **1999**, *18*, 2568.

(35) (a) Giardello, M. A.; Conticello, V. P.; Brard, L.; Sabat, M.; Rheingold, A. L.; Stern, C. L.; Marks, T. J. *J. Am. Chem. Soc.* **1994**, *116*, 10212. (b) Giardello, M. A.; Conticello, V.

P.; Brard, L.; Gagne, M. R.; Marks, T. J. *J. Am. Chem. Soc.* **1994**, *116*, 10241. (c) Gagné, M. R.; Brard, L.; Conticello, V. P.; Giardello, M. A.; Stern, C. L.; Marks, T. J. *Organometallics* **1992**, *11*, 2003.

(36)   (a) Quinet, C.; Ates, A.; Markó, I. E. *Tetrahedron Lett.* **2008**, *49*, 5032. (b) Hultzsch, K. C.; Hampel, F.; Wagner, T. *Organometallics* **2004**, *23*, 2601. (c) Bürgstein, M. R.; Berberich, H.; Roesky, P. W. *Chem. Eur. J.* **2001**, *7*, 3078. (d) Kim, Y. K.; Livinghouse, T.; Bercaw, J. E. *Tetrahedron Lett.* **2001**, *42*, 2933.

(37)   See also reference 36d. (a) Kim, Y. K.; Livinghouse, T. *Angew. Chem. Int. Ed.* **2002**, *41*, 3645. (b) Kim, Y. K.; Livinghouse, T.; Horino, Y. *J. Am. Chem. Soc.* **2003**, *125*, 9560. (c) Kim, J. Y.; Livinghouse, T. *Org. Lett.* **2005**, *7*, 4391.

(38)   Kim, J. Y.; Livinghouse, T. *Organic Letters* **2005**, *7*, 1737.

(39)   (a) Aillaud, I.; Collin, J.; Duhayon, C.; Guillot, R.; Lyubov, D.; Schulz, E.; Trifonov, A. *Chem. Eur. J.* **2008**, *14*, 2189. (b) Riegert, D.; Collin, J.; Meddour, A.; Schulz, E.; Trifonov, A. *J. Org. Chem.* **2006**, *71*, 2514. (c) Collin, J.; Daran, J.-C.; Jacquet, O.; Schulz, E.; Trifonov, A. *Chem. Eur. J.* **2005**, *11*, 3455. (d) Collin, J.; Daran, J.-C.; Schulz, E.; Trifonov, A. *Chem. Commun.* **2003**, 3048.

(40)   (a) Chapurina, Y.; Guillot, R.; Lyubov, D.; Trifonov, A.; Hannedouche, J.; Schulz, E. *Dalton Trans.* **2013**, *42*, 507. (b) Aillaud, I.; Collin, J.; Hannedouche, J.; Schulz, E.; Trifonov, A. *Tetrahedron Lett.* **2010**, *51*, 4742. (c) Aillaud, I.; Lyubov, D.; Collin, J.; Guillot, R.; Hannedouche, J.; Schulz, E.; Trifonov, A. *Organometallics* **2008**, *27*, 5929. (d) Riegert, D.; Collin, J.; Daran, J.-C.; Fillebeen, T.; Schulz, E.; Lyubov, D.; Fukin, G.; Trifonov, A. *Eur. J. Inorg. Chem.* **2007**, 1159.

(41)   Hong, S.; Tian, S.; Metz, M. V.; Marks, T. J. *J. Am. Chem. Soc.* **2003**, *125*, 14768.

(42)   (a) Reznichenko, A. L.; Nguyen, H. N.; Hultzsch, K. C. *Angew. Chem. Int. Ed.* **2010**, *49*, 8984. (b) Yuen, H. F.; Marks, T. J. *Organometallics* **2009**, *28*, 2423. (c) Gribkov, D. V.; Hultzsch, K. C.; Hampel, F. *J. Am. Chem. Soc.* **2006**, *128*, 3748. (d) Ryu, J.-S.; Li, G. Y.; Marks, T. J. *J. Am. Chem. Soc.* **2003**, *125*, 12584. (e) Li, Y.; Marks, T. J. *J. Am. Chem. Soc.* **1998**, *120*, 1757. (f) Li, Y.; Marks, T. J. *Organometallics* **1996**, *15*, 3770.

(43) Mg^{2+}, Ca^{2+}, Sr^{2+} and insoluble Ba are not toxic, however Be^{2+}, soluble Ba^{2+} and Ra are.

(44)   Harder, S. *Chem. Rev.* **2010**, *110*, 3852.

(45)   (a) Crimmin, M. R.; Casely, I. J.; Hill, M. S. *J. Am. Chem. Soc.* **2005**, *127*, 2042. (b) Datta, S.; Roesky, P. W.; Blechert, S. *Organometallics* **2007**, *26*, 4392. (c) Buch, F.; Harder, S. *Z. Naturforsch.* **2008**, *63b*, 169. (d) Datta, S.; Gamer, M. T.; Roesky, P. W. *Organometallics* **2008**, *27*, 1207. (e) Barrett, A. G. M.; Crimmin, M. R.; Hill, M. S.; Hitchcock, P. B.; Kociok-Köhn, G.; Procopiou, P. A. *Inorg. Chem.* **2008**, *47*, 7366. (f) Crimmin, M. R.; Arrowsmith, M.; Barrett, A. G. M.; Casely, I. J.; Hill, M. S.; Procopiou, P. A. *J. Am. Chem. Soc.* **2009**, *131*, 9670. (g) Arrowsmith, M.; Hill, M. S.; Kociok-Köhn, G. *Organometallics* **2009**, *28*, 1730. (h) Wixey, J. S.; Ward, B. D. *Chem. Commun.* **2011**, *47*, 5449. (i) Wixey, J. S.; Ward, B. D. *Dalton Trans.* **2011**, *40*, 7693. (j) Jenter, J.; Köppe, R.; Roesky, P. W. *Organometallics* **2011**, *30*, 1404.

(46)   (a) Horrillo-Martínez, P.; Hultzsch, K. C. *Tetrahedron Lett.* **2009**, *50*, 2054. (b) Dunne, J. F.; Fulton, D. B.; Ellern, A.; Sadow, A. D. *J. Am. Chem. Soc.* **2010**, *132*, 17680. (c) Zhang, X.; Emge, T. J.; Hultzsch, K. C. *Organometallics* **2010**, *29*, 5871. (d) Arrowsmith, M.; Crimmin, M. R.; Barrett, A. G. M.; Hill, M. S.; Kociok-Köhn, G.; Procopiou, P. A. *Organometallics* **2011**, *30*, 1493. (e) Neal, S. R.; Ellern, A.; Sadow, A.

D. *J. Organomet. Chem.* **2011**, *696*, 228. (f) Arrowsmith, M.; Hill, M. S.; Kociok-Köhn, G. *Organometallics* **2011**, *30*, 1291.

(47)   Arrowsmith, M.; Hill, M. S.; Kociok-Köhn, G. *Organometallics* **2011**, *30*, 1291.

(48)   See references 45c,h,i and 46a,e

(49)   Zhang, X.; Emge, T. J.; Hultzsch, K. C. *Angew. Chem. Int. Ed.* **2012**, *51*, 394.

(50)   Neal, S. R.; Ellern, A.; Sadow, A. D. *J. Organomet. Chem.* **2011**, *696*, 228.

(51)   Liu, B.; Roisnel, T.; Carpentier, J.-F.; Sarazin, Y. *Angew. Chem. Int. Ed.* **2012**, *51*, 4943.

(52)   Pauling ionic radii. Cotton, A. F.; Wilkinson, G. *Advanced Inorganic Chemistry*; Wiley: New York, NY, 1980.

(53)   (a) Barrett, A. G. M.; Brinkmann, C.; Crimmin, M. R.; Hill, M. S.; Hunt, P.; Procopiou, P. A. *J. Am. Chem. Soc.* **2009**, *131*, 12906. (b) Brinkmann, C.; Barrett, A. G. M.; Hill, M. S.; Procopiou, P. A. *J. Am. Chem. Soc.* **2012**, *134*, 2193.

(54)   Seayad, J.; Tillack, A.; Hartung, C. G.; Beller, M. *Adv. Synth. Catal.* **2002**, *344*, 795.

(55)   (a) J. D. Danforth, *French Patent 917060,* **1946**. (b) J. D. Danforth, *U. S. Patent 2,449,644,* **1948**. (c) A. W. Weston , *U. S. Patent 2,437,984,* **1948**. (d) J. D. Danforth , *Canadian Patent 461783,* **1949**.

(56)   Howk, B. W.; Little, E. L.; Scott, S. L.; Whitman, G. M.; *J. Am. Chem. Soc.* **1954**, *76*, 1899.

(57)   (a) Closson, R. D.; Napolitano, J. P.; Ecke, G. G.; Kolka, A. J. *J. Org. Chem.* **1957**, *22*, 646. (b) Wollensak, J.; Closson, R. D. *Org. Synth.* **1963**, *43*, 45.

(58)   Lehmkuhl, H.; Reinehr, D. *J. Organomet. Chem.* **1973**, *55*, 215.

(59)   (a) Pez, G. P.; Galle, J. E. *Pure Appl. Chem.* **1985**, *57*, 1917. (b) 21 − 34% conversion observed in 1 − 3 hours at 80 − 110°C and 90 − 120 atm.

(60)   Khedkar, V.; Tillack, A.; Benisch, C.; Melder, J.-P.; Beller, M. *J. Mol. Catal. A: Chem.* **2005**, *241*, 175.

(61)   See ref. 58 for the use of LiH and NaH as hydroamination catalysts under more forcing reaction conditions.

(62)   Horrillo-Martínez, P.; Hultzsch, K. C.; Gil, A.; Branchadell, V. *Eur. J. Org. Chem.* **2007**, 3311.

(63)   120°C, 1:2 ratio of vinylarene:amine allowed for high selectivity of the monosubstituted product.

(64)   7% *ee* with α-methyl styrene and *p*-methoxy benzyl amine; 14% *ee* with trans-β-methyl styrene and *p*-methoxy benzyl amine.

(65)   <u>Intermolecular Hydroamination of styrene derivatives:</u> See also reference 62. (a) Kumar, K.; Michalik, D.; Garcia Castro, I.; Tillack, A.; Zapf, A.; Arlt, M.; Heinrich, T.; Böttcher, H.; Beller, M. *Chem. Eur. J.* **2004**, *10*, 746. (b) Beller, M.; Breindl, C. *Chemosphere* **2001**, *43*, 21. (c) Hartung, C. G.; Breindl, C.; Tillack, A.; Beller, M. *Tetrahedron* **2000**, *56*, 5157. (d) Beller, M.; Breindl, C.; Riermeier, T. H.; Eichberger, M.; Trauthwein, H. *Angew. Chem. Int. Ed.* **1998**, *37*, 3389. (e) Beller, M.; Breindl, C. *Tetrahedron* **1998**, *54*, 6359. (f) Narita, T.; Teruo, Y.; Tsuruta, T. *Bull. Chem. Soc. Jap.* **1973**, *46*, 3825. (g) Schlott, R. J.; Falk, J. C.; Narducy, K. W. *J. Org. Chem.* **1972**, *37*, 4243. (h) Asahara, T.; Senō, M.; Tanaka, S.; Den, N. *Bull. Chem. Soc. Jap.* **1969**, *42*, 1996. (i) Wegler, R.; Pieper, G. *Chem. Ber.* **1950**, *83*, 1.

(66)   <u>Intermolecular hydroamination of 1,3-dienes:</u> See also reference 65g. (a) Takabe, K.; Katagiri, T.; Tanaka, J.; Fujita, T.; Watanabe, S.; Suga, K. *Org. Syn.* **1989**, *67*, 44. (b)

Fujita, T.; Suga, K.; Watanabe, S. *Aust. J. Chem.* **1974**, *27*, 531. (c) Fujita, T.; Suga, K.; Watanabe, S. *Chem. Ind.* **1973**, 231. (d) Narita, T.; Imai, N.; Tsuruta, T. *Bull. Chem. Soc. Jap.* **1973**, *46*, 1242. (e) Takabe, K.; Katagiri, T.; Tanaka, J. *Tetrahedron Lett.* **1972**, *39*, 4009. (f) Imai, N.; Narita, T.; Tsuruta, T. *Tetrahedron Lett.* **1971**, *12*, 3517.

(67) Intermolecular HA to Ethylene: See references 56-60.

(68) Intermolecular HA to Aliphatic Olefins: See ref. 56, 57a, 58-60.

(69) (a) Fujita, H.; Tokuda, M.; Nitta, M.; Suginome, H. *Tetrahedron Lett.* **1992**, *33*, 6359. (b) Ates, A.; Quinet, C. *Eur. J. Org. Chem.* **2003**, *2003*, 1623. (c) Quinet, C.; Jourdain, P.; Hermans, C.; Ates, A.; Lucas, I.; Markó, I. E. *Tetrahedron* **2008**, *64*, 1077.

(70) See reference 69c. Details on these experiments were not reported in formal catalytic tables, they were discussed in the results and discussion section on page 1079.

(71) Tsuchida, S.; Kaneshige, A.; Ogata, T.; Baba, H.; Yamamoto, Y.; Tomioka, K. *Org. Lett.* **2008**, *10*, 3635.

(72) (a) Martinez, P. H.; Hultzsch, K. C.; Hampel, F. *Chem. Commun.* **2006**, 2221. (b) Martínez, P. H. Ph. D. Dissertation, Institut für Organische Chemie, Friedrich-Alexander Universität Erlangen-Nürnberg, **2008**.

(73) (a) Deschamp, J.; Collin, J.; Hannedouche, J.; Schulz, E. *Eur. J. Org. Chem.* **2011**, 3329. (b) Deschamp, J.; Olier, C.; Schulz, E.; Guillot, R.; Hannedouche, J.; Collin, J. *Adv. Synth. Catal.* **2010**, *352*, 2171.

(74) One ligand contained a pyridyl group where four carbons separate the nitrogen's, three of which are contained on a rigid aromatic ring.

(75) Lebeuf, R.; Robert, F.; Schenk, K.; Landais, Y. *Org. Lett.* **2006**, *8*, 4755.

(76) Ogata, T.; Ujihara, A.; Tsuchida, S.; Shimizu, T.; Kaneshige, A.; Tomioka, K.; *Tetrahedron Lett.* **2007**, *48*, 6648.

(77) (a) Reznichenko, A.; Hultzsch, K. *Top. Organomet. Chem.* Springer Berlin/Heidelberg: **2013**, *43*, 51-114. (b) Aillaud, I.; Collin, J.; Hannedouche, J.; Schulz, E. *Dalton Trans.* **2007**, 5105. (c) Hultzsch, K. C. *Adv. Synth. Catal.* **2005**, *347*, 367.

(78) (a) Manna, K.; Xu, S.; Sadow, A. D. *Angew. Chem. Int. Ed.* **2011**, *50*, 1865. (b) Manna, K.; Ellern, A.; Sadow, A. D. *Chem. Commun.* **2010**, *46*, 339.

(79) (a) Lauzon, J. M. P.; Schafer, L. L. *Dalton Trans.* **2012**, *41*, 11539. (b) Roesky, P. W. *Angew. Chem. Int. Ed.* **2009**, *48*, 4892.

(80) (a) Chen, E. Y.-X.; Marks, T. J. *Chem. Rev.* **2000**, *100*, 1391. (b) Watson, P. L.; Parshall, G. W. *Acc. Chem. Res.* **1985**, *18*, 51.

(81) Gribkov, D. V.; Hultzsch, K. C. *Angew. Chem. Int. Ed.* **2004**, *43*, 5542.

(82) Knight, P. D.; Munslow, I.; O'Shaughnessy, P. N.; Scott, P. *Chem. Commun.* **2004**, 894.

(83) Bexrud, J. A.; Beard, J. D.; Leitch, D. C.; Schafer, L. L. *Organic Lett.* **2005**, *7*, 1959.

(84) Watson, D. A.; Chiu, M.; Bergman, R. G. *Organometallics* **2006**, *25*, 4731.

(85) Ayinla, R. O.; Gibson, T.; Schafer, L. L. *J. Organomet. Chem.* **2011**, *696*, 50.

(86) (a) Majumder, S.; Odom, A. L. *Organometallics* **2008**, *27*, 1174. (b) Stubbert, B. D.; Marks, T. J. *J. Am. Chem. Soc.* **2007**, *129*, 6149.

(87) See also 78a. (a) Kim, H.; Kim, Y. K.; Shim, J. H.; Kim, M.; Han, M.; Livinghouse, T.; Lee, P. H. *Adv. Synth. Catal.* **2006**, *348*, 2609. (b) Kim, H.; Lee, P. H.; Livinghouse, T. *Chem. Commun.* **2005**, 5205.

(88) Ackermann, L.; Kaspar, L. T.; Gschrei, C. J. *Org. Lett.* **2004**, *6*, 2515.

(89) Kaspar, L. T.; Fingerhut, B.; Ackermann, L. *Angew. Chem. Int. Ed.* **2005**, *44*, 5972.

(90)   (a) Marcseková, K.; Doye, S. *Synthesis* **2007**, *2007*, 145. (b) Anderson, L. L.; Arnold, J.; Bergman, R. G. *J. Am. Chem. Soc.* **2005**, *127*, 14542.

(91)   (a) Wood, M. C.; Leitch, D. C.; Yeung, C. S.; Kozak, J. A.; Schafer, L. L. *Angew. Chem. Int. Ed.* **2007**, *46*, 354. (b) Gott, A. L.; Clarke, A. J.; Clarkson, G. J.; Scott, P. *Organometallics* **2007**, *26*, 1729.

(92)   (a) Zhang, F.; Song, H.; Zi, G. *Dalton Trans.* **2011**, *40*, 1547. (b) Reznichenko, A. L.; Emge, T. J.; Audörsch, S.; Klauber, E. G.; Hultzsch, K. C.; Schmidt, B. *Organometallics* **2011**, *30*, 921.

(93)   See also reference 92a. (a) Zi, G.; Zhang, F.; Song, H. *Chem. Commun.* **2010**, *46*, 6296. (b) Eisenberger, P.; Ayinla, R. O.; Lauzon, J. M. P.; Schafer, L. L. *Angew. Chem. Int. Ed.* **2009**, *48*, 8361. (c) Herzon, S. B.; Hartwig, J. F. *J. Am. Chem. Soc.* **2008**, *130*, 14940. (d) Herzon, S. B.; Hartwig, J. F. *J. Am. Chem. Soc.* **2007**, *129*, 6690. (e) Nugent, W. A.; Ovenall, D. W.; Holmes, S. J. *Organometallics* **1983**, *2*, 161.

(94)   See also references 20d and 20g. (a) Reznichenko, A. L.; Hultzsch, K. C. *Chiral Amine Synthesis*; Wiley-VCH Verlag: **2010**, p 341. (b) Hartwig, J. F. *Pure Appl. Chem.* **2004**, *76*, 507. (c) Beller, M.; Breindl, C.; Eichberger, M.; Hartung, C. G.; Seayad, J.; Thiel, O. R.; Tillack, A.; Trauthwein, H. *Synlett* **2002**, 1579. (d) Nobis, M.; Drießen-Hölscher, B. *Angew. Chem. Int. Ed.* **2001**, *40*, 3983.

(95)   (a) Kawatsura, M.; Hartwig, J. F. *J. Am. Chem. Soc.* **2000**, *122*, 9546. (b) Nettekoven, U.; Hartwig, J. F. *J. Am. Chem. Soc.* **2002**, *124*, 1166. (c) Johns, A. M.; Utsunomiya, M.; Incarvito, C. D.; Hartwig, J. F. *J. Am. Chem. Soc.* **2006**, *128*, 1828. (d) Sievers, C.; Jiménez, O.; Knapp, R.; Lin, X.; Müller, T. E.; Türler, A.; Wierczinski, B.; Lercher, J. A. *J. Mol. Catal. A: Chem.* **2008**, *279*, 187.

(96)   (a) Casalnuovo, A. L.; Calabrese, J. C.; Milstein, D. *J. Am. Chem. Soc.* **1988**, *110*, 6738. (b) Dorta, R.; Egli, P.; Zürcher, F.; Togni, A. *J. Am. Chem. Soc.* **1997**, *119*, 10857. (c) Zhao, J.; Goldman, A. S.; Hartwig, J. F. *Science* **2005**, *307*, 1080. (d) Zhou, J.; Hartwig, J. F. *J. Am. Chem. Soc.* **2008**, *130*, 12220.

(97)   Komeyama, K.; Morimoto, T.; Takaki, K. *Angew. Chem. Int. Ed.* **2006**, *45*, 2938.

(98)   Shen, X.; Buchwald, S. L. *Angew. Chem. Int. Ed.* **2010**, *49*, 564.

(99)   (a) Liu, Z.; Yamamichi, H.; Madrahimov, S. T.; Hartwig, J. F. *J. Am. Chem. Soc.* **2011**, *133*, 2772. (b) Liu, Z.; Hartwig, J. F. *J. Am. Chem. Soc.* **2008**, *130*, 1570.

(100) Julian, L. D.; Hartwig, J. F. *J. Am. Chem. Soc.* **2010**, *132*, 13813.

(101) Takemiya, A.; Hartwig, J. F. *J. Am. Chem. Soc.* **2006**, *128*, 6042.

(102) Bauer, E. B.; Andavan, G. T. S.; Hollis, T. K.; Rubio, R. J.; Cho, J.; Kuchenbeiser, G. R.; Helgert, T. R.; Letko, C. S.; Tham, F. S. *Org. Lett.* **2008**, *10*, 1175.

(103) (a) Hesp, K. D.; Stradiotto, M. *Org. Lett.* **2009**, *11*, 1449. (b) Hesp, K. D.; Tobisch, S.; Stradiotto, M. *J. Am. Chem. Soc.* **2010**, *132*, 413.

(104) (a) Kashiwame, Y.; Kuwata, S.; Ikariya, T. *Organometallics* **2012**, *31*, 8444. (b) Tobisch, S. *Chem. Eur. J.* **2012**, *18*, 7248. (c) Kashiwame, Y.; Kuwata, S.; Ikariya, T. *Chem. Eur. J.* **2010**, *16*, 766.

(105) Bender, C. F.; Widenhoefer, R. A. *J. Am. Chem. Soc.* **2005**, *127*, 1070.

(106) (a) Bender, C. F.; Hudson, W. B.; Widenhoefer, R. A. *Organometallics* **2008**, *27*, 2356. (b) Lavery, C. B.; Ferguson, M. J.; Stradiotto, M. *Organometallics* **2010**, *29*, 6125.

(107) (a) Cochran, B. M.; Michael, F. E. *Org. Lett.* **2007**, *10*, 329. (b) Michael, F. E.; Cochran, B. M. *J. Am. Chem. Soc.* **2006**, *128*, 4246.

(108) Cochran, B. M.; Michael, F. E. *J. Am. Chem. Soc.* **2008**, *130*, 2786.

(109) Ohmiya, H.; Moriya, T.; Sawamura, M. *Org. Lett.* **2009**, *11*, 2145.

(110) Han, X.; Widenhoefer, R. A. *Angew. Chem. Int. Ed.* **2006**, *45*, 1747.

(111) Bender, C. F.; Widenhoefer, R. A. *Chem. Commun.* **2006**, 4143.

(112) Bender, C. F.; Widenhoefer, R. A. *Org. Lett.* **2006**, *8*, 5303.

(113) Bender, C. F.; Widenhoefer, R. A. *Chem. Commun.* **2008**, 2741.

(114) (a) Zhang, J.; Yang, C.-G.; He, C. *J. Am. Chem. Soc.* **2006**, *128*, 1798. (b) Liu, X.-Y.; Li, C.-H.; Che, C.-M. *Org. Lett.* **2006**, *8*, 2707.

(115) (a) Utsunomiya, M.; Hartwig, J. F. *J. Am. Chem. Soc.* **2004**, *126*, 2702. (b) Takaya, J.; Hartwig, J. F. *J. Am. Chem. Soc.* **2005**, *127*, 5756.

(116) Coulson, D. R. *Tetrahedron Lett.* **1971**, *12*, 429.

(117) (a) Beller, M.; Eichberger, M.; Trauthwein, H. *Angew. Chem. Int. Ed. Engl.* **1997**, *36*, 2225. (b) Beller, M.; Trauthwein, H.; Eichberger, M.; Breindl, C.; Müller, T. E. *Eur. J. Inorg. Chem.* **1999**, 1121. (c) Beller, M.; Trauthwein, H.; Eichberger, M.; Breindl, C.; Herwig, J.; Müller, T. E.; Thiel, O. R. *Chem. Eur. J.* **1999**, *5*, 1306.

(118) Utsunomiya, M.; Kuwano, R.; Kawatsura, M.; Hartwig, J. F. *J. Am. Chem. Soc.* **2003**, *125*, 5608.

(119) Sevov, C. S.; Zhou, J.; Hartwig, J. F. *J. Am. Chem. Soc.* **2012**, *134*, 11960.

(120) Pan, S.; Endo, K.; Shibata, T. *Org. Lett.* **2012**, *14*, 780.

(121) Utsunomiya, M.; Hartwig, J. F. *J. Am. Chem. Soc.* **2003**, *125*, 14286.

(122) Li, K.; Horton, P. N.; Hursthouse, M. B.; Hii, K. K. *J. Organomet. Chem.* **2003**, *665*, 250.

(123) Hu, A.; Ogasawara, M.; Sakamoto, T.; Okada, A.; Nakajima, K.; Takahashi, T.; Lin, W. *Adv. Synth. Catal.* **2006**, *348*, 2051.

(124) Additional examples: Nickel: (a) Pawlas, J.; Nakao, Y.; Kawatsura, M.; Hartwig, J. F. *J. Am. Chem. Soc.* **2002**, *124*, 3669. Palladium: (b) Löber, O.; Kawatsura, M.; Hartwig, J. F. *J. Am. Chem. Soc.* **2001**, *123*, 4366.

(125) See also reference 114a. Taylor, J. G.; Whittall, N.; Hii, K. K. *Org. Lett.* **2006**, *8*, 3561.

(126) Zhang, Z.; Lee, S. D.; Widenhoefer, R. A. *J. Am. Chem. Soc.* **2009**, *131*, 5372.

2

Intramolecular Hydroamination of Diamidobinaphthyl Based Lithium Amides

2.1 Introduction

The base – catalyzed hydroamination[1] of olefins and 1,3 dienes can be traced back to the 1940's,[2] however the intramolecular variant was not reported until later. The asymmetric hydroamination/cyclization of aminoalkenes with *n*-butyllithium in THF has been reported on multiple occasions.[3] These studies noted that catalytic amounts of base were more effective for this transformation than stoichiometric quantities.

(*S,S,S*)-**25**

(*R*)-**26a**; R = C$_6$H$_5$
(*R*)-**26b**; R = cyclopentyl
(*R*)-**26c**; R = cyclohexyl
(*R*)-**26d**; R = isopropyl
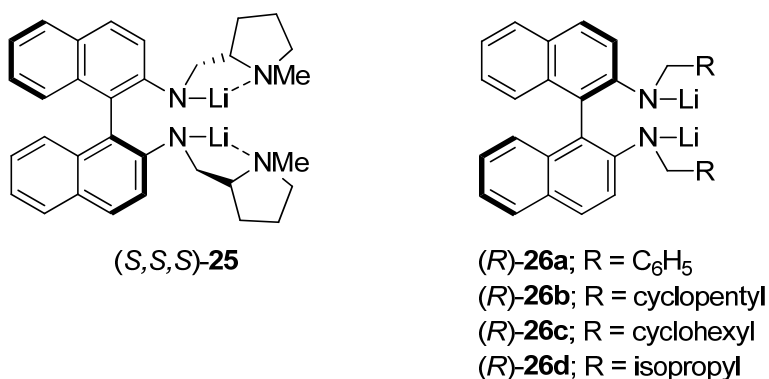
Figure 2-1. Dilithium salts used in the hydroamination/cyclization of Thorpe Ingold activated aminoalkene substrates.

The asymmetric base – catalyzed intramolecular hydroamination/cyclization of aminoalkenes was mediated by chiral dilithium salt (*S,S,S*)-**25** in 2006.[4] This catalyst induced up to 85% enantiomeric excess on *gem*-dialkyl substituted substrates. Kinetic data demonstrated a first order dependence on both catalyst and substrate concentrations,[5] and enantioselectivities could be improved by lowering the reaction temperature. A related series of complexes (*R*)-**26a-d** were also reported to cyclize aminoalkenes and aminodienes.[6] These complexes did not containing L-donor sidearms[7] and reported up to 65% enantiomeric excess for aminodienes and up to 58% *ee* for one aminoalkene substrate.

$$(2\text{-}1)$$
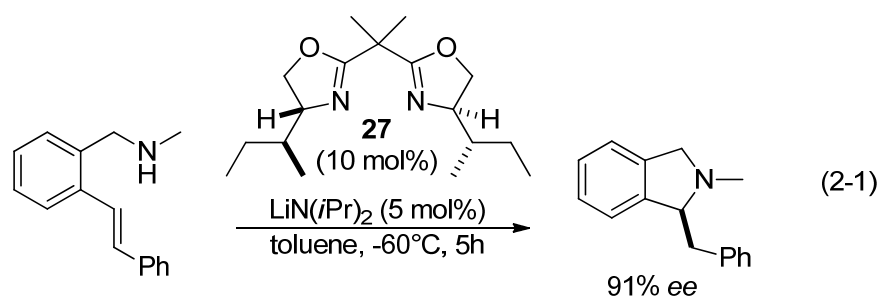
Formation of bicyclic products by the intramolecular hydroamination of stilbene and subsequent aminolithiation have also been reported.[8] The stoichiometry and temperature of this reaction can be modified to control product distribution. Incorporation of chiral bisoxazoline allowed up to 91% enantiomeric excess at -60°C (Eq. 2-1).[9]

2.2 Ligand Synthesis

Previously reported ligand H$_2$-(*S,S,S*)-**25** contains two elements of internal chirality.[10] Enantiopure DABN has axial chirality and each proline sidearm contains a chiral center. TMEDA can solvate lithium and is used to deaggregate lithium bases, often increasing their activity.[11] A new chiral ligand (*R*)-**54** was synthesized to contain flexible sidearms similar to TMEDA, with its sole source of chirality being the axial chirality from diaminobinaphthyl.
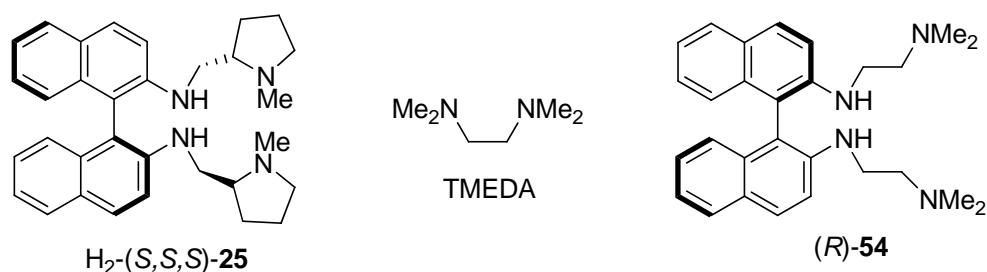
Figure 2-2. Left: Previously reported ligand H$_2$-(*S,S,S*)-**25** used for intramolecular hydroamination/cyclization upon lithiation. Center: TMEDA, a ligand used to deaggregate organolithium reagents. Right: Ligand (*R*)-**54**, which incorporates TMEDA into the chiral diaminobinaphthyl ligand scaffold.
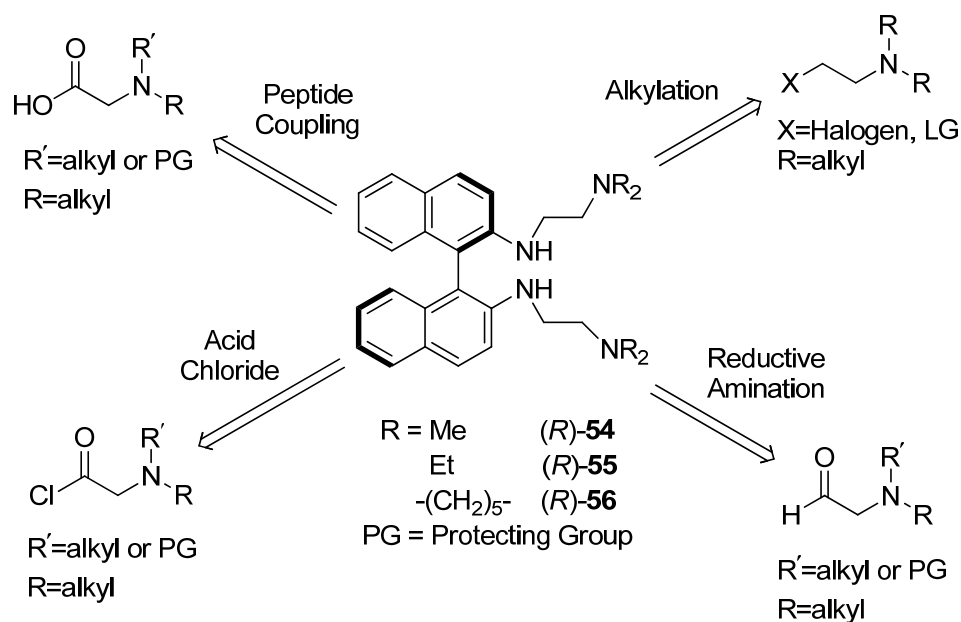
Scheme 2-1. Outline of retrosynthetic pathways to the desired ligands.

Addition of the desired side chain to commercially available enantiopure DABN was the general approach. Approaches to amine and amide bond formation include alkylation,[12] reductive amination,[13] peptide coupling[14] or addition to an acid chloride. High selectivity for the desired product was a priority because the separation of tertiary amine containing mixtures is difficult. Ultimately, reductive amination prevailed as the most efficient and selective pathway to the desired ligands. Three commercially available β-amino alcohols were used to synthesize ligands (R)-**54**, (R)-**55** and (R)-**56** allowing the effects of steric bulk on the chelating amine to be studied. An analog of these ligands, (R)-**63** containing a methoxy coordinating group on the side chain was prepared as well.

(2-1)
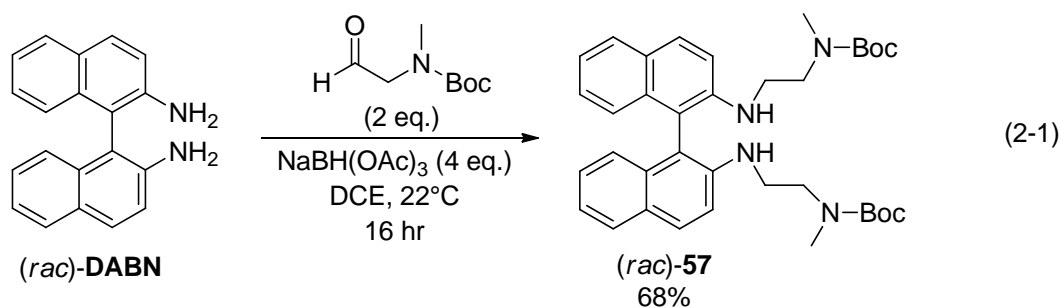
Reductive amination[15] is often a clean, selective method for amine bond formation under appropriate conditions. The coupling of NOBIN[16] and aniline derivatives[17] to Boc-amine containing aldehydes by reductive amination has been reported. The homolog of the desired aldehyde has been formed by Swern oxidation,[18] however its purification was modified due to the increased volatility of the desired aldehyde. The synthesis of (*rac*)-**57** was completed in 68% yield (Eq. 2-1). Reduction of this compound with LiAlH$_4$ yielded a mixture of products in which Boc was either reduced or cyclized.[19] Attempts to isolate pure products from this mixture were unsuccessful. This route was not attempted with other carbamate protecting groups because reduction would generate the same aldehyde intermediate which is capable of cyclization.

The proline analog of these ligands[4] was synthesized by coupling DABN to the acid chloride of Boc-L-proline and a similar route yielded (*rac*)-**58**. In theory, stepwise reduction of Boc followed by amide reduction could allow the secondary amine to prevent cyclization. This did not occur and a similar mixture of reduced and cyclized products was obtained.

(2-2)
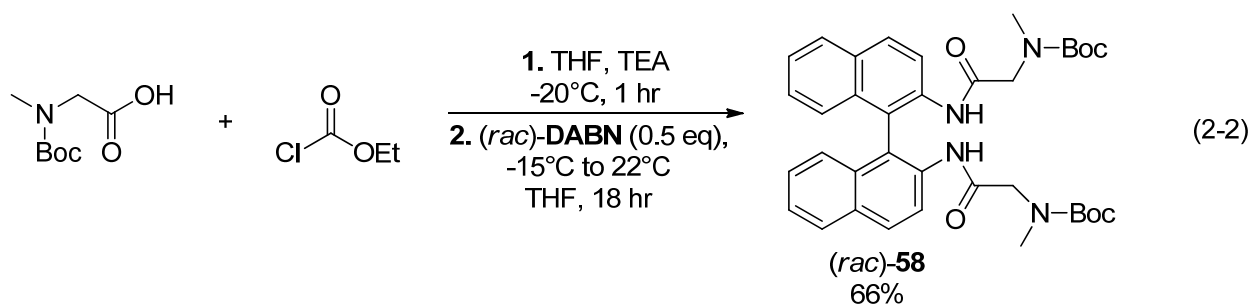
The use of protecting groups is deeply ingrained into the field of amine synthesis. Demand for more atom economic[20] routes to amines has driven the development of protecting group-free methods leading to these target molecules.[21] Amine bond formation by reductive amination using an unprotected α-amino aldehyde has been documented,[13b,22] however yields are often low and experimental details minimal or omitted. Crude mixtures containing aldehydes are used, most of which have significantly higher boiling points than aldehyde **59** (Eq. 2-3).

The desired ligands (*R*)-**54**, (*R*)-**55** and (*R*)-**56** were synthesized by reductive alkylation of diaminobinaphyl with unprotected α-amino aldehydes (Eq. 2-4). Aldehydes **59**, **60** and **61** are not commercially available, although **59** has been reported in the literature. Documented synthetic routes include oxidation by platinum catalysis, chromium oxide and alkylation.[23] The calculated boiling point of this aldehyde is 89°C at 120 mBar.[24] Oxidation with the platinum

catalyst was not attempted because removal of the solvent, dioxane, was a concern. Chromium was not used because it is highly toxic.

$$R = Me \quad \mathbf{59}$$
$$Et \quad \mathbf{60}$$
$$-(CH_2)_5- \quad \mathbf{61}$$

(2-3)
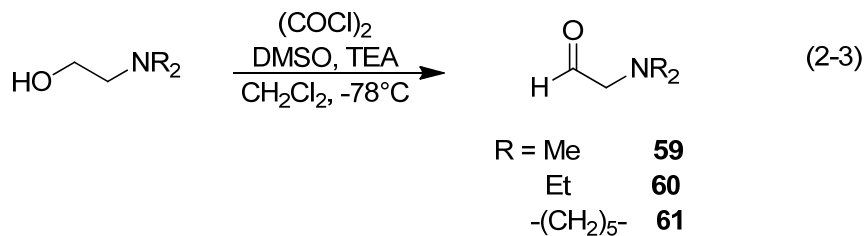
The oxidation of tertiary amine containing alcohols to their aldehydes has been reported, however the stability of these compounds is ambiguous. Crude mixtures are often used without purification, characterization and procedures are seldom reported and yields of pure products are low. The tertiary amines within the amino alcohol substrates are commonly mono- or dibenzyl protected,[25] and have higher boiling points than **59**. Oxidations on β-amino alcohols have been performed using activated DMSO. The aldehydes **59**, **60** and **61** were synthesized by Swern oxidation of their corresponding β-amino alcohols (Eq. 2-3). Immediately after an aqueous workup, the desired ligands (*R*)-**54**, (*R*)-**55** and (*R*)-**56** were synthesized by reductive alkylation. The crude aldehydes were exposed to (*R*)-diaminobinaphthyl and an excess of sodium triacetoxyborohydride.

$$R = Me \quad (R)\text{-}\mathbf{54}, 75\%$$
$$Et \quad (R)\text{-}\mathbf{55}, 86\%$$
$$-(CH_2)_5- \quad (R)\text{-}\mathbf{56}, 80\%$$

(2-4)
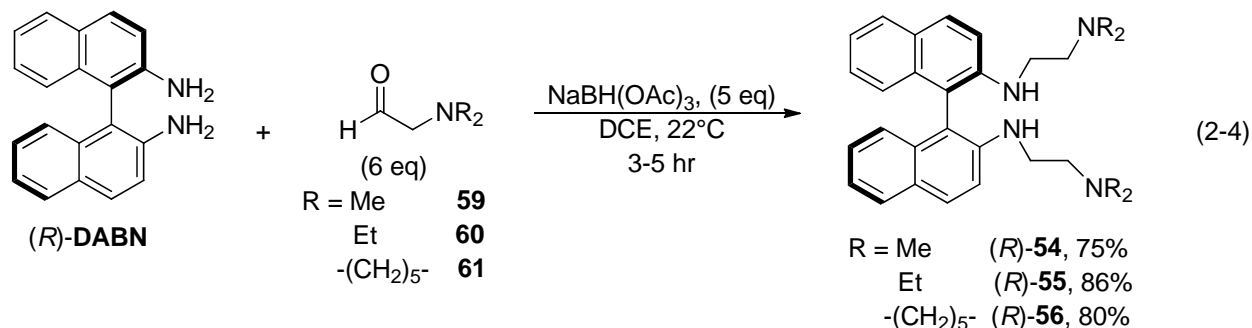
The methoxy analog of these ligands, (*R*)-**63** was synthesized by coupling (*R*)-diaminobinaphthyl to 2-methoxyacetyl chloride, followed by reduction with LiAlH₄ (Scheme 2-2).
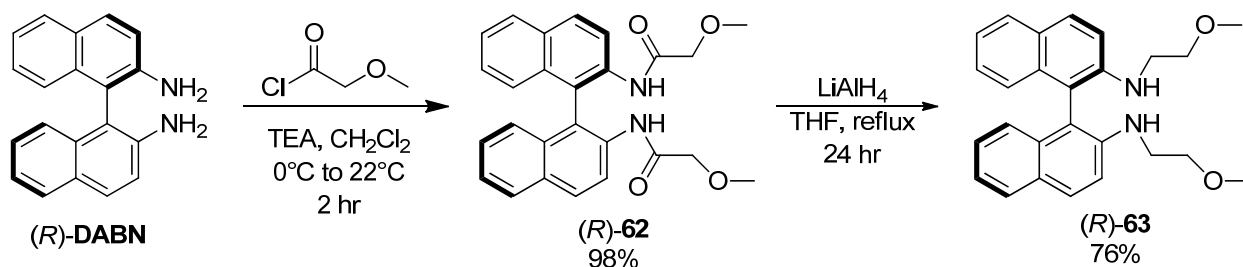
Scheme 2-2. The synthesis of (*R*)-**63**. (*R*)-diaminobinaphthyl was coupled to methoxyacetyl chloride which formed intermediate (*R*)-**62**. Reduction with LiAlH$_4$ yielded the product.

2.3 Complex Synthesis

LiCH$_2$SiMe$_3$[26] was used as the lithium source, and prepared by metal halogen exchange (Eq. 2-5). Two equivalents of LiCH$_2$SiMe$_3$ dissolved in pentane were added to benzene solutions of each ligand to form the benzene soluble dilithium salts (*R*)-**64**, (*R*)-**65** and (*R*)-**66** (Eq. 2-6). The solvents were removed by freeze drying and the purity of each dilithium salt was monitored by ^{1}H NMR spectra at high temperatures ($\geq$ 60 °C). NMR spectra at room temperature were not diagnostic for excess base due to coalescence of the signals for free LiCH$_2$SiMe$_3$ and the dilithium salts. Stock solutions of the ligand and base in benzene were combined for some catalytic and all kinetic experiments to generate the dilithium salt *in situ*.

(2-5)

(2-6)
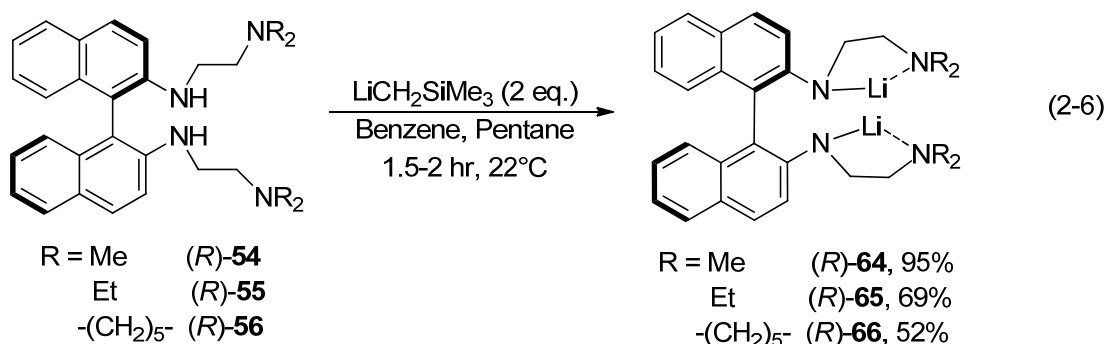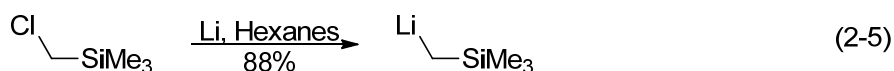
Lithiation of (R)-**63** yielded a solid which was soluble in THF and insoluble in benzene, toluene, pentane and hexane. A solution of LiCH$_2$SiMe$_3$ in benzene was layered over a solution

of (R)-**63** in benzene and the layers were allowed to slowly diffuse overnight, at which point x-ray quality crystals were obtained. These complexes were characterized in the solid state with (R)-**64** and (R)-**67** forming dimers, (R)-**65** and (R)-**66** forming monomers and (rac)-**64** forming a hexamer. Details of these structures are outlined in section 2.3 (Eq. 2-7).

$$(2\text{-}7)$$

L = NMe$_2$	(R)-**54**	
NMe$_2$	(rac)-**54**	
NEt$_2$	(R)-**55**	
-N(CH$_2$)$_5$-	(R)-**56**	
OMe	(R)-**63**	

L = NMe$_2$; n=2	(R)-**64**	
NMe$_2$; n=6	(rac)-**64**	
NEt$_2$; n=1	(R)-**65**	
-N(CH$_2$)$_5$-; n=1	(R)-**66**	
OMe; n=2	(R)-**67**	
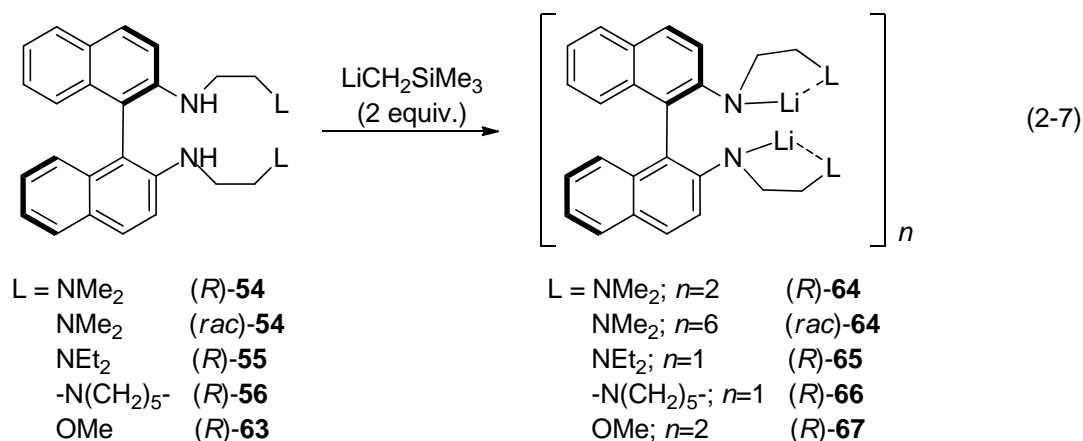
2.4 Crystal Structures

The number of structurally characterized lithium amides has grown significantly in recent years, and the majority of structures contain small molecules with strongly coordinating Lewis basic solvents such as TMEDA and THF. These solvents may prevent weak interactions such as Li···C(π) coordination from being observed. Literature precedence for such interactions has been reported up to 2.8 Å,[27] however Li···C(π) contacts between 2.5–2.8 Å are present in many structures and often not discussed. Significant distortion of bond angles is the rule rather than the exception, making the nature of Li···C(π) contacts ambiguous in some cases.

Lithium typically forms coordination number of four through six, although it has been assigned coordination numbers of up to eight in spite of its small size.[28] Higher coordination numbers are attributed to the electrostatic nature of its bonding which leads to distortion of the expected geometry.

Reports of structurally characterized lithium salts uncomplexed by coordinating solvents are somewhat limited. Ring stacking and laddering are commonly observed in such systems, along with the formation of oligomers and polymers.[29] The structures discussed herein contain one or two Lewis basic sites contained within a ligand per lithium amide which forces Li···C(π) contacts to complete the formation of a tetrahedron. Nonetheless, contacts of up to 3.0 Å will be

discussed with the understanding that current precedence suggests such interactions do not stabilize the metal.

Related dilithium salts of diamidobinaphthyl analogs have been reported, two of which are monomeric. Aggregation of these complexes is prevented by steric bulk on the sidearms[30] along with coordination from an L-donor solvent.[6b] Another structure contained chelating sidearms and was dimeric.[4] A common feature in these structures is the stabilizing metal-carbon(π) interactions with the nearest naphthyl ring. The η^2 and η^3 binding of lithium to conjugated amido and π electrons has been reported,[31] along with its stabilization by an aromatic ring.[32] Another feature observed is the dimerization of both metal amido bonds to form a four membered ring, in which bond strengths are heavily influenced by the steric bulk of the L-donor moiety.

2.3.1 *Molecular Structure of (R)-(Bis(dimethylamino-2-yl-ethyl)amido)binaphthyl-di-lithium ([(R)-**64**]₂).*

Two equivalents of LiCH$_2$SiMe$_3$ were added to a solution of (R)-**54** in benzene. Pentane was added by vapor diffusion over 1–2 days and bright orange crystals of [(R)-**64**]$_2$ suitable for X-ray diffraction formed at 22°C over 1–3 weeks. The ORTEP diagram of [(R)-**64**]$_2$ is shown in Figure 2-3, selected bond lengths, bond angles and dihedral angles are tabulated in Table 2-1.
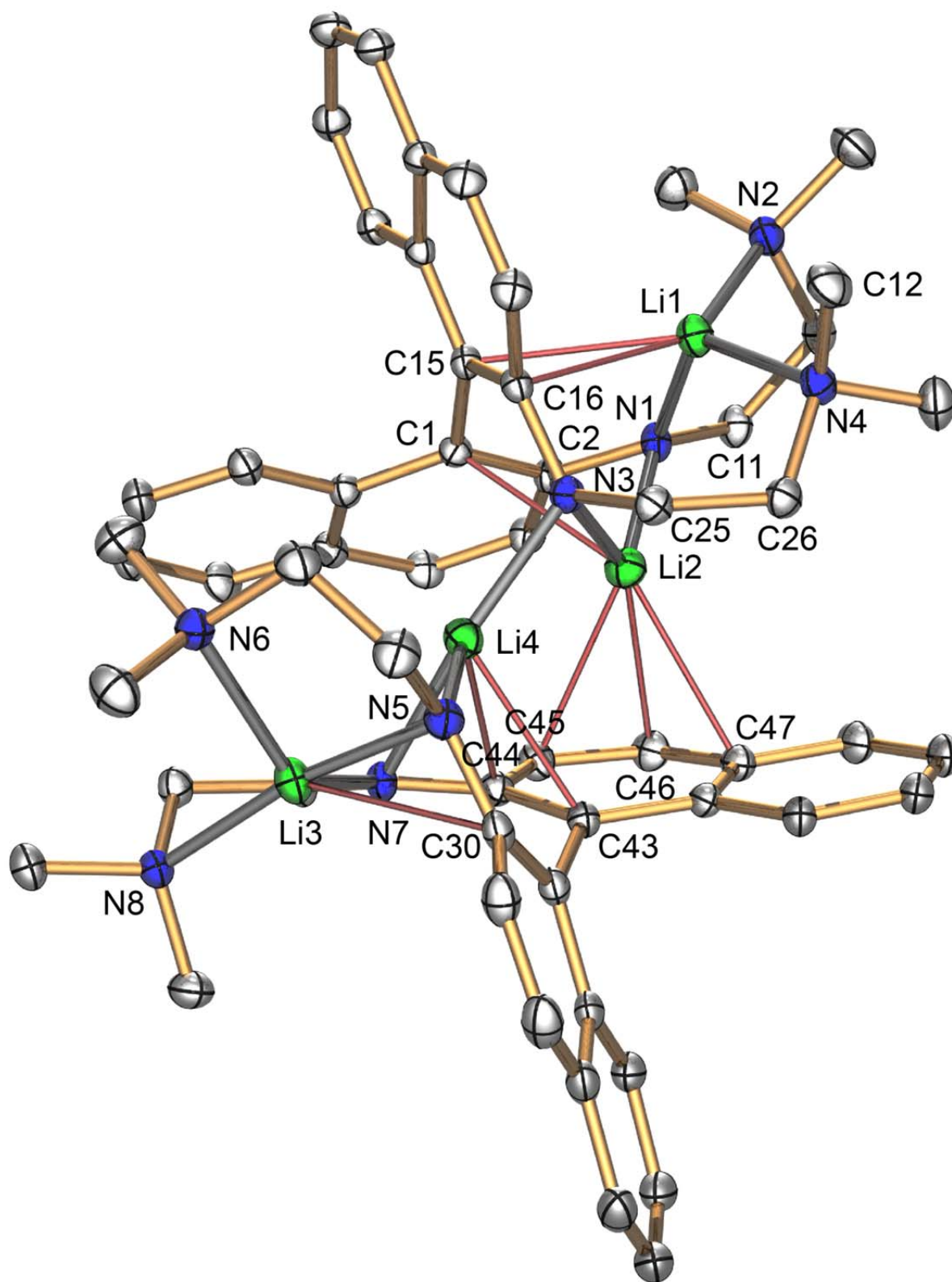
Figure 2-3. ORTEP Diagram of the molecular structure of [(*R*)-**64**]₂ (side view). Thermal ellipsoids are shown at the 50% probability level and hydrogens are omitted for clarity.

Table 2-1. Selected bond lengths, Li$\cdots$C(π) interatomic distances ($\leq$ 3.0 Å) and dihedral angles (°) for [(R)-**64**]$_2$.

Bond Lengths			
Li1-N1 (amido)	1.957(3)	Li1$\cdots$C15 (π)	2.654(3)
Li2-N1 (amido)	2.030(3)	Li1$\cdots$C16 (π)	2.501(3)
Li2-N3 (amido)	1.986(3)	Li2$\cdots$C1 (π)	2.563
Li3-N5 (amido)	2.100(3)	Li2$\cdots$C2 (π)	2.237
Li3-N7 (amido)	1.975(3)	Li2$\cdots$C45 (π)	2.566
Li4-N3 (amido)	2.031(3)	Li2$\cdots$C46 (π)	2.371
Li4-N5 (amido)	1.966(3)	Li2$\cdots$C47 (π)	2.603
Li4-N7 (amido)	2.152(3)	Li3$\cdots$C30 (π)	2.643
Li1-N2 (amine)	2.101(3)	Li4$\cdots$C43 (π)	2.484
Li1-N4 (amine)	2.158(3)	Li4$\cdots$C44 (π)	2.249
Li3-N6 (amine)	2.269(3)		
Li3-N8 (amine)	2.169(3)		

Dihedral Angles	
N1-C11-C12-N2 (sidearm)	38.28(16)
N3-C25-C26-N4 (sidearm)	63.42(15)
C2-C1-C15-C16	81.56(16)
C10-C1-C15-C24	67.49(15)
Mean Planes	75.79
N5-C39-C40-N6 (sidearm)	61.50(16)
N7-C53-C54-N8 (sidearm)	43.74(15)
C30-C29-C43-C44	76.65(16)
C38-C29-C43-C52	66.70(15)
Mean Planes	73.55

[(R)-**64**]$_2$ is dimeric with respect to ligand (R)-**54** and contains four distorted tetrahedral lithium atoms in different coordination environments. The terminal lithium atoms, Li1 and Li3 interact exclusively with one ligand. Li1 forms one amido bond (Li1-N1 1.957(3) Å) and is chelated by two amine nitrogens (Li1-N2 2.101(3) Å, Li1-N4 2.158(3) Å). An η^2 interaction with the adjacent π system (Li1-C16 2.501(3) Å, Li1-C15 2.654(3) Å) provides additional

stabilization. Li3 interacts with one amido nitrogen (Li3-N7 1.975(3) Å) and two amine nitrogens (Li3-N6 2.270(3) Å, Li3-N8 2.169(3) Å,). An η^2 interaction of Li3 with N5 and C30 is present, with a slightly elongated amido bond (Li3-N5 2.100(3) Å) and a weaker π Li···C interaction (Li3-C30 2.643 Å).

The two ligands are joined exclusively through interactions of the internal lithium atoms Li2 and Li4. Li4 forms two amido interactions (Li4-N3 2.031(3) Å, Li4-N5 1.966(3) Å) and an η^3 π stabilization occurs with an adjacent naphthyl ring (Li4-N7 2.152(3) Å, Li4-C43 2.484 Å, Li4-C44 2.249 Å). Li2 forms one amido bond (Li2-N3 1.986(3) Å) while being sandwiched between two naphthyl rings on different ligands via η^3 π interactions. The more closely bound allylic system is formed by one amido nitrogen and two aromatic carbons (Li2-N1 2.030(3) Å, Li2-C2 2.237 Å, Li2-C1 2.563 Å) while the other contains three aromatic carbons (Li2-C45 2.566 Å, Li2-C46 2.371 Å, Li2-C47 2.603 Å).

The side arms of [(R)-**64**]$_2$ are flexible compared to the previously reported [(S,S,S)-**25**]$_2$ which has a proline ring incorporated into each sidearm.[4] The proline moiety limits their flexibility creating more uniform NCCN dihedral angles (46.2°–55.5°, avg. 52.1°) due to a rigid ligand framework. Dihedral angles for the sidearms on [(R)-**64**]$_2$ have a wider range (38.3°–63.4°, avg. 51.7°). The difference between dihedral angles of the sidearms on each ligand is 17.8° and 25.1° compared with 0.1° and 9.3° in [(S,S,S)-**25**]$_2$. The angles between the mean planes[33] of each naphthyl ring in [(R)-**64**]$_2$ are similar (73.5°, 75.8°). In [(S,S,S)-**25**]$_2$, however, these angles were larger (77.4°, 98.7°) and had a significant difference in values.

2.3.2 *Molecular structure of (rac)-(Bis(dimethylamino-2-yl-ethyl)amido)binaphthyl-di-lithium ([(rac)-**64**]$_6$).*

Two equivalents of LiCH$_2$SiMe$_3$ were added to a solution of (rac)-**54** in benzene. Pentane was added by vapor diffusion over 1–2 days and bright orange crystals of [(rac)-**64**]$_6$ suitable for X-ray diffraction formed at 22°C over 1–3 weeks. The ORTEP diagram of [(rac)-**64**]$_6$ is shown in Figure 2-4 and 2-5, selected bond lengths, bond angles and dihedral angles are tabulated in Table 2-2.

[(rac)-**64**]$_6$ forms a hexameric heterometallacycle. Each molecule contains 12 pseudo tetrahedral lithium atoms in two different coordination environments. Li1 binds to two different

ligands. One ligand is bound through an amido nitrogen (Li1-N1 2.018(4) Å) and an amine nitrogen (Li1-N2 2.122(3) Å). The other ligand binds via one amido nitrogen (Li1-N3A 2.062(4) Å) a π interaction (Li1-C12A 2.519(4) Å). Li1 has additional contacts to the carbon atoms adjacent to C12A (Li1···C11A 2.927 Å, Li1···C1A 2.991 Å, Li1···C10A 2.977 Å, Li1···C9A 2.951 Å). Although these contacts are slightly long to be considered formal Li-C(π) interactions, it is worth noting that the uniformity in their length is unique to this structure. Li2 is bound only to one ligand via two amido nitrogens (Li2-N3 2.005(4) Å; Li2-N1 2.164(4) Å), one amine nitrogen (Li2-N4 2.078(4) Å) and a formal Li-C(π) interaction (Li2-C2 2.315(4) Å).

The torsion angle of the sidearms in [(*rac*)-**64**]$_6$ (59.7°–66.1°, avg. 62.9°) are larger than many other observed values, and have larger average than the dimeric species (~10°), and monomeric species (~10–20°). The angle between the mean planes of the naphthyl rings (75.9°) are close in value for those found in [(*R*)-**64**]$_2$ which is the enantiopure variant of this compound.

Table 2-2. Selected bond lengths, Li···C(π) interatomic distances (≤ 3.0 Å) and dihedral angles (°) for [(*rac*)-**64**]$_6$.

Bond Lengths			
Li1-N1 (amido)	2.018(4)	Li1···C12' (π)	2.519(4)
Li1-N3' (amido)	2.062(4)	Li2···C2 (π)	2.315(4)
Li2-N1 (amido)	2.164(4)	Li1···C1' (π)	2.991
Li2-N3 (amido)	2.005(4)	Li1···C9' (π)	2.951
Li1-N2 (amine)	2.122(3)	Li1···C10' (π)	2.977
Li2-N4 (amine)	2.078(4)	Li1···C11' (π)	2.927
Dihedral Angles			
N1-C21-C22-N2 (sidearm)		66.1(2)	
N3-C25-C26-N4 (sidearm)		59.7(2)	
C2-C1-C11-C15		71.1(2)	
C10-C1-C11-C20		75.9(2)	
Mean Planes		75.29	
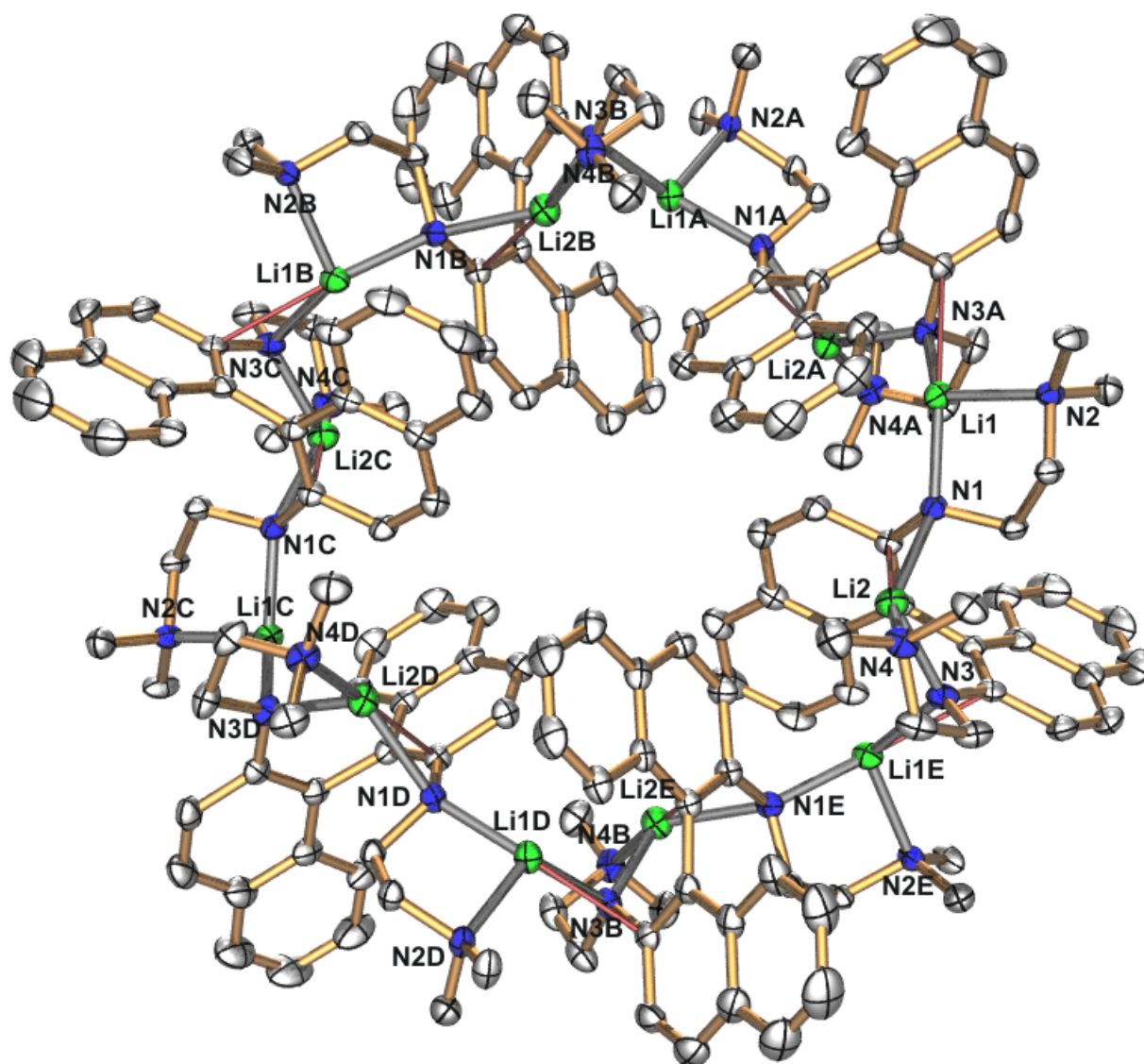
Figure 2-4. ORTEP Diagram of the molecular structure of [(*rac*)-**64**]₆ (top view). Thermal ellipsoids are shown at the 50% probability level and hydrogens are omitted for clarity.
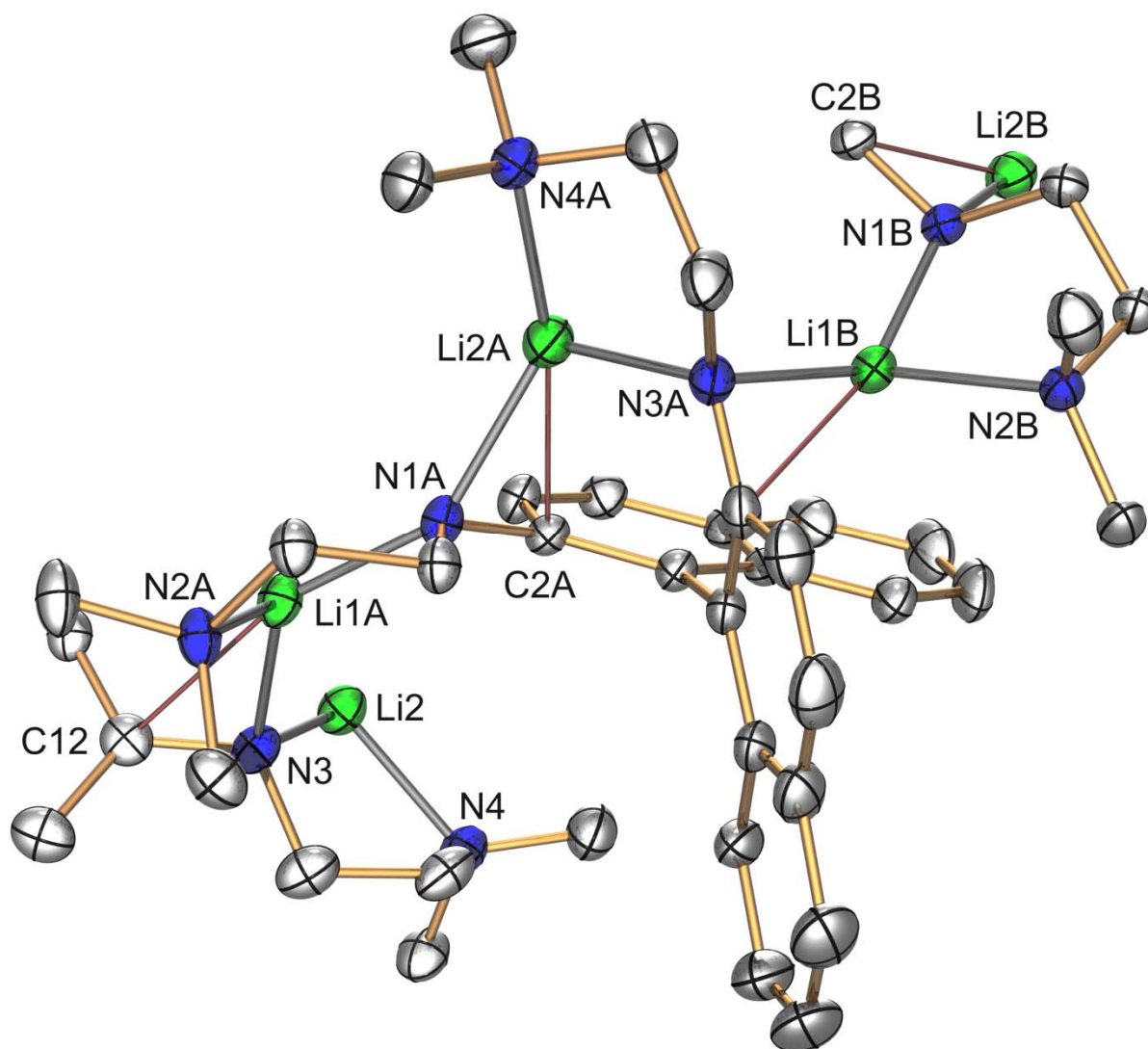
Figure 2-5. Partial ORTEP diagram of the molecular structure of [(*rac*)-**64**]$_6$ (top view), with Li2 and Li2B being cutoff points. Thermal ellipsoids are shown at the 50% probability level and hydrogens are omitted for clarity.

2.3.3 *Molecular Structure of (R)-(Bis(dimethylamino-2-yl-ethyl)amido)binaphthyl-di-lithium ([(R)-**68**]).*

LiCH$_2$SiMe$_3$ (3.7 equiv.) was added to a solution of (*R*)-**54** in benzene. This was added to a solution of **S3** (10 equiv.) in benzene (Eq. 2-8). The hydroamination reaction was allowed to proceed at 22°C, then was frozen at -27°C for several weeks and was then slowly warmed to room temperature due to an unexpected freezer failure. Bright orange crystals of (*R*)-**68** suitable

for X-ray diffraction were obtained. The ORTEP diagram of (*R*)-**68** is shown in Figure 2-6, selected bond lengths, bond angles and dihedral angles are tabulated in Table 2-3.

$$\text{(2-8)}$$
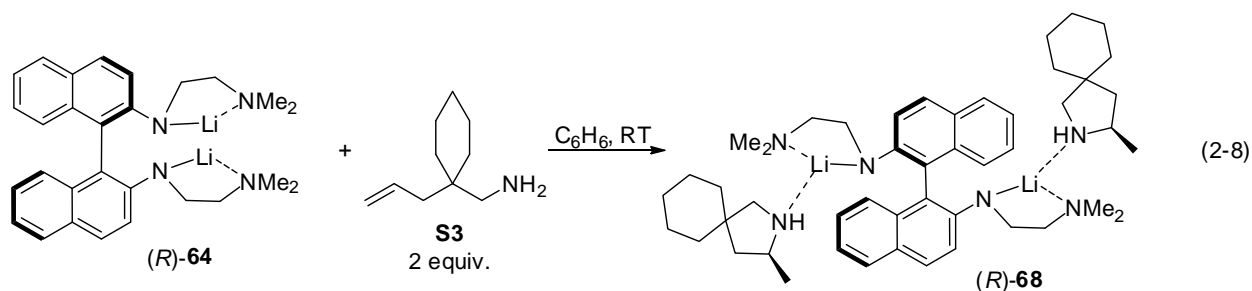
(*R*)-**68** contains 2 lithium atoms in identical coordination environments. Li1 is bound to one amido nitrogen (Li1a-N1a 1.936(5) Å), two amine nitrogens (Li1a-N2a 2.133(5) Å, Li1a-N3a 2.016(5) Å), and forms an η^1 interaction with the π system of one naphthyl ring (Li1a···C3b 2.635(5) Å). Li1a is also in close proximity to C2b and C4b (Li1a···C2b 2.817 Å; Li1a···C4b 2.936 Å) however, these terminal bond distances are longer than the internal Li1a···C3b contact ruling out an η^3 assignment.
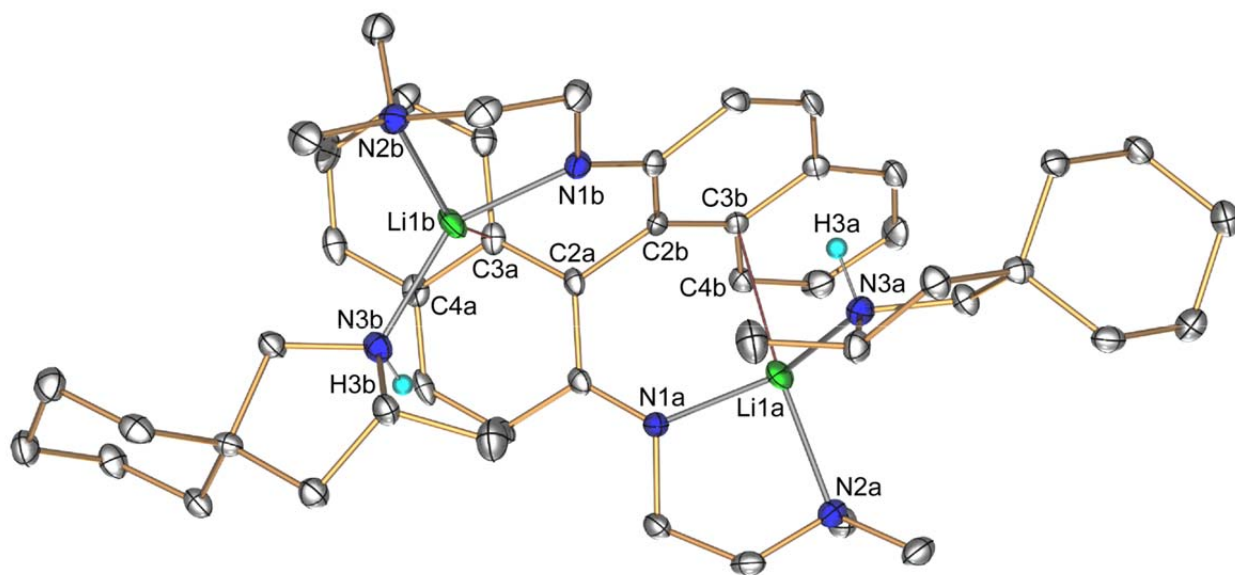
Figure 2-6. ORTEP diagram of the molecular structure of (*R*)-**68** (top view). Thermal ellipsoids are shown at the 50% probability level and hydrogens, except for H3a and H3b are omitted for clarity.

Table 2-3. Selected bond lengths, Li···C(π) interatomic distances (≤ 3.0 Å) and dihedral angles (°) for (*R*)-**68**.

Bond Lengths			
Li1a-N1a (amido)	1.936(5)	Li1a···C3 (π)	2.635(5)
Li1a-N2a (amine)	2.133(5)	Li1a···C2 (π)	2.817
Li1a-N3a (amine)	2.015(5)	Li1a···C4 (π)	2.936
Dihedral Angles			
N2b-C12b-C11b-N1b (sidearm)		48.15	
C1b-C2b-C2a-C1a		113.68	
C3b-C2b-C2a-C3a		108.38	
Mean Planes		64.85	

2.3.4 *Molecular Structure of (rac)-(Bis(diethylamino-2-yl-ethyl)amido)binaphthyl-di-lithium ([(rac)-65]).*

Yellow-orange crystals of (*rac*)-**65** suitable for X-ray diffraction were obtained from a reaction mixture of LiCH$_2$SiMe$_3$ (2 equiv.) with (*rac*)-**55** in benzene after 2 weeks at 22°C. Two independent monomeric molecules, (*rac*)-**65A** and (*rac*)-**65B** are located within the unit cell. The conformation of these molecules is similar, but slight variation in the coordination environments on each of their lithium atoms is different. A single puckered ring containing two amido ligands bridging two lithium atoms is found within each monomer. This feature is commonly observed in aggregated lithium salts, and is present in the structure of [(*R*)-**67**]$_2$ and in the previously reported [(*S,S,S*)-**25**]$_2$.[4]

The ORTEP diagram of (*rac*)-**65A** is shown in Figure 2-7, selected bond lengths, bond angles and dihedral angles are tabulated in Table 2-4. (*rac*)-**65A** contains lithium atoms in similar, albeit slightly different coordination environments. Li1 is bound to two amido nitrogens (Li1-N1 1.880(4) Å, Li1-N3 2.102(4) Å) and one amine nitrogen (Li1-N2 2.068(4) Å). Additional stabilization occurs through an η^3-aza allyl interaction with N3 and the adjacent π system of the naphthyl ring (Li1···C11 2.661Å, Li1···C12 2.272(4) Å). Li2 is also bound to two amido nitrogens (Li2-N3 1.898(4) Å, Li2-N1 2.131(4) Å) and one amine nitrogen (Li2-N4 2.109(4) Å). A similar η^3-aza allyl interaction with N1 and its adjacent naphthyl ring is also observed (Li2···C1 2.287(4) Å, Li2···C10 2.635(4) Å).

The ORTEP diagram of (*rac*)-**65B** are shown in Figure 2-8, selected bond lengths, bond angles and dihedral angles are tabulated in Table 2-5. (*rac*)-**65B** also contains lithium atoms in similar, albeit slightly different coordination environments. Li3 is bound to two amido nitrogen (Li3-N5 1.880(4) Å, Li3-N7 2.090(4) Å) and one amine nitrogen (Li3-N6 2.073(4) Å). Additional stabilization occurs through an η^3-aza allyl interaction with N7 and the adjacent π system of the naphthyl ring (Li3···C43 2.667Å, Li3···C44 2.293(4) Å). Li4 is also bound to two amido nitrogens (Li4-N7 1.896(4) Å, Li4-N5 2.146(4) Å) and one amine nitrogen (Li4-N8 2.099(4) Å). A similar η^3-aza allyl interaction with N5 and the adjacent π system of the naphthyl ring is also observed (Li4···C33 2.270(4) Å, Li4···C42 2.619(4) Å).

The shortest Li-N(amido) bonds reported in these structures occur in (*rac*)-**65**. The sidearm torsion angles are 38.4° and 47.6° for (*rac*)-**65A** and 35.9° and 48.2° for (*rac*)-**65B**. The angle between planes of the naphthyl rings of (*rac*)-**65A** (65.8°) and (*rac*)-**65B** (66.4°) are small compared to the other similar complexes.
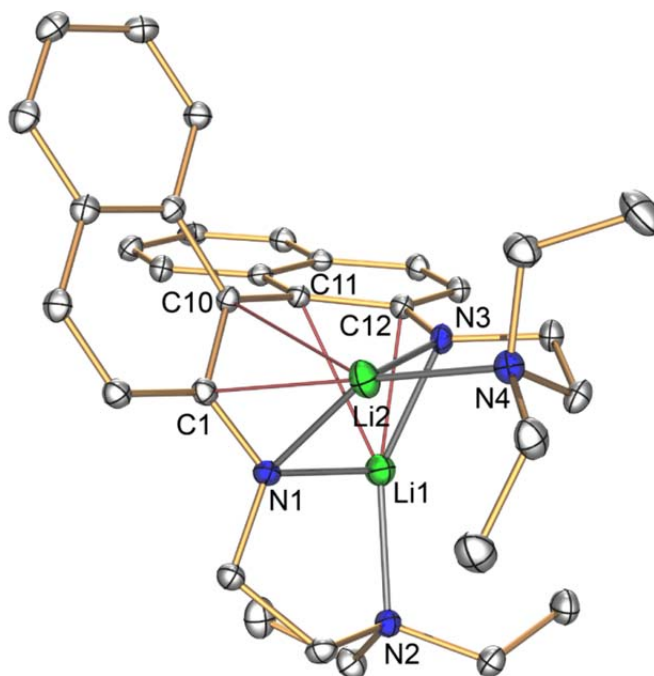
Figure 2-7. ORTEP diagram for the molecular structure of (*rac*)-**65A** (side view). Thermal ellipsoids are shown at the 50% probability level and hydrogens are omitted for clarity.
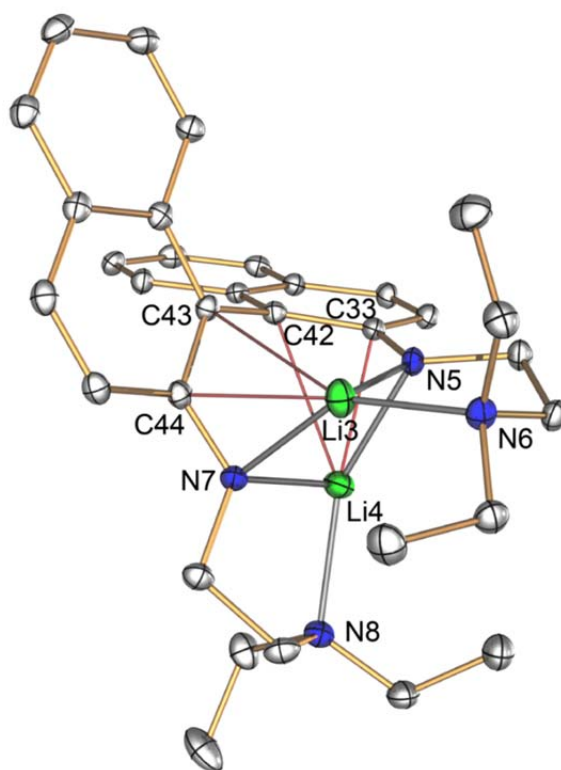
Figure 2-8. ORTEP diagram for the molecular structure of (*rac*)-**65B** (side view). Thermal ellipsoids are shown at the 50% probability level and hydrogens are omitted for clarity.

Table 2-4. Selected bond lengths, Li···C(π) interatomic distances (≤ 3.0 Å) and dihedral angles (°) for (*rac*)-**65A**.

Bond Lengths			
Li1-N1 (amido)	1.880(4)	Li1···C11 (π)	2.661
Li1-N3 (amido)	2.102(4)	Li1···C12 (π)	2.272(4)
Li2-N1 (amido)	2.131(4)	Li2···C1 (π)	2.287(4)
Li2-N3 (amido)	1.898(4)	Li2···C10 (π)	2.635
Li1-N2 (amine)	2.068(4)		
Li2-N4 (amine)	2.109(4)		

Dihedral Angles	
N1-C21-C22-N2 (sidearm)	38.4(2)
N3-C27-C28-N4 (sidearm)	47.6(2)
C9-C10-C11-C20	60.6(2)
C1-C10-C11-C12	72.3(2)
Mean Planes	65.78

Table 2-5. Selected bond lengths, Li···C(π) interatomic distances (≤ 3.0 Å) and dihedral angles (°) for (*rac*)-**65B**.

Bond Lengths			
Li3-N5 (amido)	1.880(4)	Li3···C43 (π)	2.677
Li3-N7 (amido)	2.090(4)	Li3···C44 (π)	2.293(4)
Li4-N5 (amido)	2.146(4)	Li4···C33 (π)	2.270(4)
Li4-N7 (amido)	1.896(4)	Li4···C42 (π)	2.619
Li3-N6 (amine)	2.073(4)		
Li4-N8 (amine)	2.099(4)		

Dihedral Angles	
N5-C53-C54-N6 (sidearm)	35.9(2)
N7-C59-C60-N8 (sidearm)	48.2(2)
C41-C42-C43-C52	61.1(2)
C33-C42-C43-C44	71.9(2)
Mean Planes	66.40

2.3.5 *Molecular Structure of (rac)-(Bis(piperidin-2-yl-ethyl)amido)binaphthyl-di-lithium* ([(*rac*)-**66**]).

LiCH$_2$SiMe$_3$ (2 equiv.) was added to a solution of (*rac*)-**56** in benzene and pentane was added by vapor diffusion over 1–2 days. Yellow-orange crystals of (*rac*)-**66** suitable for x-ray diffraction grew at 22°C over 1–3 weeks. The ORTEP diagram of (*rac*)-**66** are shown in Figure 2-9, selected bond lengths, bond angles and dihedral angles are tabulated in Table 2-6.

(*rac*)-**66** is monomeric and contains two pseudo tetrahedral lithium atoms in distinct coordination environments. Li1 interacts with one amido nitrogen (Li1-N1 1.929(2) Å), one piperidine nitrogen (Li1-N2 2.058(2) Å) and is bound η^2 to the adjacent aromatic rings (Li1-C11 2.333(2) Å; Li1-C20 2.449(2) Å). Two additional carbon atoms (C12 and C15) are slightly more remote at the borderline of a bonding interaction. Li2 interacts with one amido nitrogen (Li2-N3 1.915(2) Å) and one piperidine nitrogen (Li2-N4 2.114(2) Å), and is bound η^2 to other amido and its adjacent aromatic ring (Li2-C2 2.377(2) Å, Li2-N1 2.050(2) Å). Close proximity of Li2 to C1 is observed (Li2-C1 2.809 Å).

The increased steric bulk on the chelating amine of (*rac*)-**66** slightly weakened the Li-N(amido) bonds, and increased the sidearm torsional angles (53.7°, 54.2°). These angles are much closer to those observed in the dimeric species [(*S,S,S*)-**25**]$_2$,[4] as is the angle between the planes of the naphthyl rings (*rac*)-**65** (85.7°).
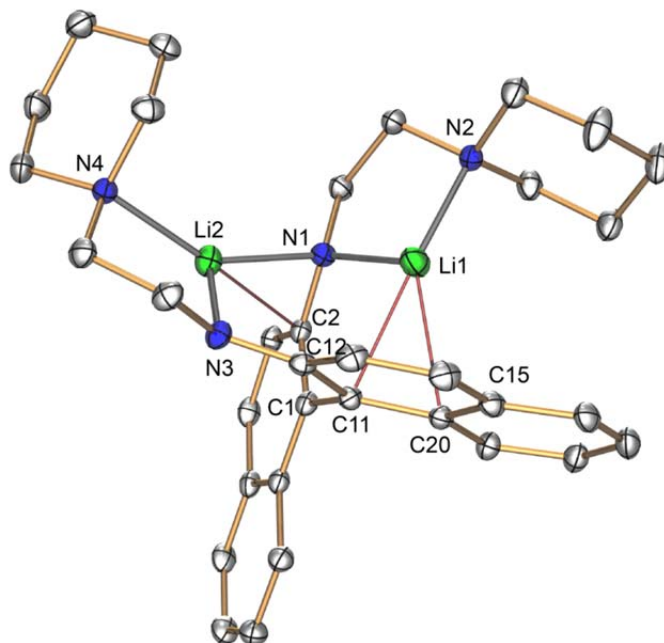
Figure 2-9. ORTEP diagram for the molecular structure of (*rac*)-**66** (side view). Thermal ellipsoids are shown at the 50% probability level and hydrogens are omitted for clarity.

Table 2-6. Selected bond lengths, Li···C(π) interatomic distances (≤ 3.0 Å) and dihedral angles (°) for (*rac*)-**66**.

Bond Lengths			
Li1-N1 (amido)	1.929(2)	Li1···C11 (π)	2.333(2)
Li2-N1 (amido)	2.050(2)	Li1···C20 (π)	2.449(4)
Li2-N3 (amido)	1.915(2)	Li2···C2 (π)	2.377(2)
Li1-N2 (amine)	2.058(2)	Li1···C12 (π)	2.702
Li2-N4 (amine)	2.114(2)	Li1···C15 (π)	2.906
		Li2···C1 (π)	2.809

Dihedral Angles	
N1-C21-C22-N2 (sidearm)	53.65(11)
N3-C28-C29-N4 (sidearm)	54.21(11)
C2-C1-C11-C12	79.86(11)
C10-C1-C11-C20	81.72(11)
Mean Planes	85.34

2.3.6 *Molecular Structure of (R)-(Bis(methoxy-2-yl-ethyl)amido)binaphthyl-di-lithium* ([(R)-**67**]₂).

Addition of LiCH₂SiMe₃ to (*R*)-**63** leads to the formation of a solid which is insoluble in benzene and toluene. A solution of LiCH₂SiMe₃ in benzene was layered over a solution of (*R*)-**63** in benzene. Overnight, orange solids formed at the interface containing X-ray quality crystals. The ORTEP diagram of [(*R*)-**67**]₂ is shown in Figure 2-10, selected bond lengths, bond angles and dihedral angles are tabulated in Table 2-7.

[(*R*)-**67**]₂ is dimeric and all four lithium atoms are separately equivalent and therefore situated in identical coordination environments. Each complex contains two N-Li-N-Li four membered cycles which hold the two ligands together. A total of eight lithium amide bonds hold together this dimer along with four Li-O interactions from each chelating sidearm. The N-Li-N-Li rings are puckered and stacked in a slightly staggered manner with each Li and N being stacked on one another, uniformly separated by a distance of 3.513 Å. The positioning of these rings is reminiscent of ring stacking interactions commonly observed in organolithium complexes, however distances separating Li and N do not exceed 2.0 Å.

Each lithium forms two amido bonds (Li1a-N1d 2.028(3) Å, Li1a-N1a 2.225(3) Å) with the one being slightly lengthened by a chelating interaction with the oxygen on the sidearm (Li1a-O1a 1.886(3) Å). An η^2 interaction forms with the π system on one ligand (Li1a-C3b 2.506 Å; Li1a-C2b 2.231 Å), with an additional carbon atom in close proximity (Li1a-C1b 2.697(3) Å). Two carbon atoms (Li1a-C1d 2.822 Å, Li1a-C2d 2.908 Å) on the opposite naphthyl ring are in close proximity to Li1a, however, they are beside the ring and outside of the π electron cloud.

The insolubility of this complex in non-coordinating solvents including benzene and toluene distinguish it from the related complexes [(*S,S,S*)-**25**]$_2$, [(*R*)-**64**]$_2$, (*R*)-**65**, (*R*)-**66**. Insolubility is a common phenomenon observed in organolithium chemistry and is often attributed to the formation of oligomers and polymers upon metalation. Examination of intermolecular contacts within several unit cells did not reveal any interaction unique to this system. [(*R*)-**67**]$_2$ is held together by more and stronger inter-ligand interactions than related dimers [(*S,S,S*)-**25**]$_2$ and [(*R*)-**64**]$_2$, possibly as a result of lack of steric bulk on the chelating sidearm. Because of these strong bonds, dissociation of this complex into a soluble monomeric species likely does not occur in non-coordinating solvents.
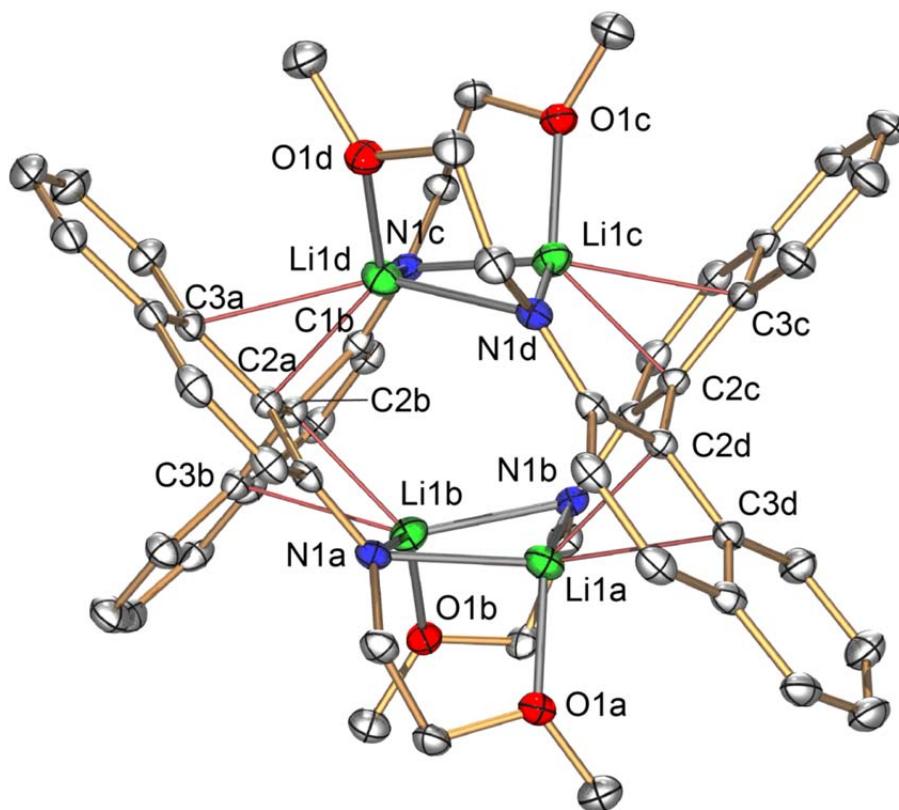
Figure 2-10. ORTEP diagram for the molecular structure of [(*R*)-**67**]$_2$ (side view). Thermal ellipsoids are shown at the 50% probability level and hydrogens are omitted for clarity.

Table 2-7. Selected bond lengths, Li···C(π) interatomic distances ($\leq$ 3.0 Å) and dihedral angles (°) for [(*R*)-**67**]$_2$.

Bond Lengths			
Li1d-O1d	1.886(3)	Li1d···C1a (π)	2.697(3)
Li1d-N1c (amido)	1.929(3)	Li1d···C2a (π)	2.231
Li1d-N1d (amine)	2.058(3)	Li1d···C3a (π)	2.506
		Li1d···C1b (π)	2.822
		Li1d···C2b (π)	2.908
Dihedral Angles			
N1-C11-C12-O1 (sidearm)		62.11(15)	
C1a-C2a-C2b-C1b		108.26	
C3a-C2a-C2b-C3b		92.78	
Mean Planes		83.85	

2.5 Solution Studies on Precatalyst components and mixtures

2.5.1 Introduction

It is widely accepted that organolithium reagents are powerful bases capable of acting as nucleophiles when conditions are tailored to allow it. Less known and understood are their solution structures and which variables affect them. The solution structures of lithium reagents with and without Lewis basic solvents have been studied. Low temperature NMR of isotopically labelled compounds, the method of continuous variation (Job plots) and DFT studies have allowed chemists to probe their structures. DOSY-NMR[34] has recently emerged as a tool for the assessment of aggregation in lithium amides/alkyls[35] and bimetallic lithium containing superbases.[36] The interaction of these bases and reagents with substrates is even less understood. Their high reactivity requires the use of rapid inject NMR or *in situ* IR spectroscopy[37] because the reaction timescale does not lend itself to traditional kinetic studies.

Organolithium typically exist as mixtures of aggregates while in solution, where higher aggregates can dissociate into monomeric species and/or lower aggregates (Eq. 2-9).

(2-9)
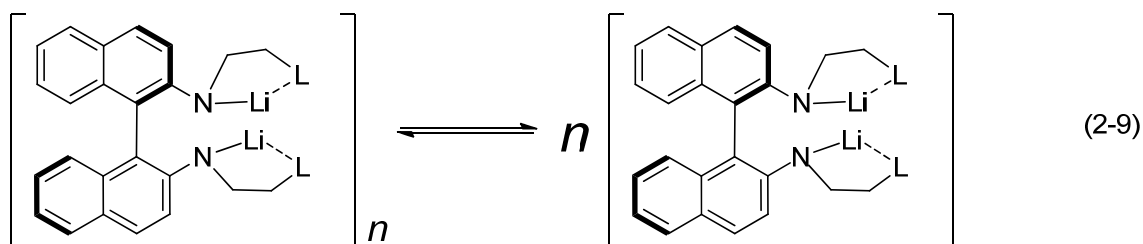
2.5.2 DOSY Study

DOSY NMR is a pseudo two dimensional NMR experiment which allows the diffusion of a molecule in solution to be observed. The attenuation rate of a given signal can be plotted according to the diffusion coefficient which is proportional the compounds size based on the Stokes-Einstein equation (Eq. 2-10). The frictional coefficient (f) is variable based on molecular geometry and for spherical molecules is given by Eq. 2-11.

$$D = \frac{k_b\,T}{f} = \frac{k_b\,T}{6\pi\,\eta\,r_s} \qquad (2-10)$$

Where: D = diffusion coefficient, k_b = Boltzmann's constant, T = temperature (K)

$$f = 6\,\pi\,\eta\,r_s \qquad (2-11)$$

Where: η = viscosity; r_s = hydrodynamic radius or Stokes radius

Substitution of the experimental diffusion coefficient and the solvent viscosity into this equation produces the hydrodynamic radius of the compound.[34] Discrepancies in the density and viscosity of unknown solutions compared with pure solvents are a major source of error when using this approach.[35e] An experimentally determined solution viscosity is often used and can minimize this error.[34c] To compensate for method and instrumental errors, Williard has established an alternate approach, formula weight prediction by internal reference.[35e] This method has been used to study lithium amides, alkyls and bimetallic lithium containing superbases.[36]

DOSY analysis of the ligands and dilithium salts discussed herein was performed (Table 2-8). The objective was to understand the aggregation of these complexes during catalytic experiments. Experiments were performed at catalytic concentrations of ≤ 0.03 M. Data for each experiment was analyzed using both the Stokes-Einstein equation and formula weight prediction

by internal reference. The internal standards cyclooctene (COE), tetradecene (TDE) and squalene (SQU) were included and these experiments were performed using a non-convection corrected pulse sequence (Varian, Dbppste). For the Stokes-Einstein calculation, the viscosity of benzene was used rather than the experimentally determined solution viscosity.

DOSY analysis of H_2-(*S*,*S*,*S*)-**25** and [(*S*,*S*,*S*)-**25**]$_2$ revealed hydrodynamic radii of 8.79 and 11.25 Å respectively.[5] The related ligands (*R*)-**54** and (*rac*)-**54** demonstrated smaller molecular volumes (*R*-**54** 6.78 ± 0.29 Å, *rac*-**54** 6.03 ± 0.18 Å) and fomula weights averaged slightly lower than their theoretical weight (*R*-**54** 418 ± 27, *rac*-**54** 381 ± 10, theoretical 427). The hydrodynamic radii of the dilithium salts for these complexes are smaller than in the previously reported complex, and an increase of approximately 30% is observed upon metalation ([(*R*)-**64**]$_2$ 8.73 ± 0.21 Å, [(*rac*)-**64**]$_6$ 8.75 ± 0.15 Å). The fomula weights for the complexes demonstrated aggregation ([(*R*)-**64**]$_2$ 669 ± 26, [(*rac*)-**64**]$_6$ 637 ± 18, theoretical 439). These results suggest aggregation for both of these complexes and a similarity in their solution structure. The aggregation numbers vary based on the method used to process the data, with values between 1.4 and 2.1. This could indicate the presence of a monomer-dimer equilibrium at room temperature for both of these complexes.

Related complexes (*R*)-**65** and (*R*)-**66** are monomeric in the solid state due to increased steric bulk on their chelating sidearm amines. The molecular volume of (*R*)-**55** (3.80 ± 0.12 Å) and formula weight (355 ± 23, theoretical 483) are lower than expected. The monomeric structure exhibited in the solid state by this complex is long and narrow, and not spherical shaped. DOSY spectroscopy observes the translational motion of a molecule therefore results often reflect the width of complex rather than its length. It has been postulated that a different frictional coefficient is more appropriate for smaller molecules, although $6\pi \, \eta \, r_s$ is used in most DOSY studies.[34b] The dilithium salt of this ligand demonstrated an increase in volume ((*R*)-**65** 5.75 ± 0.2 Å), and formula weight ((*R*)-**65** 441 ± 27, theoretical= 495) upon lithiation. The ~20% increase in molecular volume is similar to that observed with H_2-(*S*,*S*,*S*)-**25** and [(*S*,*S*,*S*)-**25**]$_2$[5] and experimental formula weights are closer to theoretical values than those of the free ligand. Another momoneric species in the solid state, the free ligand (*R*)-**56** and dilithium salt (*R*)-**66** had statistically insignificant different hydrodynamic radii (*R*-**56** 5.93 ± 0.15 Å, (*R*)-**66** 5.44 ± 0.29 Å) and formula weights (*R*-**56** 434 ± 18, theoretical= 507; (*R*)-**66** 445 ± 39, theoretical = 519). The DOSY study of complexes (*R*)-**65** and (*R*)-**66** strongly suggests the presence of monomeric

species in solution. This is consistent with their solid state structures and caused by the steric bulk on the coordinating amine groups which prevent aggregation.

It should be noted that the rigid binaphthyl ligand scaffold accounts for half of these compounds molecular weights, and are structurally different from the flexible aliphatic standards used in previous studies.[38] The chiral ligands used by Williard were more flexible and similar in structure to these catalysts.

Table 2-8. Results of DOSY study at 25°C.

(*rac*)-**54**, mw = 426.6

δ (ppm)	FW_{avg} (g·mol^{-1})^a	$R_{H\text{-avg.}}$ (Å)^b
7.9–7.79	372 ± 10	6.01 ± 0.11
7.35–7.21	375 ± 18	6.04 ± 0.19
7.17–7.07	375 ± 13	6.04 ± 0.13
4.42–4.40	387 ± 10	6.17 ± 0.11
3.01–2.90	391 ± 11	6.21 ± 0.11
2.01–1.90	358 ± 14	5.85 ± 0.16

(*rac*)-**64**, mw = 438.46, $r_{crystal}$ = 11.6 Å

δ (ppm)	FW_{avg} (g·mol^{-1})^a	Agg. #^{c}	$R_{H\text{-avg.}}$ (Å)^b	Agg. #
7.76–7.65	619 ± 17	1.41 ± 0.04	8.59 ± 0.15	2.02 ± 0.04
7.16–7.14	654 ± 7	1.49 ± 0.02	8.89 ± 0.06	2.12 ± 0.01
6.89–6.80	642 ± 15	1.46 ± 0.04	8.80 ± 0.14	2.09 ± 0.03
3.12–3.02	655 ± 17	1.49 ± 0.04	8.90 ± 0.15	2.12 ± 0.04

(*R*)-**54**, mw = 426.6

δ (ppm)	FW_{avg} (g·mol^{-1})^a	$R_{H\text{-avg.}}$ (Å)^b
7.85–7.28	395 ± 24	6.51 ± 0.27
7.16–7.02	393 ± 7	6.49 ± 0.08
4.37–4.34	399 ± 0	6.56 ± 0.00
2.95–2.86	391 ± 5	6.47 ± 0.05
1.69–1.56	444 ± 8	7.06 ± 0.09

(*R*)-**64**, mw = 438.46, $r_{crystal}$ = 8.4 Å

δ (ppm)	FW_{avg} (g·mol^{-1})^a	Agg. #^{c}	$R_{H\text{-avg.}}$ (Å)^b	Agg. #^{c}
7.75–7.64	655 ± 16	1.49 ± 0.04	8.62 ± 0.14	2.05 ± 0.03
7.14–6.79	688 ± 22	1.57 ± 0.05	8.89 ± 0.18	2.12 ± 0.04
3.14–3.05	694 ± 18	1.58 ± 0.04	8.94 ± 0.15	2.13 ± 0.04
1.58–1.55	643 ± 17	1.47 ± 0.04	8.52 ± 0.14	2.03 ± 0.03

(R)-**55**, mw = 482.70

δ (ppm)	FW$_{avg}$ (g·mol^{-1})^a	R$_{H\text{-avg.}}$ (Å)^b
7.91–7.79	332 ± 8	3.68 ± 0.04
7.37–7.22	337 ± 19	3.70 ± 0.10
7.16–7.06	365 ± 13	3.85 ± 0.06
4.62–4.60	377 ± 18	3.91 ± 0.09
2.96–2.91	378 ± 11	3.91 ± 0.05
2.27–2.15	369 ± 9	3.87 ± 0.05
2.07–1.97	331± 14	3.67 ± 0.07
0.59–0.55	333 ± 2	3.68 ± 0.01

(R)-**65**, 494.57, r$_{crystal}$ = 6.2 Å

δ (ppm)	FW$_{avg}$ (g·mol^{-1})^a	R$_{H\text{-avg.}}$ (Å)^b
7.87–7.69	414 ± 19	5.55 ± 0.14
7.36–7.08	417 ± 28	5.58 ± 0.21
6.92–6.86	440 ± 21	5.74 ± 0.15
3.43–3.21	468 ± 14	5.95 ± 0.10
2.54–2.47	463 ± 10	5.91 ± 0.07
2.22–2.09	434 ± 26	5.70 ±0.19
1.95–1.86	436 ± 15	5.72 ± 0.11
1.68–1.57	440 ± 12	5.75 ± 0.08
0.55–0.31	445 ± 13	5.79 ± 0.09

(R)-**56**, mw = 506.72

δ (ppm)	FW$_{avg}$ (g·mol^{-1})^a	R$_{H\text{-avg.}}$ (Å)^b
7.93–7.80	416 ± 12	5.78 ± 0.09
7.34–7.22	421 ± 19	5.82 ± 0.15
7.15–7.04	437 ± 9	5.96 ± 0.07
4.73–4.71	440 ± 10	5.97 ± 0.08
3.00–2.92	452 ± 17	6.07 ± 0.13
2.26–2.13	431 ± 17	5.90 ± 0.14
1.99–1.90	436 ± 23	5.94 ± 0.19
1.17–0.98	440 ± 22	5.97 ± 0.18

(R)-**66**, mw = 518.59, r$_{crystal}$ = 6.3Å

δ (ppm)	FW$_{avg}$ (g·mol^{-1})^a	R$_{H\text{-avg.}}$ (Å)^b
7.87–7.66	406 ± 14	5.15 ± 0.10
7.17–7.16	465 ± 10	5.58 ± 0.08
6.89–6.86	413 ± 18	5.19 ± 0.14
3.44–3.23	465 ± 23	5.58 ± 0.16
2.29–2.21	484 ± 20	5.72 ± 0.14
1.79–1.69	484 ± 13	5.72 ± 0.09

(a) **R$_{H\text{-avg.}}$** = Average hydrodynamic radius for the range of chemical shifts determined using the Stokes-Einstein equation. (b) **FW$_{avg}$** = Average formula weight for the range of chemical shifts determined by substitution of diffusion coefficients into a standard curve. Standard deviations are calculated using the stdev.p function in Microsoft Excel = SQRT (Σ (X-X$_{MEAN}$)^2)/n) which assumes that the arguments are the

entire population. (c) **Agg. #** = Aggregation number. For Agg. # of FW$_{avg}$ values, the experimental FW$_{avg}$ was divided by the theoretical FW for a monomer. For Agg. # of R$_{H\text{-avg.}}$ values, the r$_H$ experimental was divided by the longest radius present in a related crystal structure.[39] For (*R*)-**64** and (*rac*)-**64**, the radius for [(*R*)-**64**]$_2$ was used and values were multiplied by two.

DOSY Results for (*S,S,S*)-**25** at 30°C[5]

	R$_H$ (Å)
Ligand	8.79
Complex	11.25

2.5.3 Variable Temperature DOSY-NMR

DOSY NMR has been used as a tool to assess the aggregation and size of molecules in solution and experiments are typically performed at ambient temperatures.[34] Gschwind has studied phosphoramidate ligands and their transition metal coordination compounds by DOSY-NMR at low temperatures (-93°C to -3°C; 180-270 K).[40] Temperature dependent aggregation trends were reported. Williard has studied chiral lithium amides by DOSY-NMR using diffusion coefficient-formula weight (D-fw) correlation analysis revealing the presence of mixed aggregates at ambient temperatures.[35a,e] Williard used a mixture of internal standards[38] that were included with each sample and the formula weight of the complex was obtained from a plot of log(D) versus log(fw).[41]

A VT-DOSY NMR study of complexes (*R*)-**64** and (*rac*)-**64** was performed to assess their aggregation at low temperatures. Two different pulse sequences were used, one corrected for convection (Dbppste_cc) while the other was uncorrected (Dbppste). The convection corrected DOSY pulse sequence allowed the data to be processed using both the methods of Williard and Gschwind. The non-convection corrected data was only processed using the method of Gschwind. For these experiments, a linear relationship between diffusion coefficient and formula weight for the standards was not observed.

The DOSY study with a non-convection corrected pulse sequence (Table 2-9, 2-10) and data workup as described by Gschwind (See Chapter 4.9) resulted in unreasonably low hydrodynamic radii below ambient temperature ((*rac*)-**64** 2.83±0.05 Å (-55°C), 1.84±0.05 Å (-30°C), 1.67±0.01 Å (0°C); (*R*)-**64** 3.83±0.37 Å (-55°C), 2.76±0.16 Å (-30°C), 2.65±0.05 Å (0°C)). Convection can increase a compounds movement, causing its diffusion coefficient to increase. The diffusion coeffient is inversely proportional to the hydrodynamic radius of a compound based on the Stokes Einstein equation. Therefore artifically low hydrodynamic radii

are expected and this data accounts for the use of a convection corrected pulse sequence in the Gschwind study. However, the results at amibient temperature are inconsistent from those discussed herein (*rac*)-**64** 10.48±1.72 Å (25°C); (*R*)-**64** 6.74±0.54 Å (25°C), see Table 2-10). Data analysis within the Gschwind study corrected diffusion coefficients for temperature and viscosity using a viscosity correction factor ($\eta_{CAT-298}$ / $\eta_{BLANK-298}$) which was determined by dividing D (diffusion coefficient) for TMS in the sample measured at 298K by D for TMS in a blank sample at 298 K. These values had a signficiant difference, which accounts for the differences between both complexes in this study.

$$\eta_{CAT-298} / \eta_{BLANK-298} \ (R)\text{-}\mathbf{64} \text{ at } 0.0284 \text{ M in toluene-d}_8) = 1.25$$

$$\eta_{CAT-298} / \eta_{BLANK-298} \ (rac)\text{-}\mathbf{64} \text{ at } 0.0259 \text{ M in toluene-d}_8) = 0.82$$

Our previous room temperature DOSY study[5] demonstrated a small difference in the hydrodynamic radii of (*rac*)-**64** and (*R*)-**64** at 25°C, with minimal statistical significance. In this study, (*rac*)-**64** was consistently larger than (*R*)-**64** by 10–200% with values varying based on chemical shift. The hydrodynamic radii for (*rac*)-**64** were similar to those obtained using traditional DOSY data analysis, albeit slightly higher and with a larger range.

When a convection corrected pulse sequence was used (Table 2-11), the results at low temeperature using Gschwind data analysis were also unreasonable ((*rac*)-**64** 108±6 Å (-55°C); (*R*)-**64** 203±17 Å (-55°C)). The hydrodynamic radii for data obtained at room temperature was significantly more reasonable, although different from that obtained using the standard Stokes-Einstein equation ((*rac*)-**64** 12.6±1.1 Å (25°C); (*R*)-**64** 10.2±1.3 Å (25°C)). These values are higher than those in Table 2-8 and the standard deviations are much larger. When a diffusion coefficient-formula weight (D-fw) correlation analysis was applied to the same data set, more realistic values were obtained ((*rac*)-**64** 638±78 (25°C), 1139±141 (-55°C); (*R*)-**64** 772±215 (25°C), 938±112 (-55°C)). These results were also in closer agreement with those found in Table 2-8 although the standard deviations are larger and the range of final values is broader. At low temperature (-55°C) the molecular weights are higher than those observed at room temperature, which suggests an increase in average aggregation state. The presence of many aggregation states could account for the large standard deviations found here, and separation of this data based on aggregation number could generate more statistically significant results.

Table 2-9. Results of VT-DOSY study on [0.02590 M] (*rac*)-**64** using non-convection corrected pulse sequence (Varian, Dbppste).

δ (ppm)	$R_{H-avg.}$ (Å) -55°C	$R_{H-avg.}$ (Å) -30°C	$R_{H-avg.}$ (Å) 0°C	$R_{H-avg.}$ (Å) 25°C
7.7–7.5	2.78 ± 0.07	1.79 ± 0.09	1.66 ± 0.09	9.83 ± 0.49
7.3–7.0	2.88 ± 0.03			9.44 ± 0.44
7.00–6.98				9.12 ± 0.58
6.96–6.64	2.81 ± 0.09	1.89 ± 0.04	1.68 ± 0.05	9.85 ± 0.49
3.36–2.95	2.89 ± 0.03			10.35 ± 0.16
2.28–2.19	2.88 ± 0.03			8.76 ± 0.34
1.65–1.63				12.20 ± 0.36

Table 2-10. Results of VT-DOSY study on [0.02835 M] (*R*)-**64** using a non-convection corrected pulse sequence (Varian, Dbppste).

δ (ppm)	$R_{H-avg.}$ (Å) -55°C	$R_{H-avg.}$ (Å) -30°C	$R_{H-avg.}$ (Å) 0°C	$R_{H-avg.}$ (Å) 25°C
7.68–7.49	3.88 ± 0.10	2.74 ± 0.09	2.65 ± 0.34	6.90 ± 0.27
7.31–7.22	3.83 ± 0.09	2.91 ± 0.10		
7.11–6.95	3.46 ± 0.12	2.60 ± 0.10		6.77 ± 0.56
6.96–6.67	3.64 ± 0.10	2.70 ± 0.11	2.64 ± 0.21	7.28 ± 0.24
6.68–6.64				6.20 ± 0.10
3.36–3.34	4.20 ± 0.03			
3.11–2.95				7.74 ± 0.21

Table 2-11. Results of VT-DOSY study using the convection corrected pulse sequence.

(*rac*)-**64**, 0.02590 M, 25°C, Dbppste_cc			
δ (ppm)	Gschwind $R_{H-avg.}$	Williard FW_{avg}	Williard Agg. #
7.66–7.51	11.5 ± 0.7	560 ± 51	1.3 ± 0.1
7.09–7.05	13.7 ± 0.8	715 ± 56	1.6 ± 0.1
6.80–6.67	11.8 ± 0.5	579 ± 34	1.3 ± 0.1

(*rac*)-**64**, 0.02590 M, -55°C, Dbppste_cc

δ (ppm)	Gschwind $R_{H\text{-avg.}}$	Williard FW_{avg}	Williard Agg. #
7.66–7.65	113.8 ± 17.1	1279 ± 399	2.9 ± 0.9
6.85–6.68	102.4 ± 8.7	998 ± 185	2.3 ± 0.4

(*R*)-**64**, 0.02835 M, 25°C, Dbppste_cc

δ (ppm)	Gschwind $R_{H\text{-avg.}}$	Williard FW_{avg}	Williard Agg. #
7.64–7.52	8.9 ± 1.5	557 ± 226	1.3 ± 0.5
7.10–7.01	11.4 ± 2.0	986 ± 415	2.3 ± 1.0
6.81–6.72	9.3 ± 0.7	587 ± 92	1.3 ± 0.2
3.05–2.99	11.4 ± 1.4	962 ± 282	2.2 ± 0.3

(*R*)-**64**, 0.02835 M, -55°C, Dbppste_cc

δ (ppm)	Williard FW_{avg}	Agg. #
7.67–7.53	1049 ± 196	2.4 ± 0.5
7.00–6.97	865 ± 157	2.0 ± 0.4
6.87–6.66	826 ± 154	1.9 ± 0.4
3.35–3.32	973 ± 118	2.2 ± 0.3

2.5.4 Characterization of the Precatalyst by ^{7}Li and ^{1}H VT-NMR

As discussed in Chapter 2.7, kinetic analysis of the hydroamination/cyclization of **S3** with the dilithium salt (*R*)-**64** indicates a first order rate dependence on catalyst and **S3**. A first order rate dependence on excess $LiCH_2SiMe_3$ was also observed, with saturation occurring when excess base is present beyond one equivalent with respect to (*R*)-**64**. The rate enhancing effects of excess base have previously been documented, although the nature of the effect remains ambiguous.[6] This kinetic data suggests the presence of three lithium atoms within the rate limiting transition state, more specifically one dilithium salt interacting with the lithium salt of **S3** ((*R*)-**70**, Figure 2-11). A precatalytic mixture of (*R*)-**64** and 1.0 equivalent excess base can be illustrated as (*R*)-**69** (Figure 2-11).[42] Precatalytic mixtures containing (*R*)-**64** in the presence of 0.0–2.0 equivalents of excess $LiCH_2SiMe_3$ were studied by variable temperature ^{7}Li and ^{1}H NMR (0.0 equiv. see Figures 2-12 & 2-13; 0.5 equiv. see Figures A-28 & A-29; 1.0 equiv. see Figures 2-14 & 2-15; 1.5 equiv. see Figure A-30 & A-31; 2.0 equiv. see Figure A-32 & A-33).

Figure 2-11. Left: Precatalyst (*R*)-**69**, formed by combining (*R*)-**64** with LiCH$_2$SiMe$_3$ (1.0 equiv.). Right: Based on kinetic studies (Chapter 2.7) (*R*)-**70** illustrates the components found in the rate limiting transition state for the hydroamination/cyclization of **S3** with (*R*)-**64** and excess LiCH$_2$SiMe$_3$.

The DOSY studies discussed in the previous sections (2.5.2 and 2.5.3) and the observation of broad signals in the ^{1}H NMR spectra of the dilithium salt (*R*)-**64** at ambient temperatures (25°C) suggest the presence of rapidly exchanging mixed aggregates. After addition of 0.5 equivalents of LiCH$_2$SiMe$_3$ to (*R*)-**64** the proton signals become sharper in the ^{1}H NMR spectra, and up to 5 different signals are observed in the ^{7}Li NMR spectra. The presence of 1.0 equivalent of LiCH$_2$SiMe$_3$ with (*R*)-**64** leads to further sharpening of the proton signals and one major signal is observed in the ^{7}Li spectra. The methyl signals of the pure catalyst form broad multiplets from 1.75-1.00 ppm at low temperatures. Addition of 1.0 equivalent of base leads to two sharp overlapping singlets at 1.75 ppm and additional sharpening and downfield shifts are observed for the signals of the sidearm methylene and the aromatic rings. The sharpening of these signals can be attributed to deaggregation and/or a decrease in fluxional behavior, while the deshielding can be caused by proximity to an additional metal center and/or diamagnetic anisotropy. The presence of additional base leads to more non-equivalent signals in the ^{1}H and ^{7}Li NMR spectra and indicates a more complex mixture of aggregates which suggests that excess base facilitates deaggregation by formation of a new mixed aggregate, (*R*)-**69**.

Figure 2-12. VT-NMR (^{1}H) spectra of (*R*)-**64** without excess LiCH$_2$SiMe$_3$.
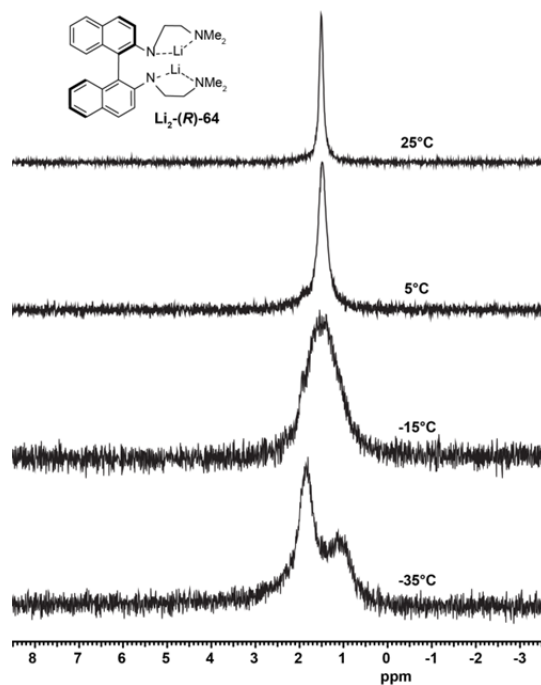
Figure 2-13. VT-NMR (^{7}Li) spectra of (*R*)-**64** without excess LiCH$_2$SiMe$_3$.
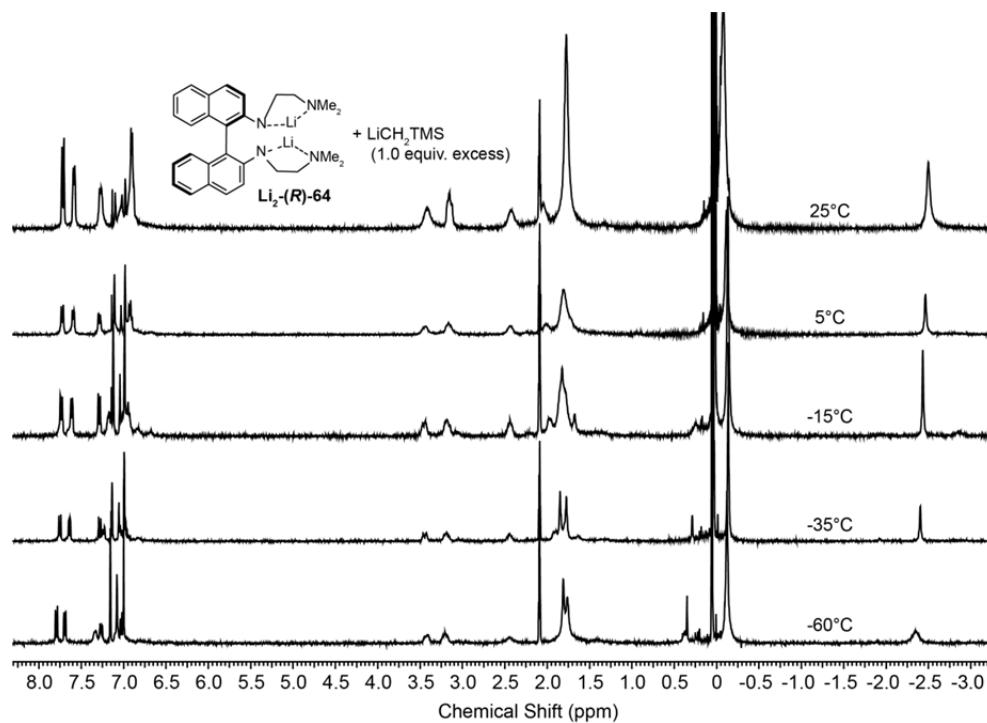
Figure 2-14. VT-NMR (^{1}H) spectra of (*R*)-**64** and 1.0 equivalent of excess LiCH$_2$SiMe$_3$.
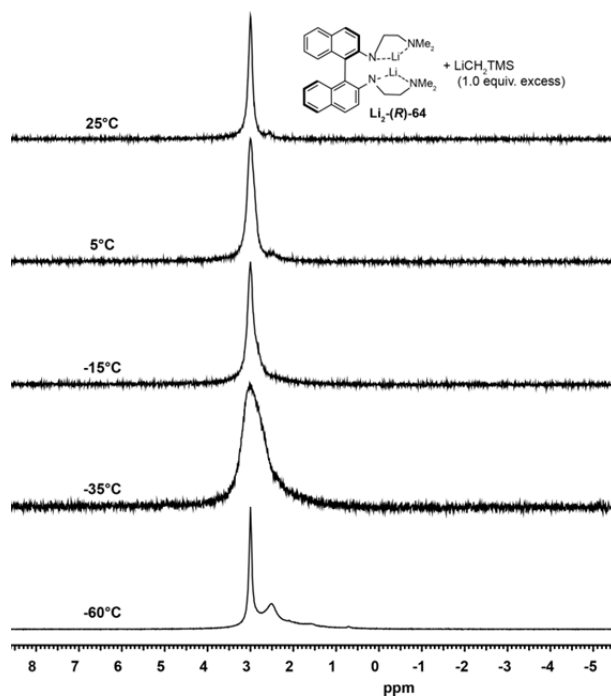
Figure 2-15. VT-NMR (^{7}Li) spectra of (*R*)-**64** and 1.0 equivalent of excess LiCH$_2$SiMe$_3$.

2.6 Intramolecular Hydroamination

2.6.1 Introduction

Intramolecular hydroamination catalysts are often model systems aimed at the development of reagents for intermolecular transformations. Aminopentene is considered a benchmark substrate for intermolecular hydroaminations because it lacks *gem*-dialkyl or diaryl activating substituents, and cyclization of this substrate at ambient temperatures indicates an active system (Eq. 2-13). Catalysts, which cannot perform the transformation, are often regarded as having limited utility. Elimination of the Thorpe-Ingold effect allows the intrinsic activity of a given catalyst to be observed, and systems which cyclize aminopentene at ambient temperature often demonstrate activity in intermolecular hydroaminations. Current research interest is shifting towards catalytic systems which function intermolecularly because the intramolecular cyclization of aminoalkenes is well developed.

$$\text{(2-13)}$$
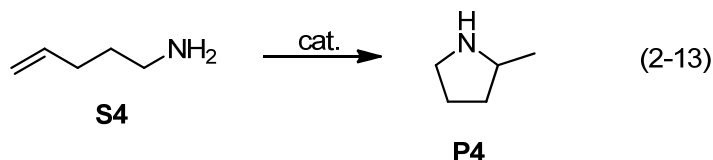
Rare earth metal based catalysts are the most studied, the most selective and the most active for intramolecular hydroamination. Cyclization of aminopentene with these reagents has been documented at ambient temperatures on multiple systems (Table 2-12, Figure 2-16) with the majority of examples being reported at 60–100°C. Lanthanocene systems have demonstrated the highest activity for this cyclization with binaphtholate rare earth metal complexes producing the highest enantioselectivities.[43]

(R)-**71** Ar = Ph
(R)-**72** Ar = 3,5-Me$_2$C$_6$H$_3$

(R)-**73** E=CH
(R)-**74** E=N

La[N(SiMe$_3$)$_2$]$_3$
75

(S)-**76** M=Sm; R* = (−)-menthyl

77

(S)

(R)

R* =

(+)-neomenthyl
(S)-**78** Ln =La; E=CH
(R)-**79** Ln =La; E=N
(R,S)-**80** Ln =Nd; E=CH
(R,S)-**81** Ln =Sm; E=CH
(S)-**82** Ln =Sm; E=N
(R)-**83** Ln =Sm; E=CH,N
(R,S)-**84** Ln =Y; E=CH
(R)-**85** Ln =Y; E=N
(R,S)-**86** Ln =Lu; E=CH

R* =

(−)-menthyl
(S)-**87** Ln =Sm; E=N
(R)-**88** Ln =Y; E=N,CH
(S)-**89** Ln =Sm; E=N
(R)-**90** Ln =Sm; E=N

R* =

(−)-phenylmenthyl
(R)-**91** Ln =Y; E=CH
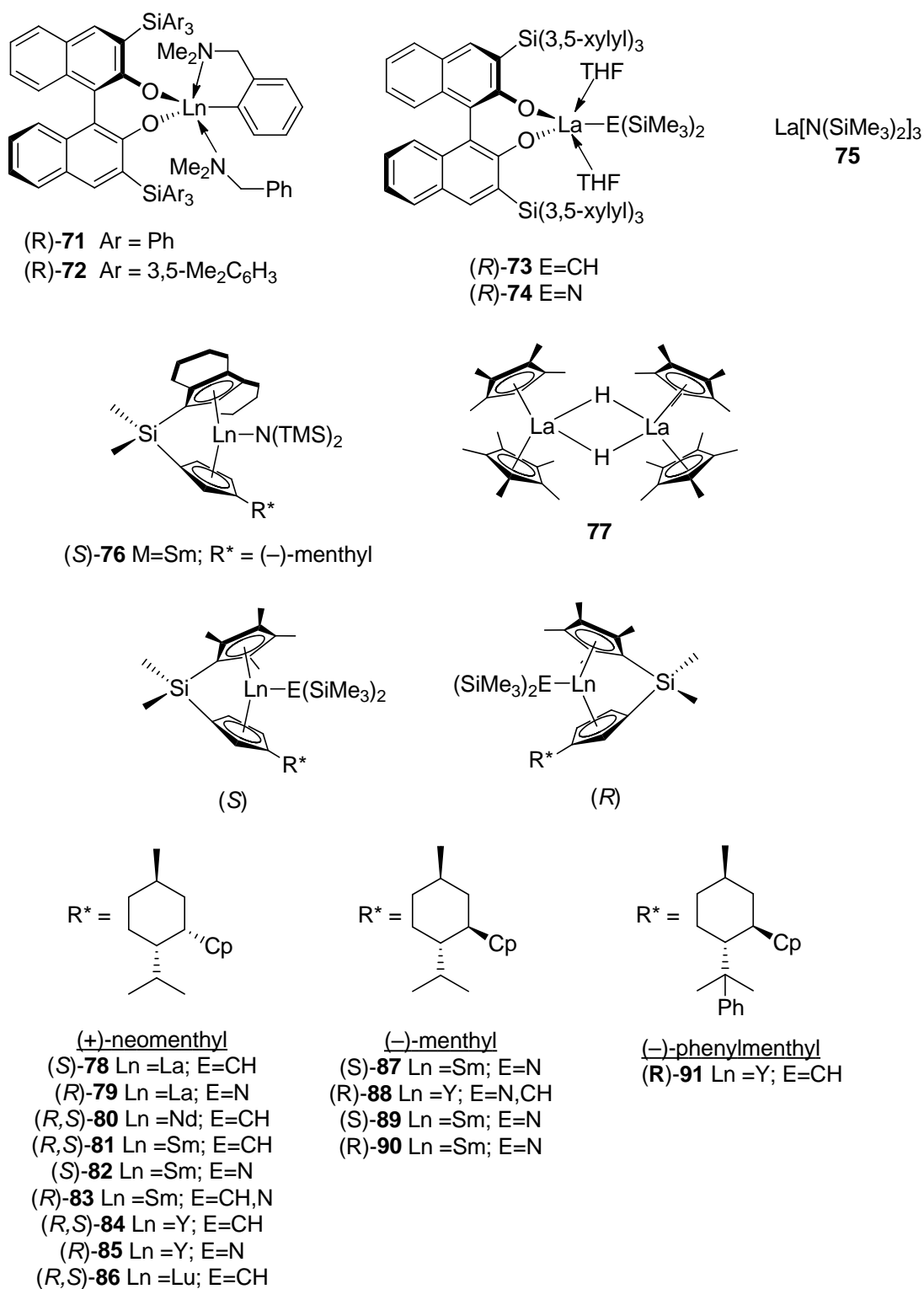
Figure 2-16. Rare earth metal-based catalysts which have completed the intramolecular hydroamination/cyclization of aminopentene (**S4**) at or below 25°C.

Table 2-12. Documented examples of rare earth metal based cyclization of aminopentene (**S4**) at or below 25°C.
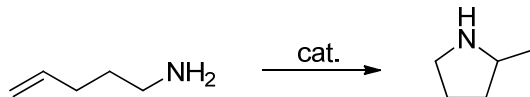
Entry	Cat.	Temp. (°C)	Time (hr.)	Conv.	*ee*	N_t (h^{-1})	Reference
1	**71**-Y	22	24 h	≥ 98	69		43d
2	**72**-Y	22	20 h	≥ 98	83		43d
3	**75**-La	23			40	0.09	43e
4	(*S*)-**87**-Sm	25			62	33	43b
5	(*S*)-**87**-Sm	0			72		43b
6	(*R*)-**88**-Y	25			69		43b
7	(*S*)-**76**-Sm	25			46	2.6	43f
8	**77**-La	25				13	43a
9	(*S*)-**78**-La	25			36		43b
10	(*R*)-**79**-La	25			31		43b
11	(*R,S*)-**80**-Nd	25			55	93	43b
12	(*R,S*)-**80**-Nd	0			64	11	43b
13	(*R,S*)-**81**-Sm	25			61	42	43b
14	(*S*)-**82**-Sm	25			55	33	43b
15	(*R*)-**83**-Sm	25			52	62	43b
16	(*R*)-**83**-Sm	0			58		43b
17	(*S*)-**89**-Sm	25			62	33	43b
18	(*S*)-**89**-Sm	0			72		43b
19	(*R*)-**90**-Sm	25			60		43b
20	(*R,S*)-**84**-Y	25			47		43b
21	(*R*)-**85**-Y	25			50		43b
22	(*R*)-**91**-Y	25			64		43b
23	(*R,S*)-**86**-Lu	25			29		43b
24	**72**-Lu	22	16.5	93	90	1.7	43c
25	**72**-Lu	0	190	92	92	0.13	43c

26	**71**-Y	25	24	95	70	2.6	43c
27	**72**-Y	22	20	94	83	2.2	43c
28	(*R*)-**73**-La	22	1.4	89	72	37	43c
29	(*R*)-**74**-La	22	5.5	95	71	≥ 33	43c

The cyclization of aminopentene has been mediated by catalysts from other portions of the periodic chart, although examples are far less common (Table 2-13, Figure 2-17), and many systems require heat to achieve conversion. Catalysts derived from groups 1,[3b,c] 2[44] and 4[45] have been reported, along with one late transition metal complex ($K_2[PtCl_4]$) in the presence of acid (0.01 M HCl, 1.99 M NaCl) at 60°C.[46] Systems derived from Group 4 metals currently have limited utility because high temperatures (110-150°C) are required for all but one catalyst, **99** which achieved 62% conversion at 23°C.[45d] The sterically congested chiral variant of this complex (**31**) demonstrated activity unparalleled by any Group 4 metal catalyst for *gem*-dialkyl-substituted substrates; however, cyclization of aminopentene was only achieved at 110°C in low yield.[45f]

Alkali and alkaline earth metal-based systems have demonstrated potential to effect this transformation, although olefin isomerization is a competing side reaction due to their high basicity. These systems are effective at the intermolecular anti-Markovnikov hydroamination of styrene derivatives which is often studied in lieu of intramolecular hydroamination. Achiral catalysts based on heavy alkali earth metals (Ca, Sr)[44b,c,d] have performed the cyclization at room temperature although their activity has not yet surpassed that of rare earth metal-based systems. A phenoxyamine magnesium catalyst produced 51% *ee* on this substrate at 80°C,[44f] making it the most selective published example of a non-rare earth metal catalyst for this transformation. *n*-Butyllithium is the only known alkali metal-based catalyst for this cyclization, but the reaction was sensitive with respect to the solvent used in the transformation. Conversion was observed at ambient temperatures, with full substrate consumption occurring at 50°C, but the resulting hydroamination product was contaminated with a mixture of isomerization products. A similar product distribution was observed with toluene as a solvent at 110°C. Selective formation of the hydroamination product was achieved in a mixed solvent system of THP and toluene (1:1) and high temperature (110°C) was required for conversion.[3c]
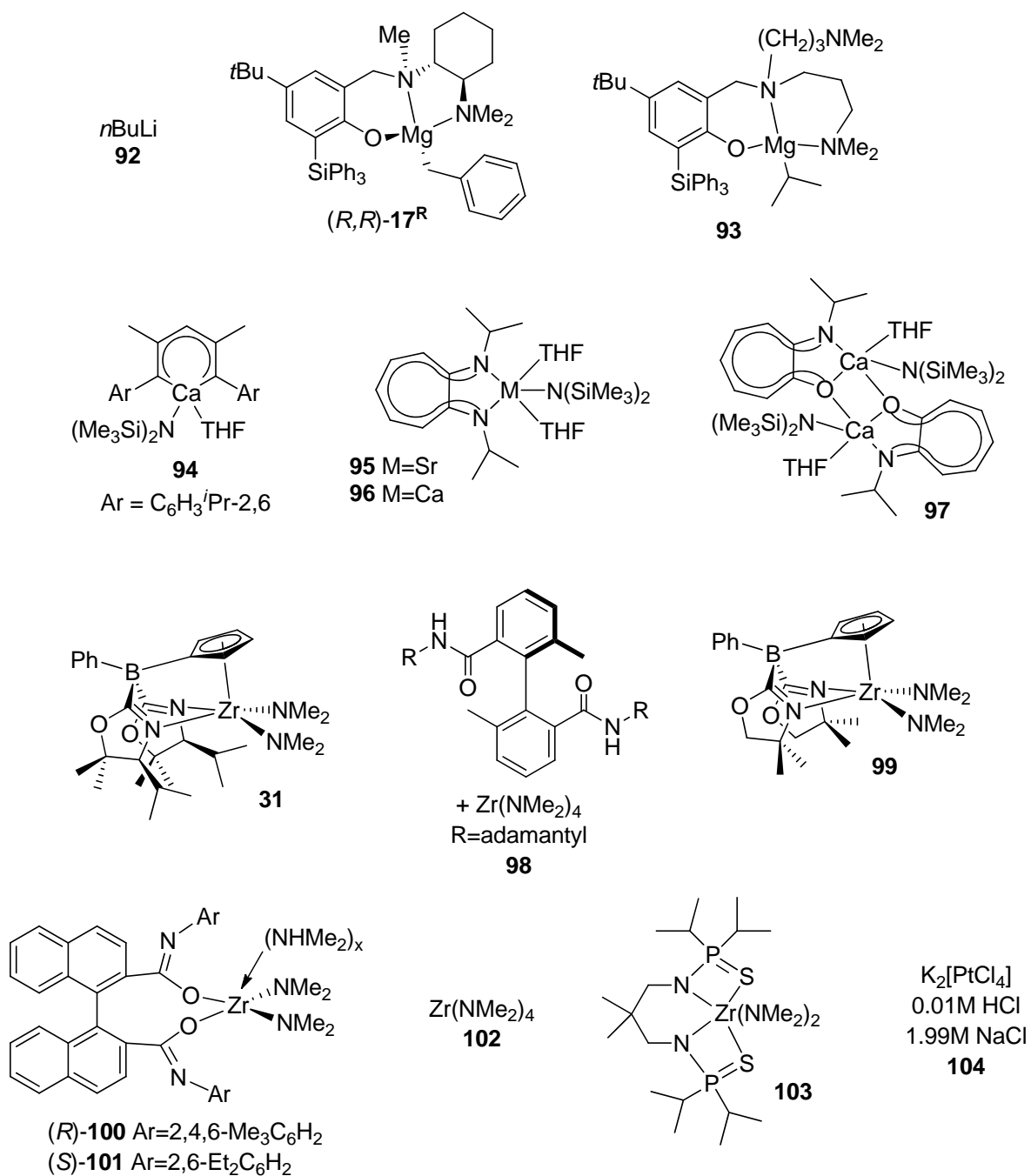
Figure 2-17. Alkali, alkaline earth, group 4 and late transition metal-based catalysts used in the intramolecular hydroamination/cyclization of aminopentene.

Table 2-13. Documented examples of aminopentene cyclization by non-rare earth metal based catalysts.
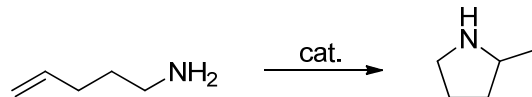
Entry	Cat.	Temp. (°C)	Time (h)	Conv.	*ee* (%)	Reference
1	**92**	110		95		3b
2	**92**	50		32		3c
3	(*R*,*R*)-**17**$^{\text{R}}$	80	72	81	51	44f
4	**93**	120	100	87		44e
5	**94**	25	21	90		44d
6	**95**	rt	72	70		44c
7	**95**	60	10	>90		44c
8	**96**	rt	40	>90		44a
9	**97**	110	10	>80		44a
10	**31**	110	5	24		45f
11	**98**	145	120	27		45e
12	**99**	23	33	62		45d
13	**100**	110	72	>95	6	45c
14	**101**	120	39	>95	7	45c
15	**102**	150	28	25		45b
16	**103**	120	41	89		45a
17	**103**	150	10	91		45a
18	**104**	60	168	67		46

Lithium amides are highly reactive bases and often applied under cryogenic conditions. Their use as nucleophiles is limited to activated substrates including Michael acceptors, dienes and styrene derivatives. Repulsion between the electron rich amido and alkene and the formation of stable aggregates in solution contributes to their lack of application to unactivated alkenes including the hydroamination of amino alkenes. Promising results have been reported on several lithium-based catalytic systems,[47] although the development and optimization of homogeneous

systems has not yet been achieved. The deduction of structure activity relationships is particularly challenging due to the complex behavior of these compounds in solution.

Accounts of dilithium diamidobinaphthyl catalyzed hydroamination have empirically demonstrated a rate enhancement by excess base although the nature of its role in this transformation is not well understood.[6] Previous studies have demonstrated good to moderate activity among diamidobinaphthyl dilithium salts even in the presence of L-donor solvents. The influence of the substituent on the diamidobinaphthyl sidearm seems to have a significant impact on enantioselectivity. Chelating sidearms of minimal steric bulk have yielded the highest enantioselectivities,[4] while bulky, non-coordinating substituents have produced minimal levels of stereoinduction with the exception of one substrate.[6a]

2.6.2 Results and Discussion

Dilithium salts (*R*)-**64**, (*R*)-**65** and (*R*)-**66** were tested in the presence of various amounts of excess LiCH$_2$TMS[48] (0.2 and 0.6 equivalents excess with respect to dilithium salt). Under these conditions some of the substrate-catalyst combinations produced slightly lower enantioselectivities as the amount of excess base was increased. Catalysts (*R*)-**64**, (*R*)-**65** and (*R*)-**66** exhibit similar catalytic activity in the cyclization of **S1** (Table 2-14, entries 1-5) as the previously studied *S,S,S*-**25**. Excess base had a significant impact on reaction rate. Higher levels of base did not produce detrimental effects on enantioselectivity, although all enantioselectivities obtained with the new dilithium salts were lower than the 64-68% *ee* induced by *S,S,S*-**25**.[4] Enantioselectivities were inversely proportional to the steric bulk on the chelating sidearm.

The reaction rates and enantioselectivities for the hydroamination/cyclization of **S2** (Table 2-14, entries 6-13) showed the highest sensitivity towards the concentration of substrate and excess base for any substrate. The steric bulk on the chelating amine had a pronounced effect on reaction rate, particularly for (*R*)-**66**, although higher levels of excess base seemed to moderate its impact (Table 2-14, entries 11-13). Enantioselectivities were minimal at best and did not demonstrate a clear trend. (*R*)-**64** and (*R*)-**65** showed increased activity and decreased enantioselectivity when the concentration of base and substrate were increased (Table 2-14, entries 6-10). The enantioselectivities reported previously (48-58% *ee*) on a related dilithium diamidobinaphthyl containing bulky aliphatic non-coordinating sidearms stand in stark contrast to these results.[6a]

The highest reaction rates and enantioselectivities were observed with **S3**, a trend previously observed with S,S,S-**25**.[4] The enantioselectivities observed on this substrate were inversely proportional to the steric bulk on the chelating sidearm, as observed for **S1**. Higher levels of excess base increased reaction rates and had a detrimental effect of statistical significance on enantioselectivity for (*R*)-**65** and (*R*)-**66** but not for (*R*)-**64** at the concentrations studied (Table 2-14, entries 14–19).

For **S4**, catalyst activity was highly dependent on the addition of excess base with cyclization occurring as low as 40°C. With (*R*)-**64**, (*R*)-**65** and (*R*)-**66** lower amounts of excess base required higher temperatures to achieve conversion and reactions stalled prior to reaching completion (Table 2-14, entries 20, 23, 25). Reactions containing 1.0 equivalent of excess base (Table 2-14, entries 21, 24, 26) proceeded to >90% conversion with all catalysts at 40°C and achieved enantioselectivities between 50–64% *ee*. Enantioselectivities for this substrate were the second highest levels observed overall. This result demonstrates the potential of lithium reagents to perform intramolecular hydroamination/cyclization at near ambient temperatures with noteworthy levels of stereoinduction. The enantioselectivities induced on **S4** with (*R*)-**64** and (*R*)-**65** are the highest values for any non-rare earth metal based catalyst for this substrate. The activity of several achiral alkaline earth metal-based catalysts is higher,[44a,c,d] although completion of this reaction at 40°C by (*R*)-**64**, (*R*)-**65** and (*R*)-**66** and excess $LiCH_2SiMe_3$ ranks them among the most active non-rare earth metal-based catalysts.

Table 2-14. Intramolecular hydroamination/cyclization of primary aminoalkenes mediated by (R)-**64**, (R)-**65** and (R)-**66** and excess LiCH$_2$SiMe$_3$.

S1: R = Me
S2: R = Ph
S3: R = Cy
S4: R = H

P1: R = Me
P2: R = Ph
P3: R = Cy
P4: R = H
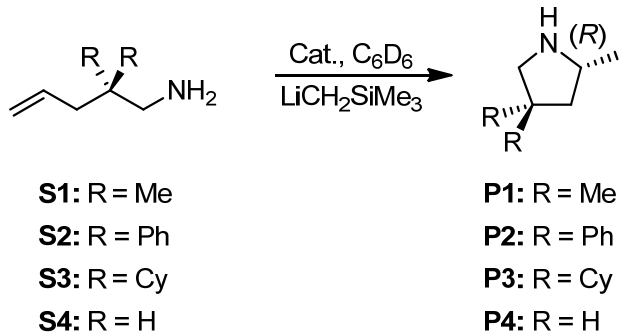
Entry #	Cat.	Cat. (mol%)	Sub.	LiCH$_2$SiMe$_3$ (eq. excess)	Temp. (°C)	Time hh:mm	Conv. %[a]	ee (%), R/S
1	(R)-**64**	10	**S1** (0.2)	0.2	22	53:15	98	58 (R)
2	(R)-**64**	11	**S1** (0.2)	0.6	22	19:00	97	55 (R)
3	(R)-**65**	9	**S1** (0.2)	0.2	22	37:05	100	48 (R)
4	(R)-**65**	10	**S1** (0.2)	0.6	22	25:00	98	46 (R)
5	(R)-**66**	10	**S1** (0.2)	0.6	22	24:55	96	36 (R)
6	(R)-**64**	9	**S2** (0.2)	0.2	40	530:20	71	4 (S)
7	(R)-**64**	10	**S2** (0.1)	0.6	22	2:12	94	2
8	(R)-**65**	10	**S2** (0.1)	0.2	22	168:00	42	24
9	(R)-**65**	9	**S2** (0.2)	0.2	22	73:55	99	18 (R)
10	(R)-**65**	10	**S2** (0.2)	0.6	22	2:05	98	10 (R)
11	(R)-**66**	9	**S2** (0.2)	0.2	60	72:00	97	7
12	(R)-**66**	10	**S2** (0.1)	0.2	40	312:40	76	8
13	(R)-**66**	10	**S2** (0.2)	0.6	22	3:35	97	15 (S)
14	(R)-**64**	10	**S3** (0.2)	0.2	22	3:00	100	67 (R)
15	(R)-**64**	10	**S3** (0.2)	0.6	22	1:03	95	64 (R)
16	(R)-**65**	10	**S3** (0.2)	0.2	22	2:05	100	57 (R)
17	(R)-**65**	10	**S3** (0.2)	0.6	22	1:10	100	53 (R)
18	(R)-**66**	10	**S3** (0.2)	0.2	22	22:50	98	46 (R)
19	(R)-**66**	9	**S3** (0.2)	0.6	22	2:20	100	38 (R)
20	(R)-**64**	10	**S4** (0.2)	0.2	100	101:00	50	66
21	(R)-**64**	10	**S4** (0.2)	1.0	40	183:45	91	64
22	(R)-**64**	10	**S4** (0.2)	2.0	40	70:24	75	51
23	(R)-**65**	8	**S4** (0.2)	0.2	60	118:00	66	42
24	(R)-**65**	10	**S4** (0.2)	1.0	40	183:30	95	56
25	(R)-**66**	8	**S4** (0.2)	0.2	100	217:20	70	33
26	(R)-**66**	10	**S4** (0.2)	1.0	40	165:35	93	50

a. Based on ^{1}H-NMR spectra, after purification of the product by distillation or column chromatography.

Substrates containing either secondary amines or internal alkenes were cyclized with all three catalysts (Table 2-15); however, conversions were low in many cases possibly because of

lower substrate concentrations. The *gem*-dimethyl-substituted substrate **S5** required elevated reaction temperatures and elongated reaction times, but conversions remained rather low (<50%). The *gem*-diphenyl-substituted substrate **S6** was cyclized at ambient temperature, although reaction times were long and conversions remained low as well. These trends are in agreement to the trends observed for primary amines. The phenyl-activated internal alkene substrates, **S7** and **S8** were cyclized as well, and *gem*-diphenyl-substituted **S8** allowed faster more complete cyclization than did *gem*-dimethyl **S7**. With diphenyl substrate **S8** a wide range in catalyst activity was observed between the three systems. Low activity is observed with (*R*)-**64** in the presence of a small amount of excess base (0.2 equivalents) as it is with **S2**. In both of these reactions (*R*)-**65** is more reactive with lower amounts of excess base, possibly due to a higher concentration of a monomeric precatalyst species. The catalysts were not screened at higher concentrations of excess base, and it is very likely that reactivity and selectivity would improve significantly if higher levels of excess base were used in this transformation.

These results are promising and indicate that alkali metal based catalysts have a broad substrate scope for intramolecular hydroamination/cyclization. Alkaline earth and rare earth metal-based catalyst systems demonstrate equally broad substrate scope. Neutral Group 4 metal-based catalyst systems cyclize exclusively primary amines, while cationic Group 4 complexes cyclize only secondary amines. The cyclization of substrates by late transition metal catalysts with primary or secondary amines and terminal olefins has been documented,[49] but the majority of intramolecular hydroaminations with these metals have involved more reactive aminoalkynes, aminoallenes and aminodienes.[1b,c] These substrates bind more readily to the late transition metal-based catalysts, which often enter the catalytic cycle by olefin activation.

Table 2-15. Intramolecular hydroamination/cyclization with substrates containing either secondary aminoalkenes or internal alkenes mediated by (*R*)-**64**, (*R*)-**65** and (*R*)-**66** and excess LiCH$_2$SiMe$_3$.
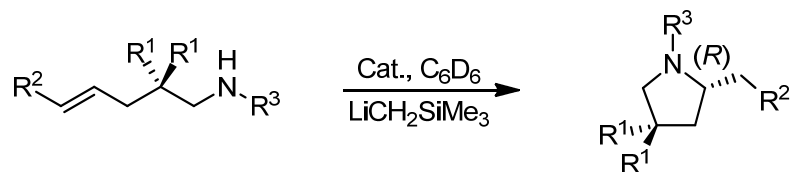
S5: R^1 = Me, R^2 = H, R^3 = Bn   **P5:** R^1 = Me, R^2 = H, R^3 = Bn

S6: R^1 = Ph, R^2 = H, R^3 = Bn   **P6:** R^1 = Ph, R^2 = H, R^3 = Bn

S7: R^1 = Me, R^2 = Ph, R^3 = H   **P7:** R^1 = Me, R^2 = Ph, R^3 = H

S8: R^1 = Ph, R^2 = Ph, R^3 = H   **P8:** R^1 = Ph, R^2 = Ph, R^3 = H

Entry #	Cat.	Cat. (mol%)	Sub. (mmol)	LiCH$_2$SiMe$_3$ (eq. excess)	Temp. (°C)	Time (hh:mm)	Conv. %[a]
1	(*R*)-**64**	10	**S5** (0.1)	0.2	60	146:00	43
2	(*R*)-**65**	10	**S5** (0.1)	0.2	60	109:10	42
3	(*R*)-**65**	10	**S5** (0.2)	0.2	60	183:55	36
4	(*R*)-**66**	10	**S5** (0.1)	0.2	100	216:55	0
5	(*R*)-**66**	10	**S5** (0.2)	0.2	60	183:35	47
6	(*R*)-**64**	10	**S6** (0.1)	0.2	22	70:50	57
7	(*R*)-**65**	10	**S6** (0.1)	0.2	22	82:55	57
8	(*R*)-**66**	10	**S6** (0.1)	0.2	22	48:45	56
9	(*R*)-**64**	5	**S7** (0.1)	0.2	80	330:10	38
10	(*R*)-**64**	10	**S7** (0.1)	0.2	60	167:25	45
11	(*R*)-**65**	5	**S7** (0.1)	0.2	60	206:35	60
12	(*R*)-**65**	10	**S7** (0.1)	0.2	40	167:30	45
13	(*R*)-**66**	5	**S7** (0.1)	0.2	80	163:50	61
14	(*R*)-**66**	10	**S7** (0.1)	0.2	60	167:35	78
15	(*R*)-**64**	5	**S8** (0.1)	0.2	22	382:50	68
16	(*R*)-**65**	5	**S8** (0.1)	0.2	22	1:10	90
17	(*R*)-**66**	5	**S8** (0.1)	0.2	40	95:50	96

a. Based on ^{1}H-NMR spectra, after purification of the product by distillation or column chromatography.

2.7 Kinetic Study of Intramolecular Hydroamination

2.7.1 Introduction

Although several systems for intramolecular lithium amide catalyzed hydroamination have been reported, kinetic studies have been disclosed on only for one system.[50] Mediation of this transformation by *n*-butyllithium and simple lithium amides has been documented.[3,8] Incorporation of chiral additives[4,6,9] and chiral chelating substrates[47b] have induced moderate to high enantioselectivities and diastereoselectivities while allowing reactions to occur under milder

conditions. The presence of a ligand accelerated[51] pathway could account for the high levels of stereoinduction.

The mechanisms of rare earth metal-catalyzed hydroamination are well understood and many catalysts are believed to proceed by σ bond metathesis.[52] A zero order dependence on substrate concentration suggesting rate limiting olefin insertion[43c,53] is often observed. The concurrent observation of a kinetic isotope effect (KIE) complicates the interpretation of these studies[53] and a similar effect has been observed for alkaline earth metal-based systems.[54,55] Rationalizations of these KIE's include the presence of a concerted non-insertive mechanism,[54] proton assistance from a proximal amine,[53] and substrate inhibition.[55] For the intramolecular cyclization of aminoalkenes, DFT studies have supported a σ-insertive mechanism with rate limiting protonolysis for alkaline earth metals[56] and rate limiting olefin insertion for rare earth metals.[57]

Similarities in the reactivity of Group 1–3 complexes exist due to their polar nature and the presence of one stable oxidation state. Because they cannot undergo oxidative addition and reductive elimination, their range of mechanistic options is somewhat limited. Very little precedence exists for the mechanisms of alkali metal-based hydroamination reactions,[58] particularly the intramolecular variant. The behavior of polar organometallic complexes for this transformation serves as a starting point for mechanistic considerations. The tendency of Group 1 and Group 2 metal-based complexes to undergo facile ligand redistribution processes[59] also adds difficulty to the understanding and elucidation of their behavior in solution.

2.7.2 Observed Rate Law

The hydroamination/cyclization of **S3** was studied to determine the empirical rate law (Eq. 2-14). In the presence of 2.5 mol% (*R*)-**64** and 0.5 equivalents excess LiCH$_2$SiMe$_3$ a first order rate dependence on substrate concentration was observed from 0.1416 M–0.5298 M (Figures 2-18, 2-19, A-3). Higher substrate concentrations did not lead to an increase in rate (0.6494 M) and the reaction did not proceed at a lower concentration (0.0766 M). A first order rate dependence on the concentration of (*R*)-**64** was observed in the presence of 0.5 and 1.0 equivalent excess LiCH$_2$SiMe$_3$ (0.5 equiv. – Figures 2-20, 2-21, A-19; 1.0 equiv. – Figures 2-22, 2-23, A-22). A similar system demonstrated observed first order dependence on catalyst and substrate which is in good agreement with these results.[5]

(2-14)
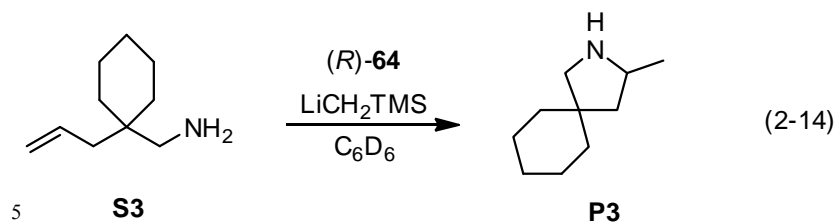
At catalyst loadings of 2.5, 5.0 and 7.5 mol% a first order rate dependence on excess $LiCH_2SiMe_3$ was also observed for up to 1.25–1.5 equivalents excess $LiCH_2SiMe_3$ with saturation or a decrease in rate occurring beyond this point (2.5 mol% catalyst – Figures 2-24, 2-25, A-6; 5.0 mol% catalyst – Figure A-7, A-10, A-11; 7.5 mol% catalyst – Figure A-12, A-15, A-16). The rate enhancing effects of excess base have previously been demonstrated.[6]

Figure 2-18. First order plot showing the consumption of **S3** in the hydroamination/cyclization with 2.5 mol% (*R*)-**64** and $LiCH_2SiMe_3$ (0.5 eq.) at various concentrations of **S3**.

Substrate Order
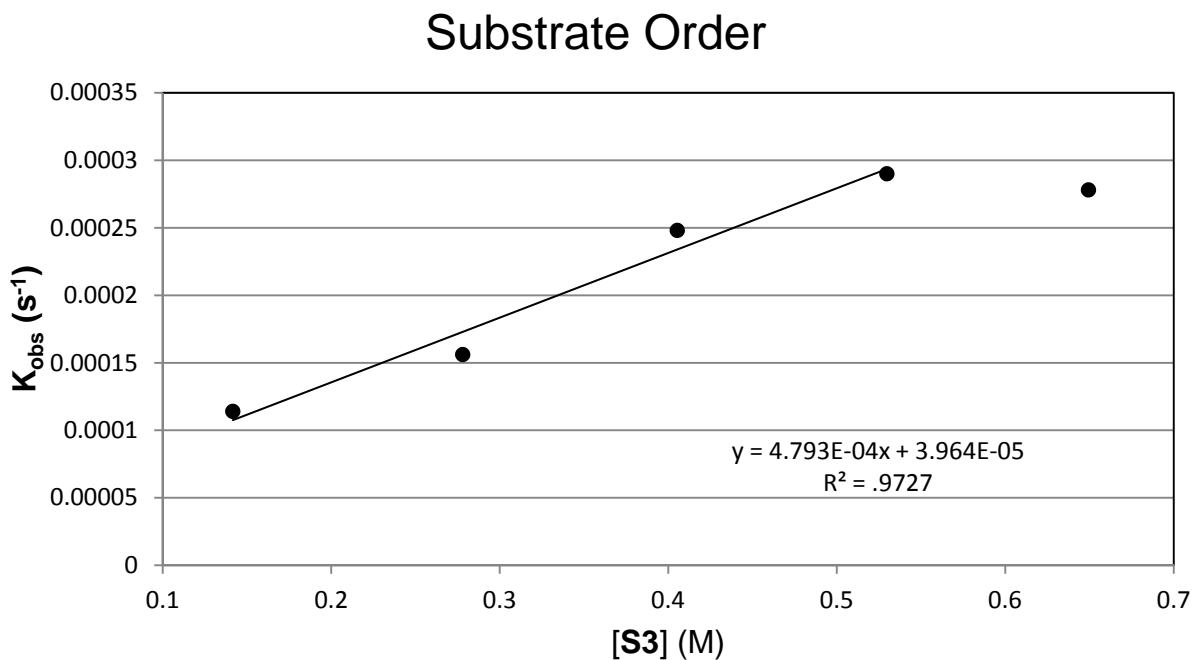
Figure 2-19. Plot of pseudo first order rate constants versus [**S3**] in the intramolecular hydroamination/cyclization of **S3** with 2.5 mol% (*R*)-**64** and LiCH$_2$SiMe$_3$ (0.5 eq.).
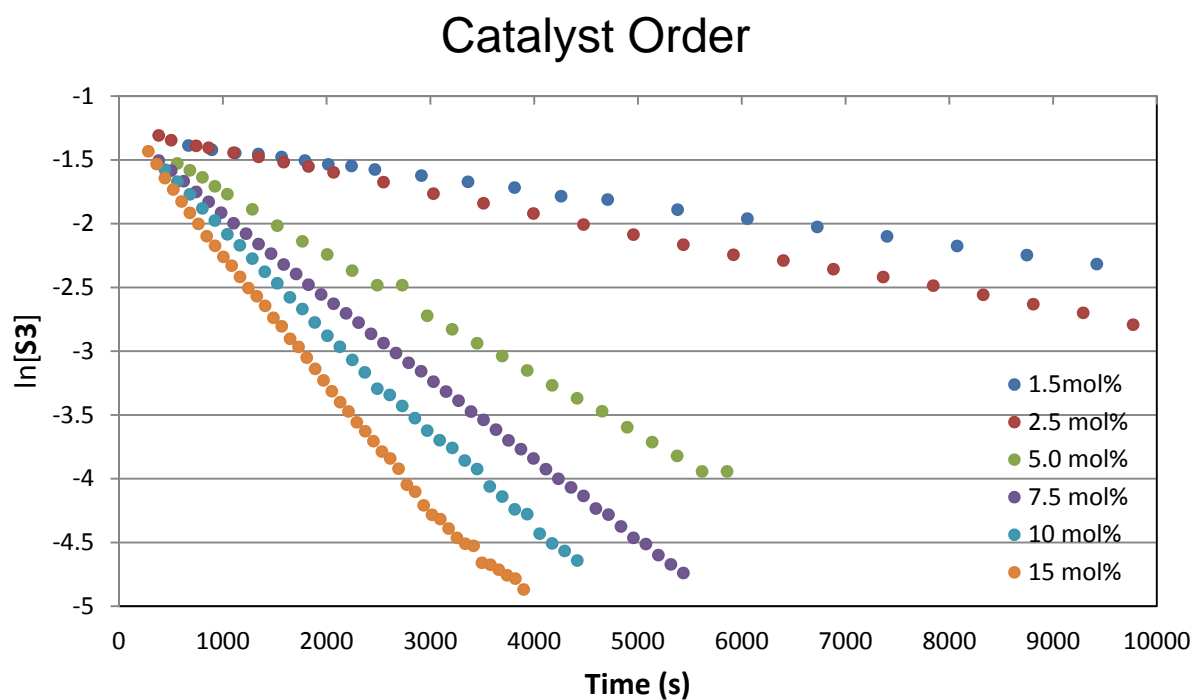
Catalyst Order

Figure 2-20. First order plot showing the consumption of **S3** in the hydroamination/cyclization with LiCH$_2$SiMe$_3$ (0.5 eq.), **S3** (0.28 M) at various catalyst loadings.
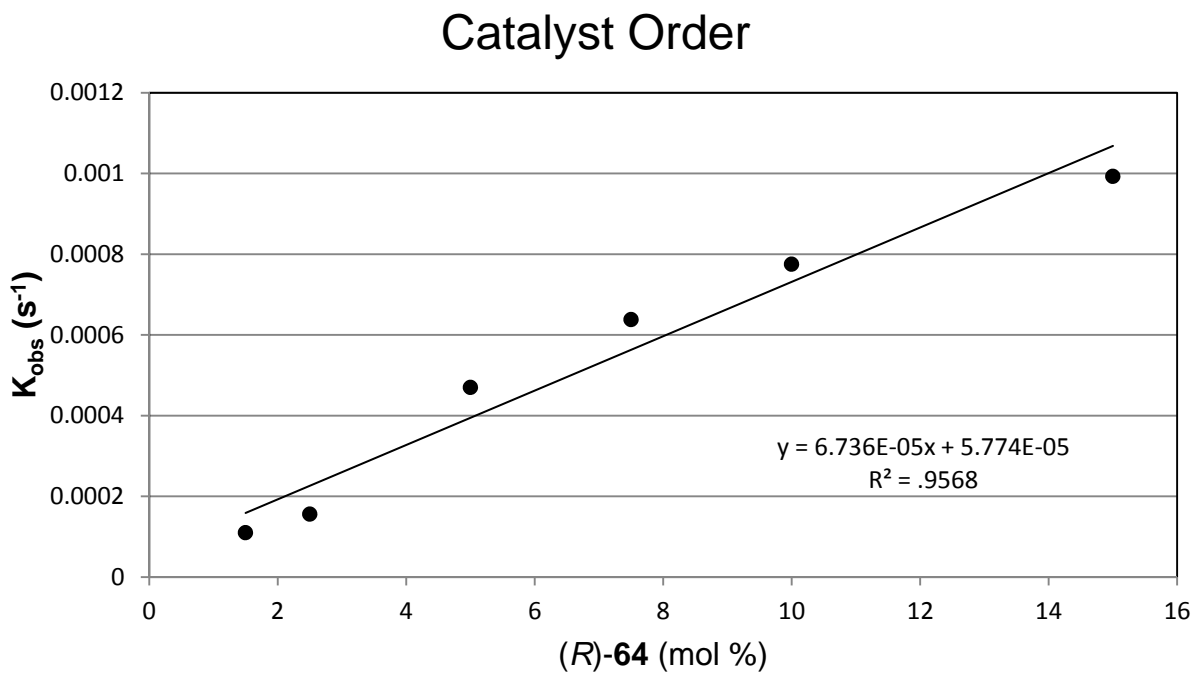
Figure 2-21. Plot of pseudo first order rate constants versus (R)-**64** (mol %) in the intramolecular hydroamination/cyclization of **S3** with $LiCH_2SiMe_3$ (0.5 eq.) and **S3** (0.28 M).
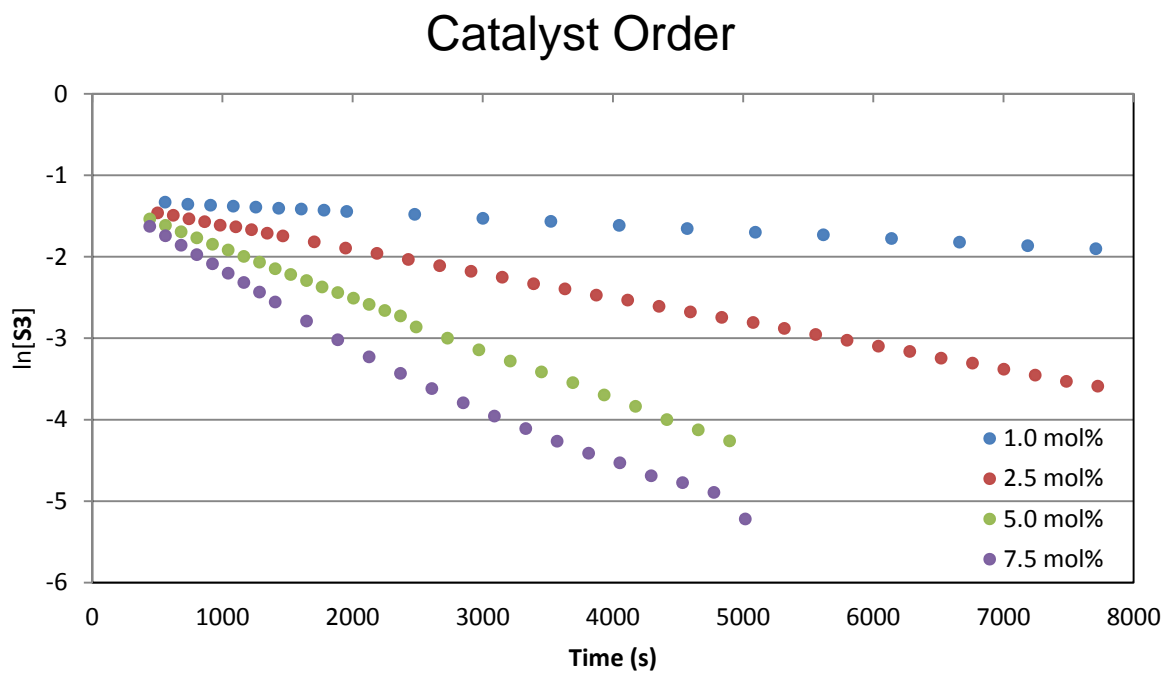
Figure 2-22. First order plot showing the consumption of **S3** in the hydroamination/cyclization with $LiCH_2SiMe_3$ (1.0 eq.), **S3** (0.28 M) at various catalyst loadings.

Catalyst Order

$$y = 1.200E\text{-}04x - 2.130E\text{-}05$$
$$R^2 = .9970$$
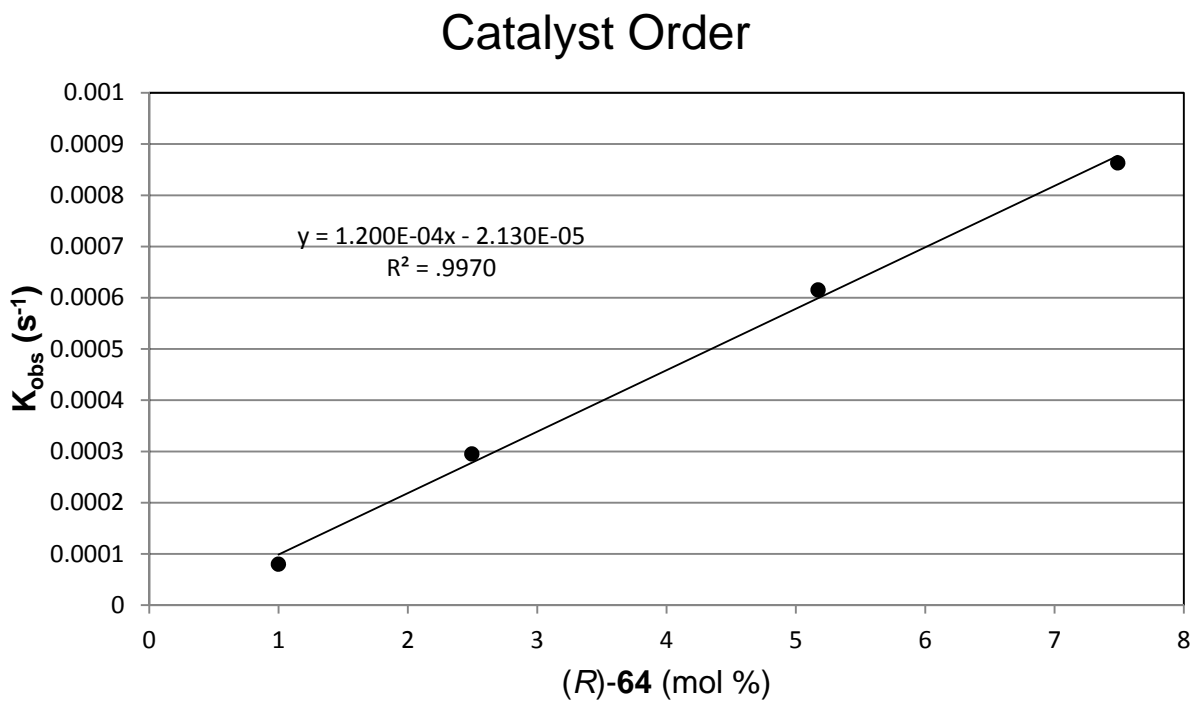
Figure 2-23. Plot of pseudo first order rate constants versus (*R*)-**64** (mol %) in the intramolecular hydroamination/cyclization of **S3** with $LiCH_2SiMe_3$ (1.0 eq.) and **S3** (0.28 M).

Order of Excess $LiCH_2SiMe_3$
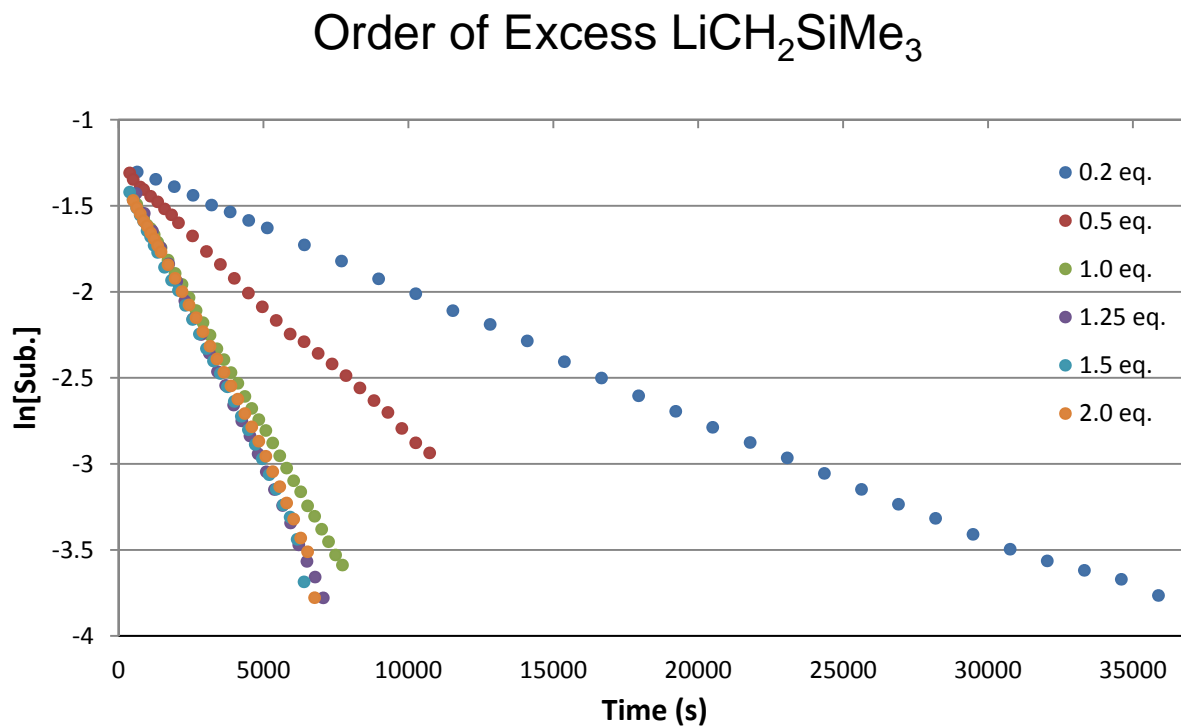
Figure 2-24. First order plot showing the consumption of **S3** in the hydroamination/cyclization with 2.5 mol% (*R*)-**64**, **S3** (0.28 M) with varied amounts of $LiCH_2SiMe_3$.

Order of Excess LiCH$_2$SiMe$_3$

y = 2.745E-04x + 1.803E-05
R^2 = .9998

Y-axis: K$_{obs}$ (s^{-1})

X-axis: LiCH$_2$SiMe$_3$ excess (eqivalents)
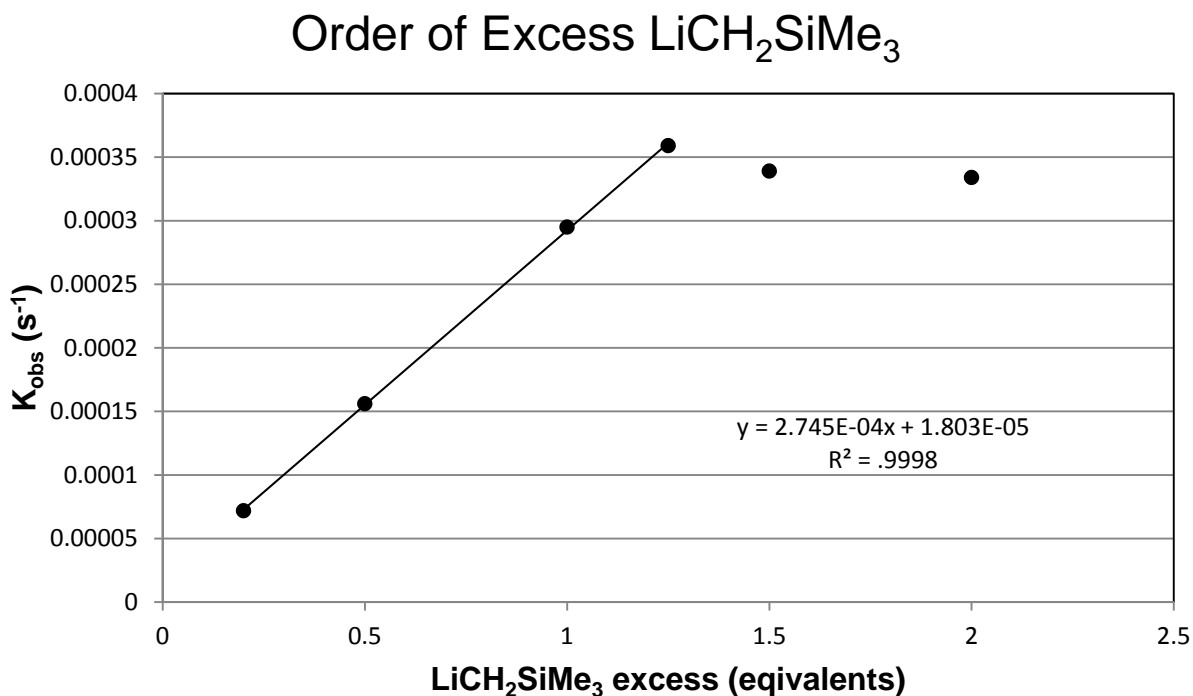
Figure 2-25. Plot of pseudo first order rate constants versus eq. excess LiCH$_2$SiMe$_3$ in the intramolecular hydroamination/cyclization of **S3** with 2.5 mol% (*R*)-**64** and **S3** (0.28 M).

2.7.3 Background Reaction and Kinetic Isotope Effect

The catalytic and stoichiometric hydroamination/cyclization of aminoalkenes with *n*-butyllithium has been documented.[3b,c] This background reaction (Eq. 2-15) was studied using **S3** and LiCH$_2$SiMe$_3$ in C$_6$D$_6$ at 25°C and demonstrated well behaved zero order kinetics (Figure 2-27, A-23). Use of N-deutero substrate **S3**-*d$_2$* yielded nearly identical results and confirmed that no KIE exists for this process with **S3**. The lack of KIE and zero order rate dependence on substrate suggests that insertion of the olefin into a Li-N bond could be the rate limiting step.

LiCH$_2$TMS
C$_6$D$_6$

S3   X = H,D

(2-15)
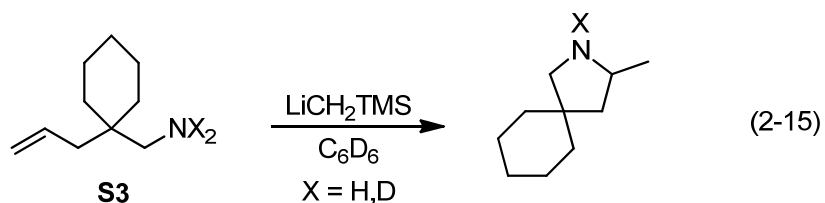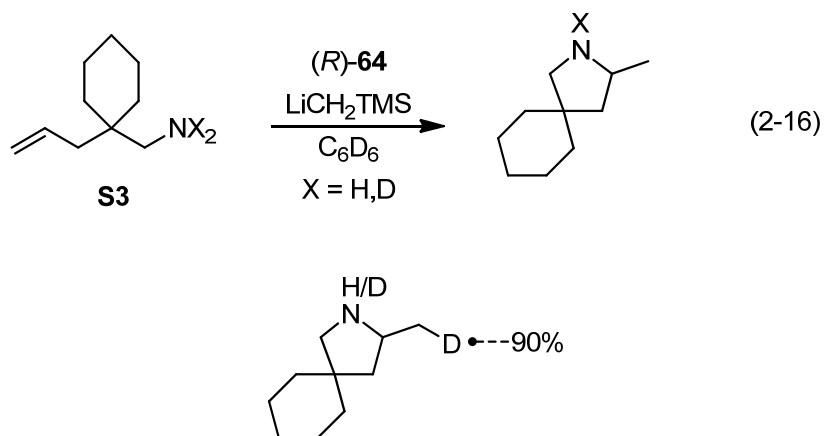
Figure 2-26. Deuterium incorporation into **P3** after hydroamination/cyclization of **S3**-d_2 (Eq. 2-15 and 2-16).

When (*R*)-**64** is present in the same reaction (Eq. 2-16), a marked rate increase occurs accompanied by a first order decay of substrate (Figure 2-28). The close proximity of two lithium atoms has been cited as the source of activity for this complex.[4] Coordination of the dilithium salt to the alkene portion of **S3** can facilitate an intramolecular interaction with the lithiated amine and generate a chiral environment. Activation of the alkene would account for the loss in zero order kinetics. In the presence of **S3**-d_2 a primary KIE of 1.6 was observed (Figure 2-28, Table 2-16, entries 6 & 7) demonstrating proton involvement in the rate determining step for the ligand accelerated process. Isotopic perturbation of enantioselectivity (Table 2-16, entries 6 & 7) was also observed. This phenomena has been reported with a cyclopentadienyl-bis(oxazolinyl)borate zirconium complex, which is believed to proceed by a concerted non-insertive mechanism.[45f,60] The first order rate dependence of $LiCH_2SiMe_3$ (≤1 equivalent excess, Section 2.7.2) on reaction rate, even in the presence of a dilithium salt suggests the presence of three lithium atoms in the rate limiting transition state.

Table 2-16. Rate constants for intramolecular hydroamination/cyclization of **S3** and **S3-d_2** with and without (*R*)-**64** (Eq. 2-15 and 2-16).

Entry	(*R*)-**64** (mol %)	LiCH$_2$SiMe$_3$ (equiv. excess)	LiCH$_2$SiMe$_3$ (mol %)	0 order k$_{obs}$ (M · s^{-1})	1st order k$_{obs}$ (s^{-1})	*ee* (%)	Sub.
1	2.5	2.0	5.0	-----	3.34×10^{-4}	66	**S3**
2	10.0	0.5	5.0	-----	7.75×10^{-4}	67	**S3**
3	-----	-----	5.0	2.66×10^{-6}	-----		**S3**
4	-----	-----	10.0	2.59×10^{-6}	-----		**S3**
5	-----	-----	10.0	2.62×10^{-6}	-----		**S3-d_2**
				k$_H$/k$_D$ = 1			
6	5.0	0.5	-----	-----	4.70×10^{-4}	68	**S3**
7	5.0	0.5	-----	-----	2.84×10^{-4}	55	**S3-d_2**
					k$_H$/k$_D$ = 1.66		
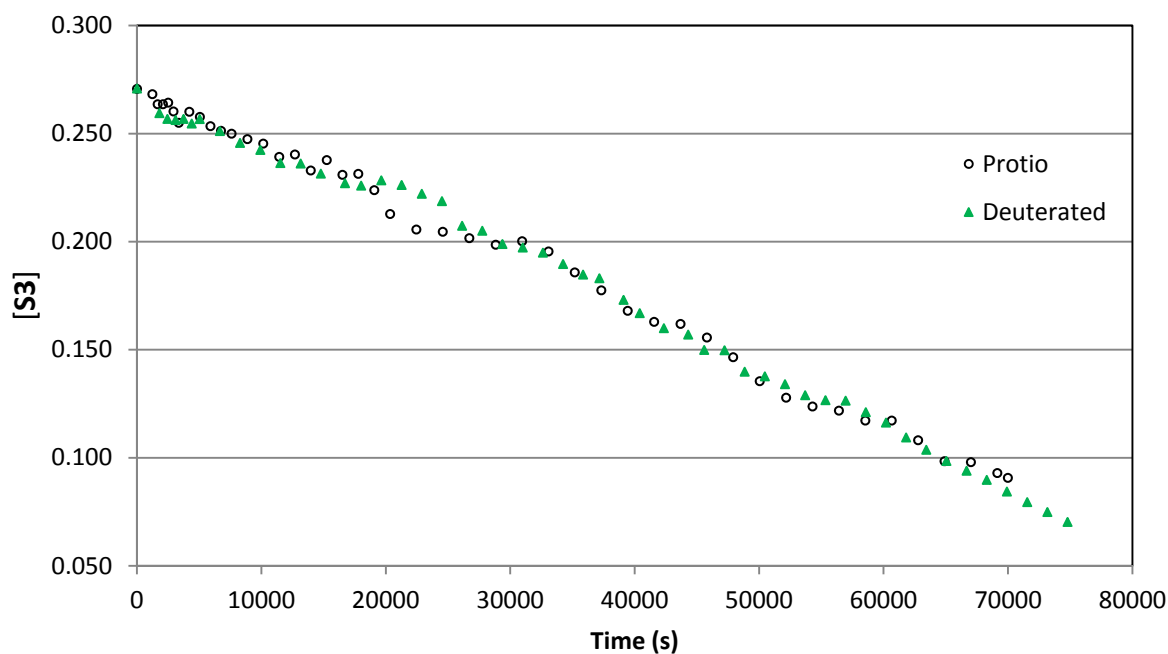
Figure 2-27. Zero order plot showing the consumption of **S3** and **S3-d_2** in the hydroamination/ cyclization with 10.0 mol% LiCH$_2$SiMe$_3$ as a catalyst.
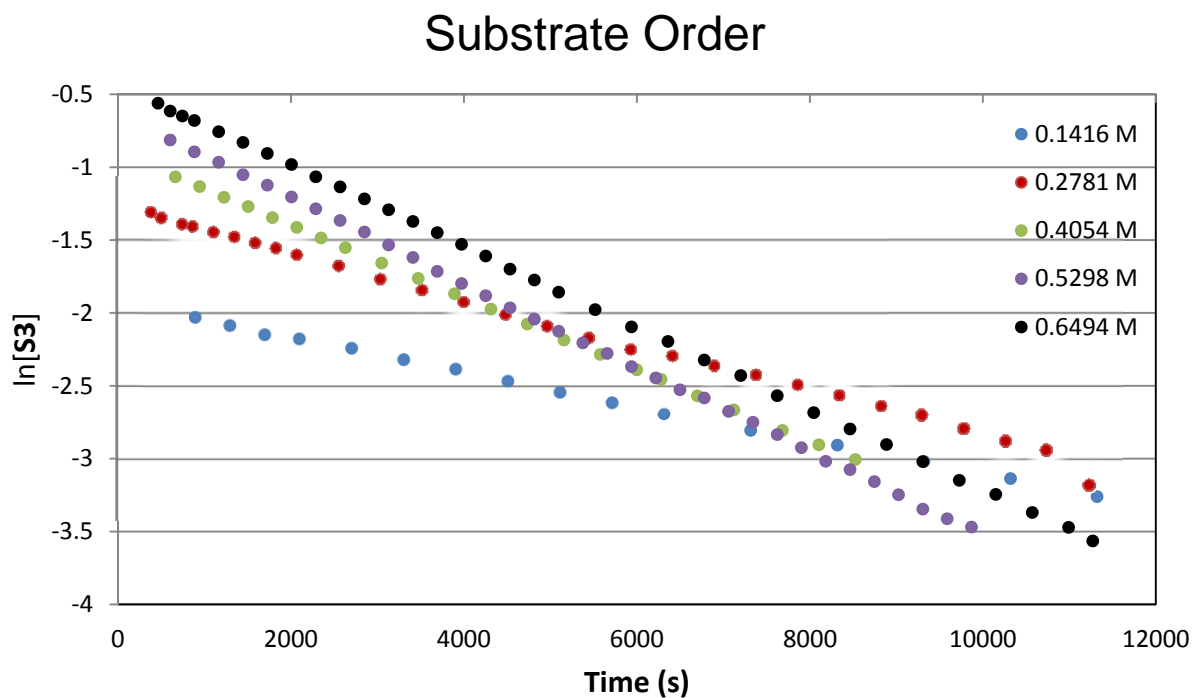
Accelerated Reaction (Eq. 2-16)
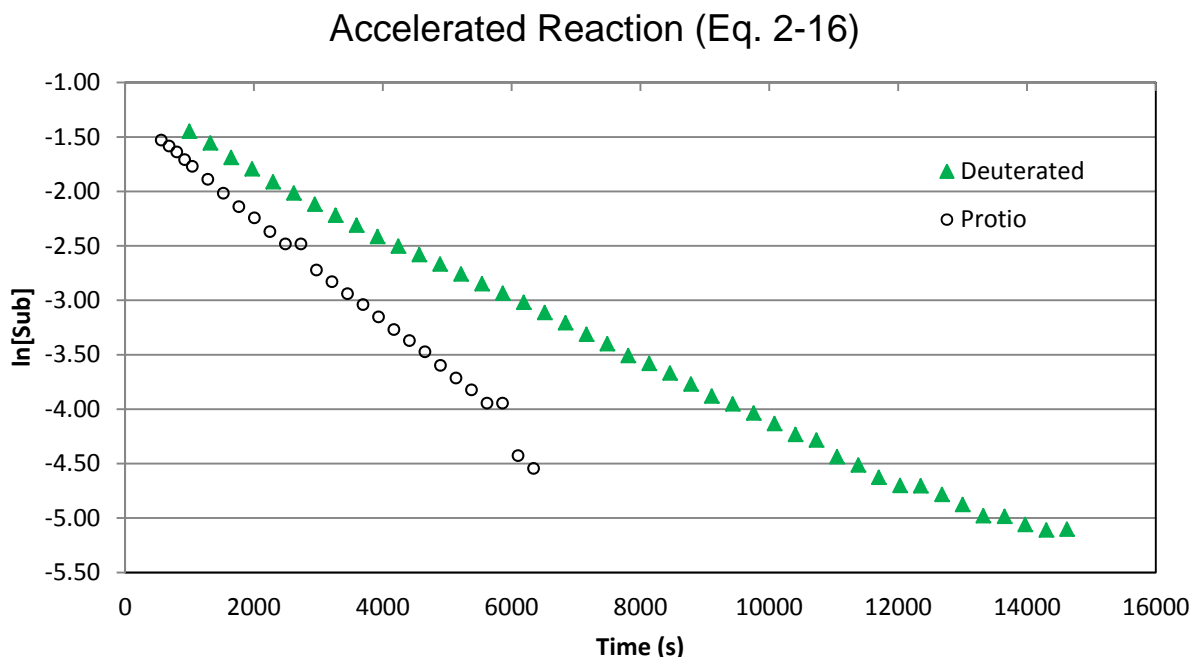
Figure 2-28. First order plot showing the consumption of **S3** and **S3-d_2** in the hydroamination/cyclization with 5.0 mol% (*R*)-**64** and LiCH$_2$SiMe$_3$ (0.5 eq. excess).

2.7.4 Reagent Stoichiometry and Enantioselectivity

As shown in Chapter 2.7.2, a first order dependence on excess LiCH$_2$SiMe$_3$ (up to 1.25-1.5 equivalents excess) was observed for the hydroamination/cyclization of **S3**. The formation of a new mixed aggregate (*R*)-**69** (Figure 2-29) was also observed by ^{1}H and ^{7}Li NMR in Chapter 2.5.4 when equimolar amounts of LiCH$_2$SiMe$_3$ and (*R*)-**64** were combined. The relationship between enantioselectivity and LiCH$_2$SiMe$_3$ was plotted for reactions containing 2.5, 5.0 and 7.5 mol % (*R*)-**64**. A linear decay of enantioselectivity was observed for the reactions containing 5.0 and 7.5 mol % (*R*)-**64** (Figures 2-30, 2-31). When the catalyst loading was lowered to 2.5 mol% (Figure A-24) this effect was observed as well; however, five of the six enantioselectivities were within 1% of each other making this trend statistically insignificant.
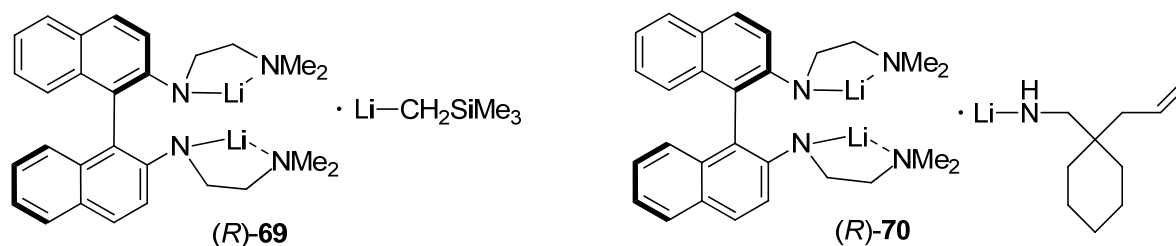
Figure 2-29. Left: Mixed aggregate (*R*)-**69**, formed when equimolar amounts of (*R*)-**64** and LiCH$_2$SiMe$_3$ are combined (Chapter 2.5.4). Right: (*R*)-**70** illustrates the components found in the rate limiting transition state for the hydroamination/cyclization of **S3** with (*R*)-**64** and excess LiCH$_2$SiMe$_3$ as determined by kinetic studies (Chapter 2.7).

The effects of catalyst loading and substrate concentration on enantioselectivity were also studied. Variation of catalyst loading from 2.5-7.5 mol% in the presence of excess LiCH$_2$SiMe$_3$ (0.2, 0.5, 1.0, 2.0 equivalents) did not vary *ee*'s a statistically significant amount (0.2 equiv. – Figure A-25; 0.5 equiv. – Figure 2-32; 1.0 equiv. – Figure A-26; 2.0 equiv. – Figure A-27). When catalyst loading was increased from 7.5 mol% to 15.0 mol % in the presence of 0.5 equivalents excess LiCH$_2$SiMe$_3$ a linear decrease in enantiomeric excess was observed (Figure 2-32). The average enantiomeric excess for each catalyst loading decreased as catalyst loading was increased. The reaction concentration did not have a significant impact on stereoinduction and similar enantioselectivities were observed from 0.1416 M to 0.6494 M of [**S3**]$_0$ (Figure 2-33).

These results demonstrate that excess LiCH$_2$SiMe$_3$ has a noteworthy impact on enantioselectivity. The presence of an unaccelerated achiral background reaction has been demonstrated (Figure 2-27), and may account for the loss in enantioselectivity. The first order dependence of LiCH$_2$SiMe$_3$ on the reaction rate suggests that LiCH$_2$SiMe$_3$, even in trace quantities, is capable of forming a new, catalytically active species generally illustrated as (*R*)-**70** (Figure 2-29).
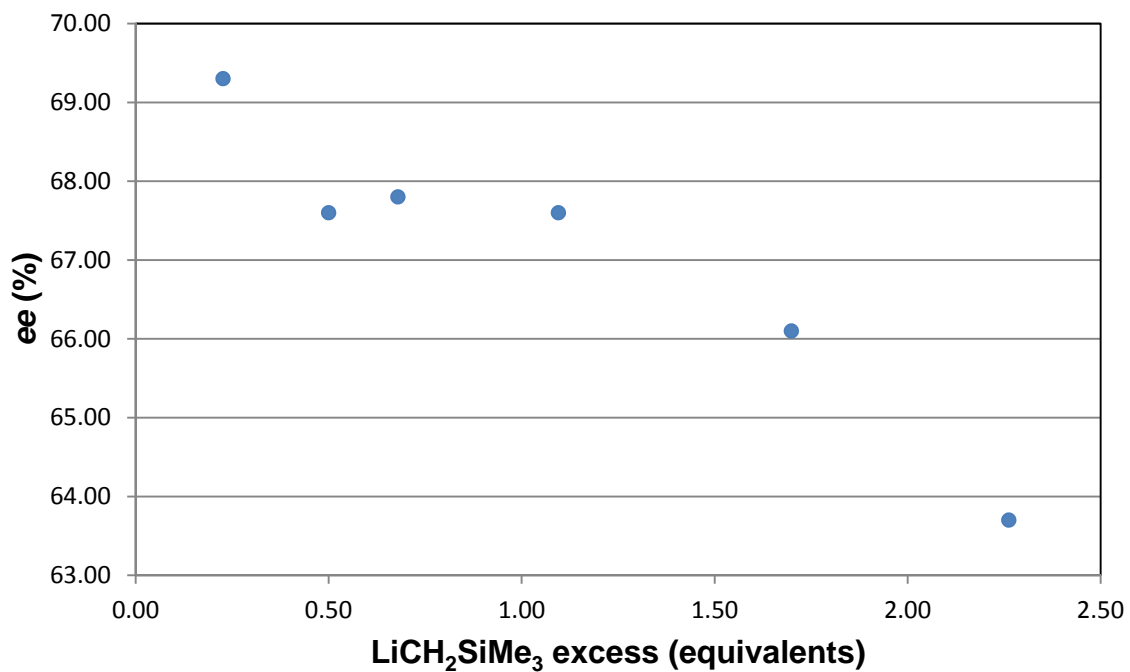
Figure 2-30. Plot of *ee* (%) vs. LiCH$_2$SiMe$_3$ (excess equivalents) for the hydroamination/ cyclization of **S3** with (*R*)-**64** (5.0 mol%) and [**S3**] (0.27–0.28 M).
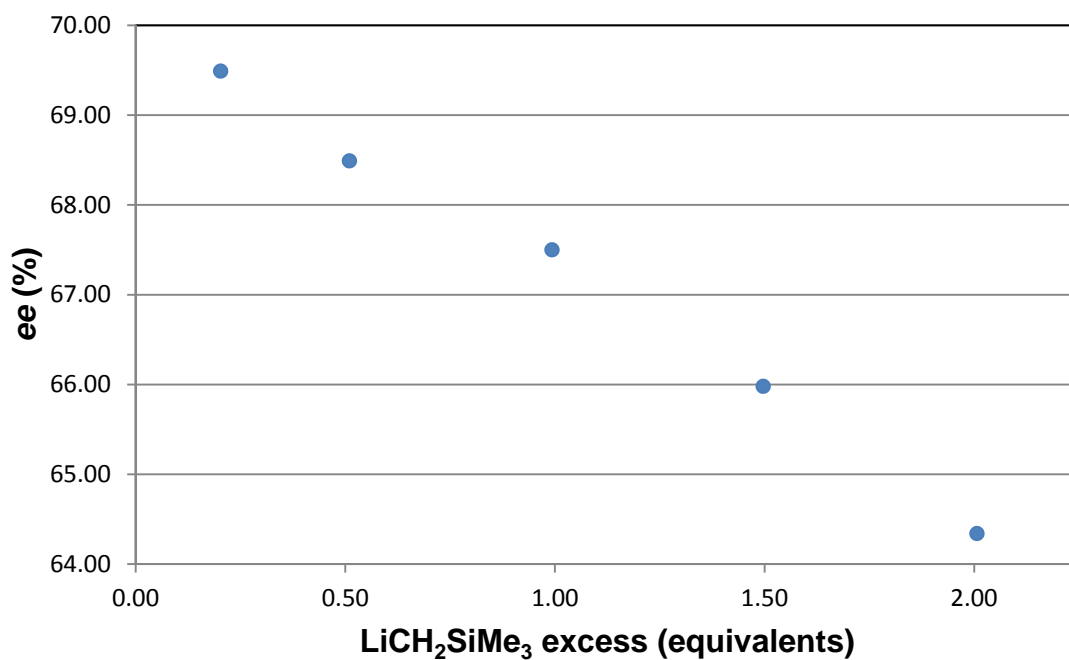
Figure 2-31. Plot of *ee* (%) vs. LiCH$_2$SiMe$_3$ (excess equivalents) for the hydroamination/ cyclization of **S3** with (*R*)-**64** (7.5 mol%) and [**S3**] (0.27–0.28 M).
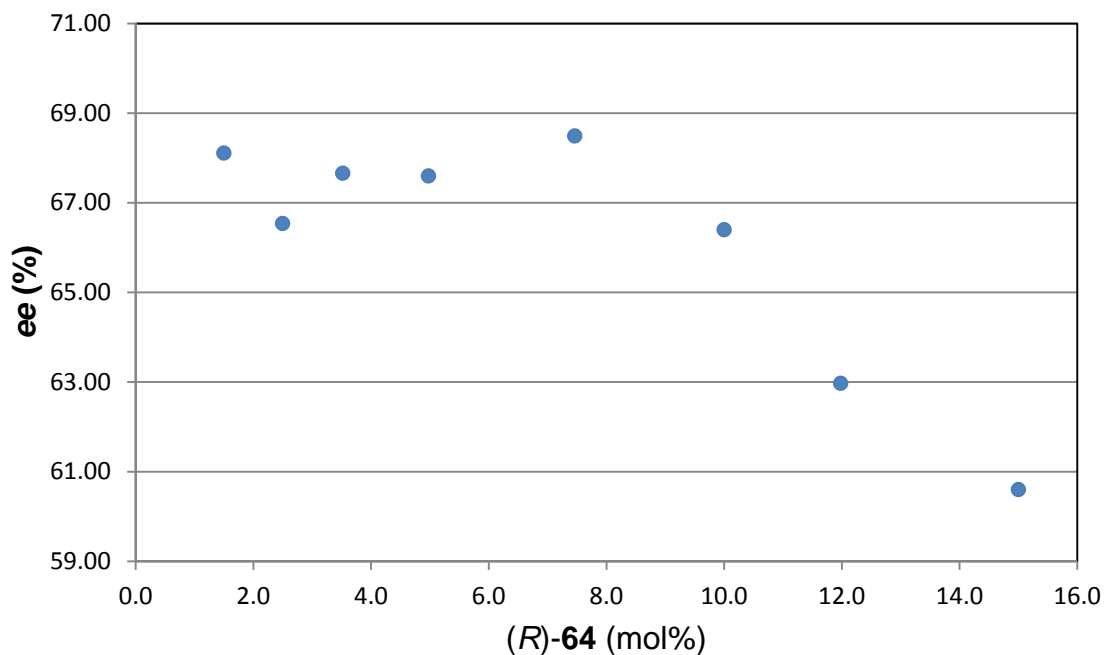
Figure 2-32. Plot of *ee* (%) vs. (*R*)-**64** (X mol%) for the hydroamination/ cyclization of **S3** with LiCH$_2$SiMe$_3$ (0.5 equiv. excess) and [**S3**] (0.27–0.28 M).
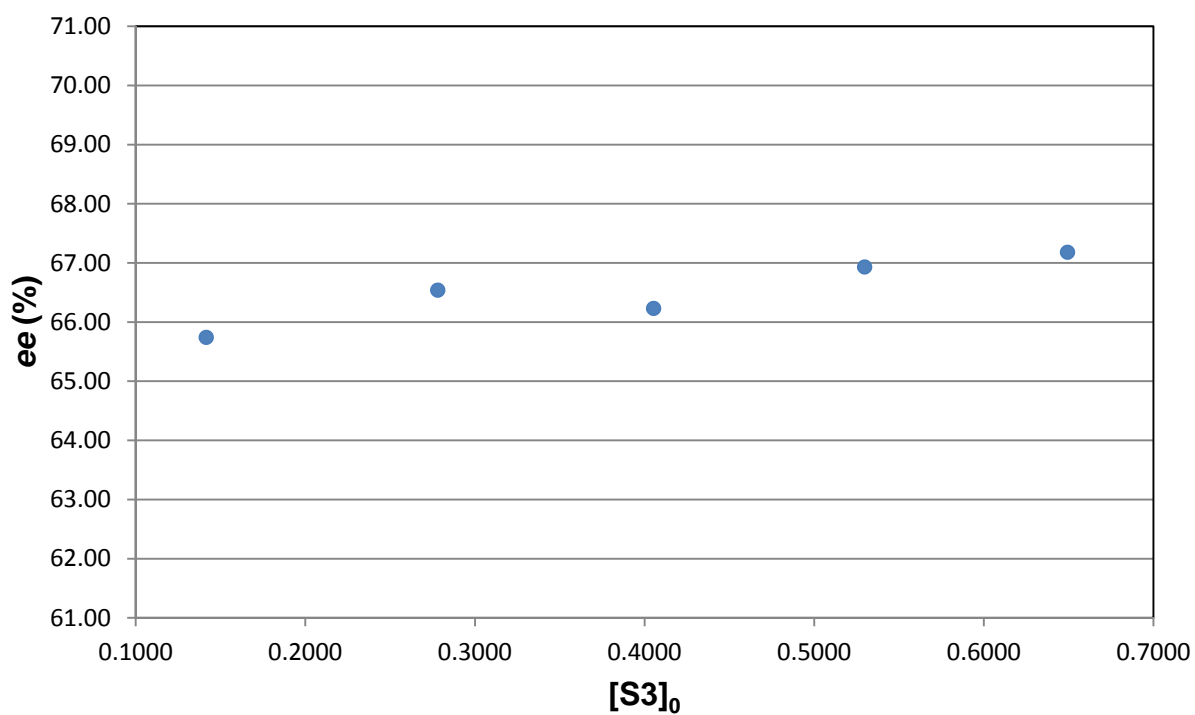
Figure 2-33. Plot of *ee* (%) vs. [**S3**]$_0$ for the hydroamination/ cyclization of **S3** with (*R*)-**64** (2.5 mol%) and LiCH$_2$SiMe$_3$ (0.5 equiv. excess).

2.8 Conclusions

Catalyst aggregation is detrimental to the activity of this system, and broad ^{1}H NMR spectra along with DOSY-NMR spectroscopy suggests that (*R*)-**64** is at least partially aggregated in solution. ^{1}H and ^{7}Li NMR of (*R*)-**64** and (*rac*)-**64** with one equivalent of LiCH$_2$SiMe$_3$ suggest that excess base facilitates deaggregation. Because the rate limiting transition step for the hydroamination/cyclization of **S3** with (*R*)-**64** and LiCH$_2$SiMe$_3$ contains three lithium atoms, it is likely that trace amounts of excess alkyl lithium were present with (*S*,*S*,*S*)-**25** allowing its reactivity.

Based on the observed rate law (Section 2.7.2), deprotonation of **S3** is essential for its entry into the catalytic cycle and accounts for the third lithium atom. Zero order kinetics with respect to the substrate have been observed in rare earth metal-mediated hydroamination and are consistent with rate limiting olefin insertion. The unaccelerated background reaction demonstrates zero order substrate kinetics and olefin insertion into the lithium amide bond is the rate determining step in this process. The loss of zero order kinetics for the accelerated process suggest that (*R*)-**64** can activate the alkene, allowing intramolecular nucleophilic attack from the metal amide. The reaction rate has a first order dependence on (*R*)-**64**, which both lowers the activation barrier of this process and generates a chiral environment. The presence of a KIE along with isotopic perturbation of enantioselectivity suggest rate limiting protonolysis or a concerted mechanism. Experimental determination of the Arrhenius activation parameters along with DFT studies will clarify the details of the rate limiting transition state.
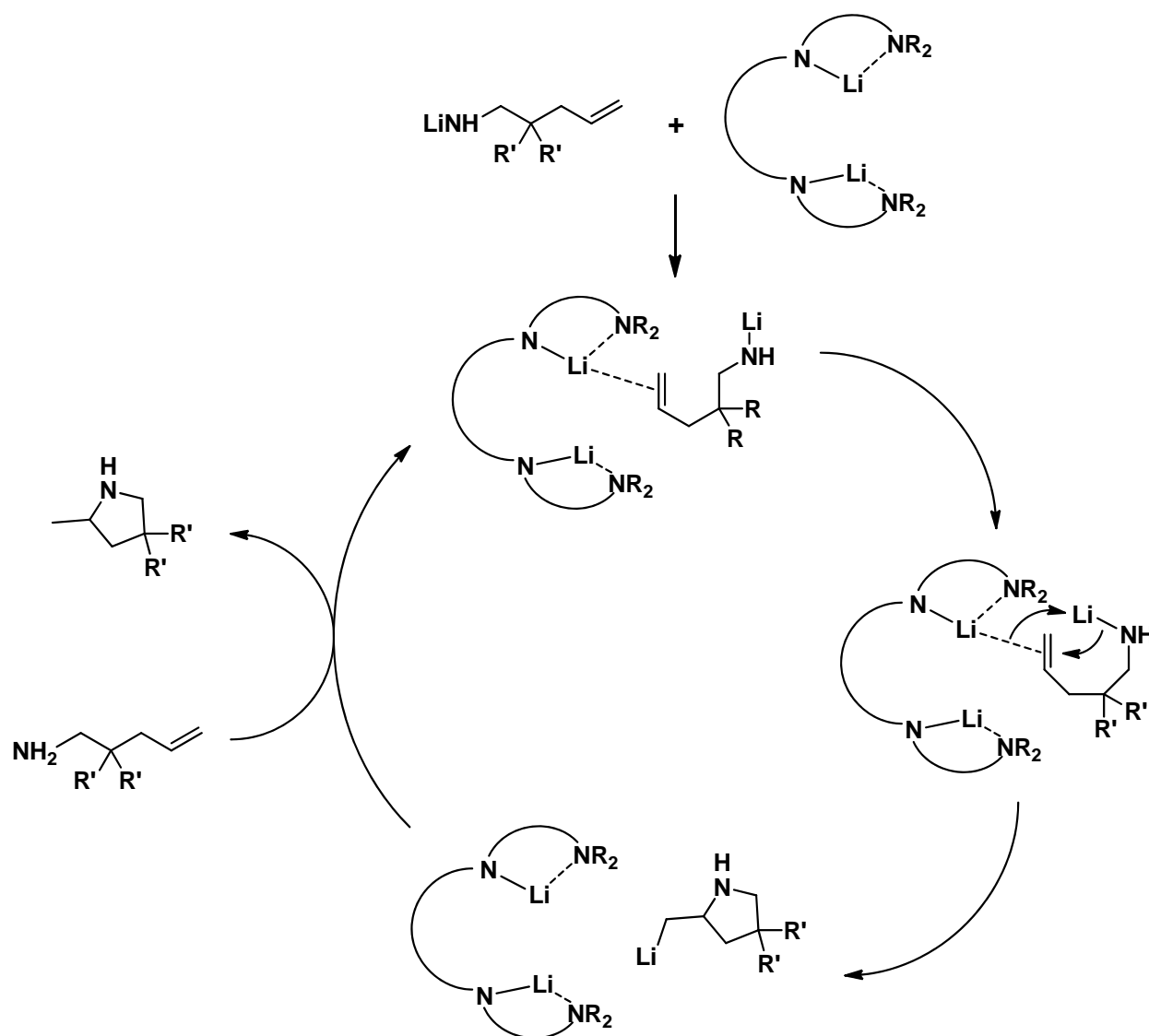
Figure 2-34. Proposed mechanism for the intramolecular hydroamination/ cyclization of **S3** with (*R*)-**64** and LiCH$_2$SiMe$_3$.

The enantioselectivities reported on (*S,S,S*)-**25** are consistently higher than those induced by (*R*)-**64**, (*R*)-**65** and (*R*)-**66**. The higher enantioselectivities induced with (*S,S,S*)-**25** compared with (*R*)-**64** may be attributed to the rigidity and additional internal chirality found in the ligand sidearms. The lower enantioselectivities produced by (*R*)-**65** and (*R*)-**66** compared with (*R*)-**64** indicate that steric bulk on the chelating amine is detrimental to stereoinduction and suggest that the amine sidearms are in close proximity during the enantioselectivity determining step. The enantioselectivities induced with (*R*)-**26a-d** also suggest that steric bulk proximal to the metal

center is detrimental to enantioselectivity. The induction of higher enantioselectivities on sterically hindered **S2** with these catalysts is unexpected, and further studies should be undertaken to clarify cause of this outcome.

Catalytic data for this system suggests that future generation catalysts will benefit from increased rigidity on the ligand sidearm and minimal steric bulk on the coordinating amine. Insufficient steric bulk on the L donor moiety leads to species such as [(*R*)-**67**]$_2$ and insufficient sidearm rigidity allows complexes such as [(*rac*)-**64**]$_6$ to form. The source of rigidity for (*S,S,S*)-**25** is the pyrollidine ring found within the sidearm, which also introduces two elements of internal chirality. Rigidity of these complexes could be increased by incorporation of a ring into the sidearm carbons, which would introduce four additional elements of internal chirality (Figure 2-35).
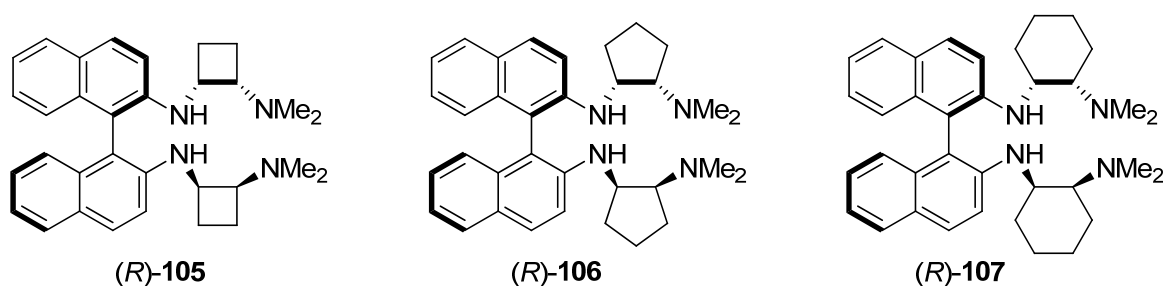
Figure 2-35. Structures of more sterically rigid diaminobinaphthyl ligands, each containing five elements of internal chirality.

These ligands would allow incremental variation of the NCCN dihedral angle on the chiral sidearms. Synthesis of a cis-selective product would be a synthetic hurdle, and require a new synthetic route. If a general route were devised, alteration of the ring size (4–6 carbons – (*R*)-**105**, (*R*)-**106**, (*R*)-**107**) could allow the impact of rigidity, steric bulk and the NCCN dihedral angle on the catalyst sidearms to be better understood. The influence of these modifications on catalyst aggregation, reactivity and enantioselectivity may allow a more complete understanding of structure activity relationships.

2.9 References

(1)   Review on base-catalyzed hydroamination: (a) Seayad, J.; Tillack, A.; Hartung, C. G.; Beller, M. *Adv. Syn. Cat.* **2002**, *344*, 795. General hydroamination reviews: (b) Müller, T.

E.; Beller, M. *Chem. Rev.* **1998**, *98*, 675. (c) Müller, T. E.; Hultzsch, K. C.; Yus, M.; Foubelo, F.; Tada, M. *Chem. Rev.* **2008**, *108*, 3795.

(2) (a) Danforth, J. D. *French Patent 917060,* **1946**. (b) Danforth, J. D. *U. S. Patent 2,449,644,* **1948**. (c) A. W. Weston, A. W. *U. S. Patent 2,437,984,* **1948**. (d) Danforth, J. D*., Canadian Patent 461783,* **1949**.

(3) Secondary aminoalkene and aminoalkyne substrates: (a) Fujita, H.; Tokuda, M.; Nitta, M.; Suginome, H. *Tetrahedron Lett.* **1992**, *33*, 6359. Primary aminoalkene substrates: (b) Ates, A.; Quinet, C. *Eur. J. Org. Chem.* **2003**, 1623. (c) Quinet, C.; Jourdain, P.; Hermans, C.; Ates, A.; Lucas, I.; Markó, I. E. *Tetrahedron* **2008**, *64*, 1077.

(4) Primary aminoalkenes: Martinez, P. H.; Hultzsch, K. C.; Hampel, F. *Chem. Commun.* **2006**, 2221.

(5) P. Horillo-Martínez, Ph. D. thesis, Institut für Organische Chemie, Friedrich-Alexander Universität Erlangen-Nürnberg (Erlangen-Nürnberg), **2008**.

(6) Primary aminoalkenes and dienes: (a) Deschamp, J.; Collin, J.; Hannedouche, J.; Schulz, E. *Eur. J. Org. Chem.* **2011**, 3329. (b) Deschamp, J.; Olier, C.; Schulz, E.; Guillot, R.; Hannedouche, J.; Collin, J. *Adv. Synth. Catal.* **2010**, *352*, 2171.

(7) One ligand contained a pyridyl group where four carbons separate the nitrogen's, three of which are contained on a rigid aromatic ring.

(8) Tsuchida, S.; Kaneshige, A.; Ogata, T.; Baba, H.; Yamamoto, Y.; Tomioka, K. *Org. Lett.* **2008**, *10*, 3635.

(9) Ogata, T.; Ujihara, A.; Tsuchida, S.; Shimizu, T.; Kaneshige, A.; Tomioka, K.; *Tetrahedron Lett.* **2007**, *48*, 6648.

(10) Kizirian, J. C. *Chem. Rev.* **2008**, *108*, 140.

(11) Collum, D. B. *Acc. Chem. Res.* **1992**, *25*, 448.

(12) (a) Romera, J. L.; Cid, J. M.; Trabanco, A. A. *Tetrahedron Lett.* **2004**, *45*, 8797. (b) Salvatore, R. N.; Nagle, A. S.; Schmidt, S. E.; Jung, K. W. *Org. Lett.* **1999**, *1*, 1893. (c) Salvatore, R. N.; Nagle, A. S.; Jung, K. W. *J. Org. Chem.* **2002**, *67*, 674.

(13) Reviews: (a) Burkhardt, E. R.; Matos, K. *Chem. Rev.* **2006**, *106*, 2617. (b) Abdel-Magid, A. F.; Mehrman, S. J. *Org. Process Res. Dev.* **2006**, *10*, 971.

(14) Peptide coupling reactions containing free tertiary amines: (a) Essawi, M. Y. H. *Pharmazie* **1999**, *54*, 575. (b) Leonov, A.; Voigt, B.; Rodriguez-Castañeda, F.; Sakhaii, P.; Griesinger, C. *Chem.-Eur. J.* **2005**, *11*, 3342.

(15) Reviews: (a) Burkhardt, E. R.; Matos, K. *Chem. Rev.* **2006**, *106*, 2617. (b) Abdel-Magid, A. F.; Mehrman, S. J. *Org. Process Res. Dev.* **2006**, *10*, 971.

(16) (a) Van Veldhuizen, J. J.; Garber, S. B.; Kingsbury, J. S.; Hoveyda, A. H. *J. Am. Chem. Soc.* **2002**, *124*, 4954. (b) VanVeldhuizen, J. J.; Gillingham, D. G.; Garber, S. B.; Kataoka, O.; Hoveyda, A. H. *J. Am. Chem. Soc.* **2003**, *125*, 12502.

(17) (a) Uehling, D. E.; Shearer, B. G.; Donaldson, K. H.; Chao, E. Y.; Deaton, D. N.; Adkison, K. K.; Brown, K. K.; Cariello, N. F.; Faison, W. L.; Lancaster, M. E.; Lin, J.; Hart, R.; Milliken, T. O.; Paulik, M. A.; Sherman, B. W.; Sugg, E. E.; Cowan, C. *J. Med. Chem.* **2006**, *49*, 2758. (b) Shearer, B. G.; Chao, E. Y.; Uehling, D. E.; Deaton, D. N.; Cowan, C.; Sherman, B. W.; Milliken, T.; Faison, W.; Brown, K.; Adkison, K. K.; Lee, F. *Bioorg. Med. Chem. Lett.* **2007**, *17*, 4670.

(18)   (a) Synthesis: Xiao, X.; Antony, S.; Kohlhagen, G.; Pommier, Y.; Cushman, M. *Bioorg. Med. Chem.* **2004**, *12*, 5147. (b) Spectral Data: Nanchen, S.; Pfaltz, A. *Helv. Chim. Acta* **2006**, *89*, 1559.

(19) ^{13}C NMR spectra contained characteristic signals from both products.

(20)   (a) Trost, B. M. *Angew. Chem. Int. Ed. Engl.* **1995**, *34*, 259. (b) Trost, B. *Science* **1991**, *254*, 1471.

(21)   (a) Hoffmann, R. W. *Synthesis* **2006**, *2006*, 3531. (b) Baran, P. S.; Maimone, T. J.; Richter, J. M. *Nature* **2007**, *446*, 404. (c) Porco, J. A. *Nature* **2007**, *446*, 383. (d) Young, I. S.; Baran, P. S. *Nature Chem.* **2009**, *1*, 193.

(22)   For experimental procedures: (a) Zhai, W.; Gerritz, S.; Andres, C. J.; Tino, J. A.; WO 2005070884, US 2005154043, **2005**. (b) O'Brien, P.; Towers, T. D. *J. Org. Chem.* **2002**, *67*, 304. (c) Yang, L.; Hofer, K. G.; WO 9814190, **1998**. (d) Gmeiner, P.; Junge, D.; Kaertner, A. *J. Org. Chem.* **1994**, *59*, 6766. For other relevant examples: (e) Hu, Y.; Green, N.; Gavrin, L. K.; Janz, K.; Kaila, N.; Li, H.-Q.; Thomason, J. R.; Cuozzo, J. W.; Hall, J. P.; Hsu, S.; Nickerson-Nutter, C.; Telliez, J.-B.; Lin, L.-L.; Tam, S. *Bioorg. Med. Chem. Lett.* **2006**, *16*, 6067. (f) Yoneda, Y.; Kawajiri, S.; Hasegawa, A.; Kito, F.; Katano, S.; Takano, E.; Mimura, T. *Bioorg. Med. Chem. Lett.* **2001**, *11*, 1261.

(23)   (a) Platinum catalyst: Korovchenko, P.; Donze, C.; Gallezot, P.; Besson, M. *Catalysis Today* **2007**, *121*, 13. (b) Chromium Oxide: Gulkova, D.; Kraus, M. *Coll. Czech. Chem. Comm.* **1992**, *57*, 2215. (c) Alkylation: Kirrmann, A.; Riehl, J. J. *Compt. Rend.* **1956**, *243*, 808.

(24)   Value obtained from ACD Labs ChemSketch.

(25)   For experimental procedures: (a) Concellon, J. M.; Riego, E.; Rodriguez-Solla, H.; Plutin, A. M. *J. Org. Chem.* **2001**, *66*, 8661. (b) Bastin, S.; Ginj, M.; Brocard, J.; Pélinski, L.; Novogrocki, G. *Tetrahedron: Asymmetry* **2003**, *14*, 1701. (c) Concellon, J. M.; Riego, E.; Rivero, I. A.; Ochoa, A. *J. Org. Chem.* **2004**, *69*, 6244. (d) Schmid, R.; Zutter, U.; US 2005272665, **2005**. (e) Hom, R.; Fang, L.; John, V.; WO 2006026533, **2006**. (f) Masuda, Y.; Tashiro, T.; Mori, K. *Tetrahedron: Asymmetry* **2006**, *17*, 3380. For a related example: (g) Kirby, A. *ChemMedChem* **2006**, *1*, 654.

(26)   (a) Tessier-Youngs, C.; Beachley Jr., O. T. *Inorg. Synth.*, **1986**; Vol. 24, 92. (b) Tecle, B.; Maqsudur Rahman, A. F. M.; Oliver, J. P. *J. Organomet. Chem.* **1986**, *317*, 267.

(27)   See ref. 6b. (a) Carey, D. T.; Mair, F. S.; Pritchard, R. G.; Warren, J. E.; Woods, R. J. *Eur. J. Inorg. Chem.* **2003**, 3464. (b) Neumann, C.; Schulz, A.; Seifert, T.; Storch, W.; Vosteen, M. *Eur. J. Inorg. Chem.* **2002**, 1040. (c)   Betz, J.; Hampel, F.; Bauer, W. *J. Chem. Soc., Dalton Trans.* **2001**, 1876. (d) Gemuend, B.; Noeth, H.; Sachdev, H.; Schmidt, M. *Chem. Ber.* **1996**, *129*, 1335.

(28)   Olsher, U.; Izatt, R. M.; Bradshaw, J. S.; Dalley, N. K. *Chem. Rev.* **1991**, *91*, 137.

(29)   (a) Von Ragué Schleyer, P. *Lithium Chemistry*; Wiley Interscience: New York, NY, **1995**. (b) Gregory, K.; von Ragué Schleyer, P.; Snaith, R. *Adv. Inorg. Chem.*; Sykes, A. G., Ed.; Academic Press, Inc: New York, NY, **1991**, p 48. (c) Armstrong, D. R.; Barr, D.; Clegg, W.; Hodgson, S. M.; Mulvey, R. E.; Reed, D.; Snaith, R.; Wright, D. S. *J. Am. Chem. Soc.* **1989**, *111*, 4719. (d) Armstrong, D. R.; Barr, D.; Clegg, W.; Mulvey, R. E.; Reed, D.; Snaith, R.; Wade, K. *J. Chem. Soc., Chem. Commun.* **1986**, 869.

(30)   Drost, C.; Hitchcock, P. B.; Lappert, M. F. *J. Chem. Soc., Dalton Trans.* **1996**, 3595.

(31) See also reference 4, 6b and 30. (a) Chen, H.; Bartlett, R. A.; Dias, H. V. R.; Olmstead, M. M.; Power, P. P. *Inorg. Chem.* **1991**, *30*, 2487. (b) Carey, D. T.; Mair, F. S.; Pritchard, R. G.; Warren, J. E.; Woods, R. J. *Eur. J. Inorg. Chem.* **2003**, 3464. (c) Blackmore, K. J.; Ziller, J. W.; Heyduk, A. F. *Inorg. Chem.* **2007**, *47*, 265. (d) Kotov, V. V.; Wang, C.; Kehr, G.; Fröhlich, R.; Erker, G. *Organometallics* **2007**, *26*, 6258.

(32) (a) Gemuend, B.; Noeth, H.; Sachdev, H.; Schmidt, M. *Chem. Ber.* **1996**, *129*, 1335. (b) Antolini, F.; Hitchcock, P. B.; Lappert, M. F.; Merle, P. *Chem. Commun.* **2000**, 1301. (c) Daniele, S.; Drost, C.; Gehrhus, B.; Hawkins, S. M.; Hitchcock, P. B.; Lappert, M. F.; Merle, P. G.; Bott, S. G. *J. Chem. Soc., Dalton Trans.* **2001**, 3179. (d) Neumann, C.; Schulz, A.; Seifert, T.; Storch, W.; Vosteen, M. *Eur. J. Inorg. Chem.* **2002**, 1040. (e) Burford, N.; D'Eon, M.; Ragogna, P. J.; McDonald, R.; Ferguson, M. J. *Inorg. Chem.* **2004**, *43*, 734.

(33) Angle between mean planes of naphthyl rings obtained in Mercury using the following procedure:

-Highlight C atoms of one naphthyl ring; -Right click on screen and select "New", then "Mean Plane";

-Repeat this procedure for second ring; -In "Picking Mode" drop down menu (located on top toolbar), select "Measure Angle"; -Select the 2 planes to be measured, angle will appear. Note: Reported angle is labeled "Angle A" in picture below.
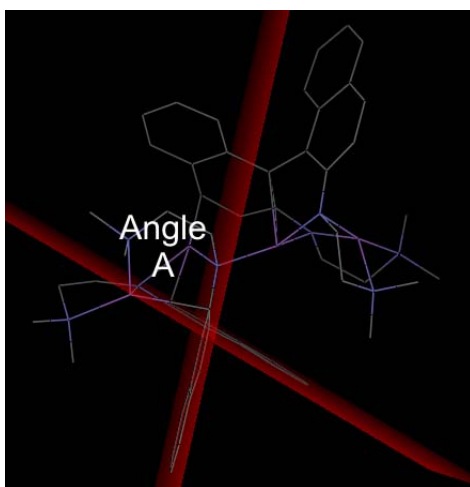
(34) Reviews – DOSY study of reactive intermediates: (a) Li, D.; Keresztes, I.; Hopson, R.; Williard, P. G. *Acc. Chem. Res.* **2008**, *42*, 270. DOSY for determining aggregation states: (b) Macchioni, A.; Ciancaleoni, G.; Zuccaccia, C.; Zuccaccia, D. *Chem. Soc. Rev.* **2008**, *37*, 479. DOSY Theory and applications: (c) Brand, T.; Cabrita, E. J.; Berger, S. In *Modern Magnetic Resonance*; Webb, G. A., Ed.; Springer: **2006**; Vol. 1, p 135. (d) Cohen, Y.; Avram, L.; Frish, L. *Angew. Chem. Int. Ed.* **2005**, *44*, 520.

(35) (a) Kagan, G.; Li, W.; Li, D.; Hopson, R.; Williard, P. G. *J. Am. Chem. Soc.* **2011**, *133*, 6596. (b) Armstrong, D. R.; García-Álvarez, P.; Kennedy, A. R.; Mulvey, R. E.; Robertson, S. D. *Chem. Eur. J.* **2011**, *17*, 6725. (c) Kagan, G.; Li, W.; Sun, C.; Hopson, R.; Williard, P. G. *J. Org. Chem.* **2010**, *76*, 65. (d) Lecachey, B.; Oulyadi, H.; Lameiras, P.; Harrison-Marchand, A.; Gérard, H.; Maddaluno, J. *J. Org. Chem.* **2010**, *75*, 5976. (e) Li, D.; Kagan, G.; Hopson, R.; Williard, P. G. *J. Am. Chem. Soc.* **2009**, *131*, 5627. (f) Kagan, G.; Li, W.; Hopson, R.; Williard, P. G. *Org. Lett.* **2009**, *12*, 520. (g) Lecachey, B.;

Duguet, N.; Oulyadi, H.; Fressigné, C.; Harrison-Marchand, A.; Yamamoto, Y.; Tomioka, K.; Maddaluno, J. *Org. Lett.* **2009**, *11*, 1907. (h) Liu, J.; Li, D.; Sun, C.; Williard, P. G. *J. Org. Chem.* **2008**, *73*, 4045. (i) Li, D.; Sun, C.; Liu, J.; Hopson, R.; Li, W.; Williard, P. G. *J. Org. Chem.* **2008**, *73*, 2373.

(36)   (a) Lithium and Magnesium: García-Álvarez, P.; Mulvey, R. E.; Parkinson, J. A. *Angew. Chem. Int. Ed.* **2011**, *50*, 9668. (b) Lithium and Zinc: Armstrong, D. R.; García-Álvarez, P.; Kennedy, A. R.; Mulvey, R. E.; Parkinson, J. A. *Angew. Chem. Int. Ed.* **2010**, *49*, 3185.

(37)   Reviews: (a) Collum, D. B.; McNeil, Anne J.; Ramirez, A. *Angew. Chem., Int. Ed.* **2007**, *46*, 3002. (b) Lucht, B. L.; Collum, D. B. *Acc. Chem. Res.* **1999**, *32*, 1035. (c) Günther, H. *J. Braz. Chem. Soc.* **1999**, *10*, 241. (d) Bauer, W. *Lithium Chemistry: A Theoretical and Experimental Overview*; Schleyer, P. v. R., Ed.; Wiley: New York, **1995**, p 125. (e) Collum, D. B. *Acc. Chem. Res.* **1993**, *26*, 227. (f) Collum, D. B. *Acc. Chem. Res.* **1992**, *25*, 448. Selected studies identifying transition states: (g) Riggs, J. C.; Singh, K. J.; Yun, M.; Collum, D. B. *J. Am. Chem. Soc.* **2008**, *130*, 13709. (h) Remenar, J. F.; Lucht, B. L.; Collum, D. B. *J. Am. Chem. Soc.* **1997**, *119*, 5567. (i) Lucht, B. L.; Bernstein, M. P.; Remenar, J. F.; Collum, D. B. *J. Am. Chem. Soc.* **1996**, *118*, 10707.

(38)   Internal standards: COE = cyclooctene (mw = 110.2); TDE = tetradecene (mw = 196.4); SQU = squalene (mw = 410.7).

(39)   Crystal data is provided for comparison purposes only and is not intended to assert that the solution and solid state structures of these complexes are identical. Data provided is based on the widest measurement found in each structure. For examples of inconsistent solution and solid state structures of lithium amides see: (a) Collum, D. B.; Kahne, D.; Gut, S. A.; DePue, R. T.; Mohamadi, F.; Wanat, R. A.; Clardy, J.; Van Duyne, G. *J. Am. Chem. Soc.* **1984**, *106*, 4865. (b) Xu, F.; Reamer, R. A.; Tillyer, R.; Cummins, J. M.; Grabowski, E. J. J.; Reider, P. J.; Collum, D. B.; Huffman, J. C. *J. Am. Chem. Soc.* **2000**, *122*, 11212.

(40)   (a) Schober, K.; Hartmann, E.; Zhang, H.; Gschwind, R. M.; *Angew. Chem. Int. Ed.* **2010**, *49*, 2794. (b) Schober, K.; Zhang, H.; Gschwind, R. M.; *J. Am. Chem. Soc.* **2008**, *130*, 12310. (c) Gschwind, R. M., *Chem. Rev.* **2008**, *108*, 3029. (d) Zhang, H.; Gschwind, R. M. *Chem. Eur. J.* **2007**, *13*, 6691.

(41)   Diffusion coefficients are typically reported as $10^{-10}\,m^2\,s^{-1}$.

(42)   This species is illustrated as a monomer for simplicity and likely exists as a mixture of aggregates in solution.

(43)   Rare earth metal catalyzed hydroamination/cyclization of aminopentene documented at or below ambient temperature. Most active: (a) Gagné, M. R.; Marks, T. J. *J. Am. Chem. Soc.* **1989**, *111*, 4108. (b) Giardello, M. A.; Conticello, V. P.; Brard, L.; Gagne, M. R.; Marks, T. J. *J. Am. Chem. Soc.* **1994**, *116*, 10241. Highest enantioselectivity: (c) Gribkov, D. V.; Hultzsch, K. C.; Hampel, F. *J. Am. Chem. Soc.* **2006**, *128*, 3748. Other examples: (d) Gribkov, D. V.; Hultzsch, K. C. *Chem. Commun.* **2004**, 730. (e) Hong, S.; Tian, S.; Metz, M. V.; Marks, T. J. *J. Am. Chem. Soc.* **2003**, *125*, 14768. (f) Douglass, M. R.; Ogasawara, M.; Hong, S.; Metz, M. V.; Marks, T. J. *Organometallics* **2002**, *21*, 283.

(44)   Group 2: (a) Datta, S.; Roesky, P. W.; Blechert, S. *Organometallics* **2007**, *26*, 4392. (b) Buch, F.; Harder, S. *Z. Naturforsch.* **2008**, *63b*, 169. (c) Datta, S.; Gamer, M. T.; Roesky, P. W. *Organometallics* **2008**, *27*, 1207. (d) Crimmin, M. R.; Arrowsmith, M.; Barrett, A.

G. M.; Casely, I. J.; Hill, M. S.; Procopiou, P. A. *J. Am. Chem. Soc.* **2009**, *131*, 9670. (e) Zhang, X.; Emge, T. J.; Hultzsch, K. C. *Organometallics* **2010**, *29*, 5871. (f) Zhang, X.; Emge, T. J.; Hultzsch, K. C. *Angew. Chem. Int. Ed.* **2012**, *51*, 394.

(45) Group 4: (a) Kim, H.; Kim, Y. K.; Shim, J. H.; Kim, M.; Han, M.; Livinghouse, T.; Lee, P. H. *Adv. Synth. Cat.* **2006**, *348*, 2609. (b) Majumder, S.; Odom, A. L. *Organometallics* **2008**, *27*, 1174. (c) Reznichenko, A. L.; Hultzsch, K. C. *Organometallics* **2010**, *29*, 24. (d) Manna, K.; Ellern, A.; Sadow, A. D. *Chem. Commun.* **2010**, *46*, 339. (e) Ayinla, R. O.; Gibson, T.; Schafer, L. L. *J. Organomet. Chem.* **2011**, *696*, 50. (f) Manna, K.; Xu, S.; Sadow, A. D. *Angew. Chem. Int. Ed.* **2011**, *50*, 1865.

(46) Ambuehl, J.; Pregosin, P. S.; Venanzi, L. M.; Ughetto, G.; Zambonelli, L. *J. Organomet. Chem.* **1978**, *160*, 329.

(47) (a) See also references 3, 4 and 6a. (b) Lebeuf, R.; Robert, F.; Schenk, K.; Landais, Y. *Org. Lett.* **2006**, *8*, 4755.

(48) Excess base = Equivalents of $LiCH_2SiMe_3$ in excess of the initial 2.0 equivalents required to form the dilithium salt. Excess base is reported with respect to ligand.

(49) (a) Bender, C. F.; Widenhoefer, R. A. *J. Am. Chem. Soc.* **2005**, *127*, 1070. (b) Komeyama, K.; Morimoto, T.; Takaki, K. *Angew. Chem. Int. Ed.* **2006**, *45*, 2938. (c) Takemiya, A.; Hartwig, J. F. *J. Am. Chem. Soc.* **2006**, *128*, 6042. (d) Michael, F. E.; Cochran, B. M. *J. Am. Chem. Soc.* **2006**, *128*, 4246. (e) Han, X.; Widenhoefer, R. A. *Angew. Chem. Int. Ed.* **2006**, *45*, 1747. (f) Bender, C. F.; Widenhoefer, R. A. *Chem. Commun.* **2006**, 4143. (g) Bender, C. F.; Widenhoefer, R. A. *Org. Lett.* **2006**, *8*, 5303. (h) Zhang, J.; Yang, C.-G.; He, C. *J. Am. Chem. Soc.* **2006**, *128*, 1798. (i) Liu, X.-Y.; Li, C.-H.; Che, C.-M. *Organic Lett.* **2006**, *8*, 2707. (j) Cochran, B. M.; Michael, F. E. *Organic Lett.* **2007**, *10*, 329. (k) Liu, Z.; Hartwig, J. F. *J. Am. Chem. Soc.* **2008**, *130*, 1570. (l) Bauer, E. B.; Andavan, G. T. S.; Hollis, T. K.; Rubio, R. J.; Cho, J.; Kuchenbeiser, G. R.; Helgert, T. R.; Letko, C. S.; Tham, F. S. *Org. Lett.* **2008**, *10*, 1175. (m) Bender, C. F.; Hudson, W. B.; Widenhoefer, R. A. *Organometallics* **2008**, *27*, 2356. (n) Cochran, B. M.; Michael, F. E. *J. Am. Chem. Soc.* **2008**, *130*, 2786. (o) Bender, C. F.; Widenhoefer, R. A. *Chem. Commun.* **2008**, 2741. (p) Hesp, K. D.; Stradiotto, M. *Organic Lett.* **2009**, *11*, 1449. (q) Hesp, K. D.; Tobisch, S.; Stradiotto, M. *J. Am. Chem. Soc.* **2009**, *132*, 413. (r) Ohmiya, H.; Moriya, T.; Sawamura, M. *Organic Lett.* **2009**, *11*, 2145. (s) Kashiwame, Y.; Kuwata, S.; Ikariya, T. *Chem. Eur. J.* **2010**, *16*, 766. (t) Lavery, C. B.; Ferguson, M. J.; Stradiotto, M. *Organometallics* **2010**, *29*, 6125. (u) Shen, X.; Buchwald, S. L. *Angew. Chem. Int. Ed.* **2010**, *49*, 564. (v) Julian, L. D.; Hartwig, J. F. *J. Am. Chem. Soc.* **2010**, *132*, 13813. (w) Liu, Z.; Yamamichi, H.; Madrahimov, S. T.; Hartwig, J. F. *J. Am. Chem. Soc.* **2011**, *133*, 2772. (x) Kashiwame, Y.; Kuwata, S.; Ikariya, T. *Organometallics* **2012**, *31*, 8444.

(50) For the first formal kinetic study on the intramolecular hydroamination of aminoalkenes see reference 5.

(51) Berrisford, D. J.; Bolm, C.; Sharpless, K. B. *Angew. Chem. Int. Ed.* **1995**, *34*, 1059.

(52) Reznichenko, A.; Hultzsch, K.; *Structure and Bonding, Vol. 137* (Ed.: P. W. Roesky), Springer Berlin / Heidelberg, **2010**, pp. 1-48.

(53) M. R. Gagné, C. L. Stern, T. J. Marks, *J. Am. Chem. Soc.* **1992**, *114*, 275.

(54) (a) Liu, B.; Roisnel, T.; Carpentier, J.-F.; Sarazin, Y. *Angew. Chem. Int. Ed.* **2012**, *51*, 4943. (b) Brinkmann, C.; Barrett, A. G. M.; Hill, M. S.; Procopiou, P. A. *J. Am. Chem.*

Soc. **2012**, *134*, 2193. (c) Arrowsmith, M.; Crimmin, M. R.; Barrett, A. G. M.; Hill, M. S.; Kociok-Köhn, G.; Procopiou, P. A. *Organometallics* **2011**, *30*, 1493. (d) Dunne, J. F.; Fulton, D. B.; Ellern, A.; Sadow, A. D. *J. Am. Chem. Soc.* **2010**, *132*, 17680.

(55)   Barrett, A. G. M.; Brinkmann, C.; Crimmin, M. R.; Hill, M. S.; Hunt, P.; Procopiou, P. A. *J. Am. Chem. Soc.* **2009**, *131*, 12906.

(56)   Tobisch, S. *Chem. Eur. J.* **2011**, *17*, 14974.

(57)   Motta, A.; Lanza, G.; Fragalà, I. L.; Marks, T. J. *Organometallics* **2004**, *23*, 4097.

(58)   (a) Pez, G. P.; Galle, J. E. *Pure Appl. Chem.* **1985**, *57*, 1917. (b) Narita, T.; Teruo, Y.; Tsuruta, T. *Bull. Chem. Soc. Jap.* **1973**, *46*, 3825.

(59)   Seyferth, D. *Organometallics* **2009**, *28*, 1598.

(60)   Tobisch, S. *Inorg. Chem.* **2012**, *51*, 3786.

3

Intermolecular Hydroamination

3.1 Introduction

Coveted by academic and industrial scientists alike are the design and optimization of catalysts to efficiently perform the intermolecular hydroamination of non-activated olefins. Even more sought after is the *anti*-Markovnikov control of this transformation. Deemed one of the "Ten Challenges for Catalysis" twenty years ago, and still unrealized is the *anti*-Markovnikov addition of ammonia to olefins (Eq. 3-1).[1] The development of efficient systems for intermolecular hydroamination will represent a significant advancement in this field, as there are currently several well developed systems for its intramolecular variant. Catalyst screening on intermolecular reactions is also more practical because the preparation of intramolecular substrates can be averted.

$$anti\text{-Markovnikov} \qquad \text{Markovnikov}$$
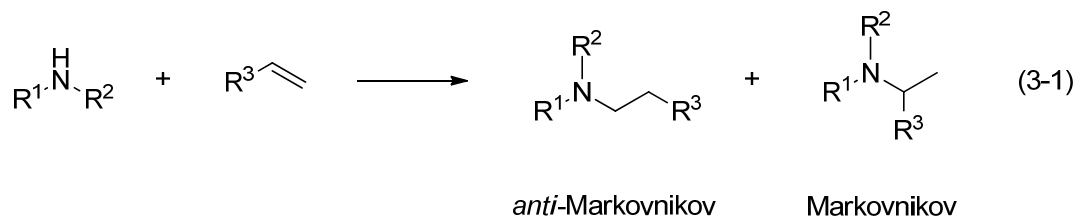
This transformation has been documented with rare earth, alkali, alkaline earth and late transition metals. Rare earth metal systems are hindered by competitive binding with substrate and product amines[2] and ten or more equivalents of excess olefin are often used to mitigate this problem. Alkaline earth metal complexes have demonstrated excellent activity for the intermolecular *anti*-Markovnikov hydroamination of styrene derivatives and 1,3-dienes.[3] Activity comparable or superior to the most active rare earth metal catalysts has been reported. Their scope includes both secondary and primary amines in the presence of equimolar amounts of olefin which demonstrates their potential to mediate this transformation in an atom economic fashion. Still in the early stages of development, their intrinsic basicity can lead to catalyst decomposition and olefin polymerization. Precatalytic equilibria are complicated by their

tendency to exist as mixed aggregates in solution allowing multiple catalytically relevant transition states and preventing high levels of stereoinduction.

3.1.1 Rare earth metal-catalyzed intermolecular hydroamination

Although rare earth metal-based catalysts are the most active and selective for intramolecular hydroamination, they are not as efficient for intermolecular reactions. A large excess of olefin and a higher reaction temperature is required to achieve conversion and increase reaction rate. Olefin insertion, which is postulated to be the rate determining step, is hindered by competitive binding with substrate and product amines. Nonetheless, the intermolecular hydroamination of olefins has been documented on multiple occasions in the groups of Marks and Hultzsch.[4] Lanthanocene and binaphtholate catalysts have mediated the addition of primary amines to styrene derivatives (*anti*-Markovnikov) and aliphatic olefins (Markovnikov) with binaptholate catalyst (**16**) achieving up to 61% enantiomeric excess.
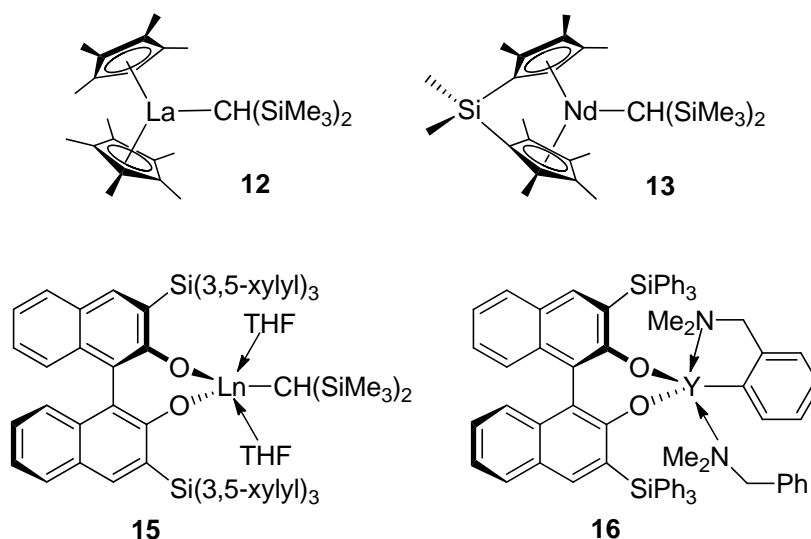
Figure 3-1. Rare earth metal-based catalysts for intermolecular hydroaminations.
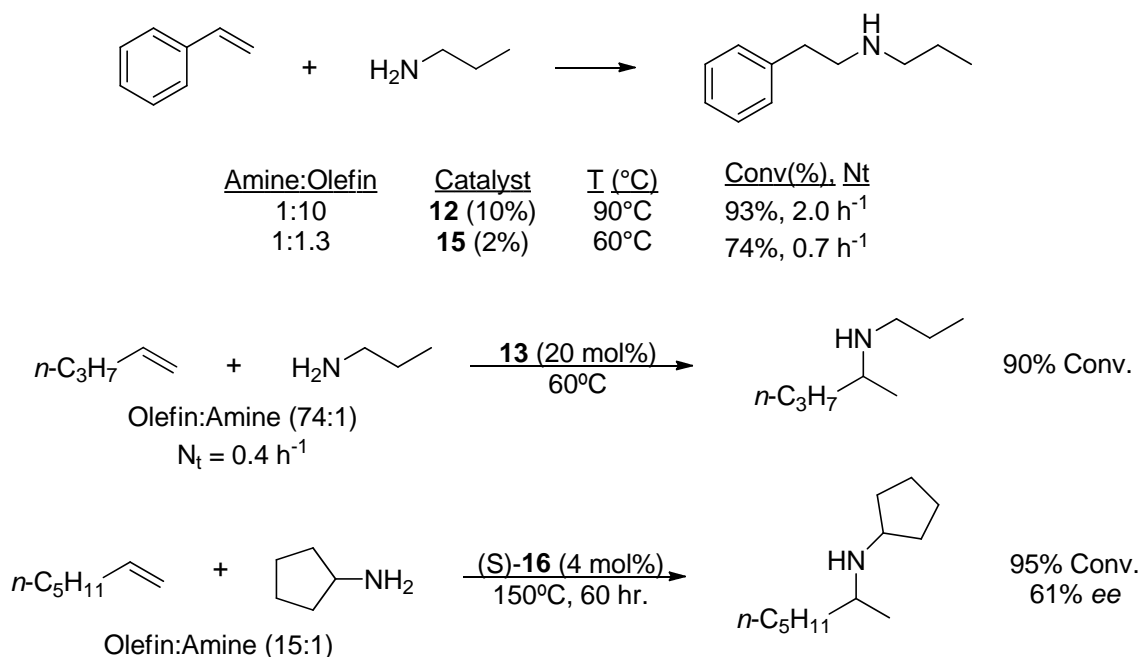
Scheme 3-1. Rare earth metal-mediated intermolecular hydroaminations.

3.1.2 Alkali metal-catalyzed intermolecular hydroamination

Alkali metal-catalyzed hydroamination[5] of olefins and 1,3-dienes can be traced back to the 1940's.[6] The addition of ammonia across ethylene (Eq. 3-2) and propylene (Eq. 3-3) as well as other amines and olefins (Eq. 3-4) was documented shortly thereafter using lithium, sodium and their hydrides as catalysts.[7] High temperatures (200–250°C) and pressures (200–1000 atm) were required to achieve conversion and mixtures of products were observed. It was later found that preformation of the alkali metal amide followed by sequential addition of ethylene to the catalyst allowed these processes to occur at slightly lower temperatures and pressures (Eq. 3-5 and 3-6).[7b,c]

$$NH_3 \quad + \quad \diagdown\!\!\diagup \quad \xrightarrow[\substack{850\text{-}975 \text{ psi} \\ 250°C}]{Na} \quad \diagup\!\!\diagdown\text{-}NH_2 \quad + \quad \diagup\!\!\diagdown\text{-}\overset{H}{N}\text{-}\diagdown\!\!\diagup \qquad (3\text{-}3)$$

$$\text{82\%} \qquad\qquad \text{8\%}$$

$$H_2N\diagdown\!\!\diagup\!\!\diagdown \quad + \quad = \quad \xrightarrow[\substack{800\text{-}1000 \text{ psi} \\ 200°C}]{Na} \quad \diagdown\!\!\diagup\!N\diagdown\!\!\diagup\!\!\diagdown \qquad (3\text{-}4)$$

$$\text{75\%}$$

(3-5)

(3-6)
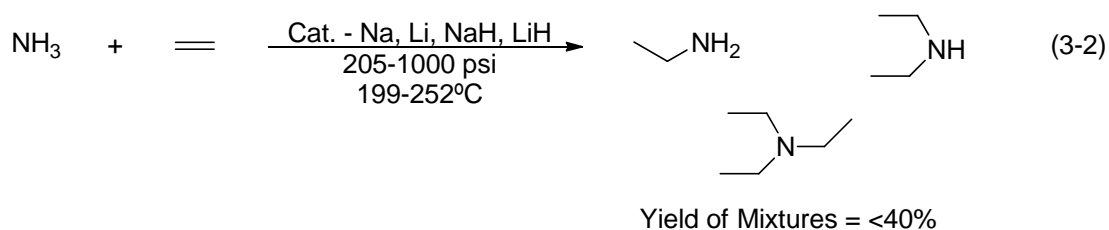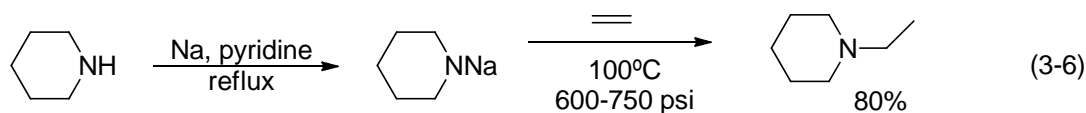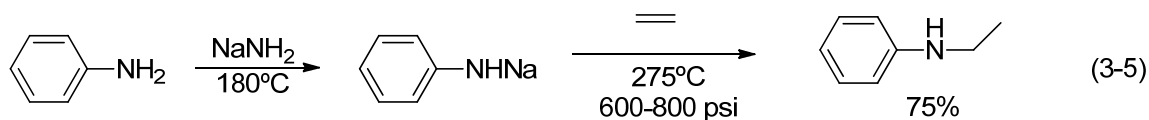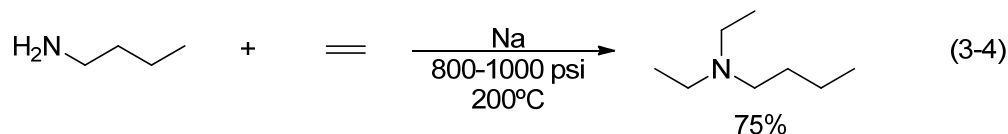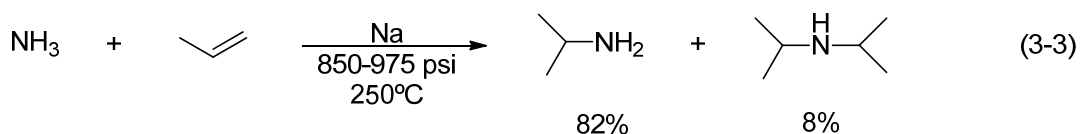
The addition of diethyl amine to ethylene occurred at lower pressures and ambient temperature in the presence of TMEDA (Scheme 3-2).[8]   Additional ligand screening and optimization of this process was later performed, with TMEDA and PMDTA allowing the highest levels of conversion and sparteine also enhancing reactivity (Figure 3-2, Table 3-1).[9]

TMEDA   TEEDA   PMDTA   (−)-Sparteine
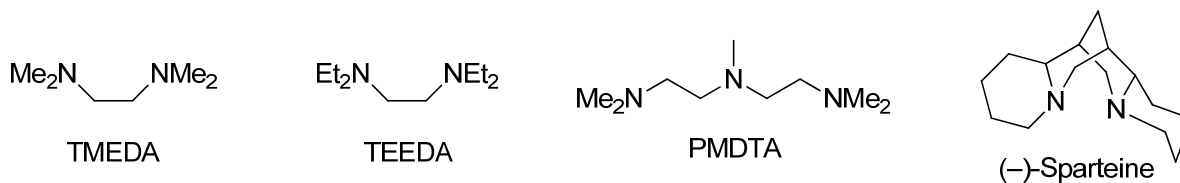
Figure 3-2. Selected chelating ligands demonstrating activity during the lithium catalyzed intermolecular hydroamination of ethylene with diethylamine.
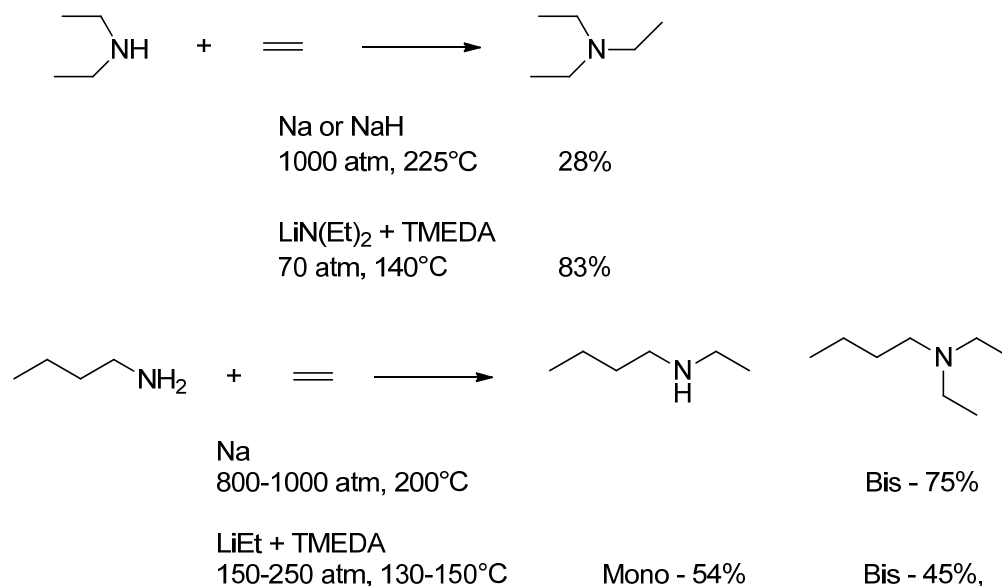
Scheme 3-2. The addition of diethylamine and butylamine to ethylene. The use of lithium diethylamide and ethyl lithium in the presence of TMEDA allowed conversion to occur at significantly lower pressures and temperatures than previously reported.

Table 3-1. Selected results from a study of ligand effects on lithium catalyzed intermolecular hydroamination of ethylene with diethylamine.

Ligand	Conv.(%)
TMEDA	92
TEEDA	19
PMDTA	90
(–)-Sparteine	36
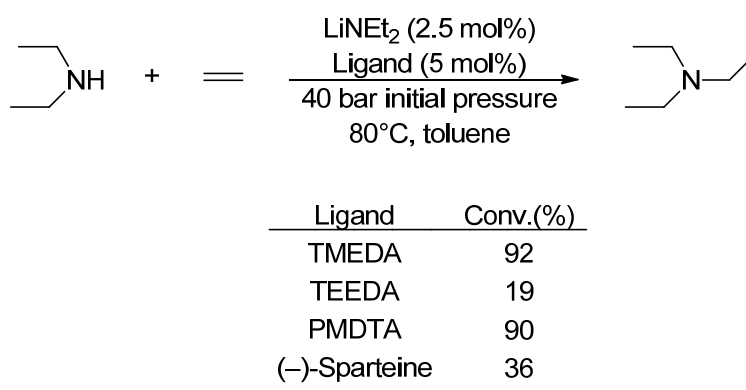
TMEDA/LiHMDS has been reported to mediate the base catalyzed *anti*-Markovnikov hydroamination of vinylarenes (Tables 3-2 and 3-3).[10] Sparteine was used in lieu of TMEDA in several examples and low levels of stereoinduction were reported.[11] Other accounts of base-catalyzed hydroamination of styrenes[12] and 1,3 dienes[13] and ethylene[14] and aliphatic amines[15] have been reported.

Table 3-2. Selected examples of the lithium catalyzed intermolecular hydroamination of α-methyl styrene by benzyl amine.
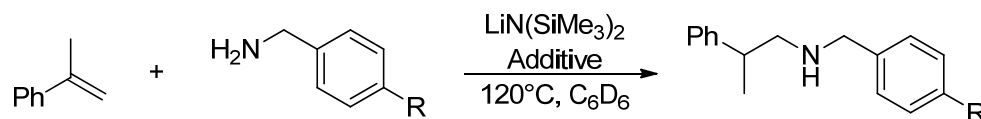
R	Additive	Yield (%)
H	TMEDA	48
H	(–)-Sparteine	57
OCH$_3$	TMEDA	38
OCH$_3$	(–)-Sparteine	40, 7% *ee*

Table 3-3. Selected examples of the lithium catalyzed intermolecular hydroamination of *trans*-β-methyl styrene by benzyl amine.

R	Additive	Yield (%)
H	TMEDA	74
H	(–)-Sparteine	71
OCH$_3$	(–)-Sparteine	60, 14% *ee*

Several examples of heavy alkali metal-based catalysts have been reported although development on a well-defined, selective system has not occurred. KHMDS/TMEDA[10] demonstrated high activity and low regioselectivity for the intermolecular hydroamination of styrene derivatives. A mixture of mono and bis alkylation products was produced along with hydroaminoalkylation products. Sodium has been reported as an effective mediator of base-catalyzed hydroamination.[16] Highly developed systems for this transformation have not been reported, possibly due to solubility and regioselectivity issues. The solid state structures of several sodium/sparteine adducts have been reported recently, along with a facile synthesis of NaCH$_2$SiMe$_3$.[17]

3.1.3 Alkaline Earth Metal-Catalyzed Intermolecular Hydroamination

The use of alkaline earth metals[18] for hydroamination catalysis is complicated by their tendency to exist in a Schlenk equilibrium[19] and their low solubility in non-coordinating solvents. Group 2 metal complexes enter their catalytic cycles by amine activation with substrate deprotonation typically initiated by an amido[20] or alkyl[21] leaving group. Alkyl leaving groups are advantageous because catalyst activation is irreversible; however, their high basicity is problematic due to competing deprotonation and anionic polymerization reactions.[21f] Lewis basic solvents including THF are used to solubilize precatalysts, potentially leading to ambiguous aggregates or stabilizing the ground states of catalytic species. Bulky multidentate ligands have demonstrated their capacity to prevent Schlenk equilibria, solubilize metal centers and generate a chiral environment.[3b,21e] Many early chiral catalysts suffered from low enantioselectivities[22] caused by ligand redistribution.

While some recent studies suggest that the reactivity of alkaline earth metal-based catalysts increases with increasing metal size,[3d] some experimental and computational studies contradict this observation.[3a,c] The evaluation of this trend is difficult with a single ligand because the metals vary in size and can form unstable complexes or mixtures of aggregates upon metalation.

Excellent activity for the intermolecular hydroamination of styrene derivatives (with *anti*-Markovnikov selectivity) and 1,3-dienes has been demonstrated by alkaline earth metal based complexes (*R,R*)-**17** and **19-24**.[3] Activity comparable to, or better than, the most active rare earth metal–based systems for *anti*-Markovnikov hydroamination of styrene has been reported (Table 3-1). Their capacity to perform this transformation with both secondary and primary amines in the presence of equimolar amounts of olefin makes their development a worthy pursuit, and optimization of amine/olefin ratios will further increase yields of the desired product.
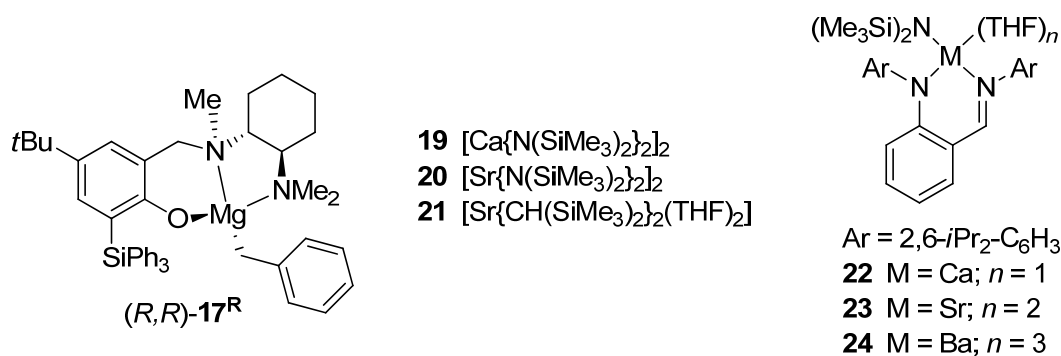
Figure 3-3. Selected alkaline earth metal-based catalysts for the intermolecular hydroamination.

Table 3-4. Selected examples of intermolecular hydroamination mediated by alkaline earth metal catalysts.

R'	R"	Amine:Olefin	Catalyst	Time, T (°C)	Conv(%), N_t	Ref
-(CH$_2$)$_5$-		1:1	**20** (5%)	72 hr, RT	92%, 0.28 h^{-1}	52
-(CH$_2$)$_5$-		1:1	**21** (5%)	10 min, RT	70%, 120.0 h^{-1}	52
-(CH$_2$)$_4$-		1.2:1	(R,R)-**17** (5%)	16 hr, 60°C	87%	50
H	Bn	1:1	**22** (2%)	18.5 hr, 60°C	34%	52
H	Bn	1:1	**23** (2%)	18.5 hr, 60°C	71%	52
H	Bn	1:1	**24** (2%)	18.5 hr, 60°C	86%	52
H	Bn	1:1	**19** (5%)	48 hr, 60°C	92%	52
H	Bn	1:1	**20** (5%)	24 hr, 60°C	78%	52

3.1.4 Late Transition metal–catalyzed intermolecular hydroamination

A number of late transition metal-based catalysts[23] for hydroamination have been developed, however this field has largely focused on the hydroamination of activated substrates including alkynes, allenes and dienes. The past fifteen years have seen a number of reports on the intermolecular hydroamination of styrene derivatives along with the hydroamination/cyclization of aminoalkenes demonstrating the potential of complexes within this class.

Late transition metal catalysts frequently operate by alkene activation instead of amine activation which distinguishes them from the more polar reagents typically employed in this transformation. The presence of multiple stable oxidations states and sensitivity to the steric bulk on substrates allows catalysts to operate under a broader range of mechanisms than observed with complexes from Groups 1–3. The three common scenarios include coordination of an alkene, alkyne or allylic complex to a catalyst which allows nucleophilic attack from an amine. Alkene insertion into late transition metal hydride complexes have been documented although it

is uncommon.[24] Redox couples are known to undergo oxidative addition with amines, and the catalytic cycle for the iridium catalyzed intermolecular hydroamination of norbornene begins by amine activation.[25] For intermolecular transformations which proceed by alkene activation, Markovnikov regioselectivity typically ensues. Nucleophilic attack occurs at the most electrophilic carbon adjacent to the aromatic ring, which makes design of catalysts for *anti*-Markovnikov transformations challenging. This mechanism also contains a β-amino alkyl metal intermediate which is susceptible to β-hydride elimination leading to oxidative amination by-products (Scheme 3-3).
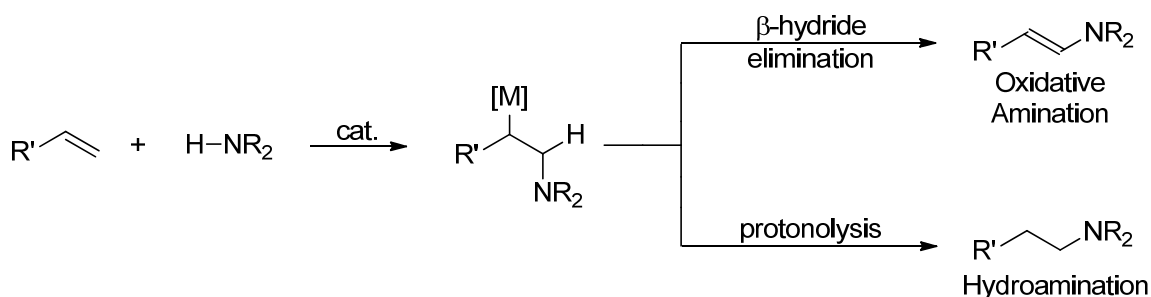
Scheme 3-3. The *anti*-Markovnikov addition of an amine to styrene forms a metal alkyl intermediate which can undergo β-hydride elimination or protonolysis leading to oxidative amination or hydroamination products.[23e]

The propensity of late transition metal catalysts to operate by alkene activation accounts for the choice of substrates in many studies. Alkenes are more desirable starting materials for hydroamination because they are less expensive, more stable and more easily synthesized than alkynes and allenes. However, they contain less electron density which makes binding to a metal center more difficult. In spite of this obstacle, the intermolecular hydroamination of styrene, norbornene and aliphatic olefins has been documented.

Late transition metal-based complexes have good functional group tolerance and low sensitivity to oxygen and moisture compared with other classes of catalysts. Acid co-catalysts are known to increase reaction rates and yields by accelerating turnover limiting protonolysis of the M-C bond. They may also suppress competitive amine binding to the metal center. Bulky, weakly coordinating counterions, frequently triflate (TfO- = F_3CSO_3-) are commonly used, and many of these reactions may be acid catalyzed.[26]

Group 8: Ru(II)

Ru(COD)(2-Me-allyl)$_2$ (**42**), DPPPent (**43**) and triflic acid is one of the most selective catalytic systems for the intermolecular *anti*-Markovnikov hydroamination of styrene derivatives.[27] Its d^6 configuration allows unique binding to the arene system of the substrate (**44**, Eq. 3-7), favoring nucleophilic attack at the terminal carbon. Moderate to high yields were reported for the addition of morpholine and piperidines to styrene at 100°C (Eq. 3-8).
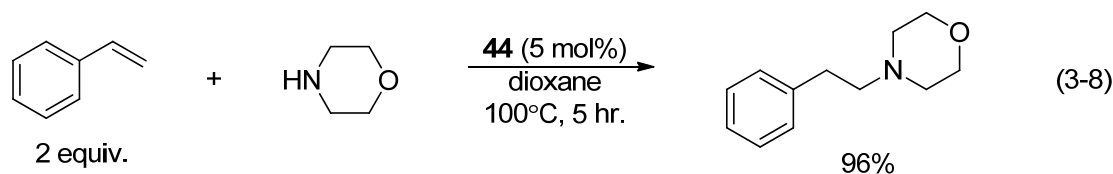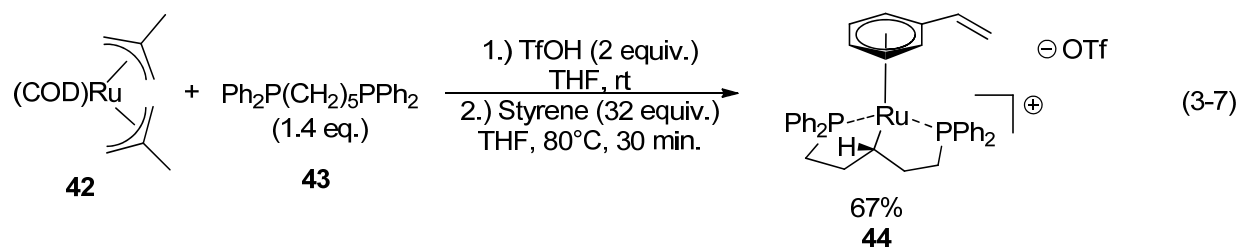
$$(3\text{-}7)$$

$$(3\text{-}8)$$

Group 9: Rh(I) and Ir(I)

Intermolecular hydroamination mediated by Rh(I)- and Ir(I)- based systems have been known since 1971,[28] although their applications are limited. Rhodium-based systems form *anti*-Markovnikov hydroamination products upon addition to styrene; however, oxidative amination is a major side-product.[29] The metal alkyl intermediate generated tends to undergo β-hydride elimination, behaving similarly to palladium complexes. High selectivity for the hydroamination product has been demonstrated when DPEphos (**45**) is used as a ligand,[30] although enamines are observed as a side-product (Eq. 3-9).

$$(3\text{-}9)$$
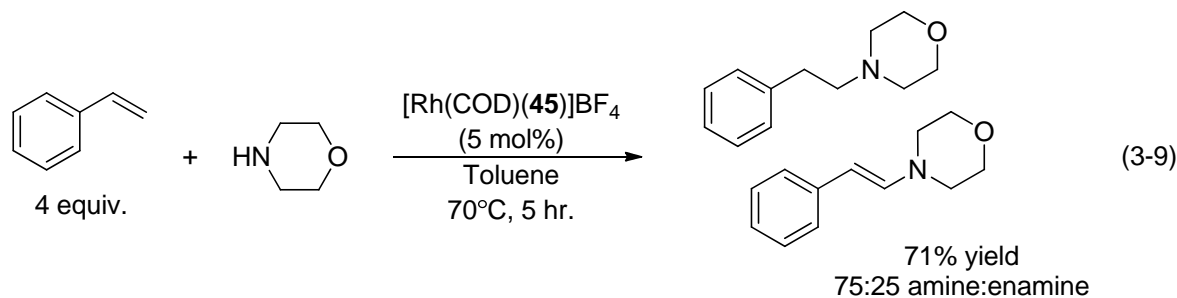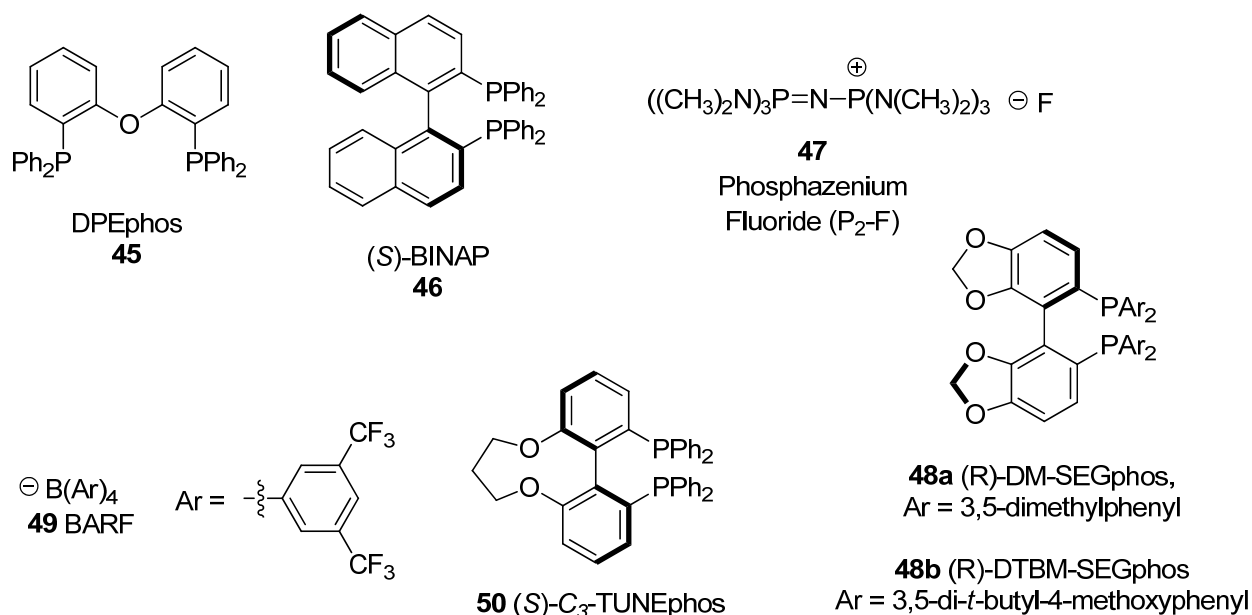
Figure 3-4. Phosphine ligands and other additives used to form Iridium catalysts for intermolecular hydroamination reactions.

The majority of intermolecular Ir(I)- mediated hydroaminations have been documented on norbornene and its derivatives. Enantioselectivities of up to 95%[25b] were reported with [IrCl((S)-**46**)]$_2$ and phosphazenium fluoride (**47**) although low TON's in addition to low substrate scope limit the utility of this catalyst. A catalytic mixture of **48a** and [Ir(COE)$_2$Cl]$_2$ and KHMDS in yielded *ee*'s up to 99% and yields up to 94% on the intermolecular addition of aniline derivatives to norbornene.[25d] The combination of high yield and enantioselectivity distinguish this system from others. The intermolecular addition of amides and sulfonamides to norbornene (in up to 93% *ee*) and aliphatic olefins was catalyzed by **48b** and [Ir(COE)$_2$Cl]$_2$ (Eq. 3-10).[31] Up to 83% *ee* was induced with [Ir(COD)$_2$]**49** and (S)-C$_3$-TUNEPHOS (**50**) for the intermolecular Markovnikov addition of heteroaromatic amines to styrene and styrene derivatives (Eq. 3-11).[32]

$$(3\text{-}10)$$

85% yield, 93% *ee*

$$\text{Ph} \diagup\diagdown \quad + \quad \text{(isoquinolin-1-amine)} \xrightarrow[\substack{\textbf{50} \text{ (10 mol\%)} \\ \text{neat, 110°C, 24 hr.}}]{[\text{Ir(COD)}_2]\textbf{49} \text{ (10 mol\%)}} \text{(product)} \qquad (3\text{-}11)$$

58% yield, 83% *ee*
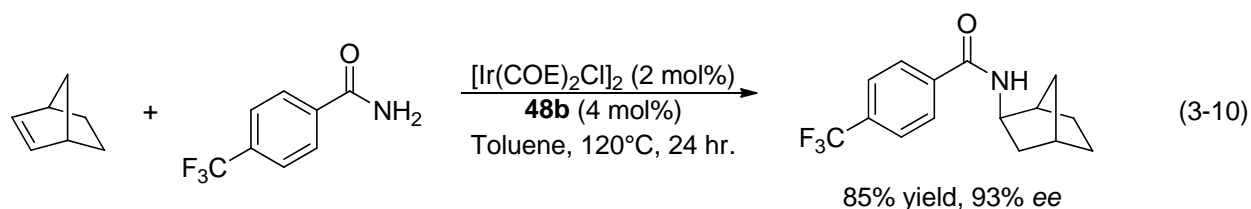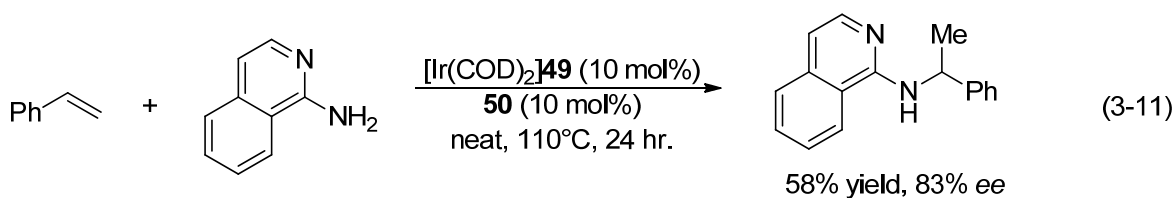
The propensity of Ir(I) catalysts to undergo oxidative addition with amine N-H bonds,[25c] distinguishes them from other systems, although this mechanism appears specific to the intermolecular addition to norbornene.[25a]

Group 10: Pd(II)

The Markovnikov addition of anilines to styrenes was mediated by $Pd(PPh_3)_2(OTf)_2$ and (**51**)Pd(TFA)$_2$ in the presence of excess triflic acid.[24a] (**51**)Pd(O$_2$CCF$_3$)$_2$ and triflic acid were also effective for this transformation.[33] [(R)-**46**]Pd(OTf)$_2$ induced *ee*'s of 81% at 25°C and 64% at 45°C for the addition of aniline to *p*-trifluoromethyl styrene and 2-vinyl naphthalene.[24a]
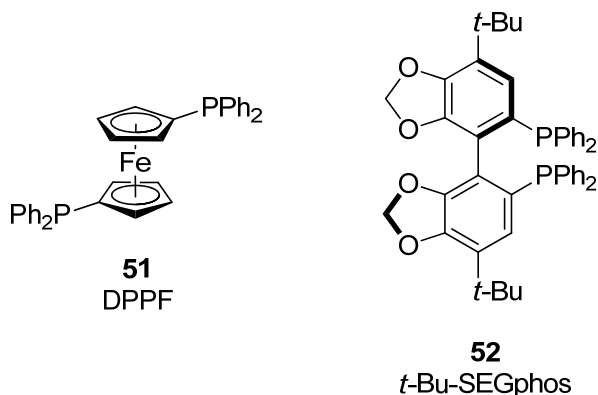
Figure 3-5. Phosphine ligands used to form Palladium catalysts for intermolecular hydroamination reactions.
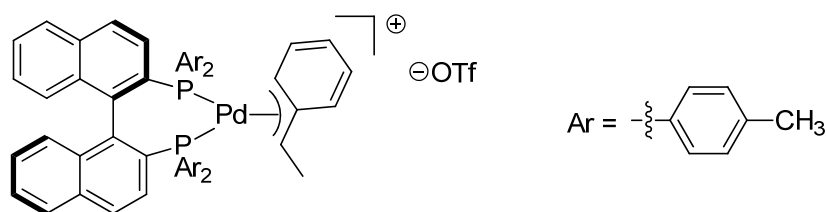
Figure 3-6. Crystallographically characterized η^3–benzyl intermediate found in the catalytic cycle for the intermolecular Markovnikov hydroamination to styrene derivatives.

A unique crystallographically characterized η^3–benzyl intermediate[24b] (Figure 3-6) allows mechanistic insight into this process and rationalization for the Markovnikov selectivity. The benzyl group binds in an η^3-fashion to the metal center, which activates the benzylic carbon for nucleophilic attack. Inversion of configuration at this carbon upon nucleophilic attack serves as proof of concept. In depth analysis on these systems revealed higher rates of nucleophilic attack on $[Pd(\eta^3\text{-allyl})Cl]_2$ complexes relative to those containing triflate and tetrafluoroborate counterions. The η^3-benzyl derivative of this complex, $[Pd(\eta^3\text{-benzyl})OTf]_2$ also demonstrated counterion effects, with tetrafluoroborate showing higher activity than triflate. Larger P-Pd-P bite angles increased their activity with Xantphos (**40**) being the most effective ligand.[24c] Additional crystallographic and catalytic data were reported for other Pd(II) complexes chelated by bidentate phosphine ligands. The intermolecular Markovnikov hydroamination of aniline to styrene (Eq. 3-12) or *p*-fluoro styrene (Eq. 3-13) was reported in up to 70% *ee* with [Pd((*R*)-**46**)(NCMe)(H$_2$O)](OTf)$_2$[34] and 84% *ee* with [Pd(**52**)(NCMe$_2$)$_2$](OTf)$_2$.[35]
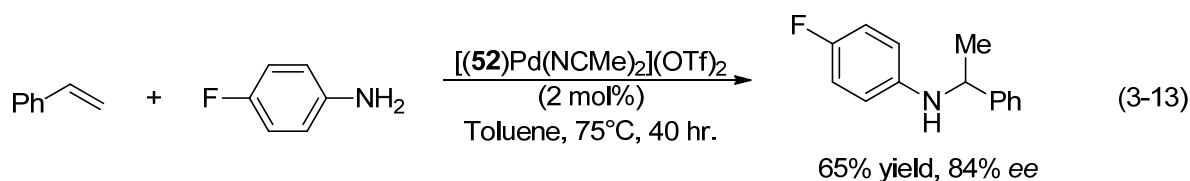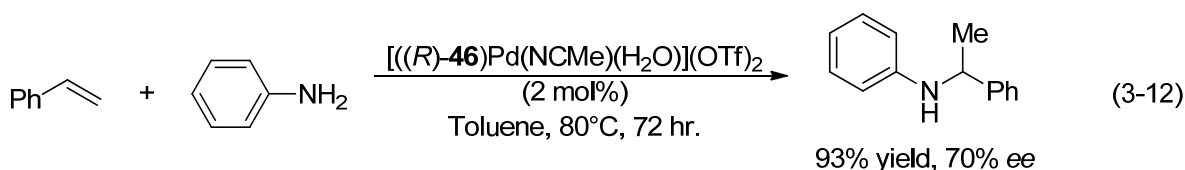
$$\text{Ph}\diagup\!\!\!\diagdown + \bigcirc\text{-NH}_2 \xrightarrow[\substack{(2\ mol\%)\\ Toluene,\ 80°C,\ 72\ hr.}]{[((R)\text{-}\mathbf{46})Pd(NCMe)(H_2O)](OTf)_2}} \quad (3\text{-}12)$$

93% yield, 70% *ee*

$$\text{Ph}\diagup\!\!\!\diagdown + \text{F}\!-\!\bigcirc\text{-NH}_2 \xrightarrow[\substack{(2\ mol\%)\\ Toluene,\ 75°C,\ 40\ hr.}]{[(\mathbf{52})Pd(NCMe)_2](OTf)_2}} \quad (3\text{-}13)$$

65% yield, 84% *ee*

Group 11: Gold(I)

Although multiple accounts of late transition metal-based hydroamination of dienes[36] and ethylene have been documented, this transformation is much more difficult with unactivated aliphatic amines. These transformations are seemingly more difficult with free amines and many systems were reported only with protected amines including sulfonamides.[37]

The Markovnikov addition of urea to unactivated alkenes and ethylene has been reported in up to 78% *ee* catalyzed by a mixture of [(*S*)-**53**](AuCl)$_2$ and AgOTf (Table 3-5).[38] Much like the rare

earth metal-mediated intermolecular hydroamination of unactivated olefins, a large excess of olefin (10–60 equivalents) was used in this study.

Table 3-5. Gold catalyzed enantioselective intermolecular Markovnikov hydroamination of unactivated alkenes with Imidazolidin-2-ones.

R	Conv(%)	ee (%)
Me	86	76
t-Bu	89	78
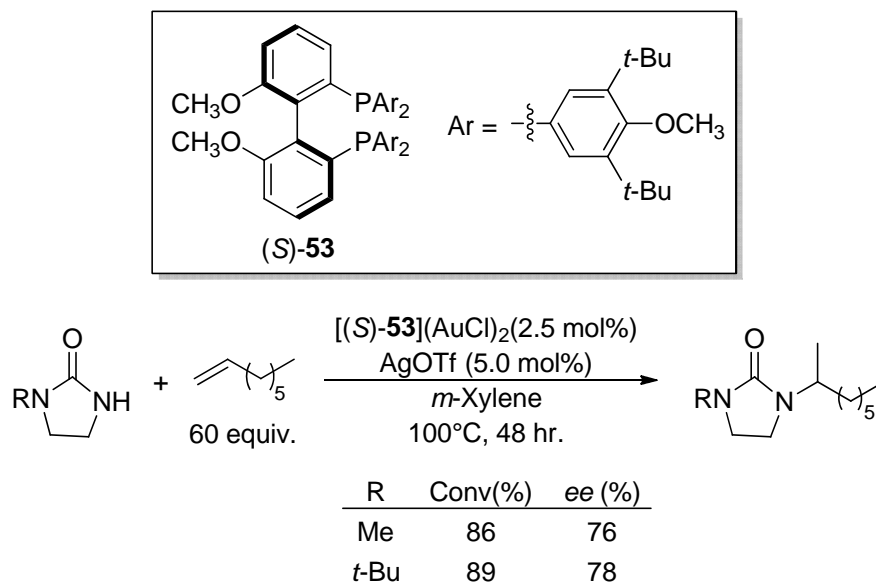
3.2 Intermolecular Carbolithiation

Although fundamentally different from lithium mediated intermolecular hydroamination, select intermolecular carbolithiations[39] may allow insight into intermolecular hydroamination. Carbolithiations are particularly important when regioselective, diastereoselective and stereoselective. The majority of substrates used contain chelating groups, which can stabilize reactive intermediates through intramolecular coordination.[40] Reports of stereoinduction on non-chelating substrates are less common. The addition of *n*-butyllithium to *trans*-β-methyl styrene in the presence of stoichiometric amount of sparteine induced 85% enantiomeric excess and 83% conversion (Eq. 3-14).[41] When a catalytic amount of sparteine (10 mol%) was used in the same transformation, 70% enantiomeric excess and 50% yield were obtained (Eq. 3-15).[42] These results show that the proper base and chiral auxiliary can induce high levels of selectivity even in intermolecular reactions. DFT studies for the carbolithiation of β-methylstyrene[43] with (–)-sparteine and either ethyl or isopropyl lithium demonstrated energy differences of 13 and 8 kJ mol^{-1} between the diastereomeric transition states leading to the product.

124

Ph–CH=CH–Me →[*n*-BuLi/hexane / (–)-Sparteine (1 equiv.)]→ Ph–CH₂–CH(Bu)(Me)   (3-14)

83% yield
85% *ee*

Ph–CH=CH–Me →[*n*-BuLi/hexane / (–)-Sparteine (10 mol%)]→ Ph–CH₂–CH(Bu)(Me)   (3-15)

50% yield
70% *ee*
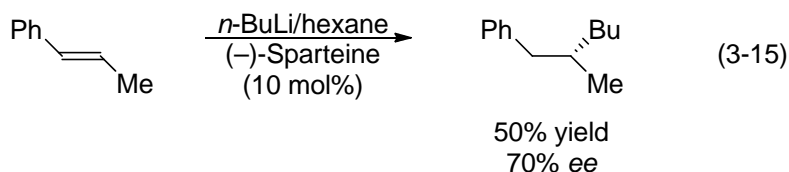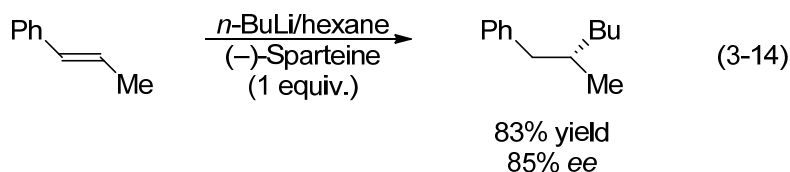
3.3 Salt Effects in Organolithium Reactions

The effects of LiCl and other salts on organolithium reagents are often overlooked by organic chemists.[44] Whether introduced by contaminated commercial lithium reagents or as a reaction byproduct, it can impact reaction rates[45] and enantioselectivities[46] (Scheme 3-4) by deaggregation[47] and/or incorporation into the desired transition state. This effect has been exploited in the field of bimetallic super base chemistry and allows difficult deprotonations on heterocyclic compounds to occur while leaving the desired product intact.[48] The solution structures of these compounds is not completely understood and studies have been undertaken to assess if they exist as ate complexes or multi-component mixtures.[49]
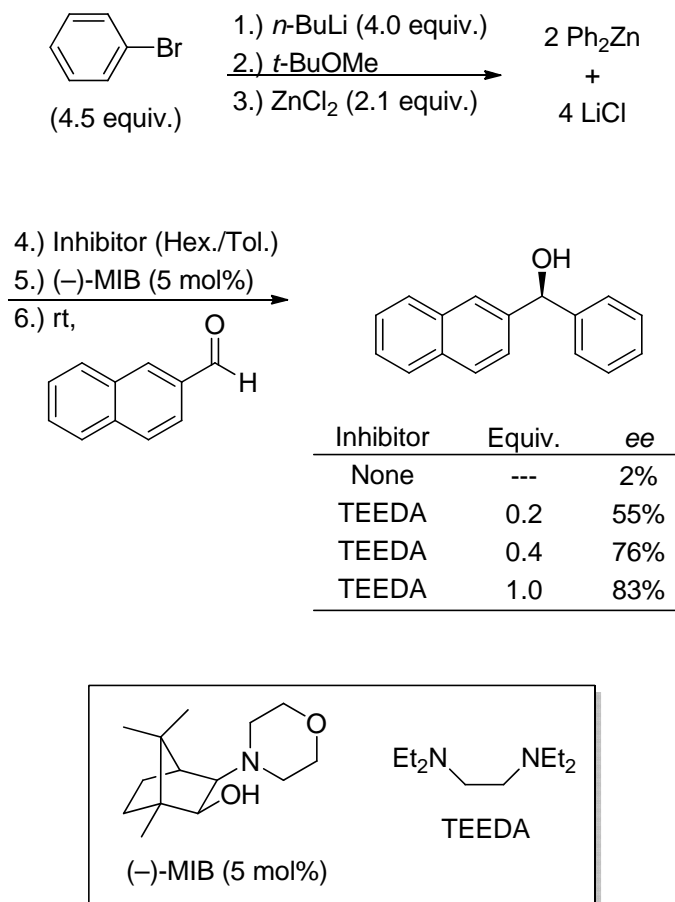
Scheme 3-4. Zinc mediated asymmetric addition of phenyl to 2-naphthaldehyde. Inclusion of TEEDA, a LiCl inhibitor, demonstrated the potential of LiCl to impact reaction enantioselectivities.

3.4 Background Reactions

As noted in Chapter 2, high levels of stereoinduction for the intramolecular hydroamination/cyclization mediated by (R)-**54** are attributed to the presence of a ligand accelerated pathway. The significant rate difference between the unaccelerated background reaction mediated by LiCH$_2$SiMe$_3$ and the accelerated containing (R)-**54** allow the majority of the product to pass through the transition state for the accelerated process. Understanding the background processes for a given reaction allows rate changes to be the first indicator for a ligands involvement in a given process.

A series of primary and secondary amines were screened for hydroamination activity using free LiCH$_2$SiMe$_3$ and NaCH$_2$SiMe$_3$ for styrene and its derivatives. The isomerization of

cis-β-methyl styrene (**108**) and allyl benzene (**110**) to form *trans*-β-methyl styrene (**109**) was observed as a background process (Scheme 3-5). This reaction was observed for all alkali metal amides tested herein and likely influences the rates of the corresponding hydroamination reactions. Regioselectivity was unaffected by this process, and exclusive formation of the *anti*-Markovnikov product was observed. Both primary and secondary amines underwent the addition reaction, showing amine scope comparable to alkaline earth metals and broader than that of rare earth metals.

R^1 = alkyl or H
R^2 = alkyl or benzyl
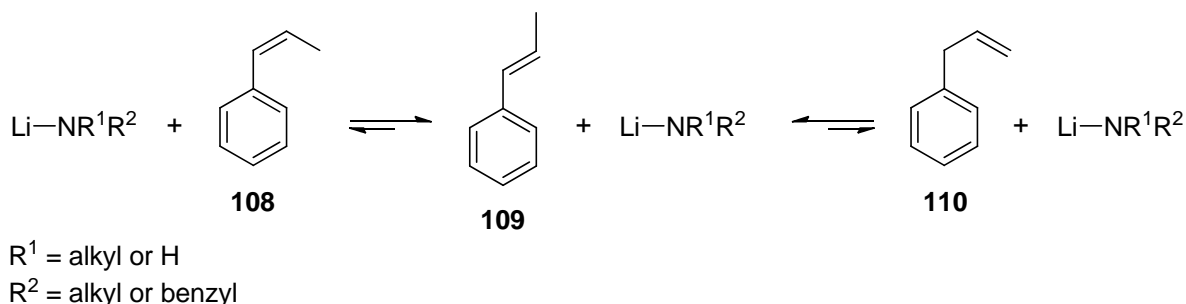
Scheme 3-5. Lithium amide catalyzed isomerization of *cis*-β-methyl styrene (**108**) and allyl benzene (**110**) to form *trans*-β-methyl styrene (**109**).
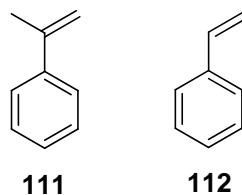
Figure 3-7. Intermolecular hydroamination substrates α-methyl styrene (**111**) and styrene (**112**).

Benzyl amine added to α-methyl styrene (**111**, Table 3-7) and cis-β-methyl styrene (**108**) or allyl benzene (**110**) in the presence of LiCH$_2$SiMe$_3$ at 50°C and 100°C respectively (Table 3-6). Overalkylation was the major side reaction and moderate isolated yields were obtained. Secondary amines showed higher activity than primary amines, which is consistent with previously published results. The addition of pyrrolidine to α-methyl styrene (**111**, Table 3-11) and cis-β-methyl styrene (**108**) or allyl benzene (**110**) with LiCH$_2$SiMe$_3$ proceeded at ambient temperatures (Table 3-10). The addition of LiCl (Table 3-10) in one example did not impact reaction rate, conversion or yield.

The hydroamination of lithium diethylamide to allylbenzene (**110**) was not observed, although the alkene was consumed by polymerization (Eq. 3-16). The hydroamination of lithium diethylamide to styrene (**112**) was observed (Table 3-9). All reactions mediated by lithium stalled prior to reaching full conversion.

When $NaCH_2SiMe_3$ was used for the addition of pyrrolidine to allylbenzene (**110**) a significant rate enhancement was observed and the reaction proceeded to completion. A twofold excess of alkene was used in this experiment because anionic olefin polymerization is observed as a side reaction. These results highlight the potential of heavy alkali metal amides to efficiently and selectively perform this transformation and demonstrate the limitations of simple lithium amides.

3.5 Screening and Studies of Ligand Effects

The impact of (–)-sparteine, axially chiral (*R*)-**54**, and lithium chloride on the intermolecular hydroamination of styrene derivatives was investigated.

The reaction rate and yield for the addition of benzyl amine to *cis*-β-methyl styrene (**108**) and allyl benzene (**110**) catalyzed by $LiCH_2SiMe_3$ was not affected by (–)-sparteine (Table 3-6) and no stereoinduction was observed. When a 3:1 ratio of (–)-sparteine:$LiCH_2SiMe_3$ was used, the product was racemic. The presence of (*R*)-**54** and LiCl (Table 3-6) produced no rate enhancement or enantioselectivity and lower conversion was observed. It is plausible that the dilithium salt is catalytically inactive, and lowers the concentration of lithium within the reaction.

Table 3-6. Lithium catalyzed intermolecular *anti*-Markovnikov hydroamination of *cis*-β-methyl styrene (**108**) and allyl benzene (**110**) with benzyl amine.
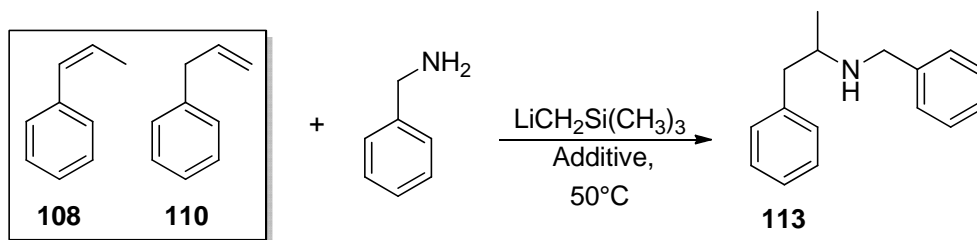
Alkene	LiCH$_2$Si(CH$_3$)$_3$ mol%	Additive (mol %)	Time (hh:mm)	Isolated Yield (%)	Conv. (%)
108	10	None	66:45	67	75
108	10	(–)-Sparteine (10)	71:25	52	80
110	5	(–)-Sparteine (15)	136:15	81	82
108	15	(*R*)-**54** (5), LiCl (4)	160:35	49	50

The addition of benzyl amine to α-methyl styrene (**111**) yielded *anti*-Markovnikov hydroamination products. The inclusion of (*R*)-**54** did not impact the reaction rate and no stereoinduction was observed (Table 3-7).

Table 3-7. Lithium catalyzed intermolecular *anti*-Markovnikov hydroamination of α-methyl styrene (**111**) with benzyl amine.
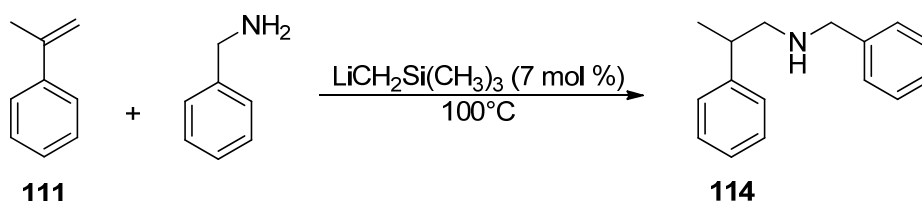
Additive (mol %)	Time (hh:mm)	Isolated Yield (%)	Conv. (%)
None	116:45	57	71
(*R*)-**54** (2)	145:50	39	65

The use of NaCH$_2$SiMe$_3$ as a base allowed the reaction to reach completion at 22°C. Inclusion of (–)-sparteine allowed high selectivity for the monohydroamination product in spite of a four fold excess of allyl benzene (**110**) being present (Table 3-8). When a (2:1) ratio of ((–)-sparteine:NaCH$_2$SiMe$_3$) was used, a rate increase occurred. This suggests that (–)-sparteine could

be involved in a pre-catalytic deaggregation process or the rate-determining step in the catalytic cycle. No stereoinduction was observed for either of these experiments.

Table 3-8. Sodium catalyzed intermolecular *anti*-Markovnikov hydroamination of allyl benzene (**110**) with benzyl amine.

Additive (mol %)	Time (hh:mm)	Isolated Yield (%)	Conv. (%)
(−)-Sparteine (20)	92:25	77	100
(−)-Sparteine (10)	121:45	80	100

When lithium diethylamide was exposed to allylbenzene (**110**), polymerization occurred with no hydroamination products being formed. The outcome of this reaction was identical when (−)-sparteine was included with consumption of the alkene occurring at the same rate.

$$\text{(3-16)}$$

*Identical results obtained with no additive and with 5 mol% (−)-Sparteine.

Exclusive formation of *anti*-Markovnikov hydroamination products were observed when lithium diethylamide was exposed to styrene (**112**, Table 3-9). The presence of (*R*)-**54** in this reaction had no impact on the reaction rate.

Table 3-9. Lithium catalyzed intermolecular *anti*-Markovnikov hydroamination of styrene (**112**) with diethylamide.
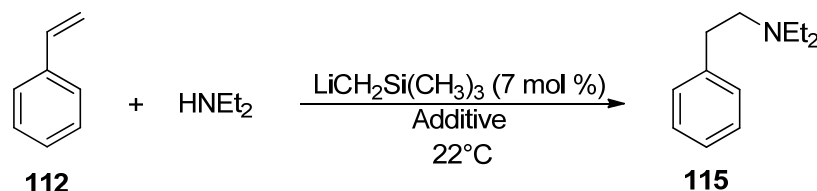
Additive (mol %)	Time (hh:mm)	Isolated Yield (%)	Conv. (%)
None	30:20	67	80
(*R*)-**54** (2)	26:15	70	77

The addition of pyrrolidine to *cis*-β-methyl styrene (**108**) and allylbenzene (**110**) catalyzed by $LiCH_2SiMe_3$ was studied under a variety of different conditions. The presence of (–)-sparteine caused a significant rate increase, even when the loading of base was decreased (Table 3-10). A rate decrease occurred upon addition of (*R*)-**54**, with a similar outcome for the addition of pyrrolidine to α-methyl styrene (**111**, Table 3-11). No stereoinduction was observed for these reactions.

For the addition of pyrrolidine to *cis*-β-methyl styrene (**108**), no conversion was achieved when H_2-(*R*)-**54** (2 mol%) and $LiCH_2SiMe_3$ (4, 5, 6 mol%) were used catalytically. Heating this mixture to 50°C allowed trace conversion to occur, however application of additional heat (100°C) did not result in additional product formation.

Table 3-10. Lithium catalyzed intermolecular *anti*-Markovnikov hydroamination of *cis*-β-methyl styrene (**108**) and allylbenzene (**110**) with pyrrolidine.
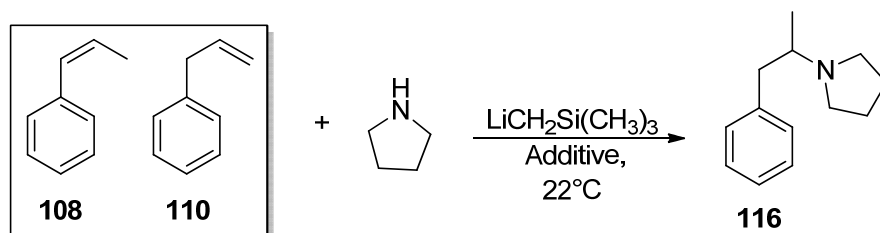
Alkene	LiCH$_2$Si(CH$_3$)$_3$ (mol %)	Additive (mol %)	Time (hh:mm)	Isolated Yield (%)	Conv. (%)
108	7	None	120:00	73	85
110	7	LiCl (7)	139:00	81	88
108	7	(*R*)-**54** (2)	120:00	32	50
110	2	(−)-Sparteine (10)	89:35	71	79
108	10	(−)-Sparteine (10)	48:40	35	77

**Table 3-11.** Lithium catalyzed intermolecular *anti*-Markovnikov hydroamination of α-methyl styrene (**111**) with pyrrolidine.
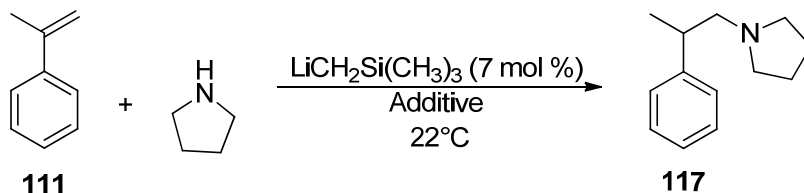
Additive (mol %)	Time (hh:mm)	Isolated Yield (%)	Conv. (%)
None	43:20	50	88
(*R*)-**54** (2)	120:00	66	85

Catalytic NaCH$_2$SiMe$_3$ allowed the intermolecular *anti*-Markovnikov hydroamination of allylbenzene (**110**) with pyrrolidine to proceed at 22°C in high conversion. Direct rate comparisons cannot be made due to discrepancies in catalyst loading although no stereoinduction was observed.

Table 3-12. Sodium catalyzed intermolecular *anti*-Markovnikov hydroamination of allylbenzene (**110**) with pyrrolidine.
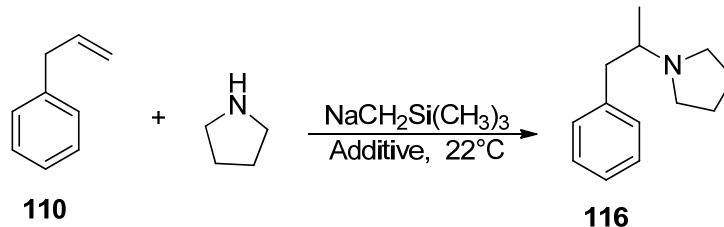
| **110**: Pyrollidine	NaCH$_2$Si(CH$_3$)$_3$ (mol %)	Additive (mol %)	Time (hh:mm)	Isolated Yield (%)	Conv. (%)
1:2	2	None	18:15	93	100
4:1	5	(–)-Sparteine (10)	20:45	83	100
4:1	10	(–)-Sparteine (10)	2:45	98	100

For the addition of pyrrolidine to *cis*-β-methyl styrene (**108**), no conversion was achieved when H$_2$-(*R*)-**54** (2.3 mol%) and NaCH$_2$SiMe$_3$ (4.6 mol%) were used as a catalyst. The addition of 0.8 equivalents (1.8 mol%) of additional NaCH$_2$SiMe$_3$ allowed polymerization of the olefin, and no hydroamination products were observed.

3.6 Conclusion

Both lithium and sodium demonstrated their capacity to perform the intermolecular hydroamination of styrene derivatives with high anti-Markovnikov selectivity. Lithium has limited potential because many reactions required heat to achieve conversion and stalled prior to reaching completion. Sodium was effective for these transformations because all reactions reached full conversion at 22°C. Although side reactions, including polymerization are problematic reaction conditions can be optimized to improve yields. Steric hindrance from (–)-sparteine was found to improve selectivity for the mono-hydroamination product for reactions with primary amines.

No rate enhancement was found when (*R*)-**54** was included in these reactions, therefore the ligand accelerated pathway for this complex is exclusive to the intramolecular process. The rates of many reactions were impacted by the presence of (–)-sparteine, although no stereoinduction was observed. Further investigation would be required to clarify if (–)-sparteine is involved in a pre-catalytic deaggregation process or is part of the rate limiting transition step for these reactions.

3.7 References

(1)   Haggin, J. *Chem. Eng. News* **1993**, *71*, 23.

(2)   (a) Giardello, M. A.; Conticello, V. P.; Brard, L.; Gagne, M. R.; Marks, T. J. *J. Am. Chem. Soc.* **1994**, *116*, 10241. (b) Gagné, M. R.; Stern, C. L.; Marks, T. J. *J. Am. Chem. Soc.* **1992**, *114*, 275.

(3)   (a) Barrett, A. G. M.; Brinkmann, C.; Crimmin, M. R.; Hill, M. S.; Hunt, P.; Procopiou, P. A. *J. Am. Chem. Soc.* **2009**, *131*, 12906. (b) Zhang, X.; Emge, T. J.; Hultzsch, K. C. *Angew. Chem. Int. Ed.* **2012**, *51*, 394. (c) Brinkmann, C.; Barrett, A. G. M.; Hill, M. S.; Procopiou, P. A. *J. Am. Chem. Soc.* **2012**, *134*, 2193. (d) Liu, B.; Roisnel, T.; Carpentier, J.-F.; Sarazin, Y. *Angew. Chem. Int. Ed.* **2012**, *51*, 4943.

(4)   (a) Reznichenko, A. L.; Nguyen, H. N.; Hultzsch, K. C. *Angew. Chem. Int. Ed.* **2010**, *49*, 8984. (b) Yuen, H. F.; Marks, T. J. *Organometallics* **2009**, *28*, 2423. (c) Gribkov, D. V.; Hultzsch, K. C.; Hampel, F. *J. Am. Chem. Soc.* **2006**, *128*, 3748. (d) Ryu, J.-S.; Li, G. Y.; Marks, T. J. *J. Am. Chem. Soc.* **2003**, *125*, 12584. (e) Li, Y.; Marks, T. J. *J. Am. Chem. Soc.* **1998**, *120*, 1757. (f) Li, Y.; Marks, T. J. *Organometallics* **1996**, *15*, 3770.

(5)   Review of base catalyzed hydroamination: Seayad, J.; Tillack, A.; Hartung, C. G.; Beller, M. *Adv. Synth. Catal.* **2002**, *344*, 795.

(6)   (a) J. D. Danforth, *French Patent 917060*, **1946**. (b) J. D. Danforth, *U. S. Patent 2,449,644*, **1948**. (c) A. W. Weston, *U. S. Patent 2,437,984*, **1948**. (d) J. D. Danforth , *Canadian Patent 461783*, **1949**.

(7)   (a) Howk, B. W.; Little, E. L.; Scott, S. L.; Whitman, G. M.; *J. Am. Chem. Soc.* **1954**, *76*, 1899. (b) Closson, R. D.; Napolitano, J. P.; Ecke, G. G.; Kolka, A. J. *J. Org. Chem.* **1957**, *22*, 646. See also: (c) Wollensak, J.; Closson, R. D. *Org. Synth.* **1963**, *43*, 45.

(8)   (a) Lehmkuhl, H.; Reinehr, D. *J. Organomet. Chem.* **1973**, *55*, 215. Mechanistic study: (b) Pez, G. P.; Galle, J. E. *Pure Appl. Chem.* **1985**, *57*, 1917.

(9)   Khedkar, V.; Tillack, A.; Benisch, C.; Melder, J.-P.; Beller, M. *J. Mol. Catal. A: Chem.* **2005**, *241*, 175.

(10)   Horrillo-Martínez, P.; Hultzsch, K. C.; Gil, A.; Branchadell, V. *Eur. J. Org. Chem.* **2007**, 3311. Reaction were ran at 120°C and a 1:2 ratio of vinylarene:amine was used because it allowed high selectivity of the monosubstituted product.

(11)   7% *ee* with α-methyl styrene and *p*-methoxy benzyl amine; 14% *ee* with *trans*-β-methyl styrene and *p*-methoxy benzyl amine.

(12)   Intermolecular HA of Styrene Derivatives: (a) See reference 10. (b) Kumar, K.; Michalik, D.; Garcia Castro, I.; Tillack, A.; Zapf, A.; Arlt, M.; Heinrich, T.; Böttcher, H.; Beller, M. *Chem. Eur. J.* **2004**, *10*, 746. (c) Beller, M.; Breindl, C. *Chemosphere* **2001**, *43*, 21. (d) Hartung, C. G.; Breindl, C.; Tillack, A.; Beller, M. *Tetrahedron* **2000**, *56*, 5157. (e) Beller, M.; Breindl, C.; Riermeier, T. H.; Eichberger, M.; Trauthwein, H. *Angew. Chem. Int. Ed.* **1998**, *37*, 3389. (f) Beller, M.; Breindl, C. *Tetrahedron* **1998**, *54*, 6359. (g) Narita, T.; Teruo, Y.; Tsuruta, T. *Bull. Chem. Soc. Jap.* **1973**, *46*, 3825. (h) Schlott, R. J.; Falk, J. C.; Narducy, K. W. *J. Org. Chem.* **1972**, *37*, 4243. (i) Asahara, T.; Senō, M.; Tanaka, S.; Den, N. *Bull. Chem. Soc. Jap.* **1969**, *42*, 1996. (j) Wegler, R.; Pieper, G. *Chem. Ber.* **1950**, *83*, 1.

(13)   Intermolecular HA of 1,3-Dienes: (a) Takabe, K.; Katagiri, T.; Tanaka, J.; Fujita, T.; Watanabe, S.; Suga, K. *Org. Synth.* **1989**, *67*, 44. (b) Fujita, T.; Suga, K.; Watanabe, S.

Aust. J. Chem. **1974**, *27*, 531. (c) Fujita, T.; Suga, K.; Watanabe, S. *Chem. Ind.* **1973**, 231. (d) Narita, T.; Imai, N.; Tsuruta, T. *Bull. Chem. Soc. Jap.* **1973**, *46*, 1242. (e) Takabe, K.; Katagiri, T.; Tanaka, J. *Tetrahedron Lett.* **1972**, *39*, 4009. (f) Imai, N.; Narita, T.; Tsuruta, T. *Tetrahedron Lett.* **1971**, *12*, 3517. (g) Also see ref. 12h.

(14)   Intermolecular hydroamination of ethylene: See references 7, 8, 9.

(15)   Intermolecular hydroamination of aliphatic olefins: See references 7a-b, 8, 9.

(16)   See Ref: 5, 7a-b, 8a, 12b,i-j, 13b-c.

(17)   (a) Clegg, W.; Conway, B.; Kennedy, A. R.; Klett, J.; Mulvey, R. E.; Russo, L. *Eur. J. Inorg. Chem.* **2011**, 721. (b) Garcia-Alvarez, P.; Kennedy, A. R.; O'Hara, C. T.; Reilly, K.; Robertson, G. M. *Dalton Trans.* **2011**, *40*, 5332. (c) Clark, N. M.; Garcia-Alvarez, P.; Kennedy, A. R.; O'Hara, C. T.; Robertson, G. M. *Chem. Commun.* **2009**, 5835.

(18)   Harder, S. *Chem. Rev.* **2010**, *110*, 3852.

(19)   Seyferth, D. *Organometallics* **2009**, *28*, 1598.

(20)   (a) Crimmin, M. R.; Casely, I. J.; Hill, M. S. *J. Am. Chem. Soc.* **2005**, *127*, 2042. (b) Datta, S.; Roesky, P. W.; Blechert, S. *Organometallics* **2007**, *26*, 4392. (c) Buch, F.; Harder, S. *Z. Naturforsch.* **2008**, *63b*, 169. (d) Datta, S.; Gamer, M. T.; Roesky, P. W. *Organometallics* **2008**, *27*, 1207. (e) Barrett, A. G. M.; Crimmin, M. R.; Hill, M. S.; Hitchcock, P. B.; Kociok-Köhn, G.; Procopiou, P. A. *Inorg. Chem.* **2008**, *47*, 7366. (f) Crimmin, M. R.; Arrowsmith, M.; Barrett, A. G. M.; Casely, I. J.; Hill, M. S.; Procopiou, P. A. *J. Am. Chem. Soc.* **2009**, *131*, 9670. (g) Arrowsmith, M.; Hill, M. S.; Kociok-Köhn, G. *Organometallics* **2009**, *28*, 1730. (h) Wixey, J. S.; Ward, B. D. *Chem. Commun.* **2011**, *47*, 5449. (i) Wixey, J. S.; Ward, B. D. *Dalton Trans.* **2011**, *40*, 7693. (j) Jenter, J.; Köppe, R.; Roesky, P. W. *Organometallics* **2011**, *30*, 1404.

(21)   (a) Horrillo-Martínez, P.; Hultzsch, K. C. *Tetrahedron Lett.* **2009**, *50*, 2054. (b) Dunne, J. F.; Fulton, D. B.; Ellern, A.; Sadow, A. D. *J. Am. Chem. Soc.* **2010**, *132*, 17680. (c) Zhang, X.; Emge, T. J.; Hultzsch, K. C. *Organometallics* **2010**, *29*, 5871. (d) Arrowsmith, M.; Crimmin, M. R.; Barrett, A. G. M.; Hill, M. S.; Kociok-Köhn, G.; Procopiou, P. A. *Organometallics* **2011**, *30*, 1493. (e) Neal, S. R.; Ellern, A.; Sadow, A. D. *J. Organomet. Chem.* **2011**, *696*, 228. (f) Arrowsmith, M.; Hill, M. S.; Kociok-Köhn, G. *Organometallics* **2011**, *30*, 1291.

(22)   See references 20c,h,i and 21a,e

(23)   (a) Reznichenko, A. L.; Hultzsch, K. C. *Chiral Amine Synthesis*; Wiley-VCH Verlag: **2010**, 341. (b) Hultzsch, K. C. *Adv. Syn. Cat.* **2005**, *347*, 367. (c) Hartwig, J. F. *Pure Appl. Chem.* **2004**, *76*, 507. (d) Roesky, P. W.; Müller, T. E. *Angew. Chem. Int. Ed.* **2003**, *42*, 2708. (e) Beller, M.; Breindl, C.; Eichberger, M.; Hartung, C. G.; Seayad, J.; Thiel, O. R.; Tillack, A.; Trauthwein, H. *Synlett* **2002**, *2002*, 1579. (f) Nobis, M.; Drießen-Hölscher, B. *Angew. Chem. Int. Ed.* **2001**, *40*, 3983.

(24)   (a) Kawatsura, M.; Hartwig, J. F. *J. Am. Chem. Soc.* **2000**, *122*, 9546. (b) Nettekoven, U.; Hartwig, J. F. *J. Am. Chem. Soc.* **2002**, *124*, 1166. (c) Johns, A. M.; Utsunomiya, M.; Incarvito, C. D.; Hartwig, J. F. *J. Am. Chem. Soc.* **2006**, *128*, 1828. (d) Sievers, C.; Jiménez, O.; Knapp, R.; Lin, X.; Müller, T. E.; Türler, A.; Wierczinski, B.; Lercher, J. A. *J. Mol. Catal. A: Chem.* **2008**, *279*, 187.

(25)   (a) Casalnuovo, A. L.; Calabrese, J. C.; Milstein, D. *J. Am. Chem. Soc.* **1988**, *110*, 6738. (b) Dorta, R.; Egli, P.; Zürcher, F.; Togni, A. *J. Am. Chem. Soc.* **1997**, *119*, 10857. (c)

Zhao, J.; Goldman, A. S.; Hartwig, J. F. *Science* **2005**, *307*, 1080. (d) Zhou, J.; Hartwig, J. F. *J. Am. Chem. Soc.* **2008**, *130*, 12220.

(26)   (a) Marcseková, K.; Doye, S. *Synthesis* **2007**, *2007*, 145. (b) Anderson, L. L.; Arnold, J.; Bergman, R. G. *J. Am. Chem. Soc.* **2005**, *127*, 14542.

(27)   (a) Utsunomiya, M.; Hartwig, J. F. *J. Am. Chem. Soc.* **2004**, *126*, 2702. (b) Takaya, J.; Hartwig, J. F. *J. Am. Chem. Soc.* **2005**, *127*, 5756.

(28)   Coulson, D. R. *Tetrahedron Lett.* **1971**, *12*, 429.

(29)   (a) Beller, M.; Eichberger, M.; Trauthwein, H. *Angew. Chem. Int. Ed. Engl.* **1997**, *36*, 2225. (b) Beller, M.; Trauthwein, H.; Eichberger, M.; Breindl, C.; Müller, T. E. *Eur. J. Inorg. Chem.* **1999**, 1121. (c) Beller, M.; Trauthwein, H.; Eichberger, M.; Breindl, C.; Herwig, J.; Müller, T. E.; Thiel, O. R. *Chem. Eur. J.* **1999**, *5*, 1306.

(30)   Utsunomiya, M.; Kuwano, R.; Kawatsura, M.; Hartwig, J. F. *J. Am. Chem. Soc.* **2003**, *125*, 5608.

(31)   Sevov, C. S.; Zhou, J.; Hartwig, J. F. *J. Am. Chem. Soc.* **2012**, *134*, 11960.

(32)   Pan, S.; Endo, K.; Shibata, T. *Org. Lett.* **2012**, *14*, 780.

(33)   Utsunomiya, M.; Hartwig, J. F. *J. Am. Chem. Soc.* **2003**, *125*, 14286.

(34)   Li, K.; Horton, P. N.; Hursthouse, M. B.; Hii, K. K. *J. Organomet. Chem.* **2003**, *665*, 250.

(35)   Hu, A.; Ogasawara, M.; Sakamoto, T.; Okada, A.; Nakajima, K.; Takahashi, T.; Lin, W. *Adv. Synth. Catal.* **2006**, *348*, 2051.

(36)   Additional examples: Nickel: (a) Pawlas, J.; Nakao, Y.; Kawatsura, M.; Hartwig, J. F. *J. Am. Chem. Soc.* **2002**, *124*, 3669. Palladium: (b) Löber, O.; Kawatsura, M.; Hartwig, J. F. *J. Am. Chem. Soc.* **2001**, *123*, 4366.

(37)   (a) Zhang, J.; Yang, C.-G.; He, C. *J. Am. Chem. Soc.* **2006**, *128*, 1798. (b) Taylor, J. G.; Whittall, N.; Hii, K. K. *Org. Lett.* **2006**, *8*, 3561.

(38)   Zhang, Z.; Lee, S. D.; Widenhoefer, R. A. *J. Am. Chem. Soc.* **2009**, *131*, 5372.

(39)   (a) Hogan, A.-M. L.; O'Shea, D. F. *Chem. Commun.* **2008**, 3839. (b) Peters, J. G.; Seppi, M.; Fröhlich, R.; Wibbeling, B.; Hoppe, D. *Synthesis* **2002**, 0381.

(40)   (a) Hogan, A.-M. L.; Tricotet, T.; Meek, A.; Khokhar, S. S.; O'Shea, D. F. *J. Org. Chem.* **2008**, *73*, 6041. (b) Hogan, A.-M. L.; O'Shea, D. F. *J. Org. Chem.* **2008**, *73*, 2503. (c) Hogan, A.-M. L.; O'Shea, D. F. *J. Am. Chem. Soc.* **2006**, *128*, 10360. (d) Klein, S.; Marek, I.; Poisson, J.-F.; Normant, J.-F. *J. Am. Chem. Soc.* **1995**, *117*, 8853.

(41)   Norsikian, S.; Marek, I.; Normant, J.-F. *Tetrahedron Lett.* **1997**, *38*, 7523.

(42)   Norsikian, S.; Marek, I.; Klein, S.; Poisson, J. F.; Normant, J. F. *Chem. Eur. J.* **1999**, *5*, 2055.

(43)   Gessner, V. H.; Koller, S. G.; Strohmann, C.; Hogan, A.-M.; O'Shea, D. F. *Chem. Eur. J.* **2011**, *17*, 2996.

(44)   (a) Hevia, E.; Mulvey, R. E. *Angew. Chem. Int. Ed.* **2011**, *50*, 6448. (b) Reich, H. J. *J. Org. Chem.* **2012**, *77*, 5471.

(45)   (a) Hoepker, A. C.; Gupta, L.; Ma, Y.; Faggin, M. F.; Collum, D. B. *J. Am. Chem. Soc.* **2011**, *133*, 7135. (b) Ma, Y.; Hoepker, A. C.; Gupta, L.; Faggin, M. F.; Collum, D. B. *J. Am. Chem. Soc.* **2010**, *132*, 15610. (c) Gupta, L.; Hoepker, A. C.; Singh, K. J.; Collum, D. B. *J. Org. Chem.* **2009**, *74*, 2231.

(46)   Salvi, L.; Kim, J. G.; Walsh, P. J. *J. Am. Chem. Soc.* **2009**, *131*, 12483. For LiCl induced *ee* enhancement with a rare-earth metal based hydroamination catalyst: (b) Chapurina,

Y.; Guillot, R.; Lyubov, D.; Trifonov, A.; Hannedouche, J.; Schulz, E. *Dalton Trans.* **2013**, *42*, 507.

(47)   (a) See also references 45a-b. (b) Lecachey, B.; Oulyadi, H.; Lameiras, P.; Harrison-Marchand, A.; Gérard, H.; Maddaluno, J. *J. Org. Chem.* **2010**, *75*, 5976.

(48)   (a) Wunderlich, S. H.; Knochel, P. *Angew. Chem. Int. Ed.* **2009**, *48*, 9717. (b) Wunderlich, S. H.; Kienle, M.; Knochel, P. *Angew. Chem. Int. Ed.* **2009**, *48*, 7256. (c) Wunderlich, S. H., Knochel, P.; *Angew. Chem. Int. Ed.* **2009**, *48*, 1501. (d) Mosrin, M., Knochel, P.; *Chem. Eur. J.* **2009**, *15*, 1468. (e) Mosrin, M., Knochel, P., *Org. Lett.* **2009**, *11*, 1837. (f) Wunderlich, S. H., Knochel, P.; *Org. Lett.* **2008**, *10*, 4705. (g) Wunderlich, S. H., Knochel, P.; *Angew. Chem. Int. Ed.* **2007**, *46*, 7685. (h) Krasovskiy, A.; Krasovskaya, V.; Knochel, P. *Angew. Chem. Int. Ed.* **2006**, *45*, 2958.

(49)   DOSY Study: (a) García-Álvarez, P.; Mulvey, R. E.; Parkinson, J. A. *Angew. Chem. Int. Ed.* **2011**, *50*, 9668. Crystal structures: (b) Blasberg, F.; Bolte, M.; Wagner, M.; Lerner, H.-W. *Organometallics* **2012**, *31*, 1001. (c) Armstrong, D. R.; García-Álvarez, P.; Kennedy, A. R.; Mulvey, R. E.; Parkinson, J. A. *Angew. Chem. Int. Ed.* **2010**, *49*, 3185. (d) García-Álvarez, P.; Graham, D. V.; Hevia, E.; Kennedy, A. R.; Klett, J.; Mulvey, R. E.; O'Hara, C. T.; Weatherstone, S. *Angew. Chem. Int. Ed.* **2008**, *47*, 8079.

4

Experimental

4.1 General Considerations

Organolithium reactions were performed under an inert atmosphere of argon in a glovebox. Ligand synthesis was performed under inert atmosphere of nitrogen on a Schlenk line. Freeze drying of catalysts was performed on Schlenk line and positive pressure was not applied (i.e. flask was kept under vacuum until inside glovebox). Dimethylaminoethanol, diethylaminoethanol, N-piperidine ethanol, dimethylsulfoxide, triethylamine, diisopropylamine and chloroform-d were distilled from calcium hydride, then stored over activated 4Å molecular sieves. Benzene, benzene-d_6 and toluene-d_8 were distilled from sodium benzophenone ketyl prior to use and stored over activated 4Å molecular sieves. Diethyl ether, tetrahydrofuran, pentane, hexane and toluene were taken from solvent purification system. Bulk dichloromethane was distilled prior to use. Dichloromethane and dichloroethane were stored over calcium hydride and carefully decanted into a separate flask prior to use in Swern oxidation and reductive amination.

4.2 Substrate Synthesis

1-Aminopent-4-ene,[1] 1,4-bromopentene,[2] 2,2-dimethyl-pent-4-enylamine,[3] 2,2-diphenyl-pent-4-enylamine,[4] *C*-(1-allyl-cyclohexyl)-methylamine,[5] (*E*)-2,2-dimethyl-5-phenylpent-4-en-1-amine,[6] *N*-benzyl-2,2-diphenylpent-4-enyl amine,[5] 2,2,5-triphenylpent-4-enyl amine[7] and *N*-benzyl-2,2-diphenylpent-4-enyl amine[5] were synthesized according to known procedures, and matched previously reported ^{1}H and ^{13}C spectra. Substrates were dried by stirring over calcium hydride for a minimum of one day then distilled. Prior to use substrates were cyclized with [La{N(SiMe$_3$)$_2$}$_3$], [Y{N(SiMe$_3$)$_2$}$_3$][8] or (*R*)-**11a** to ensure the reproducibility of catalytic results.

4.3 Ligand Synthesis

(R)-**54**
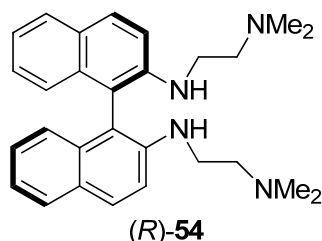
(R)-(Bis(dimethylamino-2-yl-ethyl)amine)binaphthyl ((R)-**54**). CH_2Cl_2 (200 mL) and $(COCl)_2$ (2.21 mL, $\rho = 1.46$ g·cm^{-3}, 3.22 g, 0.0254 mol) were combined in a dry flask and cooled to -78°C. Dimethylsulfoxide (2.70 mL, $\rho = 1.10$ g·cm^{-3}, 2.97 g, 0.0380 mol) was added dropwise and the solution was stirred for 15 minutes. Dimethylaminoethanol (2.12 mL, $\rho = 0.887$ g·cm^{-3}, 1.88 g, 0.0211 mmol) was added and the flask was stirred for one hour. Triethylamine (14.7 mL, $\rho = 0.726$ g·cm^{-3}, 10.67 g, 0.106 mmol) was added and the reaction was warmed to 0°C. The reaction was allowed to warm to room temperature over one hour and was extracted with water (20 mL). The aqueous layer was extracted with CH_2Cl_2 (3 × 25 mL). The organic layers were combined, dried with sodium sulfate and concentrated (using a minimum pressure of 275 mBar) to a volume of 30 mL. This solution was diluted with dichloroethane to a volume of 60 mL and divided into 3 – 20 mL portions, which were used immediately without further purification.

Sodium triacetoxyborohydride (3.73 g, 0.0176 mmol), dichloroethane (30 mL), and then (R)-DABN (1.00 g, 0.00352 mmol) were added to a dry two-neck flask which was stirred vigorously. Three portions of the crude aldehyde crude mixture (20 mL each) were added at t = 0 h, t = 2 h and t = 4 hours. The mixture was stirred for 45 additional minutes after adding the last portion of aldehyde, then 1 N NaOH (75 mL) was added. The aqueous layer was removed and diluted with water (50 mL) and extracted with CH_2Cl_2 (3 × 25 mL). The combined organic layers were extracted with water (50 mL), dried with sodium sulfate and concentrated onto silica gel and dried under high vacuum to remove residual DMSO. The product was purified by silica gel chromatography three times using 5% (10:1) MeOH: NH_4OH in CH_2Cl_2 as a mobile phase. The product was taken up in benzene (20 mL), filtered, then concentrated and dried in vacuo.

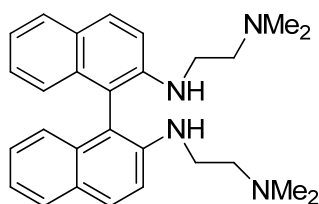Pale yellow solid, $R_f = 0.29$ in 10% (10:1) MeOH: NH_4OH in CH_2Cl_2. Yield = 1.12 g, 75%.

^{1}H NMR (400 MHz, C_6D_6, 25°C): δ 7.85 (d, 2H, $^3J_{H,H} = 9.00$ Hz), 7.76 (d, 2H, $^3J_{H,H} = 7.44$ Hz), 7.31 (dd, 2H, $^3J_{H,H} = 8.22$ Hz, $^4J_{H,H} = 0.79$ Hz), 7.19 (d, 2H, $^3J_{H,H} = 8.61$ Hz), 7.11 (ddd, 2H, $^3J_{H,H} = 8.02$ Hz, $^3J_{H,H} = 6.65$ Hz, $^4J_{H,H} = 1.30$ Hz), 7.05 (ddd, 2H, $^3J_{H,H} = 8.21$ Hz, $^3J_{H,H} = 6.75$ Hz,

$^4J_{H,H}$ = 1.47 Hz), 4.38 (t, 2H, $^3J_{H,H}$ = 5.08 Hz, NH), 2.92-2.85 (m, 4H), 2.05 (dt, 2H, $^2J_{H,H}$ = 11.74 Hz, $^3J_{H,H}$ = 6.65 Hz), 1.93 (dt, 2H, $^2J_{H,H}$ = 12.13 Hz, $^3J_{H,H}$ = 6.07 Hz), 1.70 (s, 12H). $^{13}C\{^1H\}$ NMR (100.6 MHz, C_6D_6, 25°C): 145.90, 135.11, 130.17, 128.87, 128.69, 127.34, 124.90, 122.43, 115.09, 113.52, 58.57, 45.21, 42.32. Anal Calcd for $C_{28}H_{34}N_4$: C, 78.83; H, 8.03; N, 13.13. Found: C, 78.88; H, 7.99; N, 12.98.
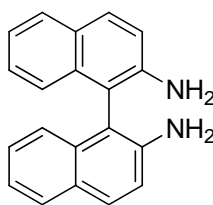
(*rac*)-**DABN**

(*rac*)-**Diaminobinaphthyl**.[9] 2-naphthol (35.0 g, 0.243 mol) and hydrazine monohydrate (4.85 mL, 0.0999 mol, 5.00 g, ρ = 1.03 g·cm^{-3}) and a stir bar were combined in a glass lined Parr bomb. The apparatus was flushed with nitrogen for 15 minutes, and then placed in a sandbath. A temperature sensor was placed in the bottom 1/3 of the sandbath, and raised to 180°C for 3 days, with stirring. The sandbath was cooled to 70°C, and the molten reaction mixture was poured into a funnel and immediately solidified. A warm mixture of 3:1 Hexane:Ethyl Acetate was used dissolve solids. The solution was cooled to 22°C, then solids were filtered and dried under vacuum. Yield = 12.4 g, light brown solid, 44%. ^1H NMR (500 MHz, CDCl$_3$, 25°C): δ 7.79 (t, $^3J_{H,H}$ = 7.95 Hz, 3H), 7.17-7.26 (m, 4H, overlapped by CDCl$_3$ signal), 7.14 (d, $^3J_{H,H}$ = 8.80 Hz, 2H), 7.08 (d, $^3J_{H,H}$ = 8.56 Hz, 2H), 3.69 (br s, 4H, NH$_2$); $^{13}C\{^1H\}$ NMR (125.7 MHz, CDCl$_3$, 25°C): δ 142.7, 133.7, 129.5, 128.5, 128.1, 126.8, 124.0, 122.4, 118.3, 112.6.
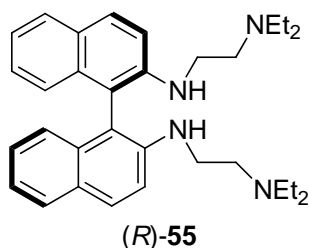

(*rac*)-**54**

(*rac*)-**(Bis(dimethylamino-2-yl-ethyl)amine)binaphthyl** ((*rac*)-**54**). CH$_2$Cl$_2$ (175 mL) and (COCl)$_2$ (2.21 mL, ρ = 1.46 g·cm^{-3}, 3.22 g, 0.0254 mol) were combined in a dry flask and cooled to -78°C. Dimethylsulfoxide (2.70 mL, ρ = 1.10 g·cm^{-3}, 2.97 g, 0.0380 mol) was added dropwise

and the solution was stirred for 15 minutes. Dimethylaminoethanol (2.12 mL, ρ = 0.887 g·cm^{-3}, 1.88 g, 0.02113 mol) was added and the flask was stirred for one hour. Triethylamine (14.7 mL, ρ = 0.726 g·cm^{-3}, 10.67 g, 0.106 mol) was added and the reaction was warmed to 0°C. The reaction was allowed to warm to room temperature over one hour. The contents of the flask were added to a separatory funnel and water (20 mL) was added. The organic layer was removed and the aqueous layer was extracted with CH_2Cl_2 (2 × 20 mL). The organic layers were combined, dried with sodium sulfate and concentrated to 30 mL. The roto-evap bath temperature was kept at 20°C and the pressure was kept at or above 300 mBar. Dichloroethane (15 mL) was added to this solution and it was divided into three equal portions of 15 mL each. These solutions of crude aldehyde were used immediately without further purification.

Sodium triacetoxyborohydride (2.24 g, 0.01056 mol) was added to a dry two-neck flask and dichloroethane (20 mL) was added followed by (*rac*)-DABN (1.00 g, 0.00352 mol). A portion of the crude aldehyde solution (15 mL) was added, and after one hour bubbling subsided. Sodium triacetoxyborohydride (1.49 g, 0.00704 mol) was added and after one hour, a second portion of crude aldehyde solution (15 mL) was added. After ninety additional minutes, the final portion of crude aldehyde solution (15 mL) was added. This solution was stirred for 16 additional hours then extracted with 1N NaOH (100 mL). The aqueous layer was extracted with CH_2Cl_2 (2 × 20 mL). The organic layers were combined and washed with water (50 mL). The water was extracted with CH_2Cl_2 (20 mL). The organic layers were combined, dried and concentrated. The residue was purified by silica gel chromatography three times using 10% (10:1) MeOH: NH$_4$OH in CH_2Cl_2 as a mobile phase. The residue was dissolved in benzene (20 mL), filtered, concentrated and dried in vacuo. Pale yellow solid. Yield = 1.021 g, 68%. Rf = 0.23 in 10% (10:1) MeOH: NH$_4$OH in CH_2Cl_2. ^{1}H NMR (500 MHz, C_6D_6, 25°C): δ 7.84 (d, 2H, $^3J_{H,H}$ = 9.0 Hz, aryl-H), 7.75 (d, 2H, $^3J_{H,H}$ = 8.0 Hz, aryl-H), 7.31 (d, 2H, $^3J_{H,H}$ = 9.0 Hz, aryl-H), 7.18 (d, 2H, $^3J_{H,H}$ = 9.0 Hz, aryl-H), 7.12-7.01 (m, 2H, aryl-H), 7.05-7.02 (m, 2H, aryl-H), 4.37 (t, 2H, $^3J_{H,H}$ = 5.0 Hz, N-H), 2.95-2.87 (m, 4H, CH$_2$), 2.06-2.01 (m, 2H, CH$_2$), 1.94-1.89 (m, 2H, CH$_2$), 1.69 (s, 12H, N-CH$_3$); ^{13}C{^{1}H} NMR (125.7 MHz, C_6D_6, 25°C): δ 145.5, 134.7, 129.8, 128.5, 128.3, 127.0, 124.5, 122.1, 114.7, 113.2 (aryl), 58.2 (CH$_2$), 44.8 (N-CH$_3$), 42.0 (CH$_2$).

(*R*)-**55**

(*R*)-(Bis(diethylamino-2-yl-ethyl)amine)binaphthyl ((*R*)-55). CH_2Cl_2 (200 mL) and $(COCl)_2$ (2.20 mL, ρ = 1.46 g·cm^{-3}, 3.22 g, 0.0253 mol) were combined in a dry flask and cooled to -78°C. Dimethylsulfoxide (2.69 mL, ρ = 1.10 g·cm^{-3}, 2.97 g, 0.0380 mol) was added and the solution was stirred for 15 minutes. Diethylaminoethanol (2.81 mL, ρ = 0.880 g·cm^{-3}, 2.47 g, 0.0211 mol) was added and the flask was stirred for one hour. Triethylamine (14.7 mL, ρ = 0.726 g·cm^{-3}, 10.66 g, 0.106 mol) was added and the mixture was warmed to 0°C. The reaction was allowed to warm to room temperature over one hour, and then was extracted with water (20 mL). The aqueous layer was extracted with CH_2Cl_2 (2 × 50 mL). The organic layers were combined, dried with sodium sulfate and concentrated (using a minimum pressure of 250 mBar) to a volume of 25 mL. This solution was diluted with dichloroethane to a volume of 40 mL and divided into 3 – 13 mL portions, which were used immediately without further purification.

Sodium triacetoxyborohydride (3.73 g, 0.0176 mol), dichloroethane (30 mL) and then (*R*)-DABN (1.00 g, 0.00352 mol) were added to a dry two-neck flask which was stirred vigorously. Two portions of the crude aldehdyde mixture (13 mL each) were added at t = 0 h, t = 2h 45m. The mixture was stirred for 2 additional hours after adding the last portion of aldehyde, then 1 N NaOH (50 mL) was added. The aqueous layer was removed and extracted with CH_2Cl_2 (2 × 50 mL). The combined organic layers were dried with sodium sulfate, concentrated and taken up in benzene (30 mL) and were then filtered. The product was purified by silica gel chromatography three times using 5% (10:1) MeOH: NH_4OH in CH_2Cl_2 as a mobile phase, then dissolved in benzene and freeze dried. Pale yellow oil, R_f = 0.24 in 10% (10:1) MeOH: NH_4OH in CH_2Cl_2. Yield = 1.45 g, 86%. ^1H NMR (400 MHz, C_6D_6, 25°C): 7.88 (d, 2H, $^3J_{H,H}$ = 9.00 Hz), 7.78 (d, 2H, $^3J_{H,H}$ = 7.83 Hz), 7.34 (dd, 2H, $^3J_{H,H}$ = 9.00 Hz, $^4J_{H,H}$ = 0.78 Hz), 7.21 (d, 2H, $^3J_{H,H}$ = 9.00 Hz), 7.12 (ddd, 2H, $^3J_{H,H}$ = 8.02 Hz, $^3J_{H,H}$ = 6.85 Hz, $^4J_{H,H}$ = 1.17 Hz), 7.05 (ddd, 2H, $^3J_{H,H}$ = 8.22 Hz, $^3J_{H,H}$ = 6.75 Hz, $^4J_{H,H}$ = 1.47 Hz), 4.60 (t, 2H, $^3J_{H,H}$ = 4.89 Hz, NH), 2.96-2.86 (m, 4H), 2.24-2.12 (m, 4H), 2.01 (dq, 8H, $^3J_{H,H}$ = 7.11 Hz, $^2J_{H,H}$ = 1.86 Hz), 0.54 (t, 12H, $^3J_{H,H}$ =7.04 Hz). $^{13}C\{^1H\}$ NMR (100.6 MHz, C_6D_6, 25°C): 145.75, 135.20, 130.00, 128.92, 128.79, 127.29,

124.92, 122.23, 114.89, 113.38, 52.34, 46.92, 41.88, 12.48. Anal. Calcd. for $C_{32}H_{42}N_4$: C, 79.62; H, 8.77; N, 11.61. Found: C, 79.86; H, 9.07; N, 10.80.
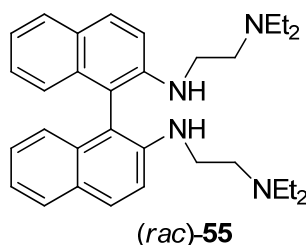
(*rac*)-**55**

(*rac*)-**(Bis(diethylamino-2-yl-ethyl)amine)binaphthyl** ((*rac*)-**55**). Oxalyl chloride (.446 mL, 0.651 g, $\rho = 1.46$ g·cm^{-3}, 0.00513 mol) was dissolved in CH_2Cl_2 (30 mL) and cooled to -78 ºC. DMSO (0.546 mL, 0.601 g, $\rho = 1.10$ g·cm^{-3}, 0.00769 mol) in CH_2Cl_2 (5 mL) was added over 5 minutes and the solution was stirred for 15 minutes. 2-diethylamino ethanol (0.568 mL, 0.500 g, $\rho = 0.880$ g·cm^{-3}, 0.00427 mol) in CH_2Cl_2 (5 mL) was added over 5 minutes and the solution was stirred for 1 hour, then TEA (2.97 mL, 2.16 g, $\rho = 0.726$ g·cm^{-3}, 0.0214 mol) was added. The -78 ºC bath was replaced with a 0 ºC bath and the mixture was stirred for 1 hour. Water (40 mL) was added and the organic layer was removed. The aqueous layer was extracted with CH_2Cl_2 (2 × 30 mL). The organic layers were combined, dried and concentrated to 12 mL using a rotoevaporator. The water bath was kept at 0°C and the pressure was not lowered below 100 mBar. A 0 °C bath was placed under the collecting flask to accelerate solvent removal. The crude mixture was used immediately without further purification.

In a dry two neck flask, (*rac*)-**DABN** (0.303 g, 0.00107 mol), NaBH(OAc)$_3$ (0.905 g, 0.00427 mol) and dichloroethane (30 mL) were combined and the flask was flushed with N_2. The mixture was stirred vigorously for 5 minutes to dissolve the solids. Acetic acid (0.122 mL, 0.128 g, $\rho = 1.05$ g·cm^{-3}, 0.00214 mol) was added dropwise. The crude mixture from the Swern oxidation was added slowly. After 45 minutes, a considerable amount of DABN was visible. Acetic acid (0.250 mL, 0.262 g, $\rho = 1.05$ g·cm^{-3}, 0.00436 mol) was added to compensate for the possible buffering effect of TEA from the Swern crude mixture. The mixture was stirred for 14 additional hours. Water (40 mL) was added followed by 25% NaOH (10 mL). The aqueous layer was extracted with CH_2Cl_2 (2 × 40 mL) and the organic layers were combined, dried, and concentrated. The residue was dissolved in CH_2Cl_2 (20 mL) and combined with silica gel (10 mL) and dried until a free flowing powder was observed. This powder was gently loaded onto a

column containing silica gel (50 mL), and the flask was rinsed with CH_2Cl_2 (2 × 10 mL). The product eluted with 1% TEA in CH_2Cl_2. Yield = 369 mg, 77%; R_f = 0.19 in 5% (10:1) $MeOH:NH_4OH$ in CH_2Cl_2. ^1H NMR (500 MHz, $CDCl_3$, 25 °C): δ 7.93 (d, 2H, $^3J_{H,H}$ = 9.1 Hz, aryl-H), 7.85-7.80 (m, 2H, aryl-H), 7.31 (d, 2H, $^3J_{H,H}$ = 8.8 Hz, aryl-H), 7.24-7.17 (m, 4H, aryl-H), 7.14-7.10 (m, 2H, aryl-H), 4.35 (br s, 2H, N-H), 3.23 (dt overlapped, 4H, $^2J_{H,H}$ = 10.9 Hz, $^3J_{H,H}$ = 5.8 Hz, C$\underline{H}_2$CH$_2$N), 2.50 (dt, 4H, $^2J_{H,H}$ = 13.0 Hz, $^3J_{H,H}$ = 6.36 Hz, CH$_2$C$\underline{H}_2$N), 2.29 (dd, 8H, $^3J_{H,H}$ = 7.1 Hz, $^3J_{H,H}$ = 4.7 Hz, NC$\underline{H}_2$CH$_3$ (overlapped with higher order multiplet $^3J_{H,H}$ = 6.1 Hz)), 0.71 (t, 12H, $^3J_{H,H}$ = 7.3 Hz, CH$_3$); $^{13}C\{^1H\}$ NMR (125.7 MHz, $CDCl_3$, 25 °C): δ 144.7, 133.8, 129.1, 127.8, 127.5, 126.2, 123.7, 121.3, 114.1, 112.3, 51.7 (CH$_2$C$\underline{H}_2$N), 46.4 (NC$\underline{H}_2$CH$_3$), 41.6 (C$\underline{H}_2$CH$_2$N), 11.5 (CH$_3$).

(R)-**56**
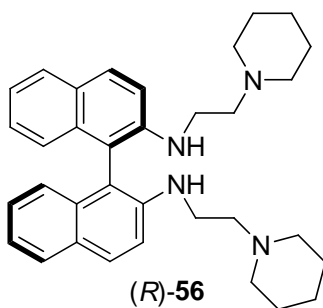
(R)-**56**. CH_2Cl_2 (200 mL) and $(COCl)_2$ (2.20 mL, ρ = 1.46 g·cm^{-3}, 3.22 g, 0.0253 mol) were combined in a dry flask and cooled to -78°C. Dimethylsulfoxide (2.69 mL, ρ = 1.10 g·cm^{-3}, 2.97 g, 0.0379 mol) was added dropwise and the solution was stirred for 15 minutes. N-piperidine ethanol (2.81 mL, ρ = 0.970 g·cm^{-3}, 2.73 g, 0.0211 mol) was added and the flask was stirred for one hour. Triethylamine (14.7 mL, ρ = 0.726 g·cm^{-3}, 10.66 g, 0.106 mol) was added and was warmed to 0°C. The reaction was warmed to room temperature over one hour then extracted with water (20 mL). The aqueous layer was extracted with CH_2Cl_2 (2 × 50 mL). The organic layers were combined, dried with sodium sulfate and concentrated (using a minimum pressure of 270 mBar) to a volume of 20 mL. The residue was diluted with dichloroethane to a volume of 50 mL, then filtered and divided into 3 portions (1 × 20 mL, 2 × 15 mL), which were used immediately without further purification.

Sodium triacetoxyborohydride (3.73 g, 0.0176 mol), dichloroethane (30 mL) and then (R)-**DABN** (1.00 g, 0.00352 mol) was added to a dry two neck flask which was stirred vigorously. Two portions of the aldehyde crude mixture were added (20 mL at t = 0; 15 mL at t = 2h). The

mixture was stirred for 1 additional hours after adding the last portion, then 1 N NaOH (50 mL) was added. The aqueous layer was removed and extracted with CH_2Cl_2 (2 × 40 mL). The combined organic layers were washed with water (15 mL) and dried with sodium sulfate. This was concentrated onto silica gel and dried under high vacuum to remove residual DMSO. The product was purified by silica gel chromatography using 10% (10:1) MeOH: NH_4OH in CH_2Cl_2 followed by two additional columns using 5% (10:1) MeOH: NH_4OH in CH_2Cl_2 as a mobile phase. The product was taken up in benzene (20 mL), filtered, then concentrated and dried in vacuo. Pale yellow solid, R_f = 0.27 in 10% (10:1) MeOH: NH_4OH in CH_2Cl_2. Yield = 1.417g, 80%. ^{1}H NMR (400 MHz, C_6D_6, 25°C): 7.89 (d, 2H, $^3J_{H,H}$ = 8.84 Hz), 7.78 (d, 2H, $^3J_{H,H}$ = 7.91 Hz), 7.31 (d, 2H, $^3J_{H,H}$ = 7.91 Hz), 7.20 (d, 2H, $^3J_{H,H}$ = 8.84 Hz), 7.11 (ddd, 2H, $^3J_{H,H}$ = 7.91 Hz, $^3J_{H,H}$ = 6.82 Hz, $^4J_{H,H}$ = 1.09 Hz), 7.03 (ddd, 2H, $^3J_{H,H}$ = 8.15 Hz, $^3J_{H,H}$ = 6.75 Hz, $^4J_{H,H}$ = 1.40 Hz), 4.70 (t, 2H, $^3J_{H,H}$ = 4.66 Hz, NH), 2.99-2.87 (m, 4H), 2.14 (dt, 2H, $^2J_{H,H}$ = 12.41 Hz, $^3J_{H,H}$ = 6.28 Hz), 2.02 (dt, 2H, $^2J_{H,H}$ = 11.79 Hz, $^3J_{H,H}$ = 5.82 Hz), 1.95-1.81 (br m, 8H), 1.20-1.07 (br m, 8H), 1.03-0.91 (br m, 4H). ^{13}C{^{1}H} NMR (100.6 MHz, C_6D_6, 25°C): 145.88, 135.24, 129.97, 128.77, 128.68, 127.36, 124.83, 122.32, 115.13, 113.52, 57.58, 54.35, 41.21, 26.45, 25.15. Anal. Calcd. for $C_{34}H_{42}N_4$: C, 80.59; H, 8.35; N, 11.06. Found: C: 80.36; H, 8.27; N, 10.94.
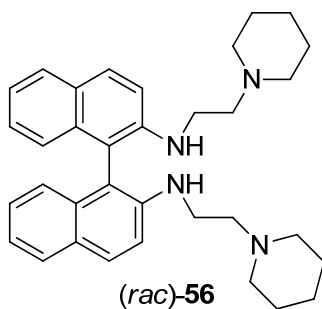
(*rac*)-**56**

(*rac*)-**56.** Oxalyl chloride (.808 mL, 1.18 g, ρ = 1.46 g·cm^{-3}, 0.00929 mol) was dissolved in CH_2Cl_2 (60 mL) and lowered to -78 ºC. DMSO (0.989 mL, 1.08 g, ρ = 1.10 g·cm^{-3}, 0.0139 mol) in CH_2Cl_2 (5 mL) was added over 5 minutes and the solution was stirred for 15 minutes. N-piperidine ethanol (1.03 mL, 1.00 g, ρ = 0.970 g·cm^{-3}, 0.00774 mol) in CH_2Cl_2 (5 mL) was added over 5 minutes and the solution was stirred for 1 hour, then TEA (5.38 mL, 3.91 g, ρ = 0.726 g·cm^{-3}, 0.0387 mol) was added. The -78 ºC bath was replaced with a 0 ºC bath and the mixture was stirred for 1 hour, and mixture was warmed to 22 ºC over 15 minutes. Water (40 mL) was added and the organic layer was removed. The aqueous layer was extracted with

CH$_2$Cl$_2$ (2 × 40 mL). The organic layers were combined, dried and concentrated to 50 mL using a rotoevaporator. The water bath was kept at 0 °C and the pressure was not lowered below 100 mBar. A 0 °C bath was placed under the collecting flask to accelerate solvent removal. The crude mixture was used immediately without further purification.

In a dry two neck flask, (*rac*)-**DABN** (0.733 g, 0.00258 mol), NaBH(OAc)$_3$ (2.30 g, 0.0108 mol) and dichloroethane (40 mL) were combined and the flask was flushed with N$_2$. The mixture was stirred vigorously for 5 minutes to dissolve the solids. The flask was placed in a 0 °C bath and the crude mixture from the Swern oxidation was added, followed by acetic acid (0.296 mL, 0.310 g, ρ = 1.05 g·cm^{-3}, 0.00516 mol). The solution was warmed to 22 °C. After 2 hours the solids appeared completely dissolved, and TLC showed consumption of DABN. The mixture was stirred for 12 additional hours. TLC did not suggest additional formation of the desired product during this time, however several UV active byproducts were observed. Water (10 mL) was added followed by 25% NaOH (10 mL), then water (40 mL). The aqueous layer was extracted with CH$_2$Cl$_2$ (2 × 50 mL) and the organics were combined, dried, and concentrated. The product was purified two times using silica gel chromatography. For each column, 50 mL silica gel was used along with 5% (10:1) MeOH:NH$_4$OH in CH$_2$Cl$_2$ as a mobile phase in the first column and 1.5% TEA in CH$_2$Cl$_2$ in the second. Yield = 0.981 g 75%; R$_f$ = 0.22 in 5% (10:1) MeOH:NH$_4$OH in CH$_2$Cl$_2$; ^{1}H NMR (500 MHz, CDCl$_3$, 25 °C): δ 7.96 (d, 2H, $^3J_{H,H}$ = 8.8 Hz, aryl-H), 7.85 (d, 2H, $^3J_{H,H}$ = 7.6 Hz, aryl-H), 7.35 (d, 2H, $^3J_{H,H}$ = 8.8 Hz, aryl-H), 7.23 (quintet, 4H, $^3J_{H,H}$ = 6.8 Hz, aryl-H), 7.14 (d, 2H, $^3J_{H,H}$ = 8.1 Hz, aryl-H), 4.45 (t, 2H, $^3J_{H,H}$ = 4.8 Hz, N-H), 3.31 (octet, 4H, $^3J_{H,H}$ = 5.8 Hz, H$_1$), 2.41 (dt, 4H, $^2J_{H,H}$ = 20.0 Hz, $^3J_{H,H}$ = 6.1 Hz, H$_2$), 2.25-2.12 (m, 8H, H$_3$), 1.35-1.25 (m, 8H, H$_4$), 1.22-1.15 (m, 4H, H$_5$); ^{13}C{^{1}H} NMR (125.7 MHz, CDCl$_3$, 25 °C): δ 144.8, 133.9, 129.2, 127.9, 127.6, 126.4, 123.7, 121.5, 114.4, 112.5, 57.4 (C$_3$), 54.0 (C$_2$), 41.0 (C$_1$), 25.6 (C$_4$), 24.2 (C$_5$).
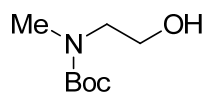

Boc-N-Methyl amino ethanol. 6.88 g (0.0916 mol) of N-methyl ethanol amine was dissolved in 100 mL CH$_2$Cl$_2$. 22.34 mL (ρ = 0.726 g·cm^{-3}, 16.22 g, 0.1603 mol) of TEA was added. 10 g (.0458 mol) of Boc anhydride was dissolved in 20 mL of CH$_2$Cl$_2$ and added to mixture. Reaction was stirred overnight (~16 hours) then poured onto water. Organic layer was washed

twice with brine, dried and concentrated. The pure product was isolated by silica gel chromatography using 0.5% NH_4OH : 4.5% MeOH : 95% CH_2Cl_2, TLC visualized with $KMnO_4$. Yield = 7.11 g, 89%. ^{1}H NMR (300 MHz, $CDCl_3$), δ 3.77 (t, 1.85H, CH_2), 3.42 (t, 1.93H, CH_2), 2.94 (s, 2.65H, CH_3), 2.2 (br s, 0.94H, OH), 1.49 (s, 9.00H, C(CH_3)$_3$). ^{13}C{^{1}H} NMR (100.6 MHz, $CDCl_3$), δ 157.37 (CO), 156.0 (CO), 80.04 (O$\underline{C}$(CH$_3$)$_3$, 61.49 (NCH$_2$), 61.40 (NCH$_2$), 51.56 (NCH$_3$), 35.68 (CH$_2$OH), 28.59 (OC($\underline{C}$H$_3$)$_3$.
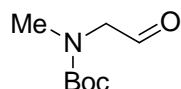

Boc-N-Methyl amino ethyl aldehyde.[10] .996 mL (ρ = 1.455 g·cm^{-3}, 1.45 g, 0.0114 mol) of oxalyl chloride was dissolved in 40 mL CH_2Cl_2, and cooled to -78°C. 1.62 mL (ρ = 1.10 g·cm^{-3}, 1.78 g, 0.0228 mol) of dimethyl sulfoxide dissolved in 10 mL CH_2Cl_2 was added dropwise to solution. Mix was stirred for 20 minutes and Boc-N-Methyl amino ethanol dissolved in 10 mL CH_2Cl_2 was added dropwise. Stirring at -78°C was continued for 40 minutes, then 4.77 mL (ρ = 0.726 g·cm^{-3}, 3.46 g, .034 mol) of triethylamine was added dropwise. The mixture was stirred at 0°C for 90 minutes. 20 mL of water and 100 mL of diethyl ether were added, then the organics were separated. Organic layer was washed twice with water and twice with brine, then dried and concentrated. Purification was performed using silica gel chromatography with a 60:1 adsorbent: absorbent ratio (75 mL silica gel) and diethyl ether as a mobile phase. Solvent was removed from pure fractions using roto-evap with flask in 0°C ice bath and full vacuum (~12 mBar). Yield = 718 mg, 73%. ^{1}H NMR (500 MHz, $CDCl_3$), δ 9.61 (s, 0.85H, CH), 3.96 (d, 2.00H, CH_2), 2.95 (d, 2.94H, CH_3), 1.46 (d, 9.46H, C(CH$_3$)$_3$). ^{13}C{^{1}H} NMR (125.7 MHz, $CDCl_3$), δ 198.81 (CHO), 156.33 (NCOO), 155.52 (NCOO), 81.65 (Me$_3$$\underline{C}$), 80.86 (Me$_3$$\underline{C}$), 59.43 (CH$_2$N), 58.98 (CH$_2$N), 36.06 (CH$_3$N), 26.60 ($\underline{C}H_3$C), 28.51 (Me$_3$C), 28.45 ($\underline{C}H_3$C). Note: Two sets of signals observed due to amide conformers.
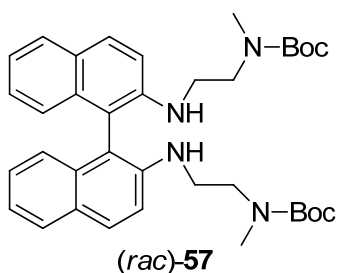
(*rac*)-**57**

(*rac*)-**57**.[11] NaBH(OAc)$_3$ (5.34 g, 25.2 mmol) and (*rac*)-**DABN** (1.79 g, 6.30 mmol) were suspended in dichloroethane (140 mL). Boc-N-Methyl amino ethyl aldehyde (2.18 g, 12.6 mmol) dissolved in dichloroethane (20 mL) was added slowly to the suspension. After the addition, some of the solids had dissolved. Solution was light brown and heterogeneous. After 16 hours, some solids were present and a small amount of bubbling could be observed. By TLC, a small amount of both starting materials was present, along with 2 new UV active products. After 43 hours, solids were still present and TLC showed little, if any change in the reaction. NaHCO$_3$ (120 mL) was added to quench the reaction. The aqueous layer was separated and extracted with CH$_2$Cl$_2$ (2 × 75 mL). The organic layers were combined, washed with brine (2 × 50 mL), dried and concentrated. Silica gel (40 mL) was added to the crude mixture while it contained a small amount of solvent. This mixture was concentrated further and dried under vacuum. Purification using silica gel chromatography (200 mL silica gel) and gradient elution (20-30% Ethyl Acetate in Hexane) afforded the product as an off white solid. Yield = 2.55 g, 68%, R$_f$ = 0.4 (30% Ethyl Acetate in Hexane). ^{1}H NMR (500 MHz, CDCl$_3$, 60°C): δ 7.87 (d, $^3J_{H,H}$ = 9.05 Hz, 2H, aryl-H), 7.73-7.82 (m, 2H, aryl-H), 7.31 (d, $^3J_{H,H}$ = 9.05 Hz, 2H, aryl-H), 7.11-7.23 (m, 5H, aryl-H), 6.99-7.03 (t, 1H, aryl-H), 6.92-6.96 (m, 2H, aryl-H), 3.67-3.89 (br s, 2H, NH), 3.30-3.39 (m, 4H, CH$_2$), 3.13-3.29 (m, 4H, CH$_2$), 2.68 (s, 6H, N-CH$_3$), 1.41(s, 18H, C(CH$_3$)$_3$); ^{13}C{^{1}H} NMR (125.7 MHz, CDCl$_3$, 60°C): δ 155.8 (CO), 144.4, 143.1, 134.1, 130.0, 128.3, 126.9, 124.0, 122.2, 118.5, 113.9, 79.7 (C(CH$_3$)$_3$), 49.3 (N-CH$_3$), 42.5 (CH$_2$), 35.2 (CH$_2$), 28.6 (C(CH$_3$)$_3$).
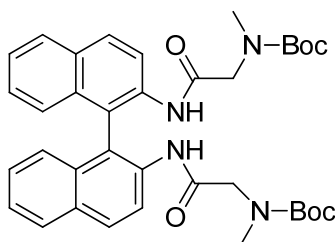
(*rac*)-**58**

(*rac*)-**58.** Boc-sacrosine (2.00 g, 10.6 mmol) was dissolved in THF (30 mL) and cooled to -20 °C. TEA (1.62 mL, 11.6 mmol, ρ = 0.726 g·cm^{-3}, 1.18 g) was added followed by dropwise addition of ethyl chloroformate (1.01 mL, 10.6 mmol, ρ = 1.14 g·cm^{-3}, 1.15 g). This mixture was kept at or below -15 °C for 1 hour. The solution was white and heterogenenous. (*rac*)-DABN (1.51 g, 5.3 mmol) in THF (15 mL) was added dropwise over 30 minutes. The flask was physically agitated to ensure stirring. Throughout addition, stirring became more apparent. The mixture was allowed to warm to 20 °C and stirred for 17 hours. The solvent and TEA were removed and the residue was dissolved in CH$_2$Cl$_2$ (150 mL), then extracted with saturated NaHCO$_3$ (2 × 75 mL) and brine (1 × 50 mL). The organic layer was dried and concentrated. The crude mixture was purified by silica gel chromatography two times (100 mL silica gel, 2% 10:1 MeOH:NH$_4$OH in CH$_2$Cl$_2$). The product was then re-crystallized from 4:1 Hexane:Toluene at 60 °C to yield 2.10 g (66%) of the pure product. ^{1}H NMR (500 MHz, CDCl$_3$, 60 °C): δ 8.58 (d, 2H, $^3J_{H,H}$ = 8.80 Hz), 8.06 (d, 2H, $^3J_{H,H}$ = 9.04 Hz), 7.93 (d, 2H, $^3J_{H,H}$ = 8.07 Hz), 7.48 (br s, 2H), 7.42 (t, 2H, $^3J_{H,H}$ = 7.46 Hz), 7.26 (t, 2H, $^3J_{H,H}$ = 7.09 Hz, overlapped with CDCl$_3$), 7.07 (d, 2H, $^3J_{H,H}$ = 8.56 Hz), 3.75-3.57 (m, 4H, CH$_2$), 2.13 (s, 6H, N-CH$_3$), 1.24 (s, 18H, CH(C$\underline{H}_3$)$_3$); ^{13}C{^{1}H} NMR (125.7 MHz, CDCl$_3$, 60 °C): δ 167.9, 134.7, 132.4, 131.5, 130.0, 128.5, 127.5, 125.7, 124.9, 121.4, 120.6, 80.5 ($\underline{C}$H(CH$_3$)$_3$), 53.6 (CH$_2$), 34.7 (N-CH$_3$), 28.1 (CH(C$\underline{H}_3$)$_3$).
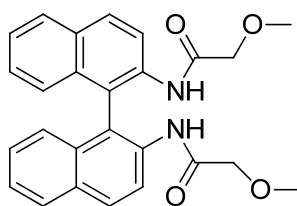

(*rac*)-**62**

(*rac*)-**62.** (rac)-**DABN** (0.14 g, 0.51 mmol) was dissolved in CH$_2$Cl$_2$ (10 mL). TEA (0.14 mL, 0.10 g, ρ = 0.73 g·cm^{-3}) was added and the mixture was briefly stirred, then cooled to 0°C.

Methoxyacetyl chloride (0.09 mL, 0.11 g, 1.0 mmol, ρ = 1.22 g·cm^{-3}) was added dropwise. After stirring for 1 hour, saturated NaHCO$_3$ (10 mL) was added. The aqueous layer was extracted with CH$_2$Cl$_2$ (3×10 mL). Combined organics were dried and concentrated. Purification was performed using silica gel chromatography (10 mL silica gel). CH$_2$Cl$_2$ eluted impurities and 1% MeOH in CH$_2$Cl$_2$ to elute the product. Fractions were concentrated and formed a thick, gummy film. Recrystallization was performed using 4:1 Hexane : Ethyl Acetate. Red-orange solid, yield = 185 mg, 85%, R_f = 0.3 (1% MeOH in CH$_2$Cl$_2$). ^{1}H NMR (500 MHz, CDCl$_3$, 25°C): δ 8.74 (d, $^3J_{H,H}$ = 9.04 Hz, 2H, N-H), 8.07 (d, $^3J_{H,H}$ = 9.04 Hz, 4H, aryl-H), 7.94 (d, $^3J_{H,H}$ = 8.32 Hz, 2H, aryl-H), 7.44 (t, $^3J_{H,H}$ = 7.21 Hz, 2H, aryl-H), 7.31 (t, $^3J_{H,H}$ = 7.09 Hz, 2H, aryl-H), 7.16 (d, $^3J_{H,H}$ = 8.56 Hz, 2H, aryl-H), 3.74 (s, 1H, CH$_2$), 3.71 (s, 1H, CH$_2$), 3.63 (s, 1H, CH$_2$), 3.60 (s, 1H, CH$_2$), 2.67 (s, 6H, OCH$_3$); ^{13}C{^{1}H} NMR (125.7 MHz, CDCl$_3$, 25°C): δ 168.1 (NCO), 134.4, 132.3, 131.1, 130.0, 128.3, 127.4, 125.4, 125.0, 120.2, 119.2, 71.8 (CH$_2$), 58.9 (OCH$_3$).
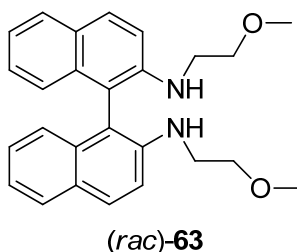

(*rac*)-**63**

(*rac*)-**63**. LiAlH$_4$ (160 mg, 4.21 mmol) was suspended in THF (25 mL) and cooled to 0°C. (*rac*)-**62** (902 mg, 2.10 mmol) dissolved in THF (6 mL) was added dropwise to the suspension. The mixture was warmed to 22°C. After 20 hours starting material was still present. Reaction was refluxed for 21 hours, and starting material remained. LiAlH$_4$ (80 mg, 2.10 mmol) was added and mixture was refluxed for 24 hours. TLC spot appearing to be starting material still remained. The mixture was cooled to 0°C and diluted with Et$_2$O (75 mL). Water (0.3 mL) was added followed by 2N NaOH (0.3 mL), then additional water (0.8 mL). Mixture was warmed to 22°C and stirred for 15 minutes. MgSO$_4$ was added, stirring was continued for 15 minutes. Liquid was decanted and concentrated. Purification with silica gel chromatography (50 mL silica gel) using gradient elution (2-5% Methanol in CH$_2$Cl$_2$) provided the product as an impure film. Recrystallization with 2:1 Hexane:Ethyl Acetate afforded the product as a yellow crystalline solid. Yield = 460 mg, 55%, R_f = 0.6 (1% MeOH in CH$_2$Cl$_2$). ^{1}H NMR (500 MHz, C$_6$D$_6$, 25°C):

δ 7.77 (d, $^3J_{H,H}$ = 9.05 Hz, 2H, aryl-H) 7.70 (d, $^3J_{H,H}$ = 8.07 Hz, 2H, aryl-H), 7.24 (d, $^3J_{H,H}$ = 8.56 Hz, 2H, aryl-H), 7.13 (d, $^3J_{H,H}$ = 8.80 Hz, 2H, aryl-H), 7.05-7.10 (m, 2H, aryl-H), 6.98-7.02 (m, 2H, aryl-H), 4.02 (br s, 2H, NH), 2.92-2.98 (m, 6H, CH$_2$), 2.85-2.91 (m, 2H, CH$_2$), 2.75 (s, 5H, OCH$_3$); ^{13}C{^{1}H} NMR (125.7 MHz, C$_6$D$_6$, 25°C): δ 145.1, 134.7, 129.9, 128.5, 128.4, 127.1, 124.5, 122.3, 114.5, 113.0, 71.5 (OCH$_2$), 58.1 (OCH$_3$), 43.7 (NCH$_2$).
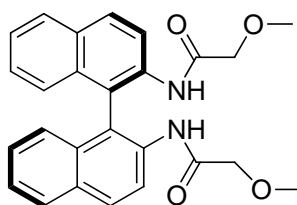

(R)-**62**

(R)-**62**. (R)-**DABN** (472 mg, 1.66 mmol) was dissolved in CH$_2$Cl$_2$ (12 mL) and triethylamine (509 μL, 370 mg, ρ = 0.726 g·cm^{-3}, 3.65 mmol) was added. The reaction was placed on ice and methoxyacetyl chloride was added dropwise. The solution turned pale yellow after addition of first drop. The solution was stirred at 22 °C for 2 hours and TLC revealed consumption of DABN. Saturated NaHCO$_3$ (15 mL) was added and the aqueous layer was extracted with CH$_2$Cl$_2$ (2 × 15 mL). The combined organics were dried and concentrated. Purification by silica gel chromatography with (1:1) Hexane:Ethyl Acetate as a mobile phase yielded the pure amide. Yield = 699 mg, 98%, Rf = 0.17 in 50:50 Hexane:Ethyl Acetate. ^{1}H NMR (400 MHz, CDCl$_3$, 25 °C): δ 8.74 (d, 2H, $^3J_{H,H}$ = 9.0 Hz, aryl-H), 8.07 (d, 2H, $^3J_{H,H}$ = 9.0 Hz, aryl-H), 7.94 (d, 2H, $^3J_{H,H}$ = 8.2 Hz, aryl-H), 7.44 (ddd, 2H, $^3J_{H,H}$ = 7.0 Hz, $^3J_{H,H}$ = 8.2 Hz, aryl-H, $^4J_{H,H}$ = 1.2 Hz,), 7.30 (ddd, 2H, $^3J_{H,H}$ = 6.7 Hz, $^3J_{H,H}$ = 8.4 Hz, $^4J_{H,H}$ = 1.2 Hz, aryl-H), 7.16 (d, 2H, $^3J_{H,H}$ = 8.6 Hz, aryl-H), 3.73 (d, 2H, $^2J_{H,H}$ = 15.7 Hz, CH$_2$), 3.61 (d, 2H, $^2J_{H,H}$ = 15.7 Hz, CH$_2$), 2.67 (s, 6H, OCH$_3$); ^{13}C NMR{^{1}H} NMR (100.6 MHz, CDCl$_3$, 25 °C): δ 168.1 (NCO), 134.4, 132.2, 131.1, 130.0, 128.3, 127.4, 125.4, 125.0, 120.2, 119.2, 71.8 (CH$_2$), 58.8 (OCH$_3$).
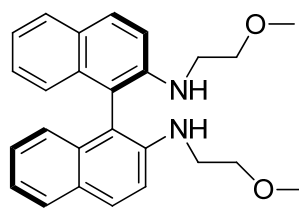
(R)-**63**

(R)-**63**. (R)-**62** (665 mg, 1.11 mmol) and LiAlH$_4$ (127 mg, 3.34 mmol) were combined in a flask, which was purged and filled with N$_2$. Et$_2$O (25 mL) was added and the suspension was refluxed at 40ºC for 20 hours. A spot with the same R$_f$ as starting material was present on TLC, so LiAlH$_4$ (220 mg, 5.79 mmol) was added and the suspension was refluxed for 24 hours. The spot possibly accounting for starting material was present at this point. Water (10 mL) was added followed by 25% NaOH (5 mL) and Et$_2$O (75 mL), then the solution was stirred for 15 minutes. The aqueous layer was removed with a pipette and the organic layer was dried with MgSO$_4$. The aqueous layer was washed with Et$_2$O (3 × 20 mL) and the combined organics were dried and concentrated. The product was purified by silica gel chromatography using 50:50 Hexane:Ethyl Acetate as a mobile phase, then freeze dried from benzene to yield the product as an orange/yellow viscous semisolid. R$_f$ = 0.24 in 50:50 Hexane:Ethyl Acetate, Yield = 490 mg, 76%; ^{1}H NMR (400 MHz, C$_6$D$_6$, 25 °C): δ 7.79 (d, 2H, $^3J_{H,H}$ = 9.0 Hz, aryl-H), 7.72 (d, 2H, $^3J_{H,H}$ = 8.2 Hz, aryl-H), 7.26 (d, 2H, $^3J_{H,H}$ = 8.2 Hz, aryl-H), 7.13 (d, 2H, $^3J_{H,H}$ = 2.4 Hz, aryl-H), 7.11-7.06 (m, 2H, aryl-H), 7.05-6.99 (m, 2H, aryl-H), 4.03 (br s, 2H, N-H), 3.00-2.85 (m, 8H, CH$_2$), 2.76 (s, 5H, OCH$_3$); ^{13}C{^{1}H} NMR (100.6 MHz, C$_6$D$_6$, 25°C) δ 145.1, 134.7, 129.9, 128.54 (C$_6$H$_6$), 128.51, 128.4 (C$_6$H$_6$), 127.1, 124.6, 122.3, 114.5, 113.0, 71.5 (CH$_2$), 58.1 (CH$_3$), 43.7 (CH$_2$).

^{1}H NMR (400 MHz, THF-d_8, 25°C): δ 7.83 (d, 2H, $^3J_{H,H}$ = 8.6 Hz, aryl-H), 7.71 (d, 2H, $^3J_{H,H}$ = 9.0 Hz, aryl-H), 7.30 (d, 2H, $^3J_{H,H}$ = 9.0 Hz, aryl-H; overlapped with C$_6$H$_6$ impurity), 7.11-7.01 (m, 4H, aryl-H), 6.88 (d, 2H, $^3J_{H,H}$ = 8.21 Hz, aryl-H), 4.10 (t, 2H, $^3J_{H,H}$ = 5.7 Hz, N-H), 3.38-3.26 (m, 8H, CH$_2$), 3.08 (s, 5H, OCH$_3$); ^{13}C{^{1}H} NMR (100.6 MHz, THF-d_8, 25 °C): δ 145.7, 135.1, 130.1, 129.0 (C$_6$H$_6$), 128.8, 128.7, 126.9, 124.7, 124.7, 122.2, 114.9, 113.1, 72.4 (CH$_2$), 58.5 (CH$_3$), 44.3 (CH$_2$).
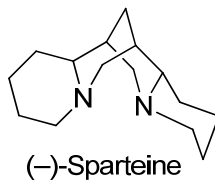
(–)-Sparteine

Isolation of (–)-Sparteine from (–)-Sparteine Sulfate Pentahydrate.[12] (–)-Sparteine Sulfate Pentahydrate (10.0 grams) was dissolved in 5% KOH in water (100 mL) and extracted with CH_2Cl_2 (2 × 100 mL). The combined organic layers were washed one additional time with 5% KOH in water (100 mL), then with brine (10 mL), then dried with sodium sulfate and concentrated *in vacuo*. The residue was dissolved in pentane (200 mL) and transferred to a clean round bottom flask, taking care to not transfer insoluble colored compounds. The pentane was removed *in vacuo*, along with residual traces of CH_2Cl_2. The viscous residue was stirred over CaH and distilled to yield pure (–)-Sparteine. The NMR data matches previously reported spectra.[13]

4.4 Complex Synthesis

Trimethylsilyl methyl lithium.[14] In the glovebox, lithium wire (0.450 g, 0.0648 mol), previously rinsed with dry hexanes and dried under vacuum, was scraped clean and cut with scissors into small (~3 × 3 cm) pieces and added to a dry schlenk flask. Flattening chunks of the lithium wire with a mortar and pestle allowed them to be cut into increasingly smaller pieces. Chlorotrimethylsilane (2.28 mL, 0.0163 mol, 2.00 g, ρ = 0.879 g·cm^{-3}) dissolved in dry hexane (20 mL) was added to this flask, and stirred vigorously at 22°C in the glovebox overnight. The solution was metallic/dark gray the following morning. Additional lithium (0.450 g, 0.0648 mol) was added followed by chlorotrimethylsilane (2.28 mL, 0.0163 mol, 2.00 g, ρ = 0.879 g·cm^{-3}) dissolved in dry hexane (20 mL). This solution was stirred for 3 additional days at 22°C. At this point, no additional pieces of lithium were floating up to the top surface of the reaction. The solution was very dark gray and metallic in appearance. The stirring was stopped and the solids were allowed to settle overnight. The flask was carefully removed from the glovebox and left to settle for several hours. Using a filter equipped cannula, the solution was filtered (on nitrogen Schlenk line). The remaining residue was dissolved in dry hexane (10 mL), allowed to settle then filtered. The hexane was removed from the filtrate under vacuum, yielding the product as a white

free flowing pyrophoric solid. Yield = 2.71 g, 88%. ^{1}H NMR (500 MHz, C_6D_6, 25 °C): δ 0.15 (s, 9H, CH_3), -2.08 (s, 2H, CH_2). $^{13}C\{^1H\}$ NMR (125.7 MHz, C_6D_6, 25 °C): δ 3.51 (s, CH_3), -4.72 (br s, CH_2).

**Trimethylsilyl methyl sodium**.[15] NaOtBu (452 mg, 4.7086 mmol) was suspended in hexane (15 mL) and $LiCH_2SiMe_3$ (444 mg, 4.7086 mmol) in pentane (5 mL) was added dropwise. The reaction was stirred for 20 hours and the liquid was removed by filtration. The solids were rinsed with hexane (3 × 5 mL) and dried *in vacuo* and transferred into a vial. Yield = 311 mg (after transfer), 60%.

(R)-**64**
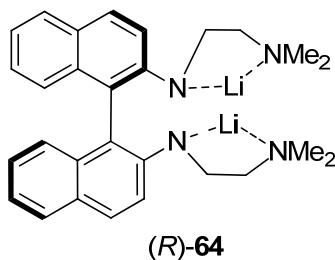
(R)-(Bis(dimethylamino-2-yl-ethyl)amido)binaphthyl-di-lithium (*(R)*-**64**). In the glovebox, *(R)*-**54** (371.1 mg, 0.869 mmol) was dissolved in benzene (4 mL). $LiCH_2SiMe_3$ (163.9 mg, 1.73 mmol) was dissolved in pentane (4 mL). The solution of $LiCH_2SiMe_3$ was added dropwise to the solution of *(R)*-**54** at 22ºC, stirred for 1.5 hours, then freeze dried and transferred to a vial. Orange solid. Yield = 362.8 mg, 95%. ^{1}H NMR (500 MHz, C_6D_6, 80°C): δ 7.69 (d, 2H, $^3J_{H,H}$ = 9.04 Hz), 7.59 (d, 2H, $^3J_{H,H}$ = 8.07 Hz), 7.13 (d, 2H, $^3J_{H,H}$ = 9.05 Hz), 6.80 (br s, 6H), 3.10 (br s, 4H), 2.21 (br s, 2H), 1.69 (br s, 2H), 1.52 (s, 12H). $^{13}C\{^1H\}$ NMR (125.7 MHz, C_6D_6, 80°C): 157.29, 138.17, 128.90, 128.85, 128.68, 126.57, 125.85, 119.18, 117.84, 117.17, 62.85, 46.36, 45.59. Anal. Calcd. for $C_{28}H_{32}Li_2N_4$: C, 76.70; H, 7.36; N, 12.78. Found: (1) C, 75.52; H, 7.88; N, 12.56. (2) C, 73.88; H, 7.13; N, 12.16. (3) C, 71.56; H, 7.26; N, 10.98 with combustion aid.
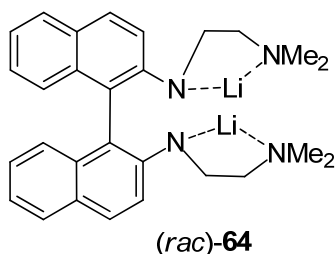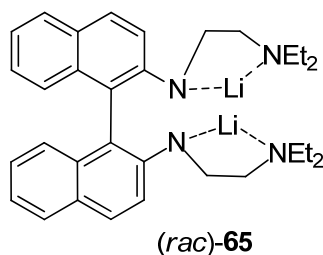
(*rac*)-**64**

(*rac*)-(Bis(dimethylamino-2-yl-ethyl)amido)binaphthyl-di-lithium ((*rac*)-**64**). In the glovebox, (*rac*)-**54** (102.5 mg, 0.240 mmol) was weighed into a vial and dissolved in benzene (0.2 mL). LiCH₂SiMe₃ (47.5 mg, 0.504 mmol) was weighed into another vial and dissolved in pentane (0.3 mL). The solution of base was layered on top of the solution containing (*rac*)-**54** and left overnight. The following day a biphasic solution remained. This solution was transferred to a larger vial with additional benzene (0.5 mL). The contents of the flask were mixed and stored at room temperature. After one week at 22ºC the solution was separated from the solids and freeze dried. The solids were dried in vacuo. All solids were combined. Yield = 77 mg, 73% (with small N-H signal present in ^{1}H NMR spectra). NMR spectra after addition of base: ^{1}H NMR (400 MHz, toluene-d₈, 80°C): δ 7.62 (d, 2H, $^3J_{H,H}$ = 9.00 Hz), 7.55-7.50 (m, 2H), 7.09 (d, 2H, $^3J_{H,H}$ = 9.00 Hz), 7.00-6.96 (m, 1H), 6.79-6.67 (m, 5H), 3.11-2.96 (m, 4H), 2.27-2.17 (m, 2H), 1.80-1.67 (m, 2H), 1.53 (s, 12H).


(*R*)-**65**
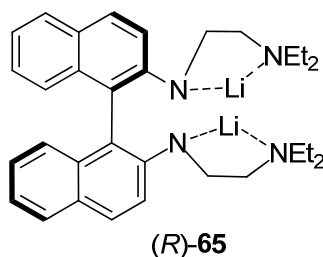
(*R*)-(Bis(diethylamino-2-yl-ethyl)amido)binaphthyl-di-lithium ((*R*)-**65**). In the glovebox, (*R*)-**55** (380.7 mg, 0.789 mmol) was dissolved in benzene (4 mL). LiCH₂SiMe₃ (148.7 mg, 1.58 mmol) was dissolved in pentane (4 mL). The solution of LiCH₂SiMe₃ was added dropwise to the solution of (*R*)-**55** at 22ºC, stirred for 1.5 hours, then freeze dried and transferred to a vial. Orange solid. Yield = 270 mg, 69%. ^{1}H NMR (500 MHz, C₆D₆, 80°C): δ 7.81 (d, 2H, $^3J_{H,H}$ = 8.80 Hz), 7.67-7.64 (m, 2H), 7.30 (d, 2H, $^3J_{H,H}$ = 8.80 Hz), 7.09-7.06 (m, 2H), 6.91-6.85 (m, 4H), 3.46-3.39 (m, 2H), 3.25 (ddd, 2H, $^2J_{H,H}$ = 12.96 Hz, $^3J_{H,H}$ = 8.56 Hz, $^3J_{H,H}$ = 4.40 Hz), 2.58-2.48 (m, 2H), 2.27-2.20 (m, 2H), 2.06-1.97 (m, 4H), 1.92-1.80 (m, 4H), 0.41 (t, 12H, $^3J_{H,H}$ = 7.22 Hz).

$^{13}C\{^1H\}$ NMR (125.7 MHz, C_6D_6, 80°C): 155.59, 137.65, 129.86, 128.90, 128.68, 126.72, 126.01, 125.75, 119.06, 117.72, 116.03, 57.61, 46.53, 46.39, 11.99, 0.31. Anal Calcd for $C_{32}H_{40}Li_2N_4$: C, 77.71; H, 8.15; N, 11.33. Found: (1) C, 72.79; H, 7.99; N, 10.16. (2) C, 74.07; H, 7.99; N, 10.14 with combustion aid.

(*rac*)-**65**
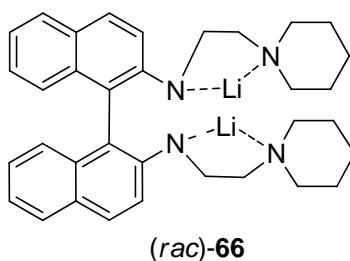
(*rac*)-(Bis(diethylamino-2-yl-ethyl)amido)binaphthyl-di-lithium ((*rac*)-**65**)**.** In the glovebox, (*rac*)-**55** (124.7 mg, 0.258 mmol) was weighed into a vial and dissolved in benzene (1.0 mL). LiCH$_2$SiMe$_3$ (51.1 mg, 0.542 mmol) was weighed into another vial and dissolved in pentane (1.0 mL). The solution of base was added dropwise to the solution of (*rac*)-**55**. The solution was stored for one week at 22°C and no solids formed. The solution was transferred to a Schlenk tube using additional benzene (2 mL), and was freeze dried. Orange powder, Yield = 93.8 mg, 73%. ^1H NMR (500 MHz, toluene-d$_8$, 65°C): δ 7.73 (d, 2H, $^3J_{H,H}$ = 8.80 Hz), 7.58 (dd, 2H, $^3J_{H,H}$ = 6.24 Hz, $^3J_{H,H}$ = 3.06 Hz), 7.22 (d, 2H, $^3J_{H,H}$ = 8.80 Hz), 6.98-6.90 (br m, 2H), 6.81 (dd, 4H, $^3J_{H,H}$ = 6.24 Hz, $^3J_{H,H}$ = 3.3 Hz), 3.42-3.32 (br m, 2H), 3.23-3.15 (m, 2H), 2.55-2.45 (br s, 2H), 2.25-2.15 (br m, 2H), 2.05-1.90 (br m, 4H, overlapped with toluene-d$_8$ signal), 1.90-1.75 (br m, 4H), 0.45-0.35 (br m, 12H).

(*R*)-**66**
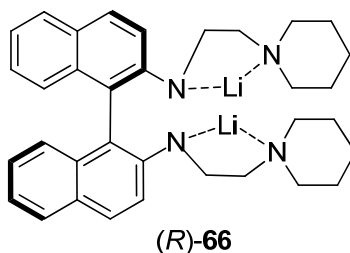
(*R*)-**66.** In the glovebox, (*R*)-**56** (400 mg, 0.789 mmol) was dissolved in benzene (4 mL). LiCH$_2$SiMe$_3$ (148.6 mg, 1.58 mmol) was dissolved in pentane (4 mL). The solution of LiCH$_2$TMS was added dropwise to the solution of (*R*)-**56** at 22°C, stirred for 2 hours, then freeze dried and transferred to a vial. Orange solid. Yield = 214 mg, 52%. ^1H NMR (500 MHz, C$_6$D$_6$,

80°C): δ 7.82 (d, 2H, $^3J_{H,H}$ = 8.80 Hz), 7.65 (d, 2H, $^3J_{H,H}$ = 7.58 Hz), 7.31 (d, 2H, $^3J_{H,H}$ = 8.81 Hz), 7.09 (d, 2H, $^3J_{H,H}$ = 7.09 Hz), 6.88 (dd – overlapped with signal at 6.85, 2H, $^2J_{H,H}$ = 12.96 Hz, $^3J_{H,H}$ = 6.36 Hz), 6.85 (dd – overlapped with signal at 6.88, 2H, $^2J_{H,H}$ = 12.96 Hz, $^3J_{H,H}$ = 6.60 Hz), 3.48-3.39 (m, 2H), 3.32-3.24 (m, 2H), 2.38-2.19 (m, 4H), 1.87 (br s, 8H), 1.52-1.10 (br m, 1H), 1.06-0.70 (m, 12H). $^{13}C\{^1H\}$ NMR (125.7 MHz, 80°C): 155.85, 137.59, 129.97, 128.90, 128.68, 126.84, 126.07, 125.65, 119.14, 117.70, 116.11, 62.53, 54.17, 46.03, 26.97, 24.63. Anal Calcd $C_{34}H_{40}Li_2N_4$: C, 78.74; H, 7.77; N, 10.80. Found: C, 72.83; H, 7.38; N, 9.75 with combustion aid.

(*rac*)-**66**

(*rac*)-(Bis(piperidin-2-yl-ethyl)amido)binaphthyl-di-lithium ((*rac*)-**66**). (*rac*)-**56** (122.0 mg, 0.240 mmol) was dissolved in benzene (1.0 mL). LiCH$_2$SiMe$_3$ (47.6 mg, 0.506 mmol) was dissolved in pentane (1.0 mL) and added dropwise to the solution of (*rac*)-**56**. This solution was stored in the freezer for one week. The solids were separated from the solution, and dried in vacuo. The solution was freeze dried. All solids were combined and rinsed with pentane (3 × 1 mL) and were then dried in vacuo. Yield = 89.5 g, 72%. ^1H NMR (400 MHz, toluene-d$_8$, 60°C): δ 7.75 (d, 2H, $^3J_{H,H}$ = 8.61 Hz), 7.61-7.56 (m, 2H), 7.25 (d, 2H, $^3J_{H,H}$ = 8.61 Hz), 7.03-6.96 (m, 2H), 6.84-6.78 (m, 4H), 3.41-3.36 (m, 2H), 3.24-3.18 (m, 2H), 2.32-2.26 (m, 2H), 2.22-2.16 (m, 2H), 1.90-1.74 (m, 8H), 1.00-0.88 (m, 8H), 0.80-0.65 (m, 4H).

Lithiation of (R)-63. (R)-**63** (47.2 mg, 0.0809 mmol) was dissolved in THF-d$_8$ (0.6 mL) and n-BuLi (63.3 µL, 2.56 M, 0.162 mmol) was added. The NMR tube was capped and shaken and a homogeneous orange solution formed. Proton and carbon spectra showed well defined peaks for this complex at 25 ºC. Spectra contains free ligand, hexane (from n-BuLi) and residual benzene. ^1H NMR (400 MHz, THF-d$_8$, 25 °C): δ 7.40 (d, 2H, $^3J_{H,H}$ = 9.0 Hz, aryl-H), 7.30 (d, 2H, $^3J_{H,H}$ = 7.05 Hz, aryl-H, overlapped with C$_6$H$_6$ impurity), 6.95 (d, 2H, $^3J_{H,H}$ = 9.0 Hz, aryl-H), 6.56 (ddd, 2H, $^3J_{H,H}$ = 8.4 Hz, $^3J_{H,H}$ = 6.7 Hz, $^2J_{H,H}$ = 1.6 Hz, aryl-H), 6.48 (t, 2H, $^3J_{H,H}$ = 7.1 Hz, aryl-H,

overlapped with 6.44), 6.44 (d, 2H, $^3J_{H,H}$ = 8.6 Hz, aryl-H, overlapped with 6.48), 4.63 (br s, 1H, N-H), 3.65-3.59 (m, 2H, overlapped with THF-d_8), 3.56-3.51 (m, 2H, overlapped with THF-d_8), 3.50-3.39 (m, 3H, overlapped with free ligand), 3.30 (s, 4H, CH$_3$), 3.20 (s, 3H, CH$_3$), 3.15 (t, 1H, $^3J_{H,H}$ = 3.7 Hz), 3.12 (t, 1H, $^3J_{H,H}$ = 3.9 Hz); ^{13}C{^{1}H} NMR & DEPT (100.6 MHz, THF-d_8, 25 °C): δ 158.3, 137.9, 128.2, 128.1, 127.7, 125.6, 125.3, 125.8, 124.6, 116.0, 115.2, 76.1 (CH$_2$O), 58.7 (CH$_3$), 58.2 (CH$_3$), 49.8 (CH$_2$), 42.3 (CH$_2$).

4.5 Crystal Structures

Data was collected using graphite monochromatized Mo-Ka x-radiation (l = 0.71073 Å) on a Bruker APEX CCD diffractometer at 100(2) K, and are summarized in Tables 5.4.1 through 5.4.6. Corrections for Lorentz, polarization, and absorption effects were applied. The Bruker APEX2 crystallographic program suite was used, which included the SAINT program for data reduction, the SHELXS program for structure solution by direct methods and the SHELXL structure refinement program.[16] All positional and atomic displacement parameters were refined using all reflection data and the full-matrix least-squares refinement on F^2 in SHELXL. All hydrogen atoms were constrained to idealized (e.g., sp^2 or sp^3) positions using a riding model in SHELXL.

ORTEP-3,[17] version 2.02 was used to generate a '.pov' file from the '.cif' file. PNG images of the complexes were rendered in POV-ray, version 3.6.2 and labels were added in Adobe Illustrator CS5, version 15.0.2. The final image was cropped in Microsoft Paint, version 6.1.

Molecular Structure of [(*R*)-64]$_2$, (*R*)-(bis(dimethylamino-2-yl-ethyl)amido)binaphthyl-di-lithium: In an argon filled glovebox, (*R*)-54 (70.6 mg, 0.165 mmol) was dissolved in benzene (0.5 mL) and transferred into a vial containing LiCH$_2$SiMe$_3$ (31.2 mg, 0.330 mmol). This solution was used to rinse the original vial, than divided evenly between both vials. The vials were placed in a larger vial (20 mL) containing pentane (1.5 mL) which was allowed to diffuse into the solutions over one day at 22°C and bright orange crystals of [(*R*)-64]$_2$ suitable for X-ray diffraction formed over 5 days at 22°C. Cell parameters were obtained from 26648 reflections within the range 1.96 < θ < 31.48°.

Molecular Structure of [(*rac*)-**64**]₆, (***rac***)-**(bis(dimethylamino-2-yl-ethyl)amido)binaphthyl-di-lithium:** In an argon filled glovebox, (*rac*)-**54** (50 mg, 0.117 mmol) was dissolved in benzene (0.5 mL) and transferred into a vial containing LiCH₂SiMe₃ (22.1 mg, 0.234 mmol). This solution was used to rinse the original vial, then divided evenly between both vials. The vials were placed in a larger vial (20 mL) containing pentane (2.5 mL) which was allowed to diffuse into the solutions over 2 days at 22°C. The vials were removed, and individually capped. Bright orange crystals of [(*rac*)-**64**]₆ suitable for X-ray diffraction were observed after 3 weeks. Cell parameters were obtained from 49606 reflections within the range $1.96 < \theta < 31.48°$.

Molecular Structure of (*rac*)-**65**, **(rac)-(bis(diethylamino-2-yl-ethyl)amido)binaphtyl-di-lithium:** In an argon filled glovebox, (*rac*)-**55** (30.1 mg, 0.623 mmol) was dissolved in benzene (0.3 mL) and transferred into a vial containing LiCH₂SiMe₃ (11.7 mg, 0.125 mmol). This solution was used to rinse the original vial, and this vial was placed in a larger vial containing hexane (1.0 mL) which was allowed to diffuse into the solutions overnight at 22°C. The inner vial was removed, capped and stored at 22°C for three weeks at which point yellow-orange crystals of (*rac*)-**65** suitable for X-ray diffraction were observed. Cell parameters were obtained from 24108 reflections within the range $1.84 < \theta < 30.56°$.

Molecular Structure of (*rac*)-**66**, (***rac***)-**(bis(piperidin-2-yl-ethyl)amido)binaphthyl-di-lithium:** In an argon filled glovebox, (*rac*)-**56** (50 mg, 0.0987 mmol) was dissolved in benzene (0.5 mL) and transferred into a vial containing LiCH₂SiMe₃ (18.6 mg, 0.197 mmol). This solution was used to rinse the original vial, than was divided evenly between both vials. The vials were placed in a larger vial (20 mL) containing pentane (2.5 mL) which was allowed to diffuse into the solutions over 2 days at 22°C. The vials were removed, and individually capped. Yellow-orange crystals of (*rac*)-**66** suitable for X-ray diffraction were observed after 3 weeks. Cell parameters were obtained from 20780 reflections within the range $1.86 < \theta < 31.56°$.

Molecular Structure of [(*R*)-**67**]₂: (***R***)-**(bis(methoxy-2-yl-ethyl)amido)binaphthyl-di-lithium:** In an argon filled glovebox, (*R*)-**63** (20.8 mg, 0.0519 mmol) was weighed into a vial and dissolved in toluene (0.5 mL). In another vial, LiCH₂SiMe₃ (10.3 mg, 0.109 mmol) was dissolved in toluene (0.5 mL). The solution of LiCH₂SiMe₃ was layered on top of the solution of

(*R*)-**63** and slow diffusion of the two layers was allowed overnight. The following day, orange solids were observed containing X-ray quality crystals of [(*R*)-**67**]$_2$. Cell parameters were obtained from 24842 reflections within the range 1.94 < θ < 31.50°. Absolute configuration could not be determined due to the flack parameter. The unit cell for the racemic structure was determined to be identical to that obtained for this structure.

Molecular Structure of [(*rac*)-**67**]$_2$: (*R*)-**(bis(methoxy-2-yl-ethyl)amido)binaphthyl-di-lithium:** In an argon filled glovebox, (*rac*)-**63** (11.2 mg, 0.0279 mmol) was weighed into a vial and dissolved in benzene (0.6 mL). In another vial, LiCH$_2$SiMe$_3$ (5.5 mg, 0.0587 mmol) was dissolved in pentane (0.8 mL). The solution of LiCH$_2$SiMe$_3$ was layered on top of the solution of (*rac*)-**63** and slow diffusion of the two layers was allowed overnight. Three days later, orange solids were observed containing X-ray quality crystals of [(*rac*)-**67**]$_2$. The unit cell for this structure is identical to that for the enantiopure structure described above.

(*R*)-(bis(dimethylamino-2-yl-ethyl)amido)binaphthyl-di-lithium (*R*)-**68.** In an argon filled glovebox, **S3** (30.8 mg, 0.201 mmol) was weighed into a vial and ferrocene was added followed by C$_6$D$_6$ (450 μL). (*R*)-**54** in C$_6$D$_6$ (143 μL, [0.1406 M], 0.0201 mmol) was added to the vial followed by LiCH$_2$SiMe$_3$ in C$_6$D$_6$ (107 μL, [0.319 M], 0.0342 mmol). This solution was shaken well and transferred to an NMR tube, then stored at 22-25°C for several hours to obtain kinetic data. The contents of the NMR tube were transferred to a vial, using an additional portion of C$_6$D$_6$ (0.2 mL) for rinsing. The vial was stored at -27°C for three and a half weeks, and slowly allowed to reach 22°C after an unexpected freezer failure. After an additional week, bright orange crystals of (*R*)-**68** suitable for X-ray diffraction were found. Cell parameters were obtained from 22161 reflections within the range 1.84 < θ < 30.56°.

4.6 Catalytic Intramolecular Hydroamination/Cyclization

General procedure for NMR scale catalytic intramolecular hydroamination/cyclization of aminoalkenes. In an argon filled glovebox, a stock solution of each ligand was made along with a solution of LiCH$_2$SiMe$_3$ in C$_6$D$_6$. In a screw cap NMR tube was added the ligand (in C$_6$D$_6$ stock solution) followed by LiCH$_2$SiMe$_3$ (in C$_6$D$_6$ stock solution). In a 1.8 mL vial was weighed

the aminoalkene substrate and C_6D_6 was added to bring the total volume to 0.7 mL, then ferrocene was added. The contents of the vial were transferred to the NMR tube, shaken and transferred back into the vial. The vial was shaken and the solution was returned to the NMR tube. This process ensures quantitative mixing of all reaction components, as the residue left behind on the vial without the second transfer would impact the actual concentration of each component in solution. If necessary, the NMR tube was placed in a thermostated oil bath at the given temperature. The conversion was monitored by ^1H NMR spectroscopy. Upon completion of the reaction, the product was purified by either vacuum transfer or column chromatography and final conversion was determined by ^1H NMR spectroscopy.

General procedure for determination of enantioselectivity by Mosher amide. (S)-[α-methoxy-α-(trifluoromethyl)phenylacetic acid chloride][18] (1.2 equiv.) was weighed into a vial and a solution of the amine (1.0 equiv. in either $CDCl_3$ or C_6D_6) was added followed by Hünig's base (1.5 equiv.) followed by a small amount of solvent (0.2 mL). The solution was allowed to sit overnight. For *ee* determination in $CDCl_3$, additional solvent was added to bring the volume to 0.6 mL. For *ee* determination in C_6D_6 or toluene-d_8 the solution was passed through a glass microfiber filter and solvent was added to bring the volume to 0.6 mL. The solutions were transferred to screwcap NMR tubes and the enantiomeric excess was determined by ^{19}F NMR spectroscopy at 70-110°C. Decomposition of excess Mosher acid chloride was performed by adding two drops of methanol, and allowing the solution to sit overnight. Formation of the methyl ester is much slower in benzene and toluene than in $CDCl_3$. For the *ee* determination of 2-Methyl-4,4-diphenylpyrrolidine, decomposition of the Mosher acid chloride was performed. This step is necessary because the acid chloride overlaps with the Mosher amide of one enantiomer in the ^{19}F spectra.

4.7 Catalytic Intermolecular Hydroamination

General procedure for base catalyzed hydroamination using LiCH$_2$SiMe$_3$: In a vial was weighed the amine. If LiCl was used, it was weighed into vial prior to addition of amine. Next, the ligand was added via microsyringe from a stock solution, followed by LiCH$_2$SiMe$_3$ also via microsyringe from a stock solution. In an NMR tube was weighed the desired alkene. The

contents of the vial were transferred to the NMR tube, and the vial was rinsed with C_6D_6 (0.2 mL) which was also transferred to the NMR tube.

General procedure for base catalyzed hydroamination using NaCH$_2$SiMe$_3$: In an NMR tube was weighed NaCH$_2$SiMe$_3$ and the ligand was added followed by the amine. C_6D_6 was added followed by the alkene and the NMR tube was shaken well.

General procedure for base catalyzed hydroamination using NaCH$_2$SiMe$_3$ and sparteine: A homogeneous solution was formed by mixing NaCH$_2$SiMe$_3$ and sparteine in C_6D_6. In an NMR tube was added amine, the stock solution containing NaCH$_2$SiMe$_3$ and sparteine, followed by the alkene. The solution was shaken well.

General workup and purification for NMR scale reactions: The contents of the NMR tube were transferred to a round bottom flask using CH_2Cl_2 and all solvents were removed *in vacuo*. The residue was taken up in 1N NaOH (20 mL) and CH_2Cl_2 (20 mL). The organic layer was separated and the aqueous layer was extracted with CH_2Cl_2 (2 × 10 mL). The organic layers were combined, dried and concentrated and purified by silica gel chromatography. Silica gel (20 mL) was used and the column was packed and loaded with CH_2Cl_2. CH_2Cl_2 (20 mL) followed by 1% MeOH in CH_2Cl_2 (20 mL) were run through the column to elute nonpolar starting materials and byproducts. 3-4% MeOH in CH_2Cl_2 was used to elute sparteine if necessary. Secondary amines were typically eluted with 5% MeOH in CH_2Cl_2 and tertiary amines with 10-20% MeOH in CH_2Cl_2.

4.8 Kinetic Studies

General procedure for the preparation of samples for intermolecular kinetic studies on the hydroamination/cyclization of S3. In an argon filled glovebox, a stock solution of each ligand was made along with a solution of LiCH$_2$SiMe$_3$ in C_6D_6. In a screw cap NMR tube was added the ligand (in C_6D_6 stock solution) followed by LiCH$_2$SiMe$_3$ (in C_6D_6 stock solution). In a 1.8 mL vial was weighed the aminoalkene substrate and C_6D_6 was added to bring the total volume to 0.7 mL, then ferrocene was added. The contents of the vial were transferred to the NMR tube, shaken and transferred back into the vial. The vial was shaken and the solution was returned to

the NMR tube. This process ensures quantitative mixing of all reaction components, as the residue left behind on the vial without the second transfer would impact the actual concentration of each component in solution. The reaction was monitored by ^{1}H NMR spectroscopy and the integration of the olefin signals was used to measure reaction progress relative to the internal standard (ferrocene). Spectra were recorded on a Varian 400 MHz NMR using the 'pad' (pre-acquisition delay) command in an arrayed ^{1}H experiment. Reaction progress was monitored by manual integration of the olefin signals and acquisition times were extracted using the 'kind' command and correlated to each spectra.

Data workup was performed in Microsoft excel. The time elapsed between addition of the catalyst to the sample and initial NMR acquisition was recorded, and added to spectral times. The natural logarithm of the raw integration values was plotted against their adjusted times, and the y-intercept for the linear portion of this plot was set as the zero time value of ln[integration]. The zero time raw integration value [integration]$_0$ was calculated using this number. A "substrate loss ratio" was calculated by dividing the integration at each time interval by the zero time integration (substrate loss ratio = [integration]$_t$/[integration]$_0$). This value was multiplied by the initial substrate concentration [Sub]$_0$ of each sample, to provide the sample concentration at each time interval [Sub].

Upon completion of the reaction, the product was purified by either vacuum transfer of column chromatography and *ee*'s were determined using the general procedure for determination of enantioselectivity by Mosher amide.

4.9 VT-DOSY NMR using Gschwind data workup:

TMS was used as an internal reference because its molecular size is known[19,20] and it does not form aggregates. Experimentally obtained diffusion coefficients (D$_{CAT-TEMP}$) were corrected for temperature and viscosity (D$_{COR}$) as shown in equation 1.[21]

(1) $D_{COR} = D_{CAT-TEMP} (\eta_{CAT-298} / \eta_{BLANK-298}) \cdot (298/T)$

The Stokes Einstein equation (equation 2) was used to determine viscosity correction factors (equation 3; $\eta_{CAT-298} / \eta_{BLANK-298}$). D for TMS in a blank sample at 298 K (D$_{BLANK-298}$) was compared with D for TMS in the catalyst solution at 298 K (D$_{CAT-TMS-298}$).

(2) $r_H = (k_B \cdot 298)/(6\pi \cdot \eta \cdot D)$

   $\eta = (k_B \cdot 298)/(6\pi \cdot r_{H\text{-}TMS} \cdot D_{TMS}) = (k_B \cdot 298)/(6\pi \cdot r_{H\text{-}TMS}) \cdot (1/D_{TMS})$

$\eta_{CAT\text{-}298} / \eta_{BLANK\text{-}298} =$

   $= [(k_B \cdot 298)/(6\pi \cdot r_{H\text{-}TMS})(1/D_{CAT\text{-}TMS\text{-}298})] / [(k_B \cdot 298)/(6\pi \cdot r_{H\text{-}TMS})(1/D_{BLANK\text{-}298})]$

   $= (1/D_{CAT\text{-}TMS\text{-}298}) / (1/D_{BLANK\text{-}298}) = D_{BLANK\text{-}298} / D_{CAT\text{-}TMS\text{-}298}$

(3) $\eta_{CAT\text{-}298} / \eta_{BLANK\text{-}298} = D_{BLANK\text{-}298} / D_{CAT\text{-}TMS\text{-}298}$

Diffusion coefficients (D_{COR}) were corrected for temperature and viscosity (equation 1) and the solution viscosity at 298 K ($\eta_{CAT\text{-}298}$) was experimentally determined (equation 4). The Stokes Einstein equation (eq. 2) was used to obtain the hydrodynamic radius.

$r_H = (k_B \cdot 298)/(6\pi \cdot \eta_{CAT\text{-}298} \cdot D_{COR}) = (k_B \cdot 298)/(6\pi) \cdot (1/(\eta_{CAT\text{-}298} \cdot D_{COR}))$

   (4) $\eta_{CAT\text{-}298} = (k_B \cdot 298)/(6\pi \cdot r_{H\text{-}TMS} \cdot D_{TMS\text{-}CAT\text{-}298})$

$r_H = [(k_B \cdot 298)/(6\pi)] \cdot [(6\pi \cdot r_{H\text{-}TMS} \cdot D_{TMS\text{-}CAT\text{-}298})/(k_B \cdot 298)] \cdot [(1/D_{CAT\text{-}TEMP})(\eta_{BLANK\text{-}298}/ \eta_{CAT\text{-}298})(T/298)]$

$= (r_{H\text{-}TMS} \cdot D_{TMS\text{-}CAT\text{-}298}) \cdot (1/D_{CAT\text{-}TEMP}) \cdot (\eta_{BLANK\text{-}298}/ \eta_{CAT\text{-}298}) \cdot (T/298)$

$= [(r_{H\text{-}TMS} \cdot D_{TMS\text{-}CAT\text{-}298} \cdot T)/(D_{CAT\text{-}TEMP} \cdot 298)] \cdot (\eta_{BLANK\text{-}298}/ \eta_{CAT\text{-}298})$

$= [(r_{H\text{-}TMS} \cdot D_{TMS\text{-}CAT\text{-}298} \cdot T)/(D_{CAT\text{-}TEMP} \cdot 298)] \cdot (D_{CAT\text{-}TMS\text{-}298} / D_{BLANK\text{-}298})$

   (5) $r_H = [(r_{H\text{-}TMS} \cdot D_{TMS\text{-}CAT\text{-}298} \cdot T)/(D_{CAT\text{-}TEMP} \cdot 298)] \cdot (D_{CAT\text{-}TMS\text{-}298} / D_{BLANK\text{-}298})$

For experiments ran at 298 K, the Stokes Einstein (eq. 5) data workup was used with the observed D of the catalyst and a calculated viscosity based on equation 2.

   (6) $r_H = (k_B \cdot 298)/(6\pi \cdot \eta_{CAT\text{-}298} \cdot D_{CAT\text{-}298})$

   $= [(k_B \cdot 298)/6\pi][(6\pi \cdot r_{H\text{-}TMS} \cdot D_{TMS\text{-}CAT\text{-}298})/(k_B \cdot 298)][1/D_{CAT\text{-}298}]$

   $= [(k_B \cdot 298)/6\pi][(6\pi \cdot r_{H\text{-}TMS} \cdot D_{TMS\text{-}CAT\text{-}298})/(k_B \cdot 298)][1/D_{CAT\text{-}298}]$

   $= (r_{H\text{-}TMS} \cdot D_{TMS\text{-}CAT\text{-}298})/(D_{CAT\text{-}298})$

   $= (2.9565 \times 10^{-10} \text{ m} \cdot D_{TMS\text{-}CAT\text{-}298})/(D_{CAT\text{-}298})$

The value of r_H (TMS)[20a] has previously been calculated:

(7) r_H (TMS) = $(\delta_{TMS}/2) \times 10^{-10}$ m = 2.9565×10^{-10} m.

Definitions:

$\eta_{CAT-298}$ = η of catalyst solution at 298 K (Pa · s)

$\eta_{BLANK-298}$ = η of blank solution at 298 K (Pa · s)

$\eta_{CAT-TEMP}$ = η of catalyst solution at experiment temperature (Pa · s)

r_{H-TMS} = calculated hydrodynamic radius of TMS (see ref. 1a)

D_{COR} = D corrected for T and η (m^2/s)

$D_{CAT-TEMP}$ = Observed D of catalyst at experiment temperature (m^2/s)

$D_{TMS-CAT-TEMP}$ = Observed D of TMS in catalyst solution at experiment temperature (m^2/s)

$D_{TMS-CAT-298}$ = Observed D of TMS in catalyst solution at 298 K (m^2/s)

$D_{TMS-298}$ = Observed D of TMS in blank sample at 298 K (m^2/s)

r_H = hydrodynamic radius

Units Used:

η = Pa · s;   T = K;   D = m^2/s

Constants & Conversion Factors:

k_B = 1.38×10^{-23} J/K; r_H (TMS) = 2.9565×10^{-10} m

J = Pa · m^3;   Å = 10^{-10} m

Experimental Data:

Pulse sequence Dbppste (not convection corrected):

For blank sample - $D_{TMS-298}$ = 17.086×10^{-10} m^{2}s^{-1}

Pulse sequence Dbppste_cc (convection corrected):

For blank sample - $D_{TMS-298}$ = 8.488×10^{-10} m^{2}s^{-1}

4.10 References

(1)   Gagné, M. R.; Stern, C. L.; Marks, T. J. *J. Am. Chem. Soc.* **1992**, *114*, 275.
(2)   Jones, I. W.; Monguchi, Y.; Dawson, A.; Carducci, M. D.; Mash, E. A. *Org. Lett.* **2005**, *7*, 2841.

(3)   Tamaru, Y.; Hojo, M.; Higashimura, H.; Yoshida, Z. *J. Am. Chem. Soc.* **1988**, *110*, 3994.

(4)   Hong, S.; Tian, S.; Metz, M. V.; Marks, T. J. *J. Am. Chem. Soc.* **2003**, *125*, 14768.

(5)   Bender, C. F.; Widenhoefer, R. A. *J. Am. Chem. Soc.* **2005**, *127*, 1070.

(6)   (a) Kondo, T.; Okada, T.; Mitsudo, T. A. *J. Am. Chem. Soc.* **2002**, *124*, 186. (b) Gribkov, D. V.; Hultzsch, K. C.; Hampel, F. *J. Am. Chem. Soc.* **2006**, *128*, 3748.

(7)   Black, D. S. C.; Doyle, J. E. *Austr. J. Chem.* **1978**, *31*, 2247.

(8)   Hultzsch, K. C.; Hampel, F.; Wagner, T. *Organometallics* **2004**, *23*, 2601.

(9)   (a) Brown, K. J.; Berry, M. S.; Murdoch, J. R. *J. Org. Chem.* **1985**, *50*, 4345. (b) NMR data: Horrillo Martínez, P., Ph. D. dissertation, Institut für Organische Chemie, Friedrich-Alexander Universität Erlangen-Nürnberg, 2008.

(10)   Nanchen, S.; Pfaltz, A. *Helv. Chim. Acta* **2006**, *89*, 1559.

(11)   (a) Van Veldhuizen, J. J.; Garber, S. B.; Kingsbury, J. S.; Hoveyda, A. H. *J. Am. Chem. Soc.* **2002**, *124*, 4954. (b) VanVeldhuizen, J. J.; Gillingham, D. G.; Garber, S. B.; Kataoka, O.; Hoveyda, A. H. *J. Am. Chem. Soc.* **2003**, *125*, 12502.

(12)   See Supporting Information for extraction procedure: Denmark, S. E.; Nakajima, N.; Stiff, C. M.; Nicaise, O. J. C.; Kranz, M. *Adv. Synth. Catal.* **2008**, *350,* 1023.

(13)   (a) Norcross, N. R.; Melbardis, J. P.; Solera, M. F.; Sephton, M. A.; Kilner, C.; Zakharov, L. N.; Astles, P. C.; Warriner, S. L.; Blakemore, P. R. *J. Org. Chem.* **2008**, *73*, 7939. (b) Golebiewskl, W. M.; Spenser, I. D. *Can. J. Chem.* **1985**, *63*, 716.

(14)   Tessier-Youngs, C.; Beachley Jr., O. T. *Inorg. Syn.* **1986**, *24*, 95.

(15)   Clegg, W.; Conway, B.; Kennedy, A. R.; Klett, J.; Mulvey, R. E.; Russo, L. *Eur. J. Inorg. Chem.* **2011**, 721.

(16)   (a) Bruker **2010**. APEX2 software for chemical crystallography, Bruker AXS, Inc., Madison, WI, USA. (b) Sheldrick, G. M. Acta Cryst. **2008**, *A64*, 112.

(17)   Farrugia, L. J. *J. Appl. Cryst.* **1997**, *30*, 565.

(18)   (a) Ward, D. E.; Rhee, C. K. *Tetrahedron Lett.* **1991**, *32*, 7165. (b) Bergman, J.; Brynolf, A. *Tetrahedron* **1990**, *46*, 1295.

(19)   Cabrita, E. J.; Berger, S. *Magn. Reson. Chem.* **2001**, *39*, S142.

(20)   Diameter calculated by hard sphere increments: (a) Ben-Amotz, D.; Herschbach, D. R. *J. Phys. Chem.* **1990**, *94*, 1038. (b) Ben-Amotz, D.; Willis, K. G. *J. Phys. Chem.* **1993**, *97*, 7736.

(21)   (a) Schober, K.; Hartmann, E.; Zhang, H.; Gschwind, R. M. *Angew. Chem. Int. Ed.* **2010**, *49*, 2794. (b) Schober, K.; Zhang, H.; Gschwind, R. M. *J. Am. Chem. Soc.* **2008**, *130*, 12310.
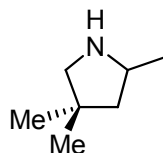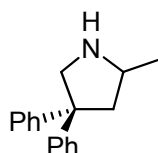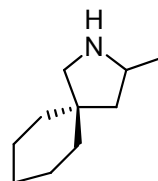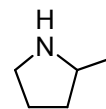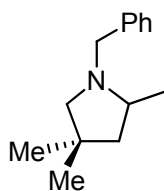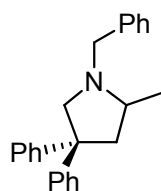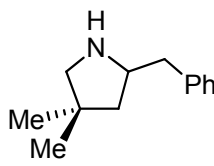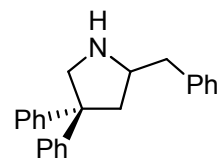
5

Appendix

5.1 Numbering of Substrates

Intramolecular Hydroamination Substrates
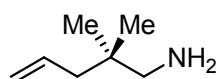
S1
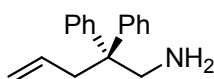
S2
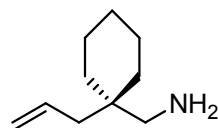
S3
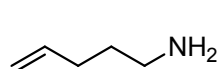
S4
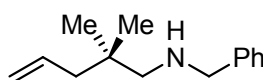
S5
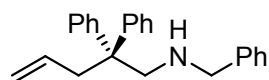
S6
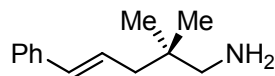
S7
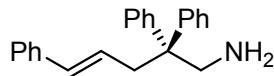
S8

Intramolecular Hydroamination Products

P1

P2

P3

P4

P5

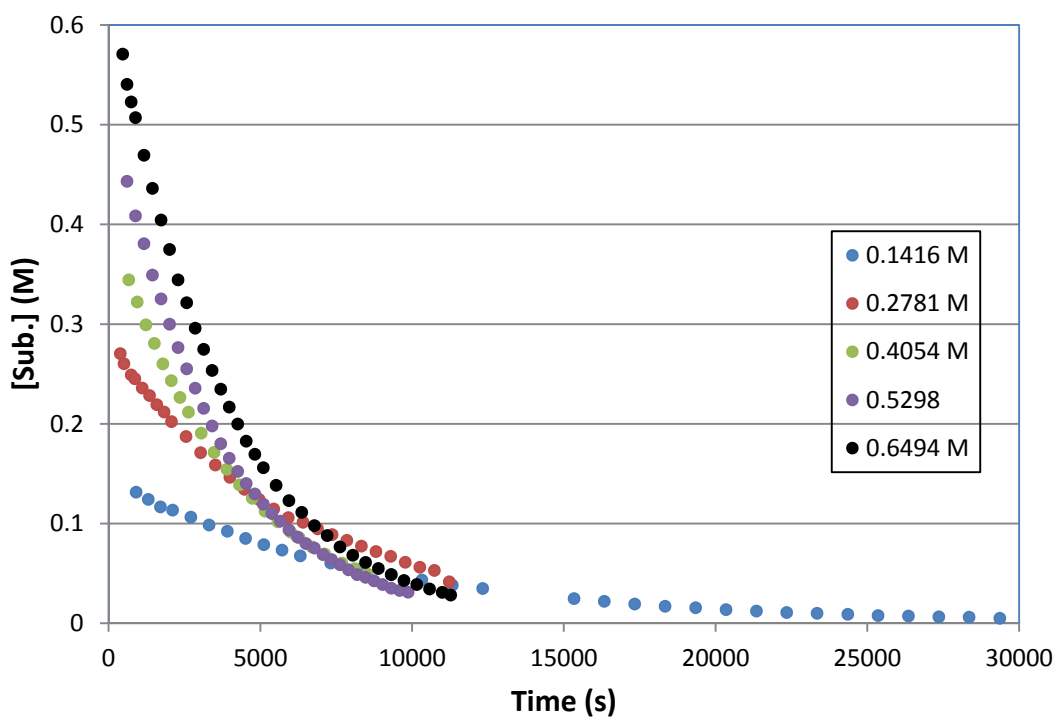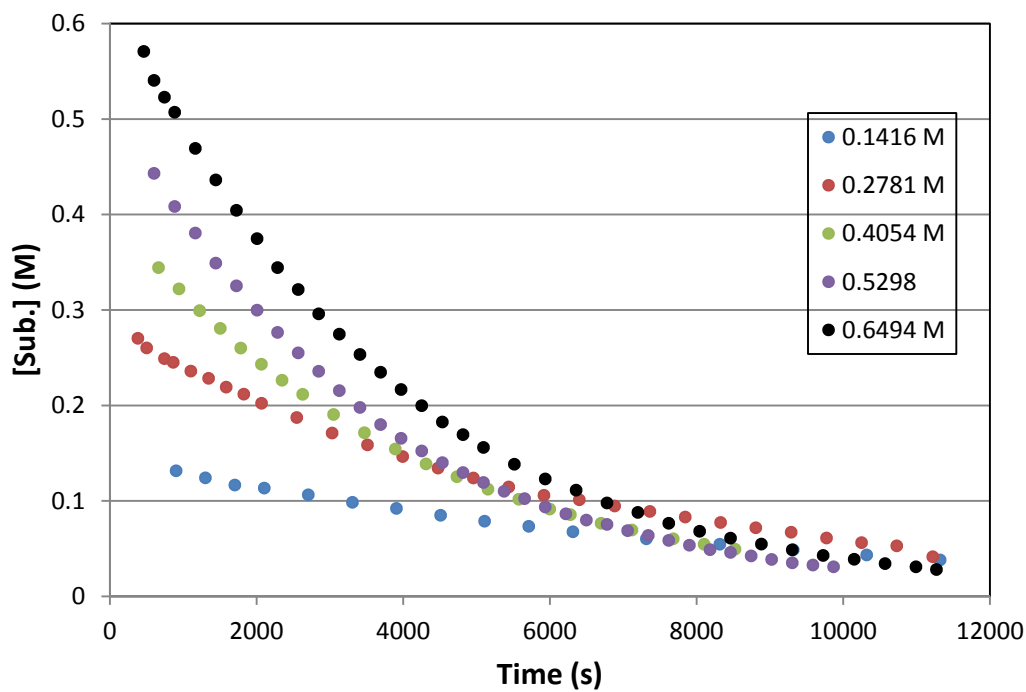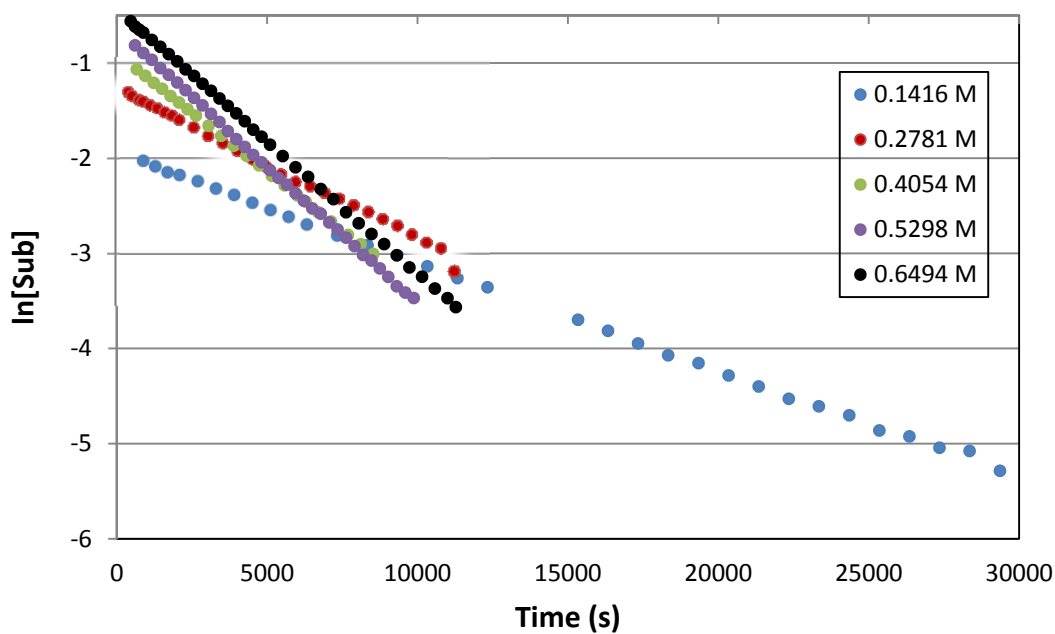**P6**

P7

P8

5.2 Charts from Kinetic Study

Figure A-1. Zero order plot showing the consumption of **S3** in the hydroamination/cyclization with 2.5 mol% (*R*)-**64** and 0.5 eq. LiCH$_2$TMS at various concentrations of **S3**.
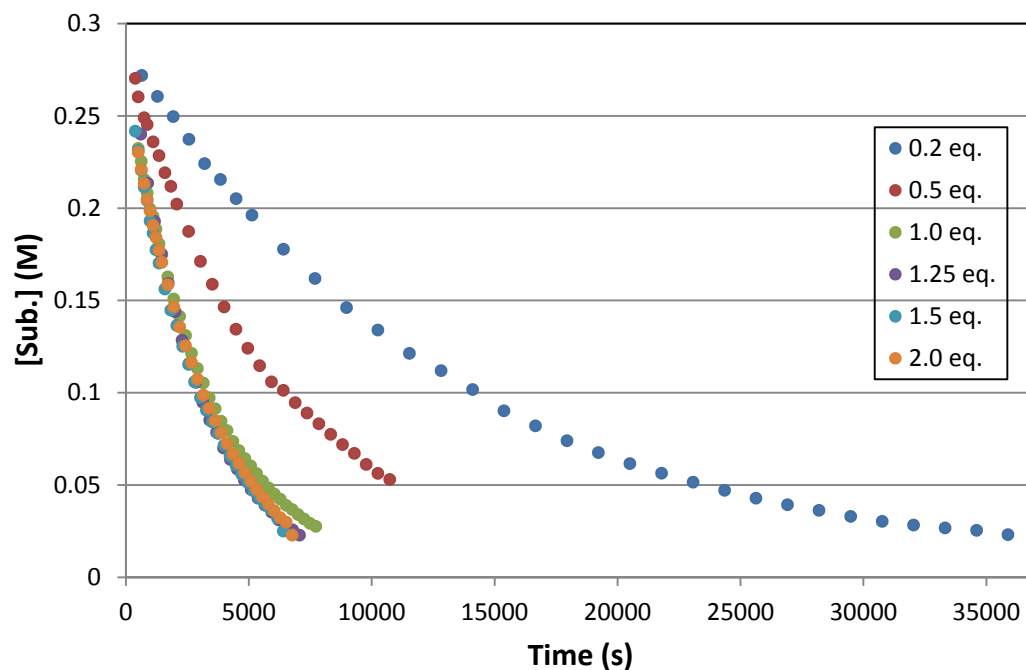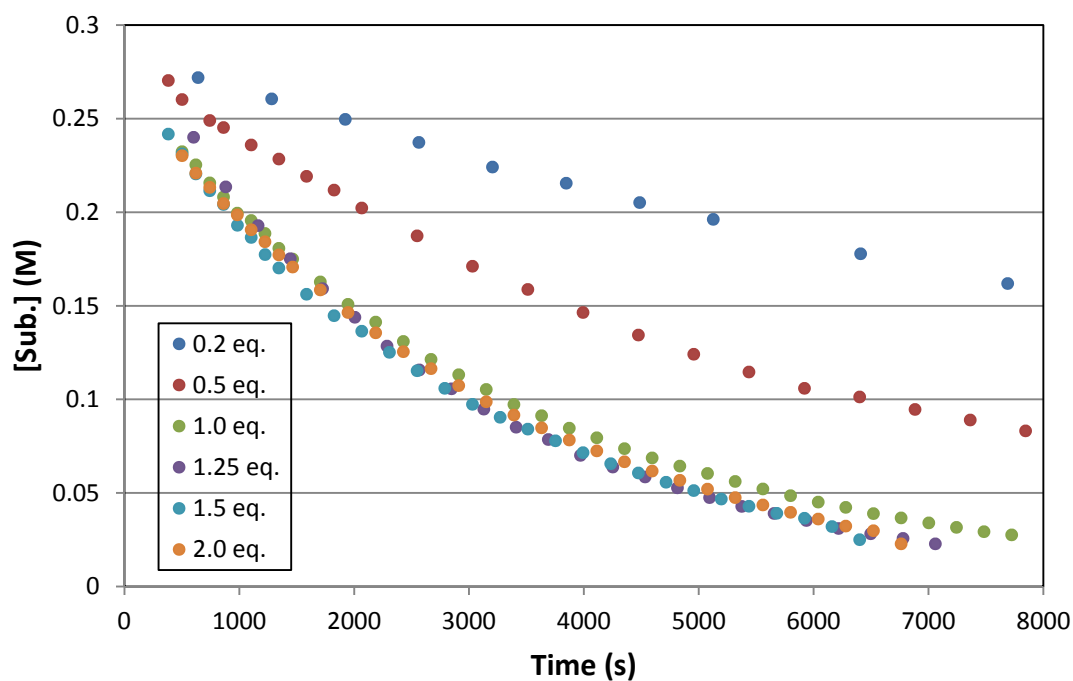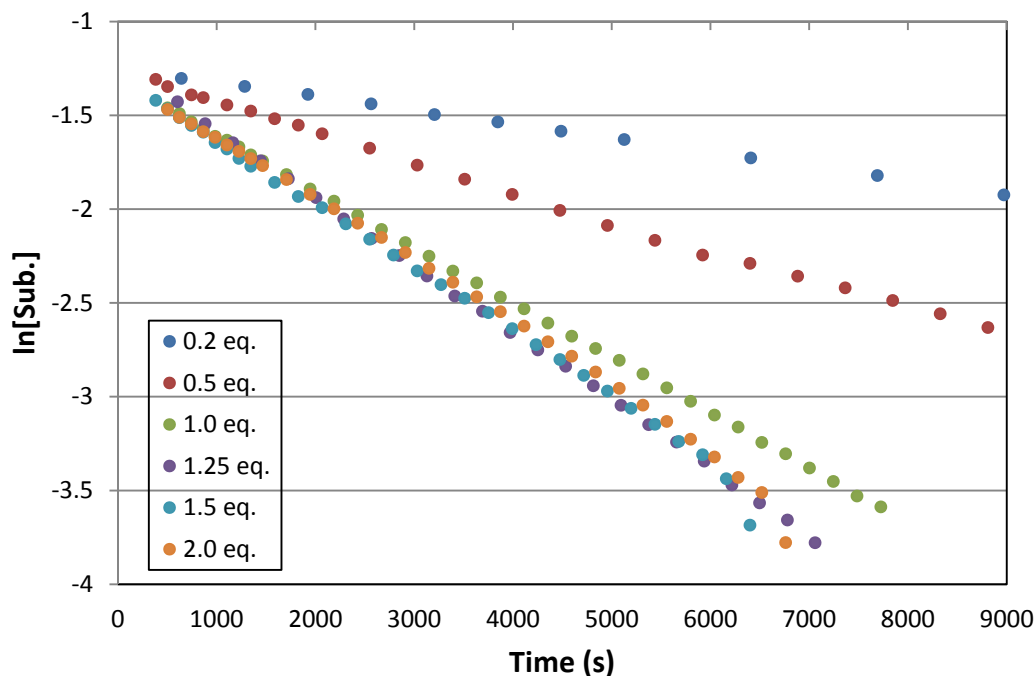
Figure A-2. Zero order plot showing the consumption of **S3** in the hydroamination/cyclization with 2.5 mol% (*R*)-**64** and 0.5 eq. LiCH$_2$TMS at various concentrations of **S3**.

Figure A-3. First order plot showing the consumption of **S3** in the hydroamination/cyclization with 2.5 mol% (*R*)-**64** and 0.5 eq. LiCH$_2$TMS at various concentrations of **S3**.

Figure A-4. Zero order plot showing the consumption of **S3** in the hydroamination/cyclization with 2.5 mol% (*R*)-**64**, 0.28 M **S3** and varied amounts of LiCH$_2$TMS.
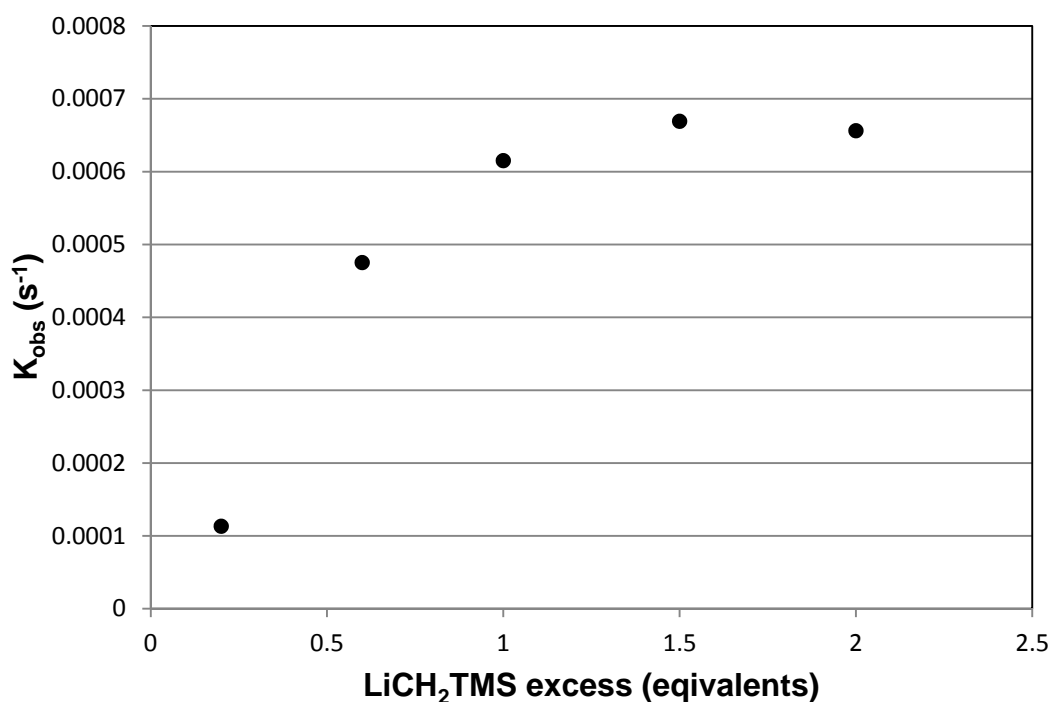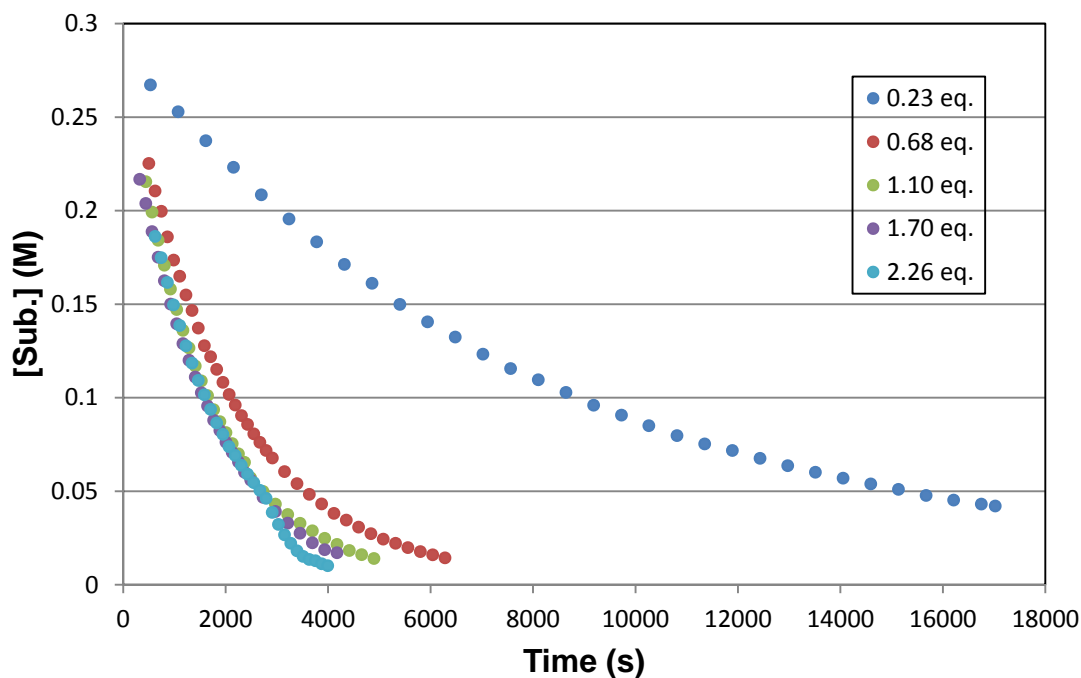

Figure A-5. Zero order plot showing the consumption of **S3** in the hydroamination/cyclization with 2.5 mol% (*R*)-**64**, 0.28 M **S3** and varied amounts of LiCH$_2$TMS.
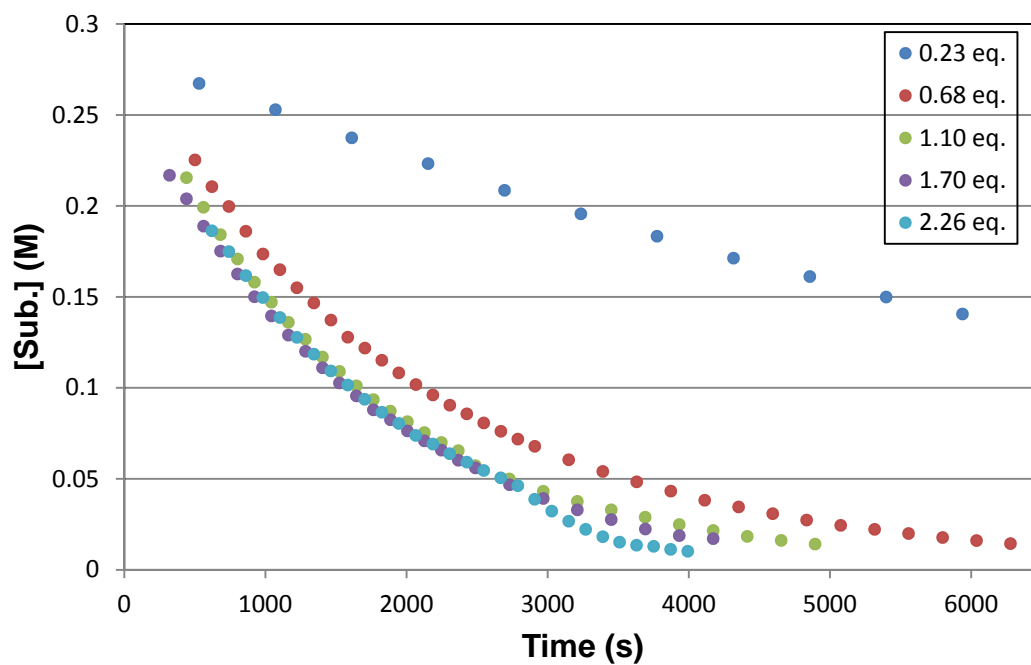
Figure A-6. First order plot showing the consumption of **S3** in the hydroamination/cyclization with 2.5 mol% (*R*)-**64**, 0.28 M **S3** and varied amounts of LiCH$_2$TMS.

Figure A-7. Plot of pseudo first order rate constants versus eq. excess LiCH$_2$TMS in the intramolecular hydroamination/cyclization of **S3** with 5.0 mol% (*R*)-**64** and 0.28 M **S3**.

Figure A-8. Zero order plot showing the consumption of **S3** in the hydroamination/cyclization with 5.0 mol% (*R*)-**64**, 0.28 M **S3** and varied amounts of LiCH$_2$TMS.
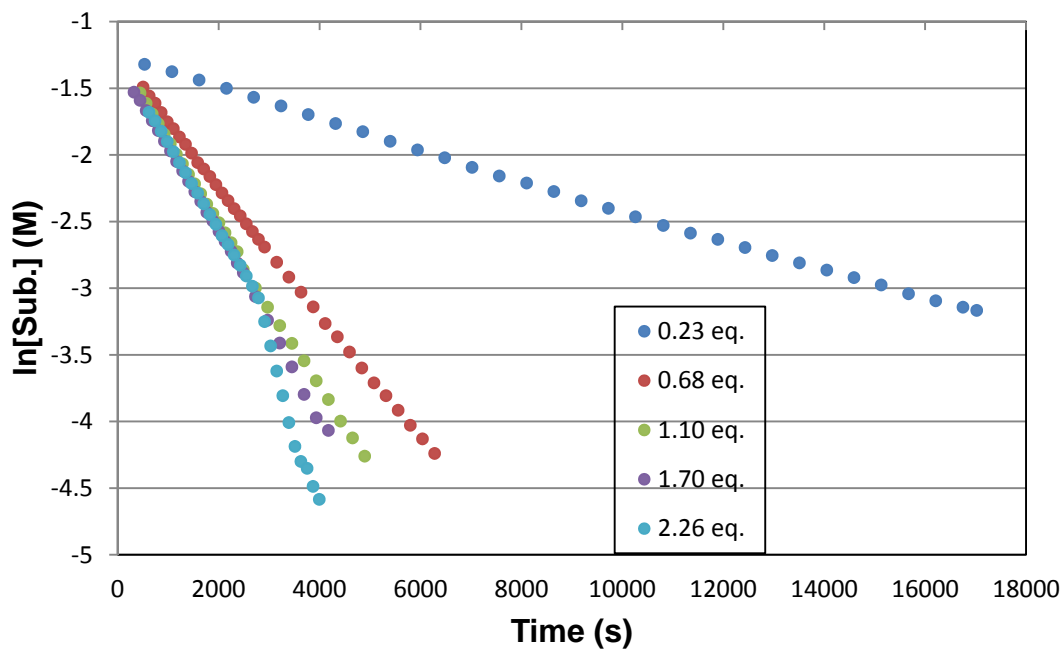

Figure A-9. Zero order plot showing the consumption of **S3** in the hydroamination/cyclization with 5.0 mol% (*R*)-**64**, 0.28 M **S3** and varied amounts of LiCH$_2$TMS.
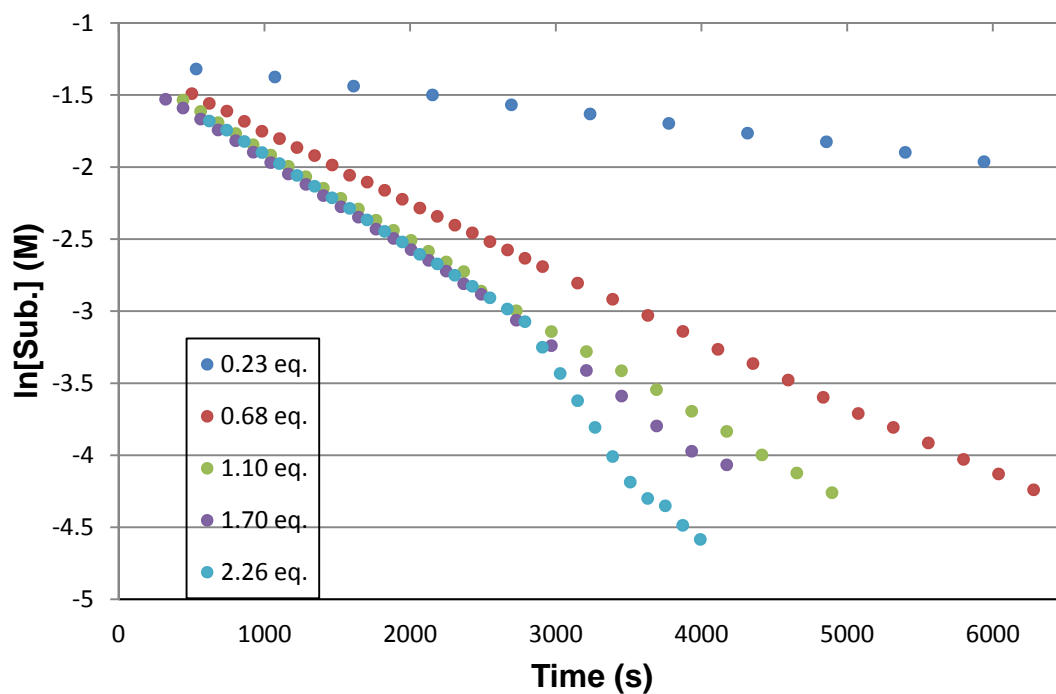
Figure A-10. First order plot showing the consumption of **S3** in the hydroamination/cyclization with 5.0 mol% (*R*)-**64**, 0.28 M **S3** and varied amounts of LiCH$_2$TMS.

Figure A-11. First order plot showing the consumption of **S3** in the hydroamination/cyclization with 5.0 mol% (*R*)-**64**, 0.28 M **S3** and varied amounts of LiCH$_2$TMS.
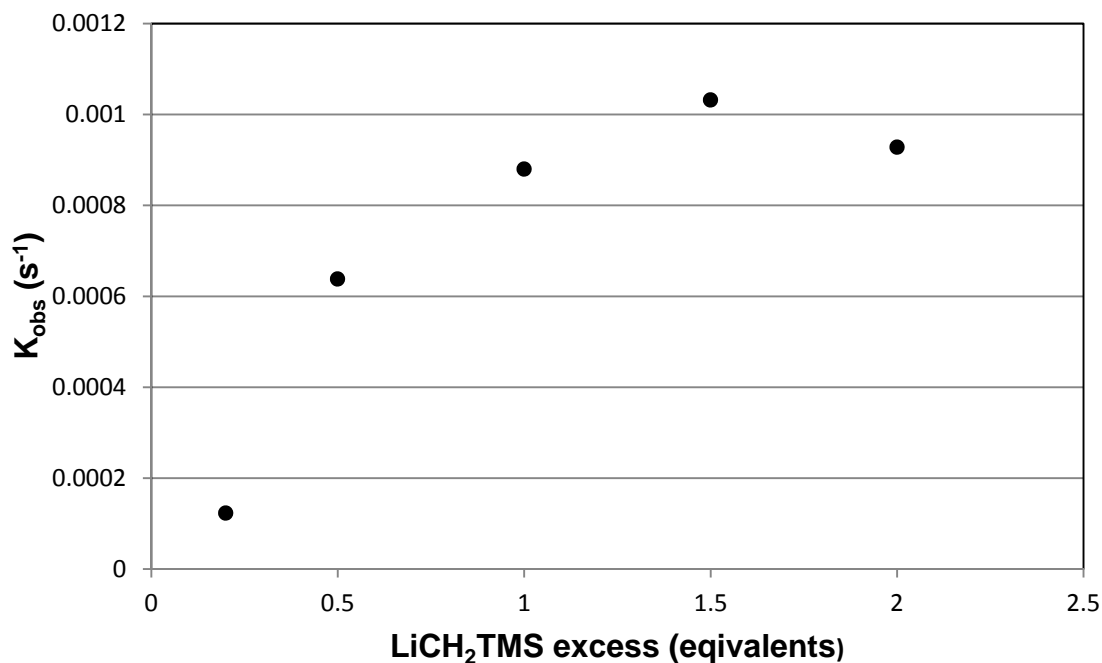
Figure A-12. Plot of pseudo first order rate constants versus equivalents excess LiCH$_2$TMS in the intramolecular hydroamination/cyclization of **S3** with 7.5 mol% (*R*)-**64** and 0.28 M **S3**.
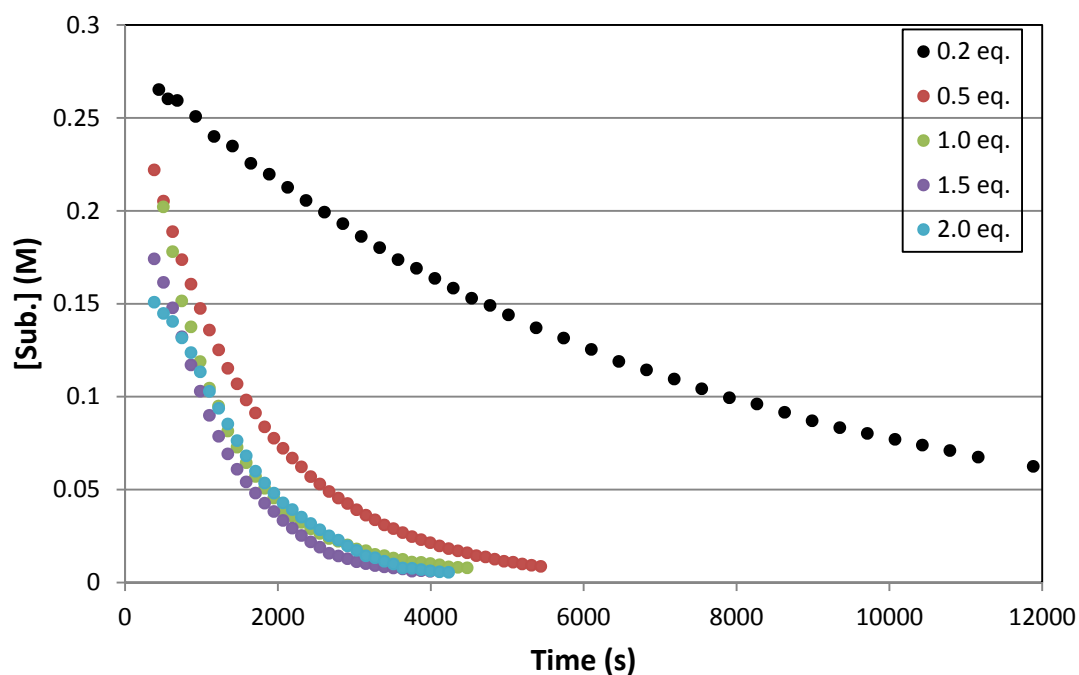

Figure A-13. Zero order plot showing the consumption of **S3** in the hydroamination/cyclization with 7.5 mol% (*R*)-**64**, 0.28 M **S3** and varied amounts of LiCH$_2$TMS.
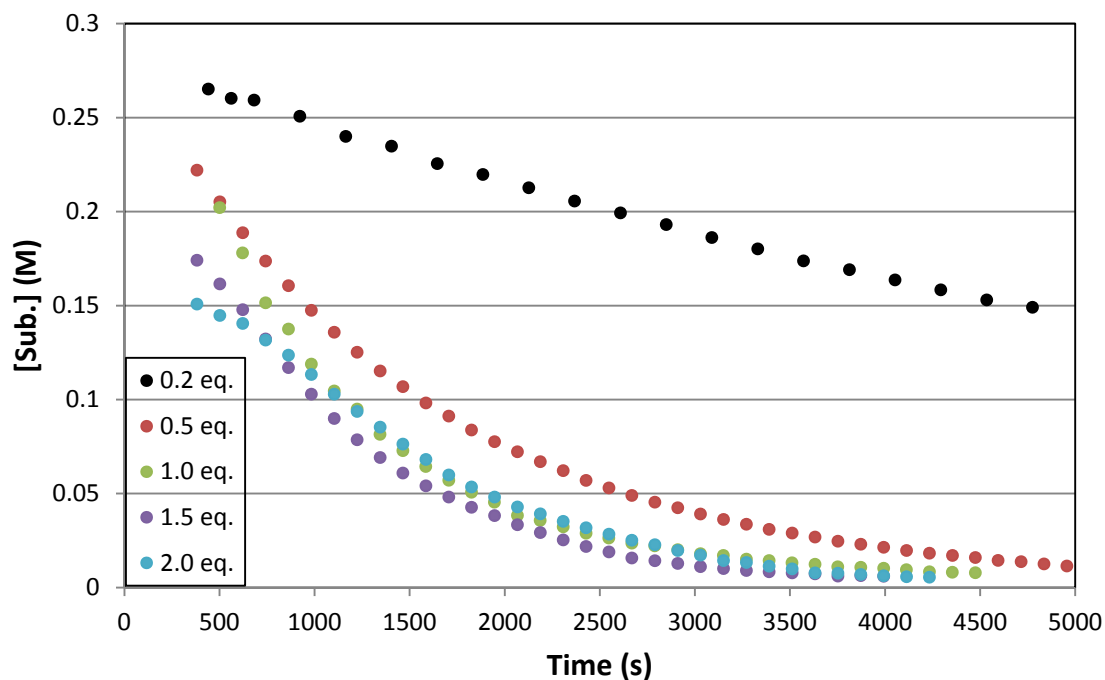
Figure A-14. Zero order plot showing the consumption of **S3** in the hydroamination/cyclization with 7.5 mol% (*R*)-**64**, 0.28 M substrate and varied amounts of LiCH$_2$TMS.

Figure A-15. First order plot showing the consumption of **S3** in the hydroamination/cyclization with 7.5 mol% (*R*)-**64**, 0.28 M substrate and varied amounts of LiCH$_2$TMS.
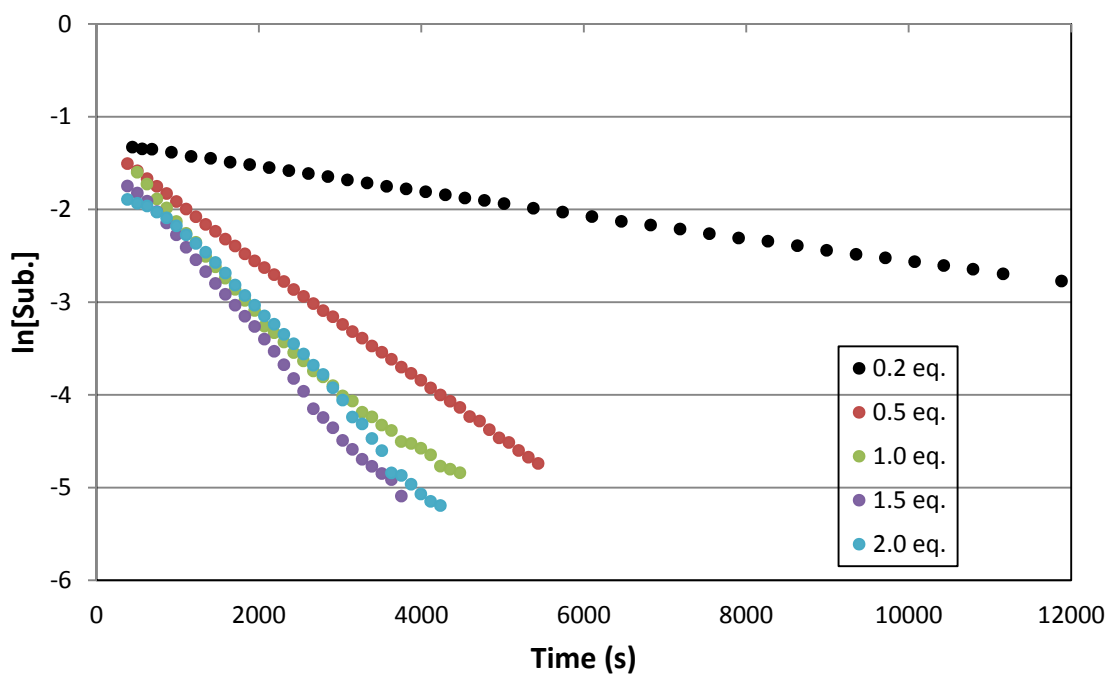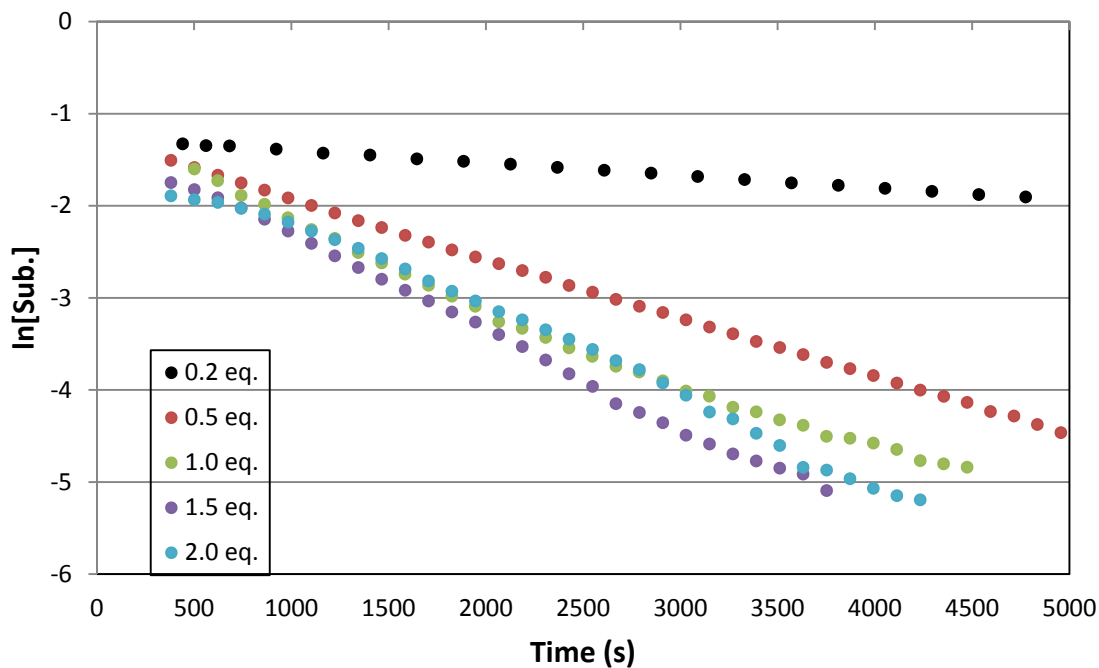
Figure A-16. First order plot showing the consumption of **S3** in the hydroamination/cyclization with 7.5 mol% (*R*)-**64**, 0.28 M substrate and varied amounts of LiCH$_2$TMS.
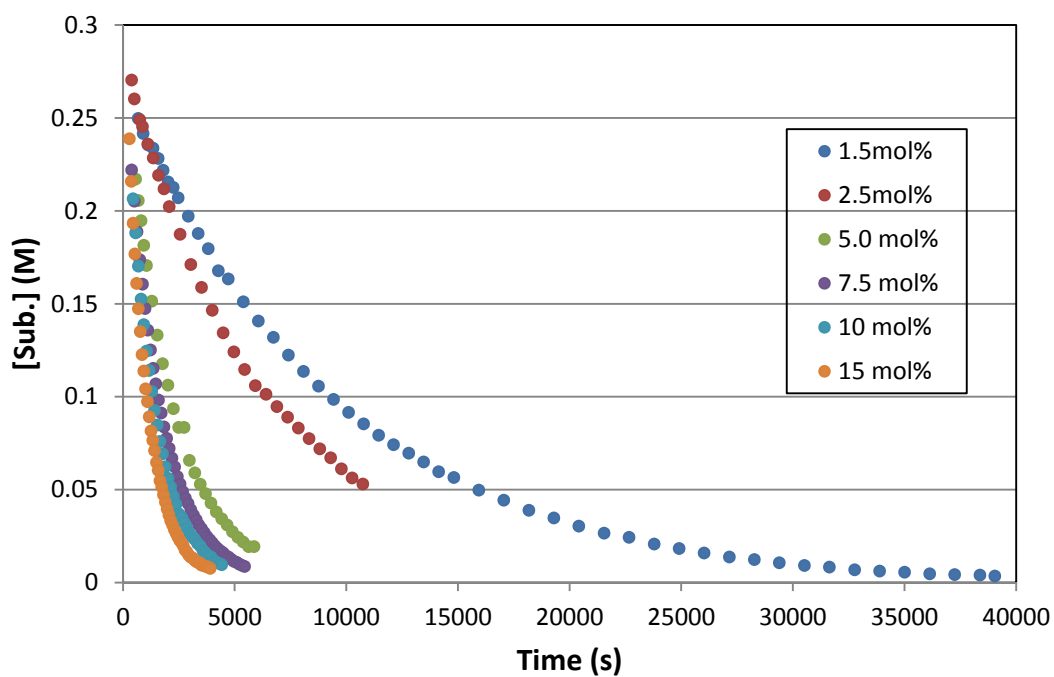

Figure A-17. Zero order plot showing the consumption of **S3** in the hydroamination/ cyclization with (*R*)-**64** and 0.5 eq. LiCH$_2$TMS, 0.28 M **S3** at various catalyst loadings.

Figure A-18. Zero order plot showing the consumption of **S3** in the hydroamination/ cyclization with (*R*)-**64** and 0.5 eq. LiCH$_2$TMS, 0.28 M substrate at various catalyst loadings.

Figure A-19. First order plot showing the consumption of **S3** in the hydroamination/ cyclization with (*R*)-**64** and 0.5 eq. LiCH$_2$TMS, 0.28 M substrate at various catalyst loadings.

Figure A-20. Zero order plot showing the consumption of **S3** in the hydroamination/ cyclization with (*R*)-**64** and 1.0 eq. LiCH$_2$TMS, 0.28 M substrate at various catalyst loadings.

Figure A-21. Zero order plot showing the consumption of **S3** in the hydroamination/ cyclization with (*R*)-**64** and 1.0 eq. LiCH$_2$TMS, 0.28 M substrate at various catalyst loadings.
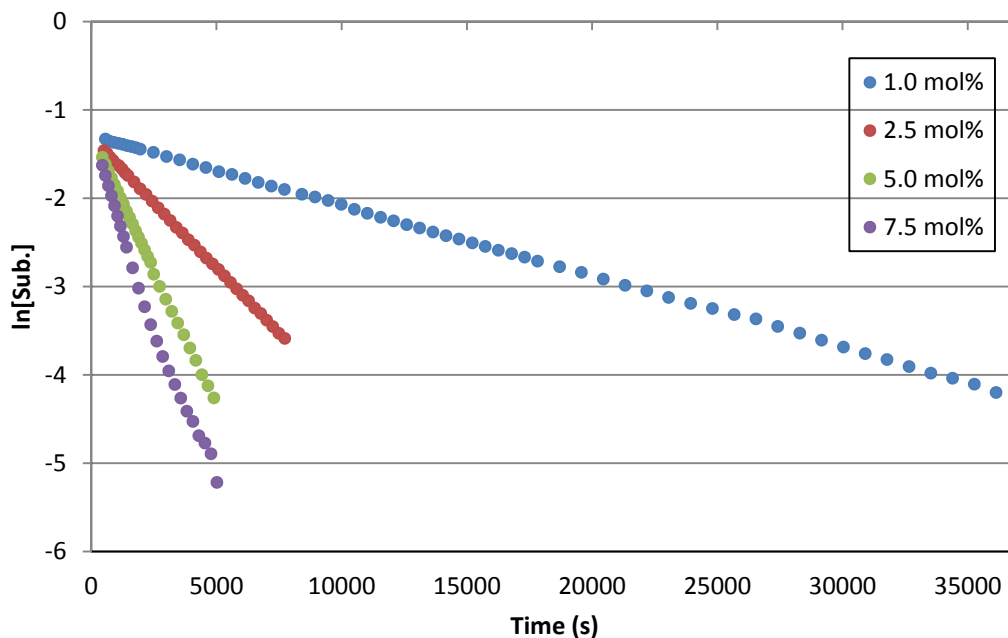
Figure A-22. First order plot showing the consumption of **S3** in the hydroamination/ cyclization with (*R*)-**64** and 1.0 eq. LiCH$_2$TMS, 0.28 M **S3** at various catalyst loadings.
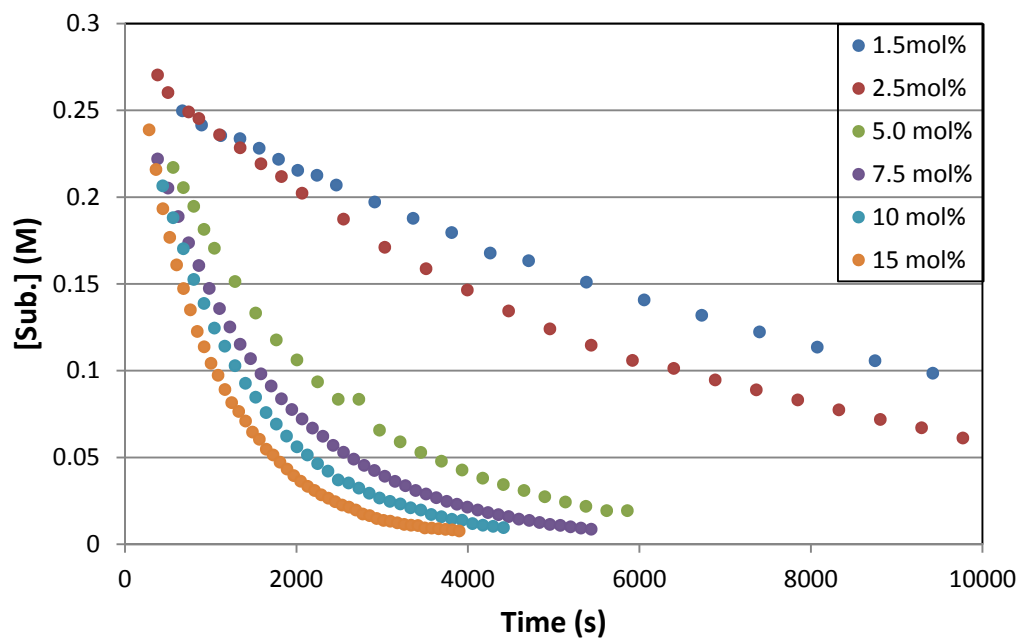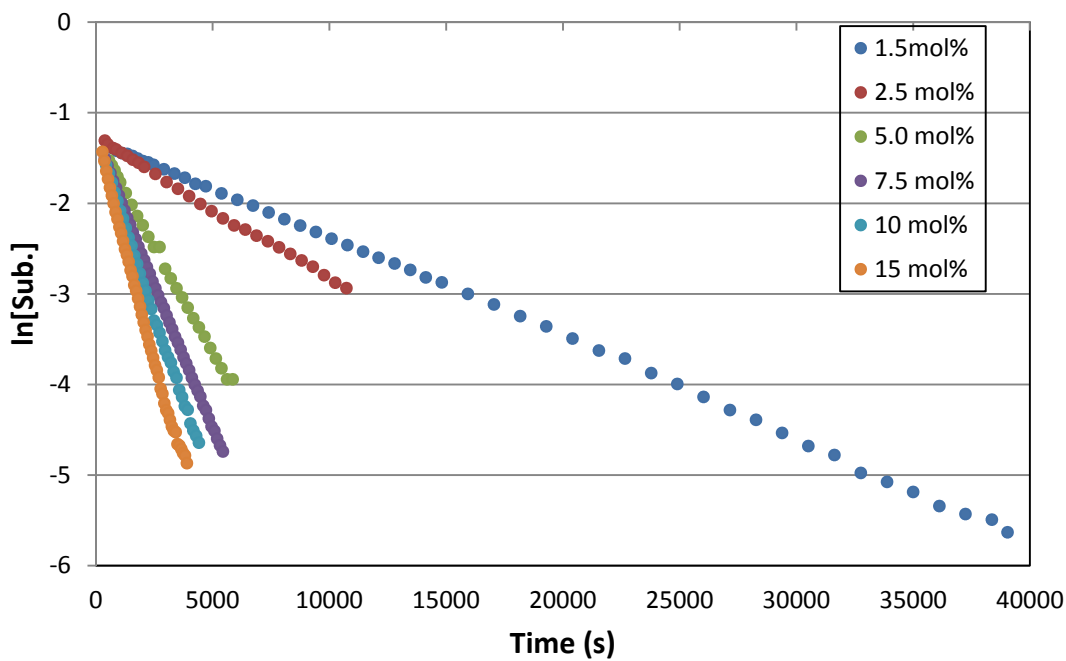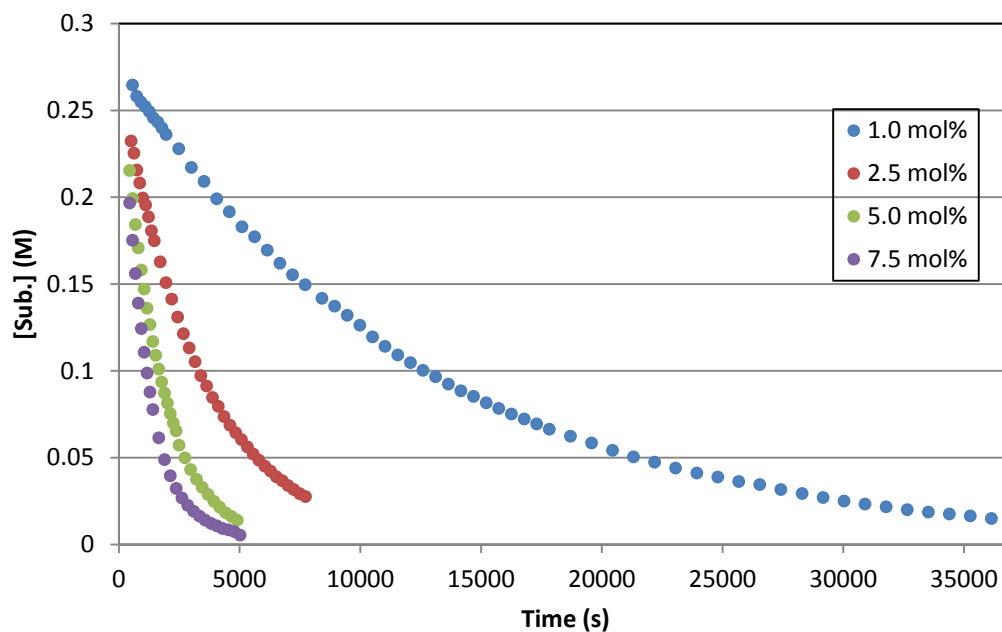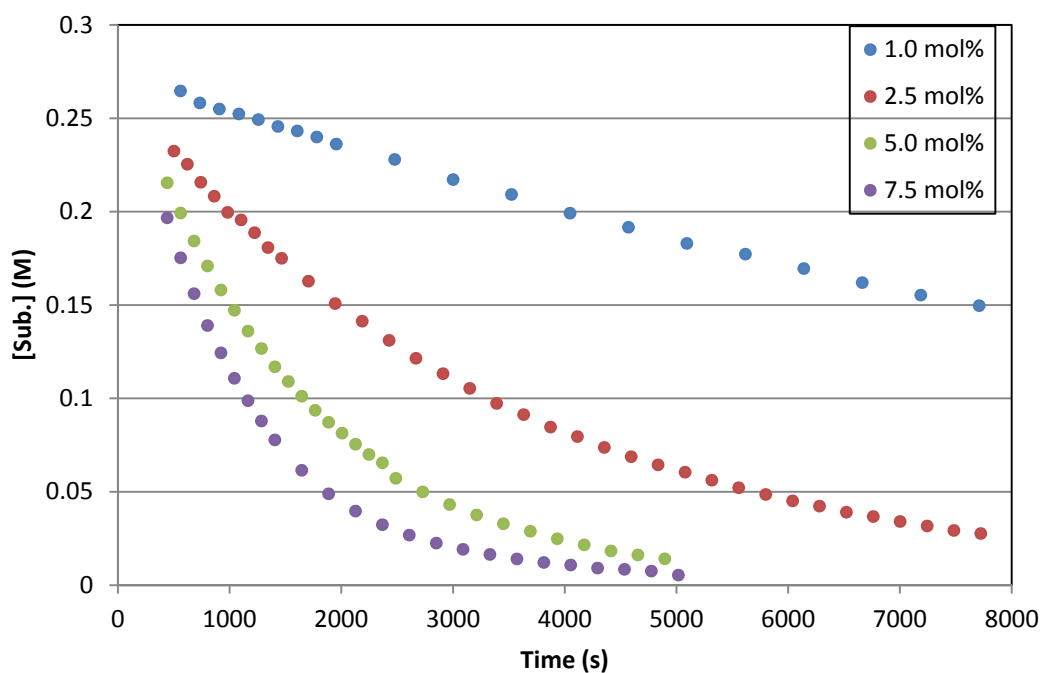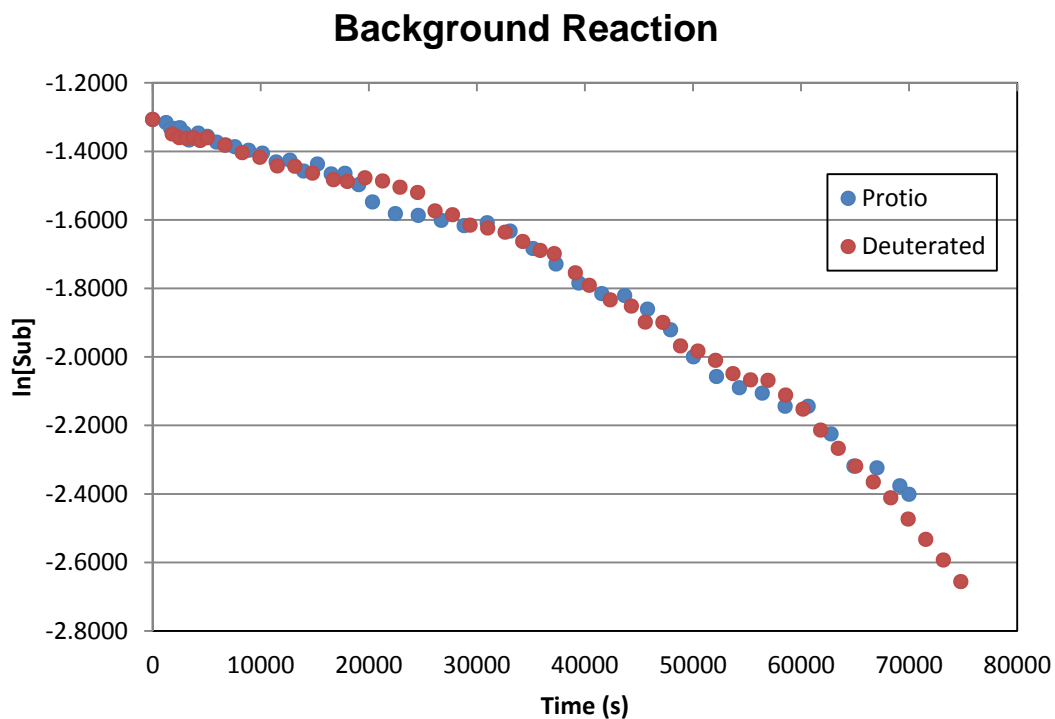

Figure A-23. First order plot showing the consumption of **S3** or **S3-*d$_2$*** in the hydroamination/ cyclization with 10.0 mol% LiCH$_2$TMS as a catalyst.
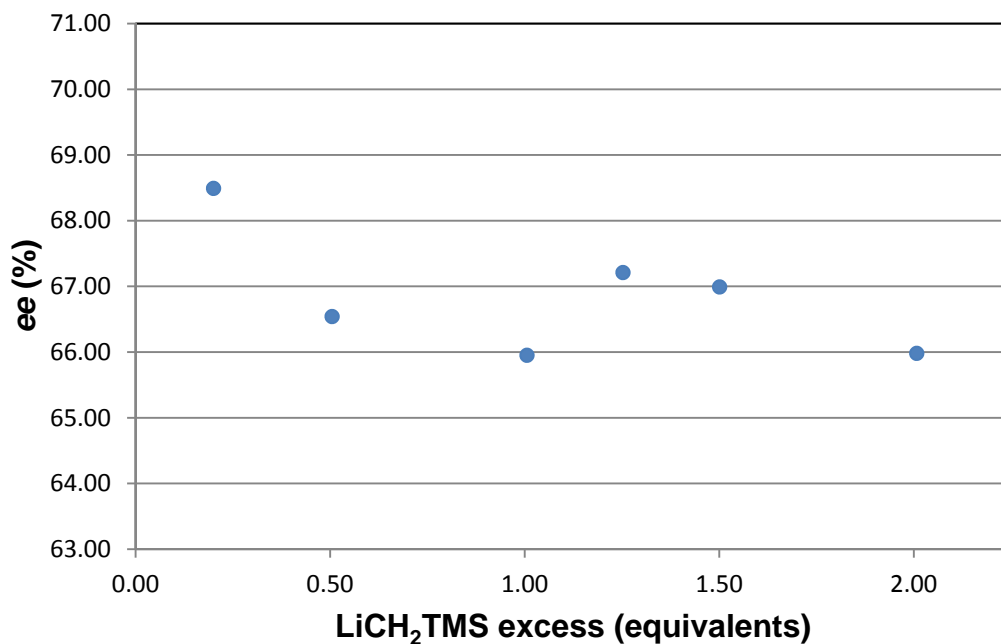
Figure A-24. Plot of *ee* (%) vs. LiCH$_2$TMS (X equiv. excess) for the hydroamination/ cyclization of **S3** (0.27-0.28 M) with (*R*)-**64** (2.5 mol%).
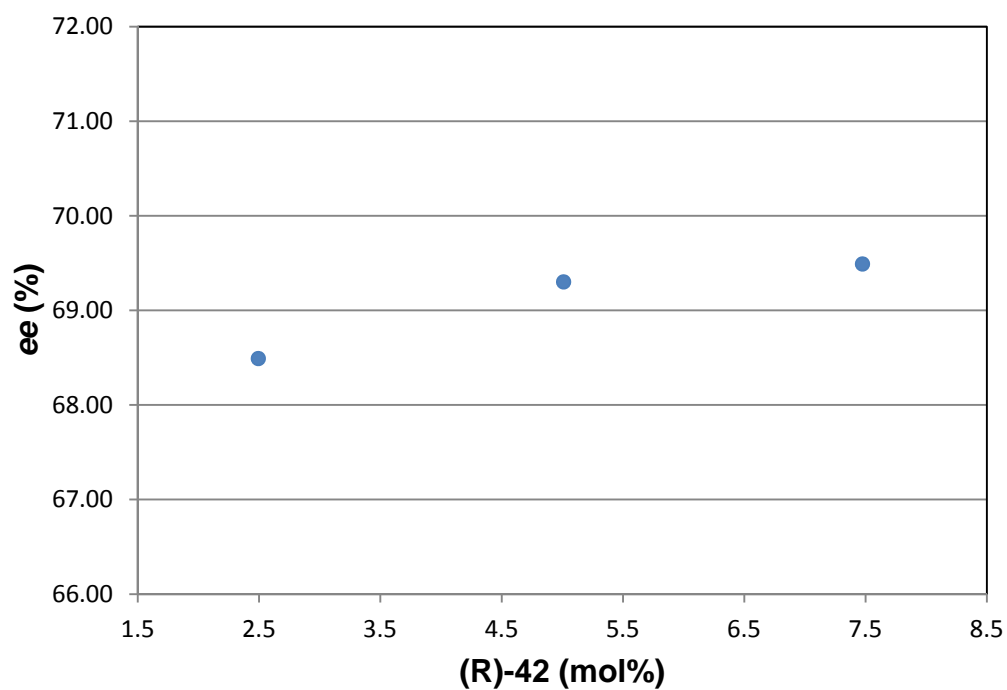
Figure A-25. Plot of *ee* (%) vs. (*R*)-**64** (X mol%) for the hydroamination/ cyclization of **S3** (0.27-0.28 M) with LiCH$_2$TMS (0.2 equiv. excess).
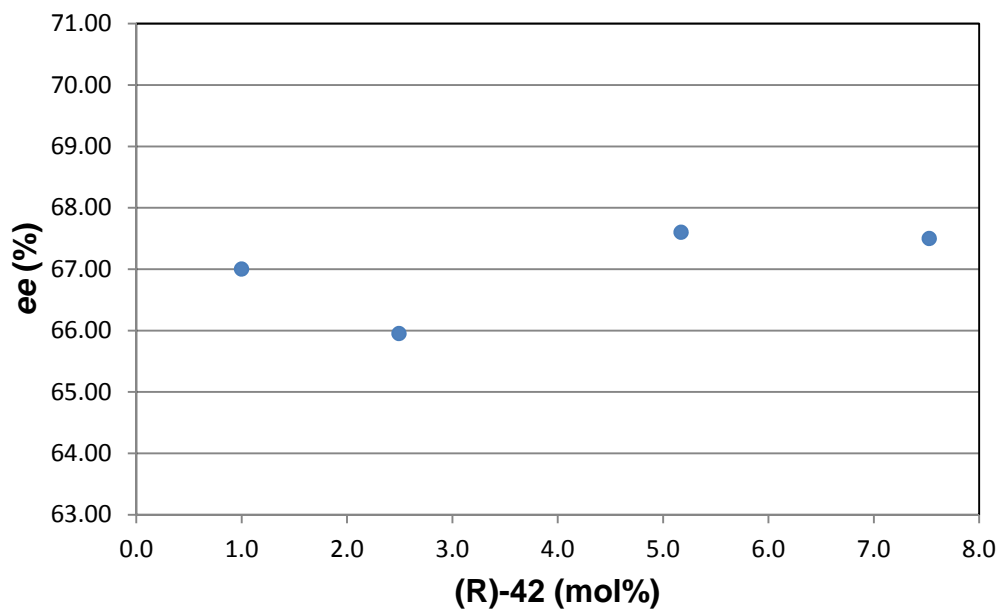
Figure A-26. Plot of *ee* (%) vs. (*R*)-**64** (X mol%) for the hydroamination/ cyclization of **S3** (0.27-0.28 M) with LiCH$_2$TMS (1.0 equiv. excess).
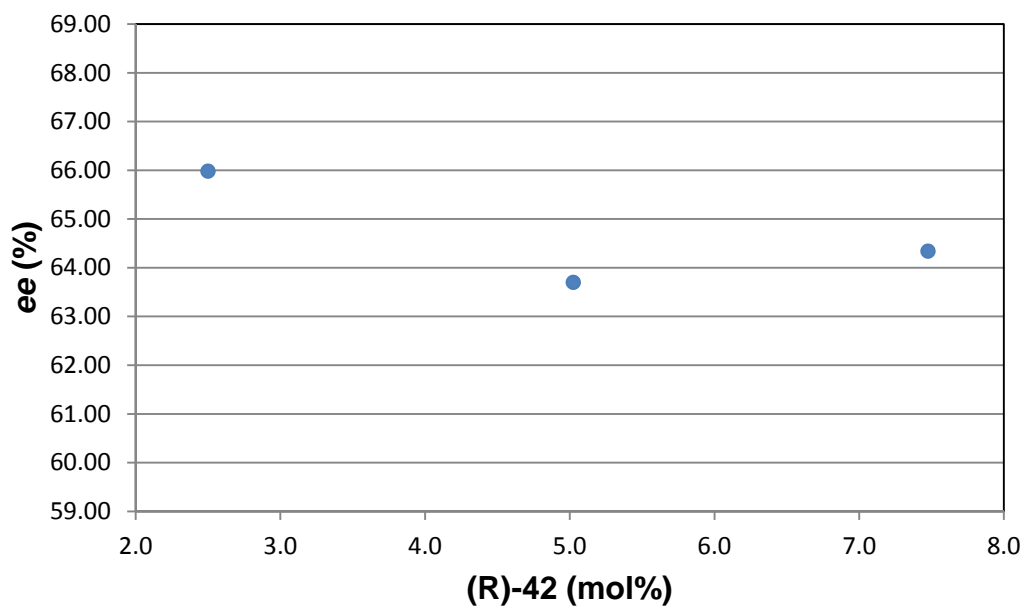
Figure A-27. Plot of *ee* (%) vs. (*R*)-**64** (X mol%) for the hydroamination/ cyclization of **S3** (0.27-0.28 M) with LiCH$_2$TMS (2.0 equiv. excess).

5.3 NMR Spectra
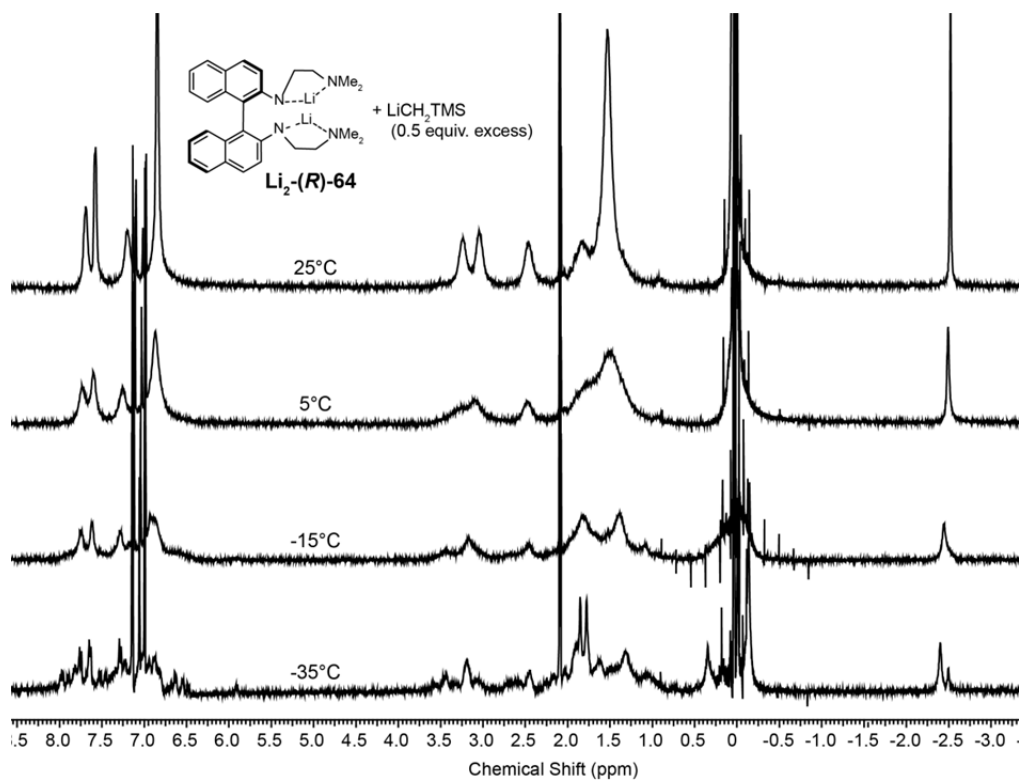
Figure A-28. VT-NMR (^{1}H) spectra of (*R*)-**64** and 0.5 equivalents of excess LiCH$_2$TMS.
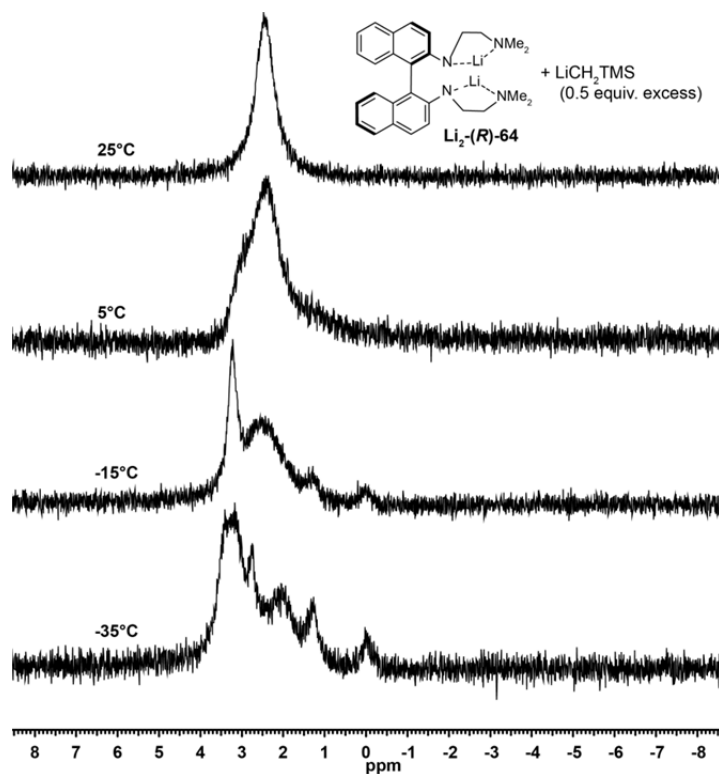
Figure A-29. VT-NMR (^{7}Li) spectra of (*R*)-**64** and 0.5 equivalents of excess LiCH$_2$TMS.
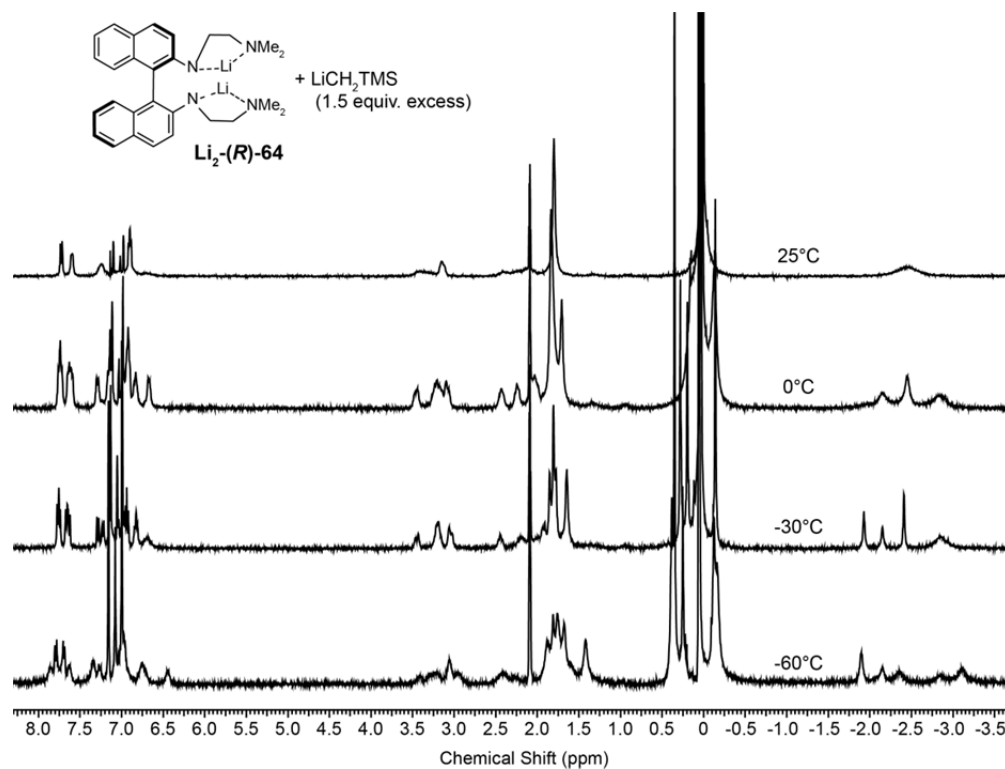
Figure A-30. VT-NMR (^{1}H) spectra of (*R*)-**64** and 1.5 equivalents of excess LiCH$_2$TMS.
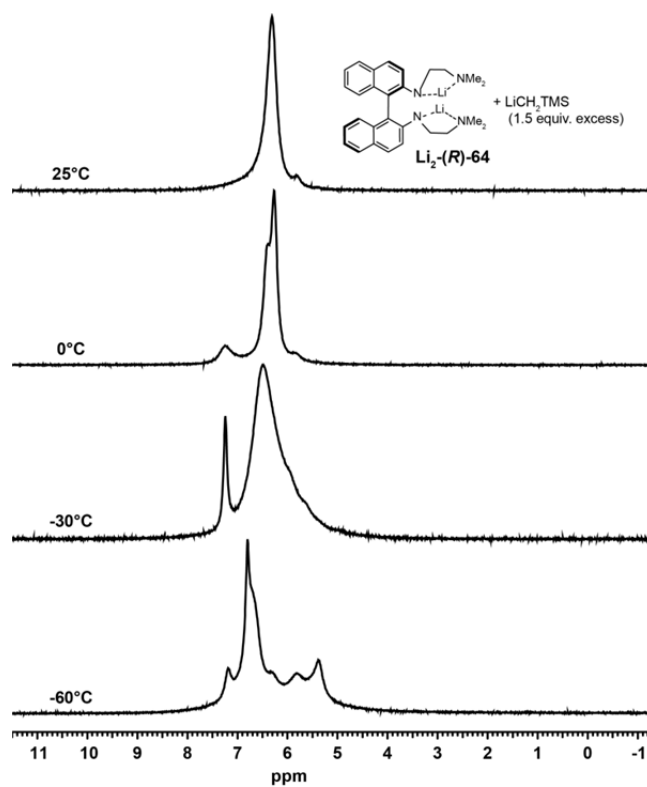
Figure A-31. VT-NMR (^{7}Li) spectra of (*R*)-**64** and 1.5 equivalents of excess LiCH$_2$TMS.
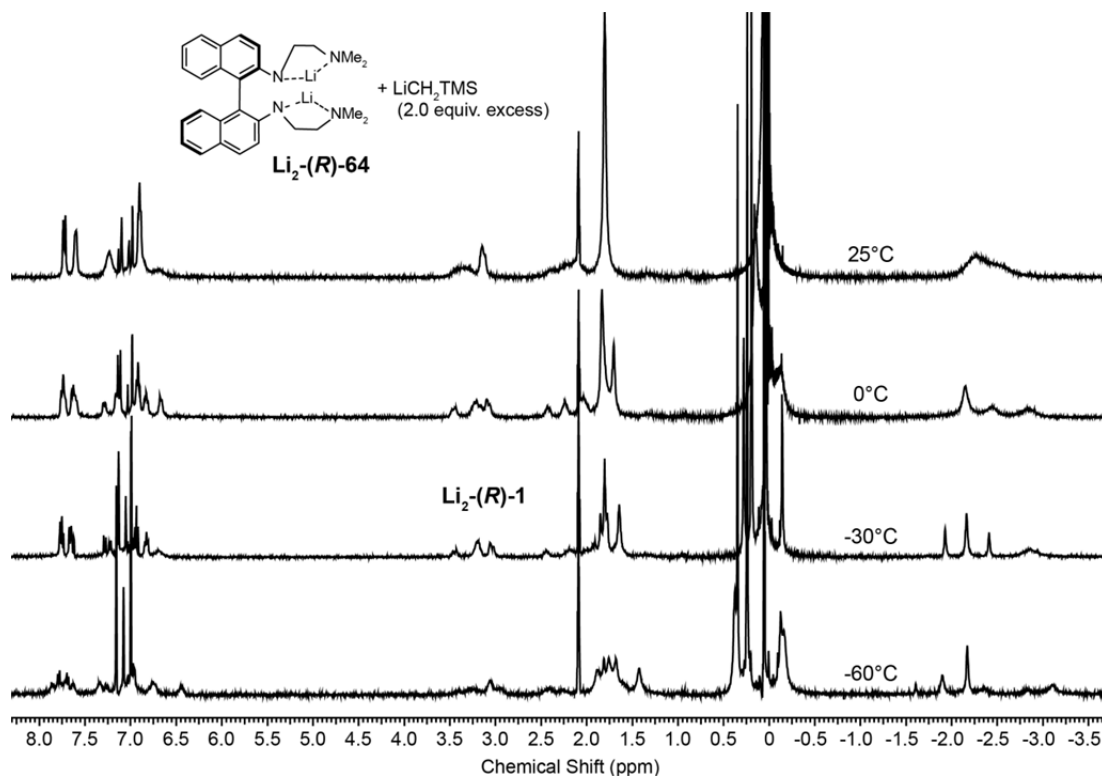
Figure A-32. VT-NMR (^{1}H) spectra of (*R*)-**64** and 2.0 equivalents of excess LiCH$_2$TMS.
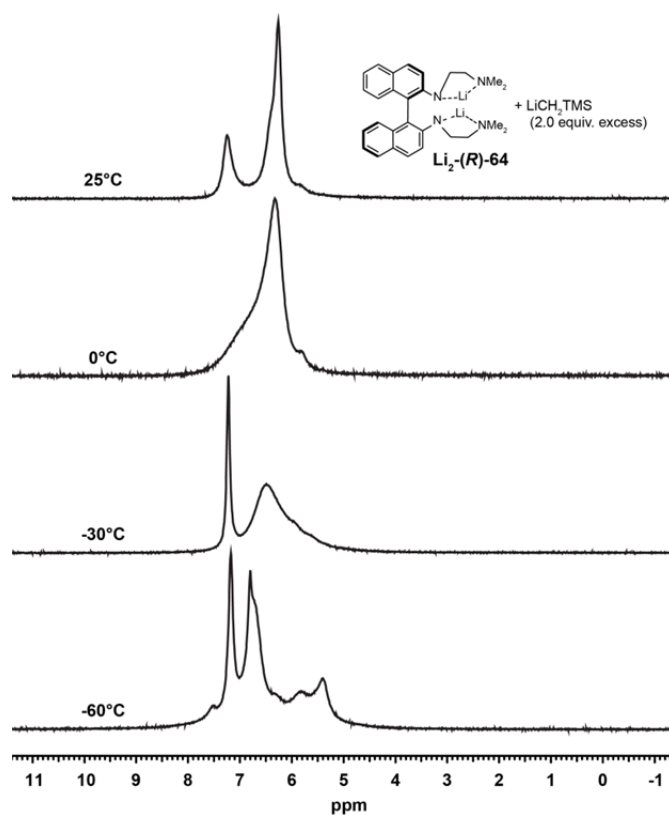
Figure A-33. VT-NMR (^{7}Li) spectra of (*R*)-**64** and 2.0 equivalents of excess LiCH$_2$TMS.
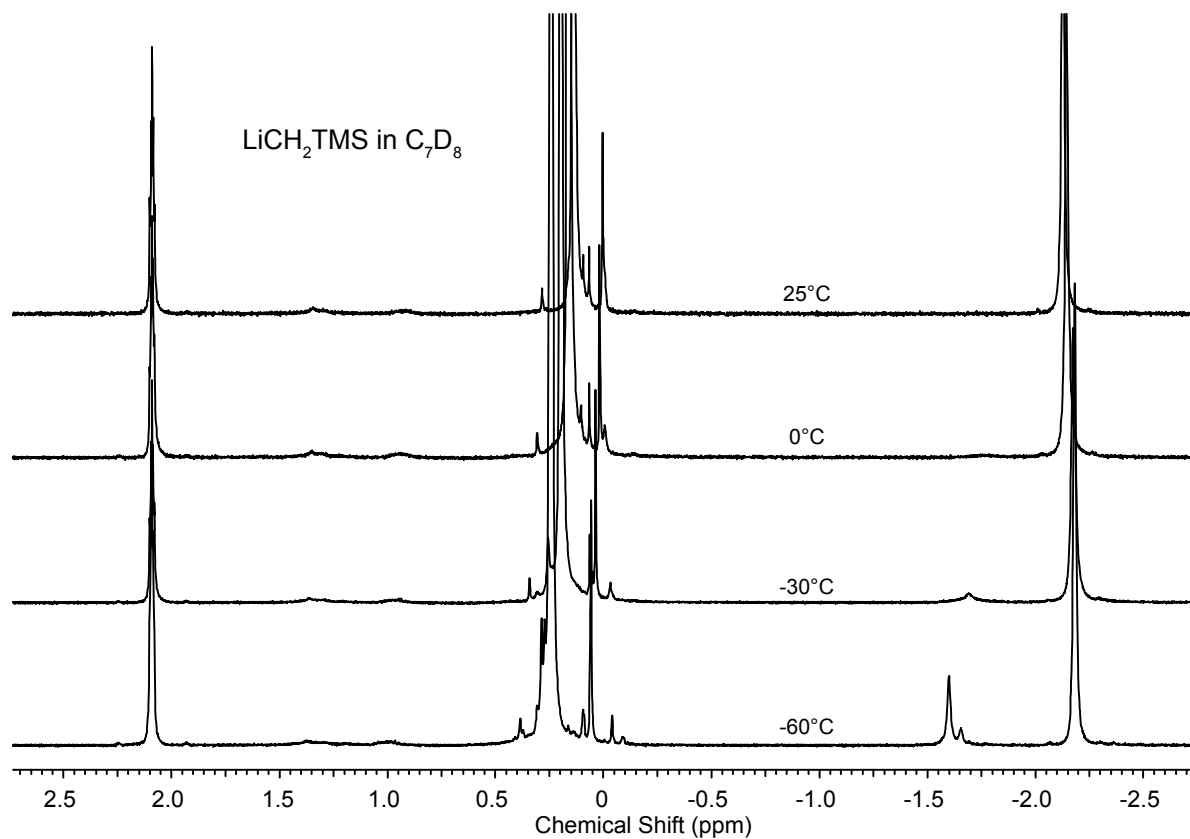
Figure A-34. VT-NMR (^{1}H) spectra of LiCH$_2$TMS in C$_7$D$_8$ with LiCl/MeOH-d_4 internal standard.
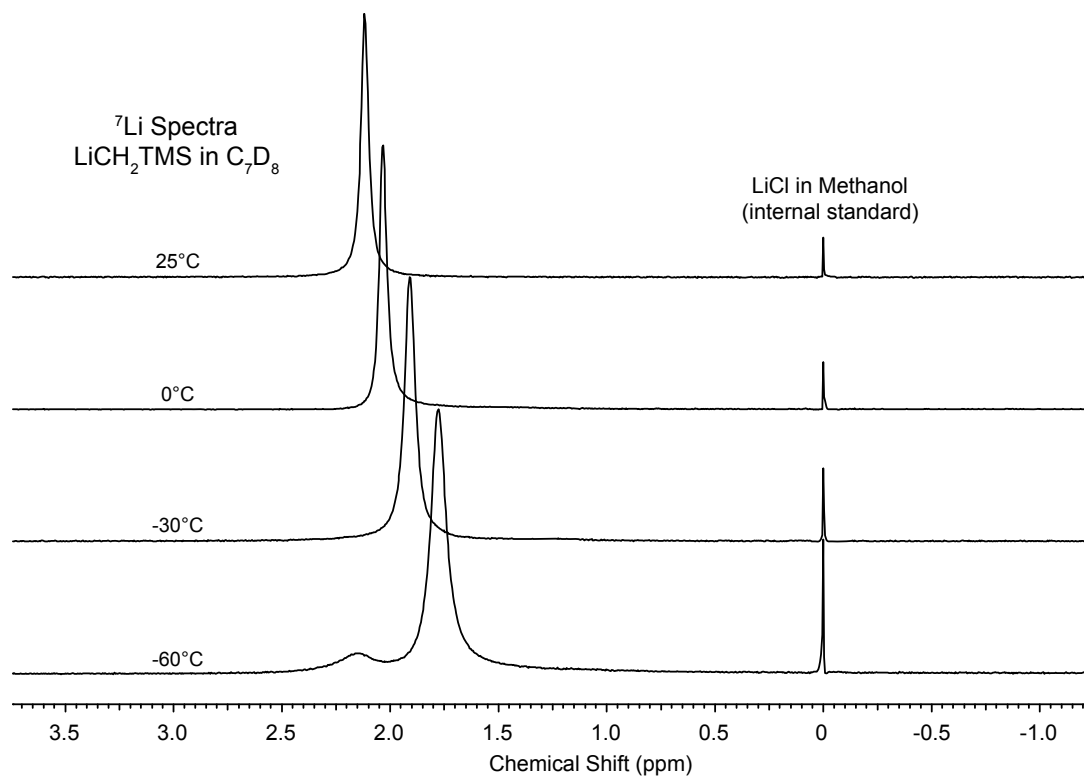
Figure A-35. VT-NMR (^{7}Li) spectra of LiCH$_2$TMS in C$_7$D$_8$ with LiCl/MeOH-d_4 internal standard.

5.4 Crystallograpic Data

Table 5-1. Crystal data and structure refinement for [(*R*)-**64**]$_2$.

|	
Identification code	[(*R*)-**64**]$_2$
Empirical formula	$C_{56}H_{64}Li_4N_8$
Formula weight	876.91
Temperature	100(2) K
Wavelength	0.71073 Å
Crystal system	Monoclinic
Space group	P2(1)
Unit cell dimensions	a = 11.4026(9) Å $\alpha = 90°$.
	b = 16.1821(13) Å $\beta = 100.292\,(2)°$.
	c = 13.8011(11) Å $\gamma = 90°$.
Volume	2505.6(3) Å^3
Z	2
Density (calculated)	1.162 Mg/m^3
Absorption coefficient	0.068 mm^{-1}
F(000)	936
Crystal size	0.43 x 0.32 x 0.23 mm^3
Theta range for data collection	1.96 to 31.48°.
Index ranges	$-16 \leq h \leq 16, -23 \leq k \leq 23, -20 \leq l \leq 20$
Reflections collected	26648
Independent reflections	15557 [R(int) = 0.0233]
Completeness to theta = 31.48°	98.5 %
Absorption correction	Semi-empirical from equivalents
Max. and min. transmission	0.984 and 0.971
Refinement method	Full-matrix least-squares on F^2
Data / restraints / parameters	15557 / 1 / 621
Goodness-of-fit on F^2	1.015
Final R indices [I>2sigma(I)]	R1 = 0.0491, wR2 = 0.1221
R indices (all data)	R1 = 0.0552, wR2 = 0.1267
Absolute structure parameter	-0.7(10)
Largest diff. peak and hole	0.486 and -0.218 e.Å^{-3}

Table 5-2. Crystal data and structure refinement for (bis(dimethylamino-2-yl-ethyl)amido)
binaphthyl-di-lithium, [(*rac*)-**64**]$_6$.

Identification code	[(*rac*)-**64**]$_6$
Empirical formula	$C_{35}H_{41}Li_2N_4$
Formula weight	531.93
Temperature	100(2) K
Wavelength	0.71073 Å
Crystal system	Rhombohedral
Space group	R-3
Unit cell dimensions	a = 23.1051(15) Å α = 90°.
	b = 23.1051(15) Å β = 90°.
	c = 30.845(2) Å γ = 120°.
Volume	14260.4(16) Å^3
Z	18
Density (calculated)	1.115 Mg/m^3
Absorption coefficient	0.065 mm^{-1}
F(000)	5133
Crystal size	0.24 x 0.24 x 0.11 mm^3
Theta range for data collection	1.98 to 29.13°.
Index ranges	$-31 \leq h \leq 31, -31 \leq k \leq 31, -41 \leq l \leq 42$
Reflections collected	49606
Independent reflections	8541 [R(int) = 0.0504]
Completeness to theta = 29.13°	99.9 %
Absorption correction	Semi-empirical from equivalents
Max. and min. transmission	0.992 and 0.984
Refinement method	Full-matrix least-squares on F^2
Data / restraints / parameters	8541 / 285 / 370
Goodness-of-fit on F^2	1.005
Final R indices [I>2sigma(I)]	R1 = 0.0710, wR2 = 0.1778
R indices (all data)	R1 = 0.1030, wR2 = 0.1987
Largest diff. peak and hole	0.869 and -0.441 e.Å^{-3}

Table 5-3. Crystal data and structure refinement for (*rac*)-**65**.

Identification code	(*rac*)-**65**
Empirical formula	$C_{32}H_{40}Li_2N_4$
Formula weight	494.56
Temperature	100(2) K
Wavelength	0.71073 Å
Crystal system	Monoclinic
Space group	Cc
Unit cell dimensions	a = 15.7250(9) Å $\quad$ α = 90°.
	b = 15.7457(9) Å $\quad$ β = 100.037(1)°.
	c = 22.4677(12) Å $\quad$ γ = 90°.
Volume	5477.9(5) Å^3
Z	8
Density (calculated)	1.199 Mg/m^3
Absorption coefficient	0.070 mm^{-1}
F(000)	2128
Crystal size	0.36 x 0.13 x 0.03 mm^3
Theta range for data collection	1.84 to 30.56°.
Index ranges	–22 ≤ h ≤ 21, –22 ≤ k ≤ 22, –32 ≤ l ≤ 31
Reflections collected	24108
Independent reflections	8295 [R(int) = 0.0262]
Completeness to theta = 30.56°	98.6 %
Absorption correction	Integration
Max. and min. transmission	0.997 and 0.975
Refinement method	Full-matrix least-squares on F^2
Data / restraints / parameters	8295 / 2 / 693
Goodness-of-fit on F^2	1.006
Final R indices [I>2sigma(I)]	R1 = 0.0424, wR2 = 0.0995
R indices (all data)	R1 = 0.0466, wR2 = 0.1021
Absolute structure parameter	0.00
Largest diff. peak and hole	0.417 and -0.213 e.Å^{-3}

Table 5-4. Crystal data and structure refinement for (bis(piperidin-2-yl-ethyl)amido)
binaphthyl-di-lithium, (*rac*)-**66**.

Identification code	(*rac*)-**66**
Empirical formula	$C_{34}H_{40}Li_2N_4$
Formula weight	518.58
Temperature	100(2) K
Wavelength	0.71073 Å
Crystal system	Triclinic
Space group	P-1
Unit cell dimensions	a = 8.9356(5) Å α = 70.673(1)°.
	b = 11.6351(7) Å β = 76.959(1)°.
	c = 15.0516(9) Å γ = 89.451(1)°.
Volume	1434.98(15) Å^3
Z	2
Density (calculated)	1.200 Mg/m^3
Absorption coefficient	0.070 mm^{-1}
F(000)	556
Crystal size	0.36 x 0.32 x 0.13 mm^3
Theta range for data collection	1.86 to 31.56°.
Index ranges	$-13 \leq h \leq 13, -17 \leq k \leq 17, -22 \leq l \leq 22$
Reflections collected	20780
Independent reflections	9426 [R(int) = 0.0192]
Completeness to theta = 31.56°	98.2 %
Absorption correction	Semi-empirical from equivalents
Max. and min. transmission	0.9910 and 0.9754
Refinement method	Full-matrix least-squares on F^2
Data / restraints / parameters	9426 / 0 / 521
Goodness-of-fit on F^2	1.007
Final R indices [I>2sigma(I)]	R1 = 0.0558, wR2 = 0.1414
R indices (all data)	R1 = 0.0653, wR2 = 0.1497
Largest diff. peak and hole	0.617 and -0.179 e.Å^{-3}

Table 5-5. Crystal data and structure refinement for [(*R*)-**67**]$_2$.

Identification code	[(*R*)-**67**]$_2$
Empirical formula	$C_{26}H_{26}Li_2N_2O_2$
Formula weight	412.37
Temperature	100(2) K
Wavelength	0.71073 Å
Crystal system	Tetragonal
Space group	P4(2)2(1)2
Unit cell dimensions	a = 14.8656(7) Å $\alpha = 90°$.
	b = 14.8656(7) Å $\beta = 90°$.
	c = 9.8701(5) Å $\gamma = 90°$.
Volume	2181.15(18) Å^3
Z	4
Density (calculated)	1.256 Mg/m^3
Absorption coefficient	0.078 mm^{-1}
F(000)	872
Crystal size	0.10 x 0.08 x 0.04 mm^3
Theta range for data collection	1.94 to 31.50°.
Index ranges	$-21 \leq h \leq 21, -21 \leq k \leq 21, -14 \leq l \leq 14$
Reflections collected	24842
Independent reflections	3639 [R(int) = 0.0503]
Completeness to theta = 31.50°	100.0 %
Absorption correction	Semi-empirical from equivalents
Max. and min. transmission	0.9969 and 0.9923
Refinement method	Full-matrix least-squares on F^2
Data / restraints / parameters	3639 / 0 / 146
Goodness-of-fit on F^2	1.067
Final R indices [I>2sigma(I)]	R1 = 0.0524, wR2 = 0.1181
R indices (all data)	R1 = 0.0636, wR2 = 0.1239
Absolute structure parameter	-0.8(14)
Largest diff. peak and hole	0.426 and -0.167 e.Å^{-3}

Table 5-6. Crystal data and structure refinement for (*R*)-**68**.

Identification code	(*R*)-**68**
Empirical formula	$C_{24}H_{35}LiN_3$
Formula weight	372.49
Temperature	100(2) K
Wavelength	0.71073 Å
Crystal system	Orthorhombic
Space group	P2(1)2(1)2
Unit cell dimensions	a = 12.5853(15) Å $\alpha = 90°$.
	b = 18.602(2) Å $\beta = 90°$.
	c = 9.2218(11) Å $\gamma = 90°$.
Volume	2158.9(5) $Å^3$
Z	4
Density (calculated)	1.146 Mg/m^3
Absorption coefficient	0.067 mm^{-1}
F(000)	812
Crystal size	0.28 x 0.22 x 0.12 mm^3
Theta range for data collection	1.95 to 28.30°.
Index ranges	$-16 \leq h \leq 16, -24 \leq k \leq 24, -12 \leq l \leq 12$
Reflections collected	22161
Independent reflections	5380 [R(int) = 0.0615]
Completeness to theta = 28.30°	100.0 %
Absorption correction	Semi-empirical from equivalents
Max. and min. transmission	0.9921 and 0.9816
Refinement method	Full-matrix least-squares on F^2
Data / restraints / parameters	5380 / 0 / 256
Goodness-of-fit on F^2	1.001
Final R indices [I>2sigma(I)]	R1 = 0.0735, wR2 = 0.1547
R indices (all data)	R1 = 0.0840, wR2 = 0.1607
Absolute structure parameter	-1(3)
Largest diff. peak and hole	0.399 and -0.237 $e.Å^{-3}$

5.5 Summary of Crystal Structure Data

Table 5-7. Summary of crystal structure data: Range of bond lengths and intermolecular distances for selected interactions (≤ 3.0 Å).

	Li-N(amido)	Li-N(amine), Li-O	Li···C(π) (Short Contacts)	Li···C(π) (Long Contacts)
[(*S,S,S*)-**25**]$_2$	1.94 – 2.26	2.10 – 2.20	2.25 – 2.54	2.77 – 2.98
[(*R*)-**64**]$_2$	1.96 – 2.15	2.10 – 2.70	2.24 – 2.50	
[(*rac*)-**64**]$_6$	2.01 – 2.16	2.08, 2.12	2.32, 2.52	2.93 – 2.99
(*R*)-**68**	1.94	2.01, 2.13	2.64	2.82, 2.94
(*R*)-**65A**	1.88 – 2.13	2.07, 2.11	2.27, 2.29	
(*R*)-**65B**	1.88 – 2.15	2.07, 2.10	2.29, 2.70	
(*R*)-**66**	1.92 – 2.05	2.06, 2.11	2.33 – 2.45	2.70 – 2.90
[(*R*)-**67**]$_2$	1.93, 2.06	1.89	2.23 – 2.70	2.82, 2.91

Table 5-8. Summary of crystal structure data: Torsion angles and mean planes.

	Torsion Angle (Sidearm)	Torsion Angle (Naphthyl Rings)	Mean Planes
[(*S,S,S*)-**25**]$_2$	46.2 – 55.5	68.0 – 84.8	77.4, 98.7
[(*R*)-**64**]$_2$	38.3 – 63.4	66.7 – 81.6	73.6, 75.8
[(*rac*)-**64**]$_6$	59.7, 66.1	71.1, 75.9	75.9
(*R*)-**68**	48.15	108.4, 113.7	64.9
(*R*)-**65A**	38.4, 47.6	60.6, 72.3	65.8
(*R*)-**65B**	35.9, 48.2	61.1, 71.9	66.4
(*R*)-**66**	53.7, 54.2	79.9, 81.7	85.7
[(*R*)-**67**]$_2$	62.1	92.8, 108.3	83.9